Searching for New Physics in Bottom-quark Decays

DISSERTATION

zur Erlangung des akademischen Grades eines Doktors
der Naturwissenschaften
(Dr. rer. nat.)

vorgelegt von

M.Sc. Muslem Rahimi

eingereicht bei der Naturwissenschaftlich-Technischen Fakultät
der Universität Siegen

Siegen
Dezember 2022

Betreuer und erster Gutachter
Prof. Dr. Thomas Mannel
Universität Siegen

Zweiter Gutachter
Prof. Dr. Alexander Khodjamirian
Universität Siegen

Tag der mündlichen Prüfung:
03.02.2023

Abstract

In recent years, small deviations between experimental measurements and predictions from the Standard Model (SM) have been observed in bottom-quark decays, which indicate that Lepton Flavour Universality (LFU) may be violated. These small deviations, the so-called b-anomalies, have been observed in the two decay channels $b \to c\ell\bar{\nu}$ and $b \to s\ell\ell$. To ensure that the b-anomalies are not an underestimation of the systematic uncertainties, we aim in this thesis to improve the precision of flavour physics prediction while also providing insight on the tension between theory prediction and experimental measurement by incorporating New Physics (NP) effects and their impact on observables in the bottom-quark decay.

This dissertation is written in the form of a cumulative work based on our six articles, four of which have been published in international peer-reviewed journals [1–4] and the remaining two are being prepared for publication [5, 6]. First, we investigate the background signals of the inclusive decay $B \to X_c\ell\bar{\nu}$ that is relevant for the extraction of $|V_{cb}|$. In order to increase precision, we argue that removing the background signals from Monte-Carlo simulation data should be avoided because it introduces uncertainties. Instead, we can precisely compute the background signals using Heavy Quark Expansion (HQE).

In addition, we investigate the LFU symmetry of the SM in the semileptonic $B \to X_c\ell\bar{\nu}$ decays. Ratios of branching fractions between decays are used to probe the LFU hypothesis, where our calculation of the LFU ratios for the SM takes into account the mass effects in the total decay rate. We provide updated results for the branching ratio of $B \to X_c\tau\bar{\nu}$. If there is a difference between SM predictions and experimental data, this could indicate the presence of NP impacts.

We also investigate the possibility of NP effect in the inclusive semileptonic $B \to X_c\ell\bar{\nu}$ decay. The calculations rely on the HQE and use non-perturbative parameters extracted from decay spectra. The extraction of HQE parameters is done assuming the SM, but we explore the idea that NP effects might be hidden in the HQE parameters. The primary goal is to lay the groundwork for a global fit analysis that includes the full basis of NP operators, allowing for the extraction of HQE parameters and consequently an updated result for $|V_{cb}|$ with NP effects.

In the baryonic decay channel we investigate the possibility of the Lepton Flavour Violation (LFV) for the exclusive decay $\Lambda_b \to \Lambda\ell_1^-\ell_2^+$ using a full basis of NP operators for the first time. We investigate the branching ratio and forward-backward symmetry of the decay quantitatively using both a model-independent and model-dependent approach. We emphasize that the baryonic decay constrains the NP Wilson coefficients differently from the mesonic decay, which has the potential to further constrain the allowed parameter space for NP models. We can also improve the constraint of the NP models by reducing the hadronic uncertainties caused by the ten independent local form factors of $\Lambda_b \to \Lambda$. To improve the control of the uncertainties, we introduce a new parametrization for the local form factors in which the form factor parameters are bounded due to orthonormal polynomials that diagonalize the form factor contribution within their respective dispersive bounds. We show, using a Bayesian analysis of available lattice QCD data, that our model provides excellent control over systematic uncertainty when extrapolating to the region

of large hadronic recoil.

As part of this thesis's final project, we investigate the light-cone distribution amplitude (LCDA) of the B meson. We are particularly interested in three-particle LCDAs, which can be found in higher dimensional vacuum-to-meson matrix elements. These matrix elements can be parametrized in terms of two parameters. To estimate the parameters, we propose alternative diagonal QCD sum rules. The sum rules of our new approach have the advantage of being positive definite, which means that we expect the quark-hadron duality to be more accurate than the previous studied sum rules.

Zusammenfassung

In den letzten Jahren wurden kleine Abweichungen zwischen experimentellen Messungen und Vorhersagen des Standardmodells (SM) bei Bottom-Quark-Zerfällen beobachtet, was auf eine Verletzung der Lepton Flavour Universalität (LFU) hindeuten könnte. Diese Abweichungen, die sogenannten b-Anomalien, wurden in den beiden Zerfallskanälen $b \to c\ell\bar{\nu}$ und $b \to s\ell\ell$ beobachtet. Um sicherzustellen, dass die b-Anomalien nicht eine Unterschätzung der systematischen Unsicherheiten sind, zielen wir in dieser Arbeit darauf ab, die Genauigkeit der Vorhersagen der Flavour-Physik zu verbessern und gleichzeitig einen Einblick in die Spannung zwischen der theoretischen Vorhersage und der experimentellen Messung zu geben, indem wir die Effekte der Neuen Physik (NP) und ihre Auswirkungen auf die Observablen im Bottom-Quark-Zerfall berücksichtigen.

Diese Dissertation ist in Form einer kumulativen Arbeit geschrieben, die auf unseren sechs Artikeln basiert, von denen vier in internationalen, von Experten begutachteten Zeitschriften veröffentlicht wurden [1–4] und die restlichen zwei sind in Vorbereitung zur Veröffentlichung [5,6]. Zunächst untersuchen wir die Hintergrundsignale des inklusiven Zerfalls $B \to X_c\ell\bar{\nu}$, der für die Extraktion von $|V_{cb}|$ relevant ist. Um die Genauigkeit zu erhöhen, argumentieren wir, dass die Subtraktion der Hintergrundsignale aus den Monte-Carlo-Simulationsdaten vermieden werden sollte, da dies Unsicherheiten mit sich bringt. Stattdessen können wir die Hintergrundsignale mithilfe der Heavy Quark Expansion (HQE) präzise berechnen.

Darüber hinaus untersuchen wir die LFU-Symmetrie des SM in den semileptonischen $B \to X_c\ell\bar{\nu}$ Zerfällen. Unsere Berechnung der LFU-Verhältnisse für das SM berücksichtigt die Masseneffekte in der Gesamtzerfallsrate. Wir liefern aktualisierte Ergebnisse für das Verzweigungsverhältnis von $B \to X_c\tau\bar{\nu}$. Die Verzweigungsverhältnisse zwischen den Zerfällen werden verwendet, um die LFU-Hypothese zu überprüfen. Wenn es einen Unterschied zwischen den SM-Vorhersagen und den experimentellen Daten gibt, könnte dies auf das Vorhandensein von Auswirkungen der Neuen Physik hinweisen.

Wir untersuchen auch die Möglichkeit eines NP-Effekts im inklusiven semileptonischen $B \to X_c\ell\bar{\nu}$ Zerfall. Die Berechnungen beruhen auf der HQE und verwenden nicht-perturbative Parameter, die aus Zerfallsspektren extrahiert werden. Die Extraktion der HQE-Parameter erfolgt unter der Annahme des SM, aber wir untersuchen die Idee, dass NP-Effekte in den HQE-Parametern versteckt sein könnten. Das primäre Ziel ist es, den Grundstein für eine globale Fit-Analyse zu legen, die die gesamte Basis der NP-Operatoren einschließt und die Extraktion von HQE-Parametern und folglich ein aktualisiertes Ergebnis für $|V_{cb}|$ mit NP-Effekten ermöglicht.

Im baryonischen Zerfallskanal untersuchen wir erstmals die Möglichkeit der Lepton Flavour Violation (LFV) für den exklusiven Zerfall $\Lambda_b \to \Lambda\ell_1^-\ell_2^+$ unter Verwendung einer vollständigen Basis von NP-Operatoren. Wir untersuchen das Verzweigungsverhältnis und die Vorwärts-Rückwärts-Symmetrie des Zerfalls quantitativ sowohl mit einem modellunabhängigen als auch mit einem modellabhängigen Ansatz. Wir betonen, dass der baryonische Zerfall die NP-Wilson-Koeffizienten anders einschränkt als der mesonische Zerfall, was das Potenzial hat, den zulässigen

Parameterraum für NP-Modelle weiter einzuschränken. Wir können auch die Einschränkung der NP-Modelle verbessern, indem wir die hadronischen Unsicherheiten reduzieren, die durch die zehn unabhängigen lokalen Formfaktoren von $\Lambda_b \to \Lambda$ verursacht werden. Um die Kontrolle der Unsicherheiten zu verbessern, führen wir eine neue Parametrisierung für die lokalen Formfaktoren ein, bei der die Formfaktorparameter aufgrund der Verwendung von orthonormalen Polynomen begrenzt sind, die den Formfaktorbeitrag innerhalb ihrer jeweiligen dispersiven Grenzen diagonalisieren. Anhand einer Bayes'schen Analyse verfügbarer Gitter-QCD-Daten zeigen wir, dass unser Modell eine ausgezeichnete Kontrolle über die systematische Unsicherheit bei der Extrapolation in den Bereich des großen hadronischen Rückstoßes bietet.

Im Rahmen des Abschlussprojekts dieser Arbeit untersuchen wir die Lichtkegelverteilungsamplitude (LCDA) des B-Mesons. Wir interessieren uns besonders für die LCDAs von drei Teilchen, die in höherdimensionalen Vakuum-Meson-Matrixelementen gefunden werden können. Diese Matrixelemente können mit zwei Parametern parametrisiert werden. Um die Parameter abzuschätzen, schlagen wir alternative diagonale QCD-Summenregeln vor. Die Summenregeln unseres neuen Ansatzes haben den Vorteil, dass sie positiv definit sind, was bedeutet, dass wir erwarten, dass die Quark-Hadron-Dualität genauer ist als die bisher untersuchten Summenregeln.

Contents

Chapter 1

Introduction

By creating scientific theories founded on logical principles, humanity has gathered essential information and understanding of the underlying workings of the universe. We are able to predict one of the most extreme events in the universe by comparing theoretical hypotheses with empirical data obtained through experimental measurements, such as the primordial energy inferno that occurred a split of a second after the Big Bang [7]. One revolutionary idea that developed in the early 20^{th} century is quantum physics, which explains certain observations of the universe that are incompatible with classical physics understanding of the universe at the time. During the same time period, crucial experimental findings regarding the electron [8], proton [9], and neutron [10] − at that time believed to be the three basic building blocks of matter − were made, laying the groundwork for fundamental particle physics. The goal of elementary particle physics is to use the simplest set of physical principles to describe the fundamental constituents of nature and their interactions. The Standard Model (SM) of particle physics provides the best understanding of nature in these terms. The SM is a quantum field theory that describes the interactions of all known fundamental particles and provides precise predictions of a wide range of events and particle processes [11–13]. But like every theory, this one has certain drawbacks as well. For example, there are 18 free parameters in the SM that are not predicted by the theory. Six quark masses, three gauge couplings, two Higgs potential parameters, three charged-lepton masses and four Cabibbo-Kobayashi-Maskawa (CKM) quark-flavour mixing parameters that need to be determined experimentally. Specifically quark-flavour mixing parameters are affected by weak quark transitions and can be over-constrained by many independent processes to test the Standard Model. Disagreements between theory and experiment would hint the presence of New Physics (NP).

Only the electromagnetic, strong, and weak forces are explained in the SM, which makes it evident that the SM is not a full theory of nature. This is because general relativity is not sufficiently described as a quantum field theory.

Furthermore, based on cosmological studies, it is estimated that just around 5 % of the known matter is described in the Standard Model. Dark matter and dark energy make up the remaining 95 %, which the SM is unable to explain. Even though it is obvious that SM is not the full theory of nature, it is nevertheless a very practical and useful theory that can be applied at specific energy scales. Comparable

to special relativity, which is a more general theory that applies when approaching the speed of light, classical mechanics is still a very useful and practical theory for the explanation of macroscopic phenomena where velocities are much lower than the speed of light.

Nonetheless, the incredible collaborative theoretical and experimental effort over the last few years has enabled us to test the Standard Model of particle physics with unprecedented precision. This revealed various small deviations between theoretical predictions and experimental measurements, specifically in semileptonic B meson decays. These small deviations are known as b-anomalies, which point to a violation of the Lepton Flavour Universality (LFU). This is surprising given that LFU is a fundamental property of the SM. It is possible to categorize the b-anomalies into two groups: 1) deviations from the μ/e universality in the $b \to s\ell\ell$ transitions, and 2) deviations from the τ vs. light leptons universality in the $b \to c\ell\bar{\nu}$ transitions. But this is not limited to semileptonic mesonic decay only; it could also apply to semileptonic baryonic decay, such as $\Lambda_b \to \Lambda\, \ell_1^+ \ell_2^-$ where ℓ_1^-, ℓ_2^+ are two different leptons, which is forbidden in the Standard Model. Another discrepancy in the semileptonic B meson decay is the puzzling tension between the exclusive $B \to D^{(*)}\ell\bar{\nu}$ and inclusive $B \to X_c\ell\bar{\nu}$ determination of the CKM element $|V_{cb}|$, which may indicate the presence of NP. The inclusive decay sums up all of the kinematically possible final states of hadrons labeled by X_c, where X_c denotes a charm-quark containing hadron. The exclusive decay, on the other hand, fully specifies the initial and final states of semileptonic decay. While the inclusive decay alone relies on the Heavy Quark Expansion and the derivation of non-perturbative parameters from data, the exclusive decays require knowledge of the form factors. At the current state, the inclusive determination of $|V_{cb}|$ has reached an impressive relative uncertainty of $1.2 - 1.5\%$ [14, 15]. There are a few more soft spots in the SM, where tensions between theoretical predictions and experimental measurements can be observed, which are all in the flavour sector of leptons and quarks. In light of recent and possibly future experimental data, there are three reasons why it is important to increase the precision of theoretical predictions. First to determine if the b-anomalies are simply an underestimate of systematic uncertainties, statistical fluctuations or evidence of NP. Second, in order to further constrain NP effects, even if the b-anomalies are not confirmed as evidence of NP effects, greater theoretical prediction precision is necessary. Third, in order for the theory to keep up with the more precise data that will be made available by LHC Run II and Belle II, more precision is required.

Therefore, we have made it our goal in this thesis to improve the precision of semileptonic bottom-quark decays in both inclusive and exclusive while also examining the implications of potential NP effects.

The thesis is organized as follows. In Chapter 2, we will give a brief introduction to the SM. In Chapter 3, we will introduce the concept of effective theories and discuss the aspects of Heavy Quark Effective Theory. We explore the inclusive semileptonic decay of the B meson in Chapter 4 and provide an overview of how to derive the fully differential decay rate and discuss the relevant observables that are subject for this thesis. We discuss the QCD sum rule method and demonstrate how to derive a sum rule explicitly in Chapter 5. Six applications are presented in

the following chapters 6 – 11, in which the heavy quark methods are used to either improve precision or investigate the potential impacts of NP effects in bottom-quark physics. All of these applications have already been published [1–4] or have been submitted to a peer-reviewed journal [5, 6].

In Chapter 6 we discuss the background process $b \to u$ and $b \to c(\tau \to \ell\bar{\nu}\nu)\bar{\nu}$. For the extraction of the CKM element $|V_{cb}|$ we need to subtract the background decay from the experimental measured decay channel $B \to X\ell$. The background signal is subtracted in the Belle experiment using generator-level Monte Carlo data. Hence, we decided to discuss the calculation of the background signals within the framework of Heavy Quark Expansion (HQE). We compare our results qualitatively to the Monte Carlo data and argue that more precise measurements of $|V_{cb}|$ can be obtained by using the HQE results instead.

We make predictions for the inclusive $B \to X_c\ell\bar{\nu}_\ell$ LFU ratios in Chapter 7. These inclusive ratios serve as a critical cross-check of the exclusive $B \to D^{(*)}\ell\bar{\nu}_\ell$ modes, where tensions exist between predictions and measurements.

In Chapter 8 we study the effects of the full basis of the NP operators in the Weak Effective Theory on the inclusive semileptonic channel $B \to X_c\ell\bar{\nu}$ for the first time. We argue that NP could influence the moments of the inclusive decay. We compute the lepton energy, hadronic and leptonic invariant mass moments for different toy NP scenarios in order to illustrate the potential impacts of the theory and we compare the results to SM predictions and experimental measurements. We discuss how our findings could be used to perform a global fit that includes NP contributions.

In Chapter 9, we discuss Lepton Flavour Violation (LFV) for the baryonic decay $\Lambda_b \to \Lambda\ell_1^-\ell_2^+$ using a full basis of New Physics operators for the first time as well. In a model-independent framework and using two specific new physics models, we present expected bounds on the branching ratio. Finally, we highlight the orthogonality of the baryonic and mesonic LFV searches.

In Chapter 10 we investigate the ten local form factors of the $\Lambda_b \to \Lambda\ell^+\ell^-$ decay by combining information of lattice QCD and dispersive bounds. We discuss that our new approach provides a degree of control of the form-factor uncertainty at the large hadronic recoil region.

In Chapter 11, we obtain new estimates for the two parameters that appear in the second moments of the B meson light-cone distribution amplitudes, as defined in the Heavy Quark Effective Theory. We consider the two-point QCD sum rule for the diagonal correlation function and compare our results with prior findings in the literature.

In the final Chapter 12 of this thesis, we summarize and discuss our results.

Chapter 2

The Standard Model

Many theories emerged during the 1970s to explain the identities and properties of elementary particles, as well as the forces that act between them. The Standard Model emerged as a collection of theories that have survived to the present day [11, 12, 16, 17]. In the SM, particles with spin 1/2 are called fermions. The fermions are classified into two types of particles: quarks and leptons. Each group consist of six particles, which are assigned to three generations, see Table 2.1. In addition to quantum numbers such as electromagnetic charge, spin and parity, quarks carry another quantum number known as colour. According to the SM, each particle has their own anti-particle, which has the same mass but opposite electric charge Q. Particles with spin 1 are called gauge bosons. The gauge bosons serve as mediators and the interactions are characterized by local gauge symmetries. The photon mediates the electromagnetic interaction, which is associated with charged particles and is a $U(1)_Q$ gauge group. The theory of photons as well as their interactions with charged fermions are described by Quantum Electrodynamics (QED). Z^0 and $W^{\pm}$ bosons mediate the weak interaction. Whilst the $W^{\pm}$ boson have an electromagnetic charge and thus can interact with the electromagnetic force. However, they exclusively interact with left-handed particles. Contrarily, the Z^0 boson is electric neutral and can interact with both left- and right-handed particles. The theory of electromagnetic and weak interaction can be unified under the gauge group $SU(2)_L \otimes U(1)_Y$, which spontaneously breaks down to $U(1)_Q$. The gauge group $SU(2)_L$ is associated with the weak isospin I and the group $U(1)_Y$ with the hypercharge Y. The strong interaction is experienced by quarks and gluons carry the force. This is a gauge theory in which the three coloured states of each flavour belong to the group $SU(3)_C$ triplet representation. Note that, the gauge group $SU(3)_C$ is associated with the colour charge C. The theory of the strong interaction is described by Quantum Chromodynamics (QCD); for more information, see Section 2.3. Finally, the last particle in the SM is the Higgs boson and was discovered in 2012 [18,19]. The Higgs mechanism, which explains how the gauge bosons $W^{\pm}$ and Z^0, the quarks and the leptons acquire masses while maintaining gauge symmetry at the quantum level, is related to the Higgs boson, which was first proposed in the 1960s [20–23].

An overview of the Standard Model can be found in Refs. [24–28].

Generations				
1	2	3	Charge Q	Spin s
Quarks				
$\begin{pmatrix} u \\ d \end{pmatrix}$	$\begin{pmatrix} c \\ s \end{pmatrix}$	$\begin{pmatrix} t \\ b \end{pmatrix}$	$+\frac{2}{3}$ $-\frac{1}{3}$	$\frac{1}{2}$ $\frac{1}{2}$
Leptons				
$\begin{pmatrix} \nu_e \\ e \end{pmatrix}$	$\begin{pmatrix} \nu_\mu \\ \mu \end{pmatrix}$	$\begin{pmatrix} \nu_\tau \\ \tau \end{pmatrix}$	0 -1	$\frac{1}{2}$ $\frac{1}{2}$
Gauge bosons				
Photon γ			0	1
gluon g			0	1
$Z^0, W^\pm$			$0, \pm 1$	1
Higgs H^0			0	0

Table 2.1: Fundamental particle content of the Standard Model, which includes quarks, leptons and gauge bosons and their quantum numbers; electromagnetic charge and spin.

2.1 Electroweak sector

The electroweak sector of the Standard Model unifies the theory of electromagnetic and weak interactions, which was originally developed by Glashow, Weinberg and Salam [11,12,16]. The electroweak theory is based on the symmetry group $SU(2)_L \otimes U(1)_Y$, where fermions are forming left-handed doublets and right-handed singlets according to the group $SU(2)_L$. In the following we define left- and right-handed fields as:

$$\psi_{L,R} = \frac{1 \mp \gamma_5}{2} \psi \,, \tag{2.1}$$

where ψ represents the fermion field. The symmetry group $U(1)_Y$ transforms the fermion field to obtain the quantum number Y. The Gell-Mann-Nishijima formula relates the electromagnetic charge Q, hypercharge Y and the third component of the weak isospin T_3 to each other

$$Q = T_3 + \frac{Y}{2} \,, \tag{2.2}$$

where the weak isospin describes the coupling of the particle with the gauge bosons in the weak interactions, similar to the electromagnetic charge in QED.

The Lagrangian density of the electroweak sector consists of a gauge boson part, Higgs part, fermion part and a Yukawa part, which describes the interaction between fermionic and Higgs field. The Lagrangian can be expressed as:

$$\mathcal{L}_{EW} = \mathcal{L}_G + \mathcal{L}_H + \mathcal{L}_F + \mathcal{L}_Y \,. \tag{2.3}$$

The gauge bosonic part of the electroweak theory is defined as:

$$\mathcal{L}_G = -\frac{1}{4} \left(W^a_{\mu\nu} W^{\mu\nu}_a + B_{\mu\nu} B^{\mu\nu} \right) \,, \tag{2.4}$$

where the field strength tensors are given as

$$B_{\mu\nu} = \partial_\mu B_\nu - \partial_\nu B_\mu \qquad \text{for } U(1)_Y\,, \tag{2.5}$$

$$W^a_{\mu\nu} = \partial_\mu W^a_\nu - \partial_\nu W^a_\mu - g'\epsilon^{abc} W^b_\mu W^c_\nu \qquad \text{for } SU(2)_L\,. \tag{2.6}$$

The gauge bosons of the electroweak interactions $W^\pm, Z^0$ and γ can be defined via the gauge fields of Eq. (2.5) and (2.6).

The gauge bosons $W^\pm$ can be expressed as:

$$W_\mu = \frac{1}{\sqrt{2}}\left(W^1_\mu \pm i W^2_\mu\right)\,, \tag{2.7}$$

where the sign $\pm$ denotes the electromagnetic charge of the gauge boson. As already mentioned, the Z^0 boson can couple to left- and right-handed particles. However, the W^3_μ gauge field can only couple to left-handed particles to preserve the isospin. Additionally, the gauge field B_μ can not be directly related to the photon γ, since B_μ can also couple with electromagnetic neutral neutrinos in contrast to the photon. By writing a combination of the two gauge fields W^3_μ and B_μ, we can express the two gauge bosons in the following:

$$\begin{pmatrix} Z_\mu \\ A_\mu \end{pmatrix} = \begin{pmatrix} \cos\theta_W & \sin\theta_W \\ -\sin\theta_W & \cos\theta_W \end{pmatrix} \begin{pmatrix} W^3_\mu \\ B_\mu \end{pmatrix}\,, \tag{2.8}$$

where the θ_W is called Weinberg angle and is defined as:

$$\cos\theta_W = \frac{g}{\sqrt{g^2 + g'^2}}\,. \tag{2.9}$$

Under the symmetry group $SU(2)_L \otimes U(1)_Y$ the gauge bosons are massless to preserve the gauge invariance. The acquiring of the mass will be through spontaneous symmetry breaking of $SU(2)_L \otimes U(1)_Y \to U(1)_Q$. The local symmetry breaking is known as Higgs mechanism, where the Lagrangian density is given as:

$$\mathcal{L}_H = (D_\mu \phi)^\dagger (D^\mu \phi) - V(\phi)\,. \tag{2.10}$$

The complex Higgs field doublet is expressed in ϕ and the covariant derivative D_μ is defined as:

$$D_\mu = \partial_\mu + i\frac{g}{2} B_\mu - i g' T^a W^a_\mu\,, \tag{2.11}$$

where T^a are the generators of $SU(2)_L$. The potential $V(\phi) = -\mu^2|\phi|^2 + \lambda|\phi|^4$, where $\mu^2, \lambda > 0$ breaks the gauge symmetry spontaneously by means of the Higgs mechanism. Hence, the field ϕ has a non-zero vacuum expectation value, where the minimum is given as:

$$v = \left(\frac{\mu^2}{2\lambda}\right)^{1/2}\,. \tag{2.12}$$

The Higgs doublet has four real-valued component, but by choosing the unitary gauge transformation we can parametrize the Higgs doublet as:

$$\phi(x) = \frac{1}{\sqrt{2}} \begin{pmatrix} 0 \\ v + h(x) \end{pmatrix}\,, \tag{2.13}$$

where $h(x)$ describes the Higgs boson and is a real-valued field. Finally, by inserting Eq. (2.13) into Eq. (2.10) the electroweak gauge bosons $W^{\pm}, Z^0$ will acquire mass terms. Moreover, the Higgs boson acquire the mass $m_h = \sqrt{2\mu}$. Since the symmetry group $U(1)_Q$ is unbroken under the Higgs mechanism by construction, the photon remains massless. The fermionic part of the electroweak sector is described by the following Lagrangian density:

$$\mathcal{L}_F = \sum_{\psi} \bar{\psi}_L i \not{D}_L \psi_L + \bar{\psi}_R i \not{D}_R \psi_R \,. \tag{2.14}$$

The covaiant derivatives are defined as:

$$(D_L)_\mu = \partial_\mu + i\frac{g}{2} Y_L B_\mu - i g' T^a W^a_\mu \,, \tag{2.15}$$

$$(D_R)_\mu = \partial_\mu + i\frac{g}{2} Y_R B_\mu \,, \tag{2.16}$$

where $Y_{L,R}$ denotes the hypercharge quantum number. To obtain the boson-fermion interaction terms, we insert the definiton of the covariant derivative in Eq. (2.15), (2.16) and also the definition of the gauge bosons in Eq. (2.7), (2.8) into the Lagrangian $\mathcal{L}_F$:

$$\mathcal{L}_F \supseteq \mathcal{L}_{\psi W} + \mathcal{L}_{\psi A} + \mathcal{L}_{\psi Z} \tag{2.17}$$

with

$$\mathcal{L}_{\psi W} = \frac{g}{\sqrt{2}} \sum_{\psi} \left[\bar{\psi}^d_L \gamma_\mu \psi^u_L W^\mu + \text{h.c.} \right] \,, \tag{2.18}$$

$$\mathcal{L}_{\psi A} = -e \sum_{\psi} Q_\psi \bar{\psi} \gamma_\mu \psi A^\mu \,, \tag{2.19}$$

$$\begin{aligned} \mathcal{L}_{\psi Z} = \frac{g}{4\cos\theta_W} \sum_{\psi} \Big[& \bar{\psi}^u \gamma_\mu (1 - 4Q_u \sin^2\theta_W - \gamma_5) \psi^u \\ & - \bar{\psi}^d \gamma_\mu (1 + 4Q_d \sin^2\theta_W - \gamma_5) \psi^d \Big] Z^\mu \,, \end{aligned} \tag{2.20}$$

where γ_μ are the Dirac matrices. Up until now, the fermionic part is still massless. Within the electroweak sector, the Yukawa part of the $\mathcal{L}_Y$ describes the interaction between fermion fields and Higgs fields and consequently explains how fermions acquire their mass terms. We can split the Lagrangian into two parts:

$$\mathcal{L}_Y = \mathcal{L}_Y^{\text{leptons}} + \mathcal{L}_Y^{\text{quarks}} \,. \tag{2.21}$$

The first Yukawa part explains the interaction between lepton and Higgs field:

$$\mathcal{L}_Y^{\text{leptons}} = -Y^{(\ell)}_{ij} \left(\bar{L}^i_L \phi(x) \right) \ell^j_R + \text{h.c.} \,. \tag{2.22}$$

The quantity Y^ℓ is the 3×3 Yukawa matrix for leptons, $L^i_L = (\nu^i_\ell, \ell^i)^T$ is the left-handed doublet with $\ell^i = e, \mu, \tau$ and ℓ^j_R are the right-handed singlets. Except for neutrinos, the leptons acquire mass terms by inserting the Higgs field from Eq. (2.13) into Eq. (2.22).

In Section 2.2 we will go into greater detail about the second part of the Lagrangian in Eq. (2.21).

2.2 The Cabbibo-Kobayashi-Maskawa Matrix

The quark masses are obtained by the Yukawa interaction term:

$$\mathcal{L}_Y^{\text{quarks}} = -Y_{ij}^{(d)} \bar{Q}_L^i \phi(x) \bar{d}_R^j - Y_{ij}^{(u)} \bar{Q}_L^i \bar{\phi}(x) u_R^i + \text{h.c.}\,, \tag{2.23}$$

where $Y^{(u,d)}$ is the Yukawa matrix of the down-type quarks (d, s, b) and up-type quarks (u, c, t). The quantity $Q_L^i = (u_L^i, d_L^i)^T$ with $u^i = (u, c, t)$ and $d^i = (d, s, b)$ is the left-handed doublet. The fields u_R^i and d_R^i are the right-handed quark fields. Through the Higgs mechanism we obtain the mass terms, which is proportional to the Higgs vacuum-expectation value. Hence, we can express the Yukawa part as:

$$\mathcal{L}_Y^{\text{quarks}} \supseteq -\frac{v}{\sqrt{2}} \left(Y_{ij}^{(d)} \bar{d}_L^i d_R^j + Y_{ij}^{(u)} \bar{u}_L^i u_R^j + \text{h.c.} \right) . \tag{2.24}$$

We diagonalize the bilinear terms with four 3×3 matrices $V_{L,R}^{u,d}$, which yields the mass eigenstates:

$$u'_{L,R} = V_{L,R}^u u_{L,R}\,, \qquad\qquad d'_{L,R} = V_{L,R}^d d_{L,R}\,. \tag{2.25}$$

We define the diagonal mass matrices in the following way:

$$M_q = \frac{v}{\sqrt{2}} V_L^q Y^{(q)} V_R^{q\dagger} \qquad\qquad \text{with } \; q = u, d\,. \tag{2.26}$$

When we insert the the definition of the mass eigenstates in Eq. (2.25) for the quark fields, the two Lagrangian density $\mathcal{L}_{\psi A}$ and $\mathcal{L}_{\psi Z}$ remain invariant due to unitarity property of matrices $V_{L,R}^{u,d}$. However, the Lagrangian density $\mathcal{L}_{qW}$ in Eq. (2.18) will have a product of unitarity matrices, which is known as Cabbibo-Kobayashi-Maskawa (CKM) matrix [29, 30]:

$$V_{\text{CKM}} = V_L^u \cdot V_L^{d\dagger} = \begin{pmatrix} V_{ud} & V_{us} & V_{ub} \\ V_{cd} & V_{cs} & V_{cb} \\ V_{td} & V_{ts} & V_{tb} \end{pmatrix} , \qquad V_{\text{CKM}} \cdot V_{\text{CKM}}^\dagger = 1\,. \tag{2.27}$$

Moreover, the quark sector takes the form of:

$$\begin{aligned} \mathcal{L}_{qW} &= \frac{g}{\sqrt{2}} \left(\bar{u}'_L \gamma^\mu W_\mu^+ + \bar{d}'_L \gamma^\mu W_\mu^- u'_L \right) \\ &= \frac{g}{\sqrt{2}} \left(\bar{u}_L \gamma^\mu V_{\text{CKM}} W_\mu^+ \bar{d}_L V_{\text{CKM}}^\dagger \gamma^\mu W_\mu^- u_L \right) . \end{aligned} \tag{2.28}$$

Hence, the quark flavour can be changed when the interaction involves a charged weak vector boson. The CKM matrix element is proportional to the transition of down- to up-type quarks or vice versa. Transitions are possible not only between quarks of the same generation, but also between quarks of different generations.

The experimental measurements show that the entries of the CKM matrix are hierarchy based. In other words, transitions of different quark flavours between different quark generations are suppressed, which is known as CKM suppression. In fact, the CKM matrix is almost a unit matrix, where the matrix elements decrease

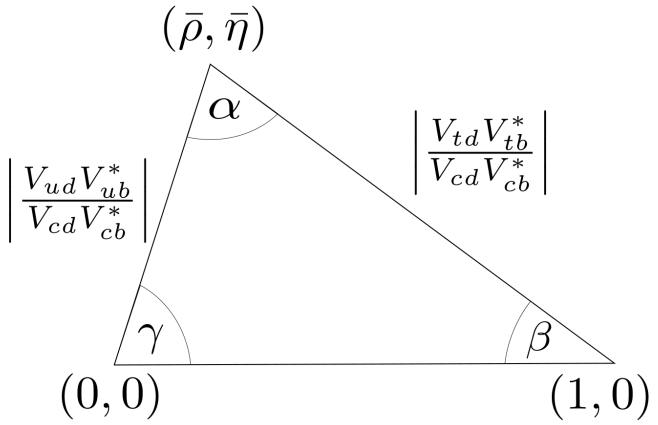

Figure 2.1: Unitarity triangle.

in size with increasing distance to the diagonal. The CKM matrix has three real angles and one phase that generates CP violation for three generations of quarks. The CKM matrix can be parametrized in terms of the four parameters A, λ, ρ, η, which was proposed by Wolfenstein [32]. In the Wolfenstein parametrization, the CKM matrix is expanded in $\lambda \simeq 0.22$:

$$V_{\text{CKM}} = \begin{pmatrix} 1-\lambda^2/2 & \lambda & A\lambda^3(\rho - i\eta) \\ -\lambda & 1-\lambda^2/2 & A\lambda^2 \\ A\lambda^3(-\rho - i\eta) & -A\lambda^2 & 1 \end{pmatrix} + \mathcal{O}(\lambda^4)\,. \tag{2.29}$$

By means of unitarity, we can display the CKM matrix as a triangle, in which unitarity implies:

$$\sum_i V_{ij}V_{ik}^* = \delta_{jk}\,, \qquad\qquad \sum_j V_{ij}V_{kj}^* = \delta_{ik}\,. \tag{2.30}$$

The above equation yields six vanishing combinations. A commonly used unitarity relation is given as:

$$V_{ud}V_{ub}^* + V_{cd}V_{cb}^* + V_{td}V_{tb}^* = 0 \qquad \Rightarrow \qquad 1 + \frac{V_{ud}V_{ub}^*}{V_{cd}V_{cb}^*} + \frac{V_{td}V_{tb}^*}{V_{cd}V_{cb}^*} = 0\,. \tag{2.31}$$

A schematically illustration of the triangle based on Eq. (2.31) is shown in Fig. 2.1.

To obtain even more precise results, the apex of the triangle can be further constrained using several independent channels and approaches, which is given as:

$$\bar{\rho} + i\bar{\eta} = \frac{V_{ud}V_{ub}^*}{V_{cd}V_{cb}^*}\,. \tag{2.32}$$

Following the notation of [33], we can define the relation:

$$\rho + i\eta = \frac{\sqrt{1 - A^2\lambda^4}(\bar{\rho} + i\bar{\eta})}{\sqrt{1-\lambda^2}\,(1 - A^2\lambda^4(\bar{\rho} + i\bar{\eta}))}\,. \tag{2.33}$$

The unitary triangle apex has been constrained significantly over the past ten years, as seen in Figure 2.2.

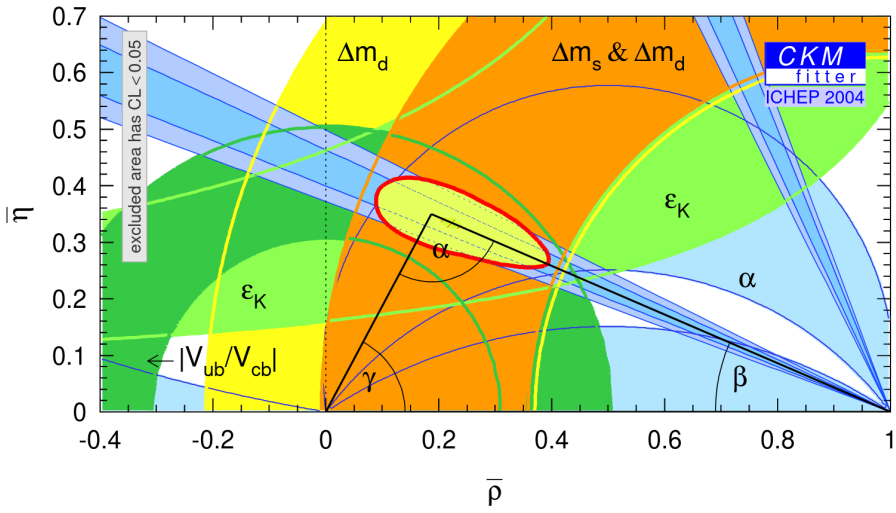

(a)

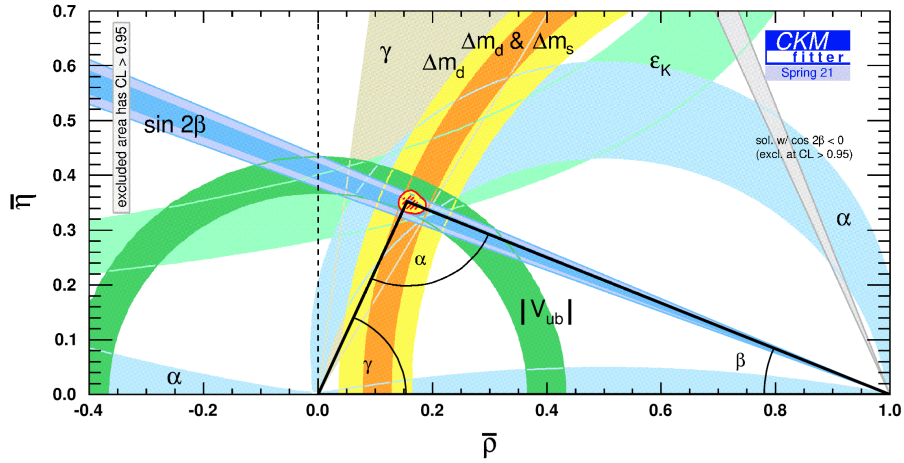

(b)

Figure 2.2: The constraints from the CKM fitter group in 2004 are shown in Fig. (a) and the most recent result from 2021 is shown in Fig. (b) [31].

2.3 Quantum Chromodynamics

In this section we briefly discuss the framework of QCD, which describes the strong interaction. The non-abelian group $SU(3)_C$ serves as the gauge group for QCD. The group introduces the colour charge, where quarks and gluons can adopt three different colours and transforms as triplets under $SU(3)_C$. Because leptons do not have a colour charge, they are not affected by the strong interaction.

In QCD, the local gauge transformation of the fields is written as:

$$\psi(x) \to e^{i\theta^a t^a}\psi(x) \qquad \text{with } a = 1, .., 8\,. \tag{2.34}$$

The quantity θ^a describes arbitrary functions and t^a are the the $SU(3)$ generators.

The Lagrangian density of QCD is given as:

$$\mathcal{L}_{\mathrm{QCD}} = -\frac{1}{4} G_a^{\mu\nu} G^a_{\mu\nu} + \sum_{\psi} \bar{\psi} \left(i \not{D} - m_{\psi} \right) \psi \,, \tag{2.35}$$

where ψ denotes the quark fields. When we substitute the partial derivative with the covariant derivative, the Lagrangian $\mathcal{L}_{\mathrm{QCD}}$ becomes gauge invariant:

$$D_\mu = \partial_\mu - i g_s t^a A^a_\mu \,, \tag{2.36}$$

where g_s is the strong coupling constant and A^a_μ the gluon field. The commutation relation of the generators are given as:

$$[t^a, t^b] \equiv i f^{abc} t^c \,. \tag{2.37}$$

Note that, f^{abc} is the structure constant of $SU(3)$. The field strength of the gluon is defined as:

$$G_{\mu\nu} = G^a_{\mu\nu} t^a = \frac{i}{g_s} [D_\mu, D_\nu] \,. \tag{2.38}$$

By inserting Eq. (2.36) into the gluon field strength we obtain:

$$G^a_{\mu\nu} = \partial_\mu A^a_\nu - \partial_\nu A^a_\mu + g_s f^{abc} A^b_\mu A^c_\nu \,. \tag{2.39}$$

The non-abelian $SU(3)$ group differs significantly from the abelian $U(1)$ group. For starters, the structure constants f^{abc} are zero for abelian groups but non-zero for non-abelian groups. When we insert Eq. (2.39) into Eq. (2.35) we see that the gluon fields obtain third and fourth powers of the gauge fields, which translates to gauge field self-interaction, a phenomenon not found in QED. The behavior of the running coupling constant is another point in which QCD and QED differ significantly, see Figure 2.3. Contrary to what the name implies, a coupling constant is not a constant but rather depends on the energy scale μ. The coupling constant is determined by the renormalisation scale μ_R. At the one-loop approximation, the running of the strong coupling constant is given as [34]:

$$\alpha_s(\mu, \mu_R) = \frac{\alpha_s(\mu_R)}{1 + \frac{\alpha_s(\mu_R)}{12\pi} (11 N_c - 2 n_f) \log\left(\mu_R / \mu\right)} \,, \tag{2.40}$$

where $\alpha_s = g_s^2 / 4\pi$, the number of colours is denoted with N_c, while the number of active quark flavours with n_f. In contrast to QCD, the coupling constant of the abelian gauge group of QED increases with the energy until it diverges, which is known as the Landau pole. As a result, the coupling constant increases over short distances. The strong coupling constant decreases for $N_c = 3$ and $n_f < 6$ for short ranges and high energy scales , i.e. $\alpha_s(\mu \to \infty) \to 0$. This is known as *asymptotic freedom* [35]. However, QCD becomes non-perturbative for large distances and low energy scales $\alpha_s(\mu \to 0) \to \infty$ with quark confinement as a consequence. In other words, larger distance between quarks increases the energy stored in the gauge fields such that a new quark-antiquark pair can be created. The QCD scale Λ_{QCD} describes the energy scale on which the strong coupling constant diverges. This is called hadronisation

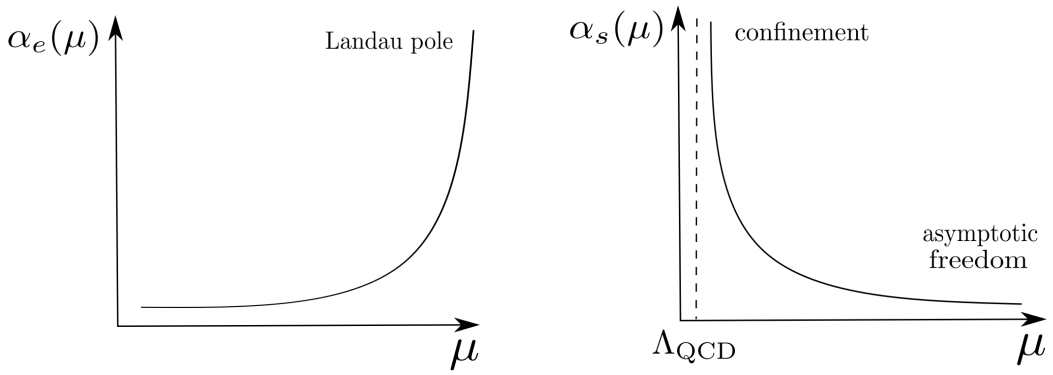

(a) (b)

Figure 2.3: The coupling constant in QED (a) and QCD (b) is depicted schematically.

and takes place on the timescale of $\mathcal{O}(10^{-24}$ s). The hadronisation of the quarks implies that they only exist in bound states called hadrons. Mesons (quark-antiquark pair) and baryons (three quarks) are two sub-types of colour neutral hadrons.
Due to the non-perturbative nature, it is quite difficult to compute hadronic quantities in QCD for low energy scales. The idea of effective field theories, such as Heavy Quark Effective Theory, is important to perform such calculation in order to overcome this challenge. More details about effective theories will be discussed in Chapter 3.

2.4 Limitations of the Standard Model

Despite being one of the most powerful and precise theories in physics, the Standard Model cannot explain all natural phenomena and has some inconsistencies with experimental measurements. In this section, we briefly discuss some notable shortcomings of the SM that motivate us to continue studying for a more fundamental theory of nature.

One of the fundamental forces in the universe is not explained within the framework of SM, namely gravity. The reason for this is that the gravitational force is several orders of magnitude weaker than the other fundamental interactions. The gravitational interaction becomes relevant at order of the Planck scale $\mathcal{O}(10^{19}$ GeV). At this scale, however, the SM becomes incompatible with another extremely successful theory, namely general relativity [36–39]. Furthermore, based on the cosmic microwave background, the rotational curves of the galaxies and the absorption lines of the hydrogen all indicate that there must be more matter than we visibly see [40, 41]. We observe that this non-baryonic matter does not or very rarely interact with particles of the SM. This unknown matter must be explained by physics beyond the SM and it is called dark matter [42]. Moreover, the vacuum energy of the SM might not explain the accelerated expansion of the universe. Therefore, the concept of dark energy has been introduced to fill the gap [43,44]. It has been shown, that only 5% is visible matter and energy described by the SM. The universe consist

of 27% of dark matter and 68% dark energy based on the latest measurements of the Planck telescope within the ΛCDM model [45].

The question: why the universe exist of matter without antimatter is also a unsolved mystery. This is puzzling, because after the big bang, we assume that matter and antimatter are distributed equally. The matter-antimatter asymmetry may be explained by later processes of CP violation, baryon number violation and interactions out of thermal equilibrium can caused an excess of matter [46]. However, only CP violations in weak decays have been experimentally observed, which is insufficient to explain the universe's matter-antimatter asymmetry [47–51].

In addition, neutrinos are assumed to be massless in the SM but it has been observed that neutrinos have a small mass. The oscillations in the neutrino flavour have been observed in solar neutrinos, atmospheric neutrinos, reactor neutrinos and neutrino beams by detecting a deficit in the predicted flavour and an enhancement of other neutrino flavors [52–59]. The mass eigenstates are linear combinations of the flavour eigenstates. This is realised through the Pontecorvo–Maki–Nakagawa–Sakata matrix, which is in analogy to the CKM matrix [60, 61]. As mentioned before, the neutrino mass is very small compared to the other particle content in the SM, which raises the question if they are generated by the Higgs mechanism.

Another mystery is why we only observe three generations of leptons and quarks, whose masses change by orders of magnitude across generations. The fact that the electroweak scale is significantly smaller than the Planck scale, which is the root of the hierarchy problem, is also not explained within the framework of the Standard Model.

There are also examples of observables with high precision predictions from theory and experimental measurements with small deviations. The most prominent example would be the measurement of the anomalous magnetic moment of muons, which is predicted by QED with high precision [62]. The experiment shows a 4.2σ deviation, which may indicate the presence of NP effects.

Chapter 3

Effective Theories

Problems with separated scales appear frequently in nature and we intuitively understand that it is most convenient to only work with degrees of freedom that are relevant at a specific scale. Otherwise, the problem quickly becomes intractable. Effective theories are distinguished by the absence of degrees of freedom that are irrelevant to the typical energy or distance scale of the problem in the Lagrangian. The calculation of heavy particle interaction at low energy scale is a common application for effective theories. When the energy scale is smaller than the heavy particle rest mass, it does not enter the final state and is therefore not a relevant degree of freedom for the effective Lagrangian.

In general, the Hamiltonian of the full theory is given as:

$$\langle f| \mathcal{H}_{\text{full}} |i\rangle \ , \tag{3.1}$$

where $|i\rangle$ denotes the initial state while $\langle f|$ the final state of the transition. The effective theory is build using a large energy scale Λ in comparison to the energies of the considered process. At a lower energy scale E, we want to define the effective theory so that $E \ll \Lambda$. By introducing the μ cut-off scale with $E \ll \mu < \Lambda$ we can separate the fields into high energy modes and low energy modes. High energy modes do not propagate over large distances; instead, they appear as virtual particles that can be removed from the theory, whereas low energy modes represent the relevant external states at the energy scale E. This is achieved by applying the path integral to these modes, which is known as integrating them out. For more details we refer to Refs. [63,64]. However, this results in a theory that is non-local on scales $\Delta x^\mu \sim 1/\Lambda$ due to the fluctuations of the high energy modes. Despite this, we can expand the result of the non-local theory in powers of $1/\Lambda$, yielding a theory of local operators $\mathcal{O}_k$ that contains just the effective theory low-energy modes.

The expansion is described by an effective Hamiltonian:

$$\langle f| \mathcal{H}_{\text{eff}} |i\rangle = \sum_k \frac{1}{\Lambda^{d_k-4}} C_k(\mu) \langle f| \mathcal{O}_k(\mu) |i\rangle \ . \tag{3.2}$$

The coefficient C_k is called Wilson coefficient and it describes the short-distance physics above Λ, which we integrated out. The long distance physics is encoded in the operators $\mathcal{O}_k$. The factor in front of the Wilson coefficient is determined by the operators mass dimension $[\mathcal{O}_k] = d_k$, such that the Wilson coefficients are dimensionless.

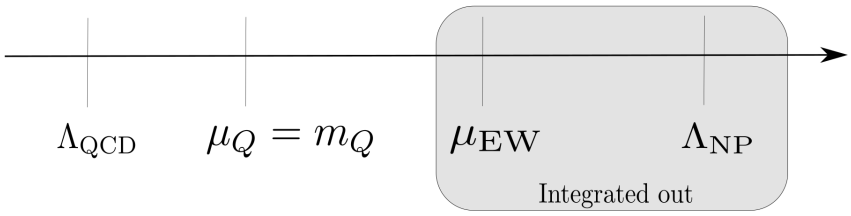

Figure 3.1: Illustration of the different energy scales in flavour physics.

The effective Hamiltonian in Eq. (3.2) does not depend on the energy scale μ. However, the values of the Wilson coefficients depend on μ. The dependence of the Wilson coefficients are encoded in the anomalous dimensions, which can be determined through the renormalization-group-equation. At low energy, each operator $\mathcal{O}_k$ contributes with:

$$\left(\frac{E}{\Lambda}\right)^{d_k-4} = \begin{cases} \gg 1 & \text{if} \quad d_k < 4\,, \\ \mathcal{O}(1) & \text{if} \quad d_k = 4\,, \\ \ll 1 & \text{if} \quad d_k > 4\,. \end{cases} \tag{3.3}$$

The dimension of the operator determines its relevance at low energies. We can systematically expand the series in Eq. (3.2) with E/Λ and truncate the series at a given operator dimension.

In this thesis we will study the weak decay of heavy hadrons. The two transitions that are interesting are $b \to s\ell^+\ell^-$ and $b \to c\ell\bar{\nu}$. The three relevant energy scales are shown in Figure 3.1. In our case the energy scale of the heavy quark will be $\mu = m_b$. The energy scale $\mu_{\rm EW}$ denotes the electroweak scale and corresponds to the mass of the $W^\pm$ boson. The size of the energy scales roughly:

$$\mathcal{O}(\Lambda_{\rm QCD}) \sim 0.2\,\text{GeV}\,, \quad \mathcal{O}(m_b) \sim 4\,\text{GeV}\,, \quad \mu_{\rm EW} \sim 80\,\text{GeV}\,. \tag{3.4}$$

Furthermore, a high energy scale $\Lambda_{\rm NP}$ can be taken into account to describe new physics phenomena. We assume that NP effects occur at far higher energy scales than the electroweak scale since particle colliders such as the LHC have not measured new degrees of freedom pushing NP to 1 TeV or higher.

Based on the energy hierarchy in Figure 3.1, one can define the following effective theories:

- When $\mu_{\rm EW} < \mu < \Lambda_{\rm NP}$, the appropriate framework is the Standard Model Effective Field Theory (SMEFT) theory, which is built with the Standard Model fields as light degrees of freedom and takes into account operators that preserve the SM symmetries. For more details we refer to Refs. [65].

- The effective theory in the region $m_b < \mu < \mu_{\rm EW}$ is the Weak Effective Theory (WET). This EFT is used to describe the decays of heavy hadrons [66].

- For the region of $\Lambda_{\rm QCD} < \mu < m_b$ we use the Heavy Quark Effective Theory (HQET). This effective theory is applied to heavy quark field interactions. Within this framework, we expand in inverse powers of m_b the Hamiltonian of the full SM interaction. This EFT will be more discussed in detail in Section 3.2.

3.1 Weak Effective Theory

The Weak Effective Theory is an effective framework for describing heavy hadron that decay weakly at the scale $\mu = m_Q$. Because the top-quark, $W^{\pm}$, Z^0, and Higgs bosons are massive in comparison to the hadron mass, i.e. $m_{\text{Had}} \ll m_{W^{\pm},Z^0,H^0,t}$ the heavy degrees of freedom associated with them can be integrated out.

In this thesis the weak semileptonic decay $b \to c\ell\bar{\nu}$ plays a significant role. Therefore, this decay will be taken as an example to see how the Hamiltonian changes. Note that, we refer to Ref. [66] for more information on the effective Hamiltonian of the transition $b \to s\ell\ell$. In the full Standard Model, the interaction of the Hamiltonian of the weak decay $b \to c\ell\bar{\nu}$ is given as:

$$\begin{aligned}\mathcal{H}^{\text{int}}_{\text{full}}(b \to c\ell\bar{\nu}) = &-\left(\frac{g'}{\sqrt{2}}\right)^2 V_{cb}\left[\bar{u}(p_c)\gamma^{\mu}P_L u(p_b)\right]\left[\bar{u}(p_e)\gamma^{\nu}P_L v(p_\nu)\right] \\ &\times \frac{1}{q^2 - m_W^2}\left(g_{\mu\nu} - \frac{q_\mu q_\nu}{m_W^2}\right),\end{aligned} \tag{3.5}$$

where $q = (p_b - p_c)$ and $P_L = (1 - \gamma_5)/2$ is the left-handed projector. Note that, the mass of the bottom-quark is much smaller than the intermediate W boson. Moreover, the maximum momentum that the W boson propagator transferred $q^2_{\text{max}} = (m_b - m_c)^2$ is also small compared to m_W^2. Hence, the propagator $1/(q^2 - m_W^2)$ can be approximated by $-1/m_W^2$ and the term $q_\mu q_\nu / m_W^2$ can be neglected. The W boson propagator can be expressed in the effective theory as:

$$\frac{1}{q^2 - m_W^2}\left(g_{\mu\nu} - \frac{q_\mu q_\nu}{m_W^2}\right) \to -\frac{g_{\mu\nu}}{m_W^2}\,. \tag{3.6}$$

Our effective Hamiltonian exhibits a four-fermion interaction:

$$\mathcal{H}^{\text{int}}_{\text{eff}}(b \to c\ell\bar{\nu}) = \frac{4G_F V_{cb}}{\sqrt{2}}\left[\bar{u}(p_c)\gamma^{\mu}P_L u(p_b)\right]\left[\bar{u}(p_e)\gamma^{\nu}P_L v(p_\nu)\right]\,, \tag{3.7}$$

where G_F is the Fermi constant and is given as

$$\frac{G_F}{\sqrt{2}} = \frac{g'^2}{8m_W^2}\,. \tag{3.8}$$

Before the W boson and the associated theory of weak interactions were discovered, Enrico Fermi proposed the four-fermion coupling. Similarly, many physical theories begin as a proposed full theory and then evolve into an effective theory of a more comprehensive theory of nature. For more details on the framework of WET, see Ref. [66].

3.2 Heavy Quark Effective Theory

The HQET, which describes systems with a single heavy quark, is introduced in this chapter. We begin by discussing the derivation of the effective Lagrangian and introducing the HQET Feynman rules. In the next section, we discuss the Heavy Quark Symmetries (HQS) that are important features of HQET from a phenomenological point of view, since these HQS are constraining the non-perturbative matrix elements at low energy scale.

3.3 Construction of the effective Lagrangian

We can derive the Lagrangian of the effective theory in two different ways. In the first approach we identify and integrate out the heavy degrees of freedom from the functional integral [67], which follows directly the idea of EFT. The second approach is based on the reduction of the Dirac equation into the non-relativistic form [68] and then recursively constructing higher order terms of the Lagrangian. The latter approach, however, does not follow the typical steps of how to construct the EFT. Hence, in the following we discuss the first approach in detail more. Note that, the two approaches will yield different results, but they can be related by a field redefinition. Both approaches leads to the same results for physical quantities.

Following the machinery of Ref. [67], our starting point is the QCD Lagrangian:

$$\mathcal{L}_{\text{QCD}} = \bar{Q}\left(i\not{D} - m_Q\right)Q + \mathcal{L}_{\text{light}}\,. \tag{3.9}$$

Here, Q denotes the heavy quark field and D_μ is the QCD covariant derivative. The Lagrangian $\mathcal{L}_{\text{light}}$ describes light quarks and gluons. For now we consider a heavy meson which contains a heavy quark Q and a light quark q with momentum $p_H = m_H \cdot v$. The quantity m_H denotes the mass of the meson and v the velocity with $v^2 = 1$. The momentum of the heavy quark can be decomposed into:

$$p_Q^\mu = m_Q v^\mu + k^\mu\,, \tag{3.10}$$

where the residual momentum is denoted with k, which satisfies $|k| \sim \mathcal{O}(\Lambda_{\text{QCD}}) \ll m_Q$. Note that, the velocity v is a conserved quantity and not a dynamical degree of freedom anymore in the heavy quark limit [69]. We redefine the heavy quark field, where we extract the large part of the momentum into a phase:

$$Q(x) = e^{-im_Q v\cdot x}\left[h_v(x) + H_v(x)\right] \tag{3.11}$$

with

$$h_v(x) = e^{im_Q v\cdot x}P_+Q(x) \quad \text{and} \quad H_v(x) = e^{im_Q v\cdot x}P_-Q(x)\,. \tag{3.12}$$

The projectors in HQET are defined as:

$$P_\pm = \frac{1 \pm \not{v}}{2}\,. \tag{3.13}$$

The fields in Eq. (3.12) satisfy the following relations with the projectors:

$$P_+h_v(x) = h_v(x)\,, \quad P_+H_v(x) = H_v(x)\,, \quad P_-h_v(x) = P_+H_v(x) = 0\,. \tag{3.14}$$

We can now re-express the QCD Lagrangian Eq. (3.9) now as:

$$\mathcal{L}_{\text{QCD}} = \bar{h}_v i(v\cdot D)h_v - \bar{H}_v(iv\cdot D + 2m_Q)H_v + \bar{h}_v i\not{D}_\perp H_v + \bar{H}_v i\not{D}_\perp h_v\,, \tag{3.15}$$

where we drop the $\mathcal{L}_{\text{light}}$ from now on. The covariant derivative $D_\perp$ is defined through $D^\mu = D_\perp^\mu + (v\cdot D)v^\mu$. The field h_v is massless but the field H_v acquired a mass term of $2m_Q$. The other terms are describing the couplings between H_v

and h_v. In the context of EFT, the field H_v denotes the heavy degrees of freedom, while h_v denotes the light degrees of freedom. For the construction of the EFT we integrate out the heavy degrees of freedom. Therefore, we integrate over the field H_v in the functional integrals. The generating functional that can be related to the heavy field H_v can be expressed as:

$$Z[J,\bar{J}] = \int \mathcal{D}H_v \mathcal{D}\bar{H}_v \exp\left(-i\int \mathrm{d}^4x \left[\bar{H}_v A H_v - \bar{J}H_v - \bar{H}_v J\right]\right), \tag{3.16}$$

where the external sources are defined as $\bar{J} = \bar{h}_v i\not{D}_\perp$, $J = i\not{D}h_v$ and $A = i(v\cdot D) + 2m_Q$. The argument of the exponential function can be re-expressed by completing the square and shifting the fields $\bar{H}_v, H_v$:

$$\bar{H}_v A H_v + \bar{J}H_v + \bar{H}_v J = \left(\bar{H}_v - \bar{J}A^{-1}\right) A \left(H_v - A^{-1}J\right) - \bar{J}A^{-1}J\,. \tag{3.17}$$

As a next step, we can perform the Gaussian integration and identify the expression:

$$Z[J,\bar{J}] = \int \mathcal{D}H_v \mathcal{D}\bar{H}_v \exp\left(-i\int \mathrm{d}^4x \bar{H}_v A H_v\right) \exp\left(i\int \mathrm{d}^4x \bar{J}A^{-1}J\right) \tag{3.18}$$

$$= \frac{\pi^{n/2}}{\sqrt{i\,\mathrm{Det}A}} \exp\left(\int \mathrm{d}^4x \bar{J}A^{-1}J\right) \sim \exp\left(i\int \mathrm{d}^4x \mathcal{L}_{\mathrm{eff}}^{H_v}\right). \tag{3.19}$$

Note that, the determinant of Eq. (3.19) is a constant, i.e. it does not depend on the gluon fields and thus has no physical effects. Hence, the effective Lagrangian corresponding to the heavy field H_v is given as:

$$\mathcal{L}_{\mathrm{eff}}^{H_v} = \bar{J}A^{-1}J = \bar{h}_v i\not{D}_\perp \frac{1}{i(v\cdot D) + 2m_Q} i\not{D}_\perp h_v\,, \tag{3.20}$$

where denominator denotes that the Lagrangian is non-local. Moreover, we can obtain the same result with the replacement

$$H_v = \left(\frac{1}{i(v\cdot D) + 2m_Q}\right) i\not{D}h_v \tag{3.21}$$

by using the equations of motion from Eq. (3.15). The propagator in Eq. (3.20) takes the form of:

$$\frac{1}{i(v\cdot D) + 2m_Q} = \frac{1}{2m_Q}\sum_{n=0}^{\infty}\left(\frac{-i(v\cdot D)}{2m_Q}\right)^n, \tag{3.22}$$

where $v\cdot D \ll 2m_Q$. Based on Eq. (3.22) our effective Lagrangian can be written as:

$$\mathcal{L}_{1/m_Q} = \bar{h}_v i(v\cdot D)h_v - \frac{1}{2m_Q}\sum_{n=0}^{N}\bar{h}_v i\not{D}_\perp \left(\frac{-i(v\cdot D)}{2m_Q}\right)^n i\not{D}_\perp h_v\,, \tag{3.23}$$

where N is the truncation order. Finally, this is the expanded QCD Lagrangian up to order $\mathcal{O}(1/m_Q^{N+1})$, where the first term

$$\mathcal{L}_{\mathrm{HQET}} = \bar{h}_v i(v\cdot D)h_v \tag{3.24}$$

represents a static heavy quark's Lagrangian moving at four velocity v. This is known as the HQET Lagrangian. Note that, we have a flavour and spin symmetry that manifest in the first term. We will discuss these two symmetry in Section 3.5 in more detail.

3.4 Feynman Rules of HQET

Here, we briefly introduce the Feynman rules of the HQET. The propagator of a heavy quark is given as:

$$\frac{\not{p} + m_Q}{p^2 - m_Q^2} = \frac{m_Q \not{v} + \not{k} + m_Q}{2m_Q v \cdot k + k^2} \longrightarrow P_+ \frac{1}{v \cdot k}\,, \tag{3.25}$$

where $m_Q \gg k$. Hence, the HQET propagator is given as:

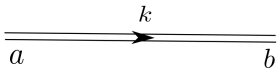

$$P_+ \frac{i}{v \cdot k + i\epsilon} \delta_{ab}\,. \tag{3.26}$$

The coefficient $a, b = 1, ..8$ are the colour indices in the adjoint representation of $SU(3)$. A vertex sandwiched between two propagators that are proportional to the projector P_+ can be replaced by the following way:

$$\gamma^\mu \to P_+ \gamma^\mu P_+ = v^\mu P_+ \to v^\mu\,. \tag{3.27}$$

Thus, the heavy-quark-gluon vertex can be expressed as:

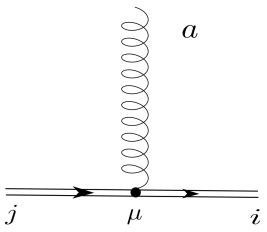

$$-ig_s v^\mu t^a_{ij}\,, \tag{3.28}$$

where $i, j = 1, 2, 3$ are colour indices in the fundamental representation of $SU(3)$. Note that, the Feynman rules concerning the interaction of light quarks with gluon and the self-interaction of gluons are remaining the same as in the full theory of QCD.

3.5 Heavy Quark Symmetries

The HQS that arise in the limit $m_Q \to \infty$ are discussed in this section [70–72]. These HQS are significant HQET features, particularly when seen in the perspective of phenomenology.

3.5.1 Flavour symmetry

The QCD Lagrangian has a flavour symmetry when the quarks become mass-degenerated. The isospin symmetry results from the up- and down-quark degeneracy. Assuming that all quarks are massless, the chiral symmetry of QCD emerges.

Because the colour charge of the quarks, rather than its mass, determines how quarks and gluons interact. In the infinite mass limit this still remains true. Hence, the flavour is no longer relevant when the heavy quark becomes a static source of colour. For instance, we consider the Lagrangian of the transition $b \to c$:

$$\mathcal{L}_{\text{HQET}}^{b\to c} = \bar{b}_v i(v\cdot D) b_v + \bar{c}_v i(v\cdot D) c_v = \left(\bar{b}_v, \bar{c}_v\right) \begin{pmatrix} i(v\cdot D) & 0 \\ 0 & i(v\cdot D) \end{pmatrix} \begin{pmatrix} b_v \\ c_v \end{pmatrix}, \quad (3.29)$$

where the velocities of the two heavy quarks are the same, i.e. $v = v'$. Eq. (3.29) has a $SU(2)$ symmetry and therefore for any unitary 2×2 matrix U we define the transformation

$$\begin{pmatrix} b'_v \\ c'_v \end{pmatrix} = U \begin{pmatrix} b_v \\ c_v \end{pmatrix} \quad (3.30)$$

in which the Lagrangian in Eq. (3.29) remains invariant.

3.5.2 Spin Symmetry

We can decompose the HQET Lagrangian into two spin components $h_v = h_v^{+s} + h_v^{-s}$ by introducing a spin vector s with $s \cdot v = 0$ and $s^2 = -1$. Hence, we can express it as:

$$h_v^{\pm s} = S_\pm h_v \quad \text{with} \quad S_\pm = \frac{1}{2}(1 \pm \gamma_5 \not{s}) \,. \quad (3.31)$$

The HQET Lagrangian can be expressed in terms of these projectors as:

$$\mathcal{L}_{\text{HQET}} = \bar{h}_v^{+s} i(v\cdot D) h_v^{+s} + \bar{h}_v^{-s} i(v\cdot D) h_v^{-s} \quad (3.32)$$

$$= \left(\bar{h}_v^{+s}, \bar{h}_v^{-s}\right) \begin{pmatrix} i(v\cdot D) & 0 \\ 0 & i(v\cdot D) \end{pmatrix} \begin{pmatrix} h_v^{+s} \\ h_v^{-s} \end{pmatrix} . \quad (3.33)$$

Once again, we have a $SU(2)$ symmetry and therefore for any 2×2 unitary matrix U we define the transformation

$$\begin{pmatrix} h_v^{+s} \\ h_v^{-s} \end{pmatrix}' = U \begin{pmatrix} h_v^{+s} \\ h_v^{-s} \end{pmatrix} . \quad (3.34)$$

In gauge theories, the interaction of the spin of a particle is given in the form of the dimension-five operator $\vec{\sigma}\cdot\vec{B}$ with coupling $g/(2m_Q)$, where $\vec{\sigma}$ are the Pauli matrices and $\vec{B}$ denotes the chromomagnetic field in QCD and magnetic field in QED. It is the QCD analogue of the Bohr magneton of the particle and consequently the spin of a particle decouples in QCD.

The HQET Lagrangian remains invariant under the transformation. Similar as in Section 3.5.1, this symmetry holds true only when the two heavy quarks have the same velocities.

3.5.3 Reparametrization Invariance

The last feature of HQET that will be discussed in this section is called reparametrization invariance (RPI). Recall that full QCD, which is Lorentz invariant, was our starting point. It is obvious that when we introduce the velocity vector v our theory is not Lorentz invariant anymore by fixing a direction that is arbitrary and could also be slightly changed. The result of an HQET constructed with v and one constructed with $v' = v + \delta v$ should be the same, see Refs. [73–76]. By varying the velocity:

$$v \to v + \delta v \quad \text{and} \quad (v + \delta v)^2 = 0 \quad \text{with} \quad v \cdot \delta v = 0 \tag{3.35}$$

we observe that the heavy-quark field and the covariant field are changing accordingly as:

$$h_v \to h_v + \frac{\delta \not{v}}{2} \left(1 + P_- \frac{i \not{D}}{2m_Q + iv \cdot D} \right) h_v \quad \text{and} \quad iD \to iD - m_Q \delta v \,. \tag{3.36}$$

Note that, the transformation in Eq. (3.36) is responsible for relating different orders in the $1/m_Q$ expansion. Therefore, taking the Lagrangian in Eq. (3.23) and inserting the definitions in Eq. (3.36) we obtain:

$$\delta_{\text{RPI}} \mathcal{L}_{1/m_Q} = \mathcal{O}(1/m_Q^{N+2}) \,, \tag{3.37}$$

where N is the truncation order. By considering the leading term of Eq. (3.23) we find

$$\delta_{\text{RPI}}\, \bar{h}_v i(v \cdot D) h_v = \bar{h}_v i(\delta v \cdot D) h_v \,. \tag{3.38}$$

The variation of the first subleading term cancels this term exactly, i.e.:

$$\delta_{\text{RPI}} \frac{1}{2m_Q} \bar{h}_v (i \not{D}^\perp)^2 h_v = -\bar{h}_v (i \delta v \cdot D) h_v \,. \tag{3.39}$$

Therefore, we have

$$\delta_{\text{RPI}} \left(\bar{h}_v i(v \cdot D) h_v + \frac{1}{2m_Q} \bar{h}_v (i \not{D}^\perp)^2 h_v \right) = \mathcal{O}(1/m_Q^2) \,. \tag{3.40}$$

The HQET Lagrangian is invariant under those shifts up to higher orders. This results in a link between parameters of different orders in $1/m_Q$. For more details on RPI, we refer to Refs. [73–78].

Chapter 4

Inclusive Semileptonic B Meson Decay

In this section we discuss the semileptonic $b \to c\ell\bar{\nu}$ decay. We can distinguish two types of decay processes: inclusive and exclusive decays. In the case of inclusive decay, we sum up all of the kinematically possible final states of hadrons labeled by X_c. The final state contains a single charm quantum number. In the case of exclusive decays, we consider the pseudo-scalar B meson decaying into either a pseudo-scalar D meson or the vector meson D^*. From an experimental point of view the inclusive channel has much higher statistics compared to the exclusive channel. In this thesis we will study the inclusive weak decays of hadrons that contain a b quark.

Our starting point is the matrix element for the inclusive process of $B \to X_c\ell\bar{\nu}$

$$\begin{aligned}\mathcal{M}(B \to X_c\ell\bar{\nu}) &= \langle X_c\ell\bar{\nu}|\,\mathcal{H}_{\text{eff}}\,|B\rangle \\ &= \frac{4G_F V_{cb}}{\sqrt{2}}\,\langle X_c\ell\bar{\nu}|\,J_{H,\mu}(0)\,J_L^{\mu}(0)\,|B\rangle\ .\end{aligned} \tag{4.1}$$

The interaction is local because we integrated out the W boson. All operators are taken at $x = 0$ unless we specify otherwise. The non-perturbative information about the hadron binding is buried in the meson matrix element, which we will look into further below. In the matrix element we also introduced the hadronic and leptonic current, which can be separated since these two do not interfere with each other. They read as

$$J_L^{\mu} = \bar{\ell}\gamma^{\mu}\,P_L\nu \quad \text{and} \quad J_H^{\mu} = \bar{c}\gamma^{\mu}\,P_L b\,. \tag{4.2}$$

For this process, the differential decay rate is given as:

$$\mathrm{d}\Gamma = \sum_{X_c}\sum_{\text{spins}}\left(\frac{\mathrm{d}^3p_\ell}{(2\pi)^3 2E_\ell}\right)\left(\frac{\mathrm{d}^3p_\nu}{(2\pi)^3 2E_\nu}\right)|\mathcal{M}(B \to X_c\ell\bar{\nu})|^2(2\pi)^4\delta^{(4)}(p_B - (p_\ell + p_\nu + p_{X_c})) \tag{4.3}$$

For more details about the differential decay rate we refer to Ref. [25]. Note that, the spins of the final states are not measured in the experiment. As a result, we must average the incoming spin states and sum the outgoing spin states. The initial particle only has one spin direction because it is a pseudo-scalar.

By decomposing the matrix element into a hadronic and leptonic part we obtain:

$$|\mathcal{M}(B \to X_c \ell \bar{\nu})|^2 = 8 G_F^2 |V_{cb}|^2 \langle B| J_{H,\nu}^\dagger |X_c\rangle \langle X_c| J_{H,\mu} |B\rangle \langle 0| J_L^{\nu\dagger} |\ell\bar{\nu}\rangle \langle \ell\bar{\nu}| J_L^\mu |0\rangle \ . \tag{4.4}$$

Therefore, the differential decay rate takes the form of:

$$\mathrm{d}\Gamma = 16\pi G_F^2 |V_{cb}|^2 \left(\frac{\mathrm{d}^3 p_\ell}{(2\pi)^3 2E_\ell}\right)\left(\frac{\mathrm{d}^3 p_\nu}{(2\pi)^3 2E_\nu}\right) W_{\mu\nu} L^{\mu\nu} \,, \tag{4.5}$$

where $W_{\mu\nu}$ denotes the hadronic part and $L^{\mu\nu}$ the leptonic part.

The leptonic tensor can be evaluate as:

$$\begin{aligned} L^{\mu\nu} &= \sum_{\text{spins}} \langle 0| J_L^{\nu\dagger} |\ell\bar{\nu}\rangle \langle \ell\bar{\nu}| J_L^\mu |0\rangle \\ &= \sum_{\text{spins}} [\bar{u}_\ell \gamma^\mu P_L v_{\bar{\nu}}] [\bar{v}_{\bar{\nu}} \gamma^\nu P_L u_\ell] \\ &= \mathrm{Tr}\left(\gamma^\mu P_L \not{p}_{\bar{\nu}} \gamma^\nu P_L \not{p}_\ell\right) \,, \end{aligned} \tag{4.6}$$

where u_ℓ and $\bar{u}_\ell$ are the spinors for incoming and outgoing particles. Furthermore, $v_{\bar{\nu}}$ and $\bar{v}_{\bar{\nu}}$ are the spinors for incoming and outgoing anti-particle. Evaluating the trace we obtain for the leptonic tensor:

$$L^{\mu\nu} = 2\left(p_\ell^\mu p_{\bar{\nu}}^\nu + p_\ell^\nu p_{\bar{\nu}}^\mu - g^{\mu\nu} p_\ell \cdot p_{\bar{\nu}} - i\epsilon^{\mu\nu\rho\sigma} p_{\ell,\rho} p_{\bar{\nu},\sigma}\right) \,. \tag{4.7}$$

We use the convention $\epsilon^{0123} = -\epsilon_{0123} = +1$ unless otherwise stated.
The hadronic tensor expresses how quarks bind in the B meson as follows:

$$W_{\mu\nu} = \frac{1}{2m_B} \sum_{X_c} \langle B| J_{H,\mu}^\dagger |X_c\rangle \langle X_c| J_{H,\nu} |B\rangle (2\pi)^3 \delta^{(4)}(p_B - q - p_{X_c}) \tag{4.8}$$

$$= -g_{\mu\nu} W_1 + v_\mu v_\nu W_2 - i\epsilon_{\mu\nu\alpha\beta} v^\alpha q^\beta W_3 + q_\mu q_\nu W_4 + (v_\mu q_\nu + v_\nu q_\mu) W_5 \,, \tag{4.9}$$

where $q^\mu = (p_\ell + p_{\bar{\nu}})^\mu$ is the momentum transfer to the leptons. In the last line we decomposed the hadronic tensor into scalar structure functions W_i. The matrix element in Eq. (4.9) will be expanded with the mass of the heavy quark, which is referred to as the Heavy Quark Expansion (HQE). Using the HQE these decays can be parametrized in perturbative Wilson coefficients and non-perturbative HQE elements. To accomplish this, we employ the optical theorem, which says that the production of intermediate states is connected to the imaginary part of the forward transition amplitude. By applying the optical theorem we place the propagator on-shell and use Cauchy theorem to obtain:

$$-\frac{1}{\pi} \mathrm{Im}\left(\frac{1}{\Delta_0 + i\epsilon}\right)^{n+1} = \frac{(-1)^n}{n!} \delta^{(n)}(\Delta_0) \,. \tag{4.10}$$

Thus, the exponent of the propagator shifts the derivative of the delta distribution. This is due to hadrons having a different mass than their constituent quarks. However, unless we sum to infinity, the higher order terms in the expansion remain

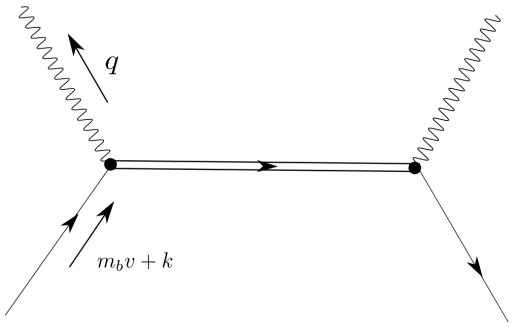

Figure 4.1: One loop forward scattering diagram, where the circle boxes represents the current $J_{H,\mu}$. The double line represents the charm quark propagating in the soft background field of the binding gluons, the solid line represents bottom-quark and the wavy line the colour-singlet external current mediating the weak decay.

local. While considering the decay with an intermediate charm-quark, we begin with a non-local forward matrix element of the form

$$\begin{aligned} T_{\mu\nu} &= -\frac{i}{2m_B}\int \mathrm{d}^4x e^{-iq\cdot x}\,\langle B|\,\mathcal{T}\{J^\dagger_{H,\mu}(x), J_{H,\nu}(0)\}\,|B\rangle \\ &= -g_{\mu\nu}T_1 + v_\mu v_\nu T_2 - i\epsilon_{\mu\nu\alpha\beta}v^\alpha q^\beta T_3 + q_\mu q_\nu T_4 + (v_\mu q_\nu + v_\nu q_\mu)T_5\,. \end{aligned} \tag{4.11}$$

Again, we can decompose the matrix element into scalar structure functions T_i. We visualize the process of Eq. (4.11) in Figure 4.1. The hadronic tensor can be expressed using the optical theorem as follows:

$$-\frac{1}{\pi}\mathrm{Im}\,T_{\mu\nu} = W_{\mu\nu} \quad \text{with} \quad -\frac{1}{\pi}\mathrm{Im}\,T_i = W_i\,. \tag{4.12}$$

Returning back to Eq. (4.11), where we insert the rephased but fully QCD b_v quark field

$$b_v(x) = e^{im_b v\cdot x} b(x)\,. \tag{4.13}$$

Hence, we express the time-ordered product as

$$T_{\mu\nu} = \frac{1}{2m_B}\,\langle B|\,\bar{b}_v\Gamma^\dagger_\nu S\Gamma_\mu b_v\,|B\rangle\ , \tag{4.14}$$

where Γ_μ denotes the gamma matrices and S the charm quark propagator with

$$S = \frac{1}{\not{p}_b - \not{q} - m_c}\,. \tag{4.15}$$

Note that, the b quark momentum consists of the four velocity vector and the residual momentum, i.e. $p_b^\mu = m_b v^\mu + k^\mu$. Following Refs. [79, 80], the charm propagator transforms into the background-field (BGF) propagator by substituting k with the covariant derivative:

$$S_{\mathrm{BGF}} = \frac{1}{\not{Q} + i\not{D} - m_c} \tag{4.16}$$

with $Q^\mu = m_b v^\mu - q^\mu$. An expansion can be obtained by writing this as a geometric series in k^μ/m_b

$$S_{\rm BGF} = \left[\sum_{n=0}^{\infty}(-1)^n\left[(\not{Q}-m_c)^{-1}(i\not{D})\right]^n\right](\not{Q}-m_c)^{-1}\,. \tag{4.17}$$

At some mass dimension m, the operator-product expansion can be cut off and the expansion takes the explicit form of

$$S_{\rm BGF} = \frac{1}{\not{Q}-m_c} - \frac{1}{\not{Q}-m_c}(i\not{D})\frac{1}{\not{Q}-m_c} + \frac{1}{\not{Q}-m_c}(i\not{D})\frac{1}{\not{Q}-m_c}(i\not{D})\frac{1}{\not{Q}-m_c} + \dots \tag{4.18}$$

We have an matrix elements in the form of:

$$\langle B|\,\mathcal{O}^{n+3}_{\mu_1\cdots\mu_n}\,|B\rangle = \langle B|\,\bar{b}_v(iD_{\mu_1})\dots(iD_{\mu_n})b_v\,|B\rangle\ . \tag{4.19}$$

These matrix elements must be evaluated and can be obtained directly from experimental data. Finally, the time-ordered product in Eq. (4.14) can be written as an OPE:

$$T_{\mu\nu} = \sum_{n=0}^{m} C^{\mu_1\cdots\mu_n}_{n,\mu\nu}(m_b, v_\mu)\,\langle B|\,\mathcal{O}^{n+3}_{\mu_1\cdots\mu_n}\,|B\rangle\ , \tag{4.20}$$

where the Wilson coefficient $C^{\mu_1\cdots\mu_n}_{n,\mu\nu}(m_b, v_\mu)$ has a perturbative expansion in the strong coupling constant α_s.

At order $\mathcal{O}(1/m_b^2)$, which is dimension 5 there are two matrix element:

$$2m_B\,\mu_\pi^2 = -\,\langle B|\,\bar{b}_v iD_\rho iD_\sigma b_v\,|B\rangle\,\Pi^{\rho\sigma}\,, \tag{4.21}$$

$$2m_B\,\mu_G^2 = \frac{1}{2}\,\langle B|\,\bar{b}_v[iD_\rho, iD_\sigma](-i\sigma_{\alpha\beta}b_v\,|B\rangle\,\Pi^{\alpha\rho}\Pi^{\beta\sigma}\,. \tag{4.22}$$

Here $\Pi^{\mu\nu} = v^\mu v^\nu - g^{\mu\nu}$ represents the projector onto the spatial components. These parameters can usually be given a physical interpretation. Because μ_π^2 is clearly related to the expectation value of the spatial momentum squared, it is known as the kinetic term. Employing $[iD_\mu, iD_\nu] = ig_sG_{\mu\nu}$ and

$$\gamma_\mu\gamma_5 \to P_+\gamma_\mu\gamma_5 P_+ = s_\mu\,, \tag{4.23}$$

$$\sigma_{\mu\nu} \to P_+\sigma\mu\nu P_+ = v^\alpha\epsilon_{\alpha\mu\nu\beta}s^\beta\,, \tag{4.24}$$

where s_μ is the spin vector. We can recognize the chromo-magnetic moment $s\cdot B$ as μ_G^2 to leading order in $1/m_b$. We define the spin-orbit term ρ_{LS}^3 and the Darwin term ρ_D^3 in dimension 6, which corresponds to $1/m_b^3$ as

$$2m_B\,\rho_D^3 = \frac{1}{2}\,\langle B|\,\bar{b}_v\,[iD_\rho,[iD_\sigma,iD_\lambda]]\,b_v\,|B\rangle\,\Pi^{\rho\lambda}v^\sigma\,, \tag{4.25}$$

$$2m_B\,\rho_{LS}^3 = \frac{1}{2}\,\langle B|\,\bar{b}_v\,\{iD_\rho,[iD_\sigma,iD_\lambda]\}\,(-i\sigma_{\mu\nu})b_v\,|B\rangle\,\Pi^{\alpha\rho}\Pi^{\beta\lambda}v^\sigma\,. \tag{4.26}$$

The spin-orbit term and Darwin term both relate to the curl $s\cdot\nabla\times E$ and divergence of the chromo-electric $\nabla\cdot E$ field, respectively.

One can observe that for higher order power-corrections the set of parameters grows factorially. For instance, dimension seven and eight each produce nine and eighteen parameters, respectively [79–81]. The factorial growth of the parameters in higher orders indicate that the HQE is an asymptotic series. Throughout the thesis we only consider power-corrections up to $\mathcal{O}(1/m_b^3)$.
Now by putting everything back to the time-ordered product in Eq. (4.20) and taking the imaginary part according to Eq. (4.10) with $\Delta_0 = (m_b v - q)^2 - m_c^2$ we obtain the hadronic tensor.

We have now covered all the crucial elements needed to describe the decay rate, therefore it is time to identify observables so that we can compare our theoretical findings to experimental measurements. By differentiating Eq. (4.3) we obtain the fully differential rate

$$\frac{\mathrm{d}\Gamma}{\mathrm{d}q^2 \mathrm{d}E_\ell \, \mathrm{d}E_\nu} = \frac{1}{2m_B} \left(\frac{\mathrm{d}^3 p_\ell}{(2\pi)^3 2E_\ell} \right) \left(\frac{\mathrm{d}^3 p_\nu}{(2\pi)^3 2E_\nu} \right) |\mathcal{M}(B \to X_c \ell \bar{\nu})|^2 \\ \times \delta(E_\ell - p_\ell^0) \delta(E_\nu - p_\nu^0) \delta(q^2 - (p_\ell + p_\nu)^2) \,. \tag{4.27}$$

The kinematical variables are the lepton energy E_ℓ, the neutrino energy E_ν and the dilepton invariant mass $q^2 = (p_\ell + p_\nu)^2$. The squared amplitude $|\mathcal{M}(B \to X_c \ell \bar{\nu})|^2$ denotes the contraction of the hadronic and leptonic tensor. After the phase-space integration over $\mathrm{d}^3 p_\ell$ and $\mathrm{d}^3 p_\nu$ we obtain for the inclusive decay $b \to c \ell \bar{\nu}$:

$$\frac{\mathrm{d}\Gamma}{\mathrm{d}q^2 \mathrm{d}E_\ell \mathrm{d}E_\nu} = \frac{G_F^2 |V_{cb}^2|}{2\pi^3} \left(W_1 q^2 + W_2 (2E_\ell E_\nu - \frac{q^2}{2}) + W_3 q^2 (E_\ell - E_\nu) \right) \theta(4E_\ell E_\nu - q^2) \,, \tag{4.28}$$

where we consider the lepton to be massless. Note that, the Lorentz scalars $W_{4,5}$ do not contribute in the case of $m_\ell \to 0$.

Observables that are relevant to this thesis can now be defined. Our observables include the following:

- We do not consider the differential decay width as an observable for the inclusive decay because there are corners in the phase-space where the OPE breaks down. Instead, we define moments using lepton energy cuts. The moments are given as:

$$\langle \mathcal{O}^n \rangle_{E_\ell > E_\ell^{\mathrm{cut}}} = \frac{\int_{E_\ell > E_\ell^{\mathrm{cut}}} \mathrm{d}\mathcal{O} \, \mathcal{O}^n \frac{\mathrm{d}\Gamma}{\mathrm{d}\mathcal{O}}}{\int_{E_\ell > E_\ell^{\mathrm{cut}}} \mathrm{d}\mathcal{O} \, \frac{\mathrm{d}\Gamma}{\mathrm{d}\mathcal{O}}}, \tag{4.29}$$

  where E_ℓ^{cut} is the lepton energy cut and n denotes the n-th order of moment. To lessen the correlation between the moments for higher order moments with $n > 1$, we consider central moments in the form of:

$$\langle (\mathcal{O} - \langle \mathcal{O} \rangle)^n \rangle = \sum_{i=0}^{n} \begin{pmatrix} n \\ i \end{pmatrix} \langle (\mathcal{O})^i \rangle \, (- \langle \mathcal{O} \rangle)^{n-i} \,. \tag{4.30}$$

  As for the observables $\mathcal{O}$ we investigate in this work the lepton energy moments $\langle E_\ell \rangle$, the hadronic invariant mass moments $\langle M_x \rangle$ with

$$M_x^2 \equiv (p_B - q)^2 = (m_B^2 + q^2 - 2m_B (v \cdot q)) \tag{4.31}$$

and the dilepton invariant mass moments $\langle q^2 \rangle$. For the q^2 moments we consider cuts of q^2_{cut} instead of lepton energy cuts. The advantage of utilizing q^2 moments is that they depend on a smaller number of HQE parameters because they are RPI observables, as demonstrated in Ref. [78]. Up to $\mathcal{O}(1/m_b^4)$, only eight parameters are required, whereas the traditional lepton energy and hadronic mass moments depend on the entire set of 13 elements.

- In addition to the standard moments, we investigate the forward-backward asymmetry observable, which was first introduced in Refs. [82]. The definition of the observable can be derived from the differential decay rate as:

$$A_{FB} = \frac{\displaystyle\int_{-1}^{0} \mathrm{d}z \frac{\mathrm{d}\Gamma}{\mathrm{d}z} - \int_{0}^{1} \mathrm{d}z \frac{\mathrm{d}\Gamma}{\mathrm{d}z}}{\displaystyle\int_{-1}^{1} \mathrm{d}z \frac{\mathrm{d}\Gamma}{\mathrm{d}z}}\,, \tag{4.32}$$

  where the variable z describes the angle of the charged lepton

$$z \equiv \cos\theta = \frac{v \cdot p_{\bar{\nu}_\ell} - v \cdot p_\ell}{\sqrt{(v \cdot q)^2 - q^2}}\,. \tag{4.33}$$

  In the rest frame of lepton anti-neutrino system ($\vec{q} = \vec{0}$), the charged lepton has the same flight direction as the B-meson.

- The branching ratio $\mathcal{B}(B \to X_c \ell \bar{\nu})$ is an additional observable that can be compared with experimental measurements. We can also construct the ratio of the total rates to test the Lepton Flavour Universality

$$R_{\ell_1/\ell_2} = \frac{\Gamma(B \to X_c \ell_1 \bar{\nu})}{\Gamma(B \to X_c \ell_2 \bar{\nu})} \quad \text{with} \quad \ell_{1,2} = \mu, e\,. \tag{4.34}$$

To conclude, we emphasize that the inclusive semileptonic $b \to c\ell\bar{\nu}$ are now the standard method for determining the CKM element $|V_{cb}|$. These calculations use the HQE and the moments of the decay spectra to directly extract the non-perturbative parameters $\mu_G^2, \mu_\pi^2, \rho_{LS}^3$, and ρ_D^3 from experimental data.

Chapter 5

QCD Sum Rule

Because of the soft-gluon exchanges between the hadron constituents, the hadronic matrix element cannot be calculated using QCD perturbation theory. We need non-perturbative approaches for the computation of hadronic matrix elements. Lattice simulations and QCD sum rules (QCDSRs) are currently the only QCD-based methods for computing hadronic matrix elements. The central idea of lattice QCD (LQCD) is to compute these integrals numerically while approximating the finite discretized Euclidean space-time with quantum field theory's path integral formulation, where correlators are substituted by integrals over all possible classical field configurations. Several advances in supercomputers and algorithms over the last few years have enabled numerous computations of hadronic matrix elements using LQCD. Note that, LQCD has the advantage of being systematically improveable, which means that the level of uncertainty can be arbitrarily reduced throughout time. However, the numerical procedures currently in use are still time and resource intensive. Furthermore, LQCD is not usually capable of providing results across the entire kinematical spectrum. Prominent examples are the form factors of $B \to K^{(*)}$ and $B \to D^{(*)}$ [83–88]. So far, we have only discussed local hadronic matrix elements; LQCD calculations of non-local matrix elements are still in the early stages of development.

This section provides an overview of the QCD sum rule method. For more insightful reviews and early development we refer to Refs. [89–95]. Sum rules are analytically determined relations between several hadronic parameters, thus this approach avoids the need for time consuming numerical evaluation. Furthermore, some sum rule analytical expressions are not affected by the transition quark flavours. For instance, the B-to-vector meson decays have the same sum rule such as $B \to K^*$ and $B \to \rho$. The input parameters stand as the only distinction between the two sum rules. As a result, using QCDSRs rather than LQCD makes obtaining theoretical predictions of various hadronic matrix elements relatively simple and quick. The primary drawback of QCDSRs is that their predictions have large uncertainties that cannot be lowered below a specific threshold. In general, sum rules are commonly dependent on an unphysical parameter known as the Borel parameter, which generates non-trivially reducible systematic uncertainty. The presumption of quark-hadron duality, which links the hadronic and partonic pictures, is another

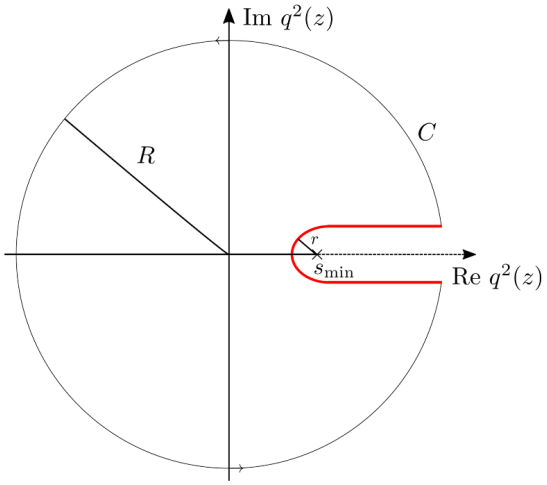

Figure 5.1: The contour C in the complex variable plane $q^2(z) = z$ around the branch cut $\mathrm{Re}\, q^2(z) > s_{\min}$.

source of uncertainty.

In this work, we focus on SVZ sum rules, which was first proposed by Shifman, Vainshtein, and Zakharov in the late 1970s [89]. The tools required, as well as how to construct sum rules, are discussed in greater detail below.

5.1 Dispersion Relation

Let us consider the vacuum-to-vacuum correlator:

$$\Pi^{\mu\nu}(q) = i \int \mathrm{d}^4x\, e^{iq\cdot x} \langle 0| \mathcal{T}\{J^\mu(x), J^{\nu,\dagger}(0)\} |0\rangle \ , \tag{5.1}$$

where $J^\mu = \bar{q}\gamma^\mu q$ is a quark current. We can decompose the tensor-valued function into a scalar-valued function

$$\Pi^{\mu\nu}(q) = (q^\mu q^\nu - q^2 g^{\mu\nu})\Pi(q^2)\,. \tag{5.2}$$

The entire real axis is the domain of the scalar function $\Pi(q^2)$. We can also expand the domain into the complex plane even though the physical world is not described by the imaginary values of q^2. However, we shall demonstrate that it is quite useful to study the scalar function $\Pi(q^2)$ in the complex plane. To analytically extend the real variable to the complex values $q^2 \to z$, the Cauchy theorem can be used to the function $\Pi(q^2)$. Hence, we have:

$$\Pi(q^2) = \frac{1}{2\pi i} \oint_C \mathrm{d}z \frac{\Pi(z)}{z - q^2}\,, \tag{5.3}$$

where q^2 is a point within the closed curve C depicted in Figure 5.1. In the $q^2 \gg 0$ region, also known as the hadronic picture, the scalar function $\Pi(q^2)$ has bound state poles and a branch cut denoted as $s_{\min}$ that begins at the lowest continuum state in the positive real axis. The singular points of a complex function are branch points

that differ from poles. They are related to the fact that the function's neighbourhood is multi-valued.

Assume $\Pi(q^2)$ decreases sufficiently fast at $|q^2| \to \infty$. Thus Eq. (5.3) can be simplified by taking the limits $R \to \infty$ and $r \to 0$ to:

$$\frac{1}{2\pi i}\oint_{|z|=R} \mathrm{d}z \frac{\Pi(z)}{z-q^2} \to 0 \quad \text{for} \quad R \to \infty \quad \text{and} \quad \frac{1}{2\pi i}\oint_{r} \mathrm{d}z \frac{\Pi(z)}{z-q^2} \to 0 \quad \text{for} \quad r \to 0\,. \tag{5.4}$$

Our expression in Eq. (5.3) simplifies to:

$$\Pi(q^2) = \frac{1}{2\pi i}\int_{s_{\min}}^{\infty} \mathrm{d}z \frac{\Pi(z+i\epsilon) - \Pi(z-i\epsilon)}{z-q^2}\,, \tag{5.5}$$

where ϵ is an infinitesimal positive number. We can reduce the numerator in the above equation to the imaginary part $\Pi(z+i\epsilon) - \Pi(z-i\epsilon) = 2i\,\mathrm{Im}\,\Pi(z)$ for $q^2 > s_{\min}$ using the Schwartz reflection principle. Finally, the hadronic dispersion relation is obtained by

$$\Pi(q^2) = \frac{1}{\pi}\int_{s_{\min}}^{\infty} \mathrm{d}z\, \frac{\mathrm{Im}\,\Pi(z)}{z-q^2-i\epsilon}\,. \tag{5.6}$$

Note that, the infinitesimal $-i\epsilon$ will not be explicitly displayed hereafter. It should be noted that the above dispersion relation does not always converge, because the assumption that $\Pi(q^2)$ decreases sufficiently fast at $|q^2| \to \infty$ does not hold in all cases. A common method to make sure Eq. (5.6) converges is to subtract from $\Pi(q^2)$ a few terms from its Taylor expansion at $q^2 = q_0^2$. Generally speaking, we can write the dispersion relation as the following:

$$\begin{aligned}\Pi(q^2) = {} & \frac{(q^2-q_0^2)^{(n+1)}}{\pi}\int_{s_{\min}}^{\infty} \mathrm{d}z \frac{\mathrm{Im}\Pi(z)}{(z-q_0^2)^{(n+1)}(z-q^2)} + \Pi(q_0^2) \\ & + (q^2-q_0^2)\frac{\mathrm{d}}{\mathrm{d}q^2}\Pi(q^2)\bigg|_{q^2=q_0^2} + \cdots + \frac{(q^2-q_0^2)^n}{n!}\left(\frac{\mathrm{d}}{\mathrm{d}q^2}\right)^n \Pi(q^2)\bigg|_{q^2=q_0^2}\,.\end{aligned} \tag{5.7}$$

Note that, the Taylor expansion subtraction terms are not always known. In Section 5.3, we will discuss a mathematical trick for overcoming this problem.

We have only covered the hadronic matrix element amplitude along the positive real axis up to this point. In the section that follows, we provide a brief explanation of how to compute the hadronic matrix element in the negative region $q^2 \ll 0$ that allows us to expand the correlator via OPE.

5.2 Operator-Product Expansion

The function $\Pi(q^2)$ is analytic for $q^2 \ll 0$, meaning there are no poles or singularities. In the local OPE in the region $m_q^2 - q^2 \gg \Lambda_{\mathrm{QCD}}^2$, where m_q is the quark mass, we can expand the amplitude as:

$$\Pi(q^2) = \sum_i C_i(q\check{\mathrm{s}}, \mu)\, \langle 0|\, \mathcal{O}_i(\mu)\, |0\rangle\,, \tag{5.8}$$

where the contribution that dominates the most comes from quarks at short distances. The mass dimension of the operator is denoted with the index i. The vacuum expectation values of the QCD fields, also known as QCD vacuum condensates, are represented by the matrix elements $\langle 0|\,\mathcal{O}_i\,|0\rangle$.

The short-distance contribution is encoded in the Wilson coefficients C_i, as we already explained in Chapter 3, while the long-distance contribution is stored in the operators $\mathcal{O}_i$. The identity matrix, which is given by mass dimension zero in Eq. (5.8), is the first matrix element:

$$\langle 0|\,\mathbb{1}\,|0\rangle = 1. \tag{5.9}$$

Here we list all the relevant operators up to dimension six:

$$\mathcal{O}_3 = \bar{q}q\,, \qquad \mathcal{O}_4 = \frac{\alpha_s}{\pi}G^a_{\mu\nu}G^{\mu\nu}_a\,, \qquad \mathcal{O}_5 = g_s\bar{q}\sigma\cdot Gq\,, \tag{5.10}$$

$$\mathcal{O}_{6,1} = g_s^3 f_{abc}G^a_{\mu\nu}G^{\nu\sigma,b}G^{\mu,c}_{\sigma}\,, \qquad \mathcal{O}_{6,2} = \alpha_s(\bar{q}\Gamma_\alpha q)(\bar{q}\Gamma^\alpha q)\,, \tag{5.11}$$

where the gluon field strength tensor is $G^a_{\mu\nu}$, f_{abc} are the $SU(3)$ structure constants, and Γ_α are combinations of the Dirac matrices. Note that, the QCD vacuum condensates are genuine non-perturbative quantities. Many estimates for the values of condensates are given in the literature, obtained from e.g. lattice QCD and sum rules [89, 91, 96–99].

5.3 Borel Transformation

In this section, we will go over the Borel transformation briefly. This transformation is frequently used in the context of sum rules because it reduces the uncertainty that stems form the quark-hadron duality approximation. The Borel transformation is defined as [89]:

$$\Pi(M^2) \equiv \mathcal{B}_{M^2}\Pi(q^2) = \lim_{\substack{-q^2,n\to\infty \\ -q^2/n=M^2}} \frac{(-q^2)^{n+1}}{n!}\left(\frac{\mathrm{d}}{\mathrm{d}q^2}\right)^n \Pi(q^2)\,, \tag{5.12}$$

where M^2 is the Borel parameter. The two most prominent Borel transformation examples are

$$\mathcal{B}_{M^2}\left(\frac{1}{z-q^2}\right)^k = \frac{1}{(k-1)!}\frac{e^{-z/M^2}}{M^{2(k-1)}} \quad \text{and} \quad \mathcal{B}_{M^2}(q^2)^k = 0 \tag{5.13}$$

with $k > 0$. For instance, using the Borel transformation on Eq. (5.7), the dispersion relation takes the form of:

$$\Pi(M^2) = \frac{1}{\pi}\int_{s_{\min}}^{\infty} \mathrm{d}z\,\mathrm{Im}\,\Pi(z)e^{-z/M^2}\,. \tag{5.14}$$

In the section that follows, we will see how much more practical the Borel transform of $\Pi(M^2)$ is for suppressing the contribution from continuum states.

5.4 Quark-Hadron Duality

In this section, we will explain briefly the concept of quark-hadron duality (QHD), which is based on the assumption that perturbative QCD amplitudes can be related to the amplitudes describing hadrons as fundamental particles [100]. More information is available in the classic review of Ref. [101].

We employ the QHD in this thesis to investigate the relationship between the hadronic and OPE imaginary parts, i.e.:

$$\int_{s_0}^{\infty} \mathrm{d}z \frac{\mathrm{Im}\,\Pi^{\mathrm{OPE}}(z)}{z-q^2} \simeq \int_{s_{\mathrm{min}}}^{\infty} \mathrm{d}z \frac{\mathrm{Im}\,\Pi^{\mathrm{had}}(z)}{z-q^2}\,, \tag{5.15}$$

where the relation is referred to as global quark-hadron duality. Typically, the OPE begins at a given threshold s_0. Note that, the effective threshold of the OPE s_0 and the continuum threshold s_{min} are generally not the same. Because we cannot compute $\Pi^{\mathrm{OPE}}(q^2)$ with infinite precision, the QHD accuracy is limited. However, if we could precisely calculate $\Pi^{\mathrm{OPE}}(q^2)$ throughout the entire q^2 complex plane, we would not need duality at all since

$$\Pi^{\mathrm{OPE}}(q^2) \equiv \Pi^{\mathrm{had}}(q^2)\,, \tag{5.16}$$

as discussed in Refs. [101]. In practice, one truncates $\Pi^{\mathrm{OPE}}(q^2)$ at a given finite order in the OPE and the strong coupling constant α_s, resulting in systematic uncertainties. But even if one could compute all terms in both series, it would be pointless because they are factorially divergent (see Refs. [101]). Another source of uncertainty is the duality violation, which occurs because $\Pi^{\mathrm{OPE}}(q^2)$ is unable to reproduce exactly the resonant structure of $\Pi^{\mathrm{had}}(q^2)$ even for large positive q^2 values [102]. These effects are expected to be small in the most of the applications, but one must nonetheless take them into consideration.
Hence, we deal with intrinsic uncertainty when using the quark-hadron duality, which is difficult to estimate.

Verifying that the tail of the OPE computation is not the main contribution to the same integral that spans the entire positive region is a check that should always be performed after calculating a sum rule. Therefore, to get reliable results from the sum rule, we ensure that

$$R_{\mathrm{cont}} = 1 - \frac{\int_{s_0}^{\infty} \mathrm{d}z\, \mathrm{Im}\,\Pi^{\mathrm{OPE}}(z) e^{-z/M^2}}{\int_{0}^{\infty} \mathrm{d}z\, \mathrm{Im}\,\Pi^{\mathrm{OPE}}(z) e^{-z/M^2}} \simeq 0.5\,. \tag{5.17}$$

This is also commonly used to determine the upper bound of the Borel parameter.

5.5 Example of a Sum Rule

After the discussion of all the necessary tools to calculate a sum rule, we demonstrate how to derive an SVZ sum rule following the example of Ref. [95]. In this example we derive the sum rule of the ρ meson decay constant f_ρ. The correlator $\Pi^{\mu\nu}_{(\rho)}(q)$ is

the same as in Eq. (5.1) with the current $J^{\mu}_{(\rho)} = 1/2(\bar{u}\gamma^{\mu}u - \bar{d}\gamma^{\mu}d)$. The expression of the OPE result is taken from Ref. [95]:

$$\Pi^{\rm OPE}_{(\rho)}(M^2) = M^2\Bigg[\frac{1}{4\pi^2}\left(1+\frac{\alpha_s(M)}{\pi}\right) + \frac{m_u+m_d}{M^4}\langle\bar{q}q\rangle + \frac{1}{12M^4}\langle\frac{\alpha_s}{\pi}G^a_{\mu\nu}G^{\mu\nu}_a\rangle - \frac{112\pi}{81}\frac{\alpha_s}{M^6}\langle\bar{q}q\rangle^2\Bigg], \tag{5.18}$$

where we performed the Borel transformation and includes the α_s-correction and QCD vacuum condensates up to mass dimension six. We proceed with the derivation of the imaginary of $\Pi^{\rm had}(q^2)$. In order to do that, we employ the unitarity relation:

$$(q^{\mu}q^{\nu} - q^2 g^{\mu\nu})\,{\rm Im}\,\Pi^{\rm had}_{(\rho)}(q^2) = \frac{1}{2}\sum\!\!\!\!\!\!\int_H {\rm d}\tau_H (2\pi)^4\delta^{(4)}(p_H - q)\,\langle 0|\,J^{\mu}(0)\,|H\rangle\,\langle H|\,J^{\dagger,\nu}(0)\,|0\rangle\,, \tag{5.19}$$

where τ_H is the spectral density function and $H(p_H)$ stands for the ρ meson as well as all other states with the same quantum numbers. The ρ meson-to-vacuum matrix element is defined as:

$$\langle 0|\,J^{\mu}_{(\rho)}\,|\rho(k,\epsilon)\rangle = \frac{i}{\sqrt{2}}\epsilon^{\mu}m_{\rho}f_{\rho}\,, \tag{5.20}$$

where ϵ^{μ} is the polarisation vector. Thus, the imaginary part of Eq. (5.19) is given as:

$$\frac{1}{\pi}{\rm Im}\,\Pi^{\rm had}_{(\rho)}(q^2) = f_{\rho}^2\delta(q^2 - m_{\rho}^2) + \tau_H(q^2)\theta(q^2 - 4m_{\pi}^2)\,, \tag{5.21}$$

where the spectral function τ_H describes all higher and continuum states. Note that, the lowest continuum state starts at the threshold $4m_{\pi}^2$. We obtain the dispersive relation and perform the Borel transformation by inserting the imaginary part into Eq. (5.14). As a result, we have:

$$\frac{1}{\pi}\int_{4m_{\pi}^2}^{\infty}{\rm d}z\,e^{-z/M^2}{\rm Im}\,\Pi^{\rm had}_{(\rho)}(z) = e^{-m_{\rho}^2/M^2}f_{\rho}^2 + \int_{4m_{\pi}^2}^{\infty}{\rm d}z\,e^{-z/M^2}\,\tau_H\,. \tag{5.22}$$

We can now match the OPE result in Eq. (5.18) with the hadronic dispersion relation. Thus, we obtain:

$$e^{-m_{\rho}^2/M^2}f_{\rho}^2 + \int_{4m_{\pi}^2}^{\infty}{\rm d}z\,e^{-z/M^2}\,\tau_H = \int_0^{\infty}{\rm d}z\,e^{-z/M^2}\Bigg[\frac{1}{4\pi^2}\left(1+\frac{\alpha_s(M)}{\pi}\right) + \frac{m_u+m_d}{M^4}\langle\bar{q}q\rangle + \frac{1}{12M^4}\langle\frac{\alpha_s}{\pi}G^a_{\mu\nu}G^{\mu\nu}_a\rangle - \frac{112\pi}{81}\frac{\alpha_s}{M^6}\langle\bar{q}q\rangle^2\Bigg]. \tag{5.23}$$

We are finally now at the stage of determining the sum rule of the decay constant, which is:

$$f_{\rho}^2 = \int_{s_0^{\rho}}^{\infty}{\rm d}z\,e^{\frac{m_{\rho}^2 - z}{M^2}}\Bigg[\frac{1}{4\pi^2}\left(1+\frac{\alpha_s(M)}{\pi}\right) + \frac{m_u+m_d}{M^4}\langle\bar{q}q\rangle + \frac{1}{12M^4}\langle\frac{\alpha_s}{\pi}G^a_{\mu\nu}G^{\mu\nu}_a\rangle - \frac{112\pi}{81}\frac{\alpha_s}{M^6}\langle\bar{q}q\rangle^2\Bigg], \tag{5.24}$$

where s_0^ρ is the duality threshold of the ρ meson channel.

In conclusion, QCD sum rules are a perturbative method for computing hadronic matrix elements in the non-perturbative domain starting from a correlator. Via the dispersion relation we compute the imaginary part of the correlator, which is described in terms of intermediate bound states in addition to a continuum of multi-particle states in the region of $q^2 \gg 0$. Both of these quantum numbers should correspond to the correlator currents. By expanding it in the OPE, we calculate the imaginary part of the hadronic matrix element in the region of $q^2 \ll 0$. Consequently, we separate the short-distance contributions from the long-distance contributions. In the SVZ sum rules, the long-distance contributions are parametrized in terms of QCD vacuum condensates. We can relate both regions of the hadronic matrix element to each other by employing quark-hadron duality. The global quark-hadron duality is used specifically to suppress the continuum contributions. A further method used to suppress the continuum contribution and the tail of the OPE computation is the Borel transformation, which also reduces the impact of potential quark-hadron duality violations.

Chapter 6

Project I: Impact of background effects on the inclusive V_{cb} determination

Published as an article in:
T. Mannel, M. Rahimi, K. K. Vos, JHEP 09 (2021) 051 [2].

Contributions of the authors to the article.
M. Rahimi contributed to the draft and did the analytical derivation and numerical analysis of all expressions obtained in the article. Prof. Dr. Vos performed an independent numerical study and worked on the draft. Prof. Dr. Mannel proposed the project, supervised the calculations, discussed them and worked on the final draft.

Abstract: The determination of the CKM element V_{cb} from inclusive semileptonic $b \to c\ell\bar{\nu}$ decays has reached a high precision thanks to a combination of theoretical and experimental efforts. Aiming towards even higher precision, we discuss two processes that contaminate the inclusive V_{cb} determination; the $b \to u$ background and the contribution of the tauonic mode: $b \to c(\tau \to \mu\nu\bar{\nu})\bar{\nu}$. Both of these contributions are dealt with at the experimental side, using Monte-Carlo methods and momentum cuts. However, these contributions can be calculated with high precision within the Heavy-Quark Expansion. In this note, we calculate the theoretical predictions for these two processes. We compare our $b \to u$ results qualitatively with generator-level Monte-Carlo data used at Belle and Belle II. Finally, we suggest to change the strategy for the extraction of V_{cb} by comparing the data on $B \to X\ell$ directly with the theoretical expressions, to which our paper facilitates.

6.1 Introduction

The determination of V_{cb} from inclusive $b \to c\ell\nu$ decays relies on the heavy quark expansion (HQE) and is in a very mature state (see e.g. [80, 103–105]). The current inclusive determination of $V_{cb} = (42.21 \pm 0.78) \cdot 10^{-3}$ [106, 107] has an impressive 2% uncertainty. The analysis includes perturbative corrections up to α_s^2 terms [108–112] and power corrections up to $1/m_b^3$. Higher-order terms up to $1/m_b^5$ have been classified [79] and studied using a lowest-lying state approximation [113]. These higher-order terms are currently studied in more detail [114] using a new method to determine inclusive V_{cb} from q^2-moments [115] using reparametrization invariance [78]. Recently, also α_s^3 corrections [116] and α_s corrections to $1/m_b^3$ terms [105] were studied. In combination with the expected data from Belle II, we therefore foresee a very precise determination of V_{cb}.

The current tension between the value of V_{cb} obtained from the inclusive determination and the one obtained from the exclusive channels $B \to D\ell\bar{\nu}$ and $B \to D^*\ell\bar{\nu}$ indicates that there may still be systematic effects which need to be understood better (see e.g. [117–120]). While the exclusive determination requires the input of form factors which are taken from lattice simulations (and/or using QCD sum rules), the inclusive determination is assumed to be theoretically cleaner, as the required hadronic matrix elements can be obtained from data, at least up to the order $1/m_b^3$ and possibly even to $1/m_b^4$. Therefore, the inclusive V_{cb} determination may be pushed towards even higher precision. At the moment, the V_{cb} determination is believed to be dominated by the theoretical uncertainties associated to missing higher-order corrections (both in the perturbative scale α_s and $1/m_b^4$).

In this quest even tiny effects and backgrounds need to be carefully studied before a precision at the level of one percent (or even less) can be claimed. The current method for extracting V_{cb} relies on taking lepton energy and hadronic invariant mass moments of the $B \to X_c\ell\bar{\nu}$ decay where $\ell = \mu, e$. However, the data taken at the B factories are based on the inclusive $B \to X\ell$ rate, from which the $B \to X_c\ell\bar{\nu}$ is extracted using Monte-Carlo simulations. While the $B \to X_c\ell\bar{\nu}$ is certainly the dominant part, aiming towards a sub-percent precision requires a modified approach. Overall, we identify two processes that contaminate the $B \to X_c$ signal and that could be constrained using the HQE:

- **The contribution of $b \to u\ell\bar{\nu}$:** Although this contribution is suppressed by a factor $(V_{ub}/V_{cb})^2$ and thus is not expected to make a significant contribution, extreme precision will require to have a good control of it.
- **The contribution of $b \to c(\tau \to \ell\bar{\nu}\nu)\bar{\nu}$:** This contribution is suppressed only by the smaller phases space and by the branching fraction of $\tau \to \ell\nu\bar{\nu}$. It may be reduced by appropriate cuts, but still needs to be described with the corresponding precision.

In the current note, we address these two contributions. Within the HQE, total rates as well as various moments of kinematic distributions can be reliably calculated and compared to the data. This may also include QED corrections, since in $B \to X\ell$ the X may not only include neutrinos but also photons. Obviously the HQE result for

$B \to X\ell$ will depend not only on m_b, m_c and V_{cb} and the HQE parameters, but also on V_{ub} and m_τ. Using HQE calculations, we may check the quality of the extraction of $B \to X_c\ell\bar{\nu}$ from $B \to X\ell$ by comparing our HQE results with the Monte-Carlo simulations of the $b \to u\ell\bar{\nu}$. In this note we study this comparison. For the $b \to c(\tau \to \ell\nu\bar{\nu})\bar{\nu}$, this comparison is more cumbersome due to different experimental cuts and Monte-Carlo data is at the moment not available. For this five-body decay, we therefore only provide the theoretical predictions. To our knowledge, no theoretical study of these effects in inclusive decays has been performed.

For the upcoming Belle II analyses we suggest to change the strategy for the extraction of V_{cb} by comparing the data on $B \to X\ell$ directly to the corresponding theoretical expressions, circumventing the problem of constructing first the data for $B \to X_c\ell\bar{\nu}$ by Monte-Carlo procedures. The aim of this note is to facilitate this strategy by supplying the necessary theoretical expressions. In Section 6.2 we discuss the lepton energy, hadronic invariant mass and q^2-moments for the three-body decay $b \to u\ell\nu$. We compare our result with the Monte-Carlo results. Moreover, we discuss the aforementioned moments for the five-body decay $b \to c(\tau \to \ell\nu\bar{\nu})\bar{\nu}$ in Section 6.4. We compare our results with the moments of three-body $b \to c\ell\nu$ decay. Finally, we conclude in Section 6.5.

6.2 Background from the $\bar{B} \to X_u\ell\bar{\nu}_\ell$ decay

The e^+e^- B factories Belle (II) and BaBar have a very clean environment, such that a fully inclusive measurement of $B \to X\ell$ can be performed, which is the basis of the current inclusive V_{cb} determination. In the current analyses the contribution of the $b \to c\ell\bar{\nu}$ transition is extracted from $B \to X\ell$ using Monte Carlo simulations of the backgrounds. After the subtraction of the backgrounds the resulting data is compared to the theoretical predictions for $B \to X_c\ell\bar{\nu}$. This procedure induces uncertainties related to the Monte Carlo simulations. At the moment, these induced uncertainties may not be relevant as the V_{cb} extraction seems limited by theoretical uncertainties related to missing higher-orders (see e.g. [14, 107, 113]). As the extraction of V_{cb} is based on lepton and hadronic mass moments of different experiments, at different energy cuts, it is challenging and clearly beyond the scope of this theoretical paper to exactly estimate the effect of the MC simulations. The aim of our paper is two-fold. First, we point out that the fully inclusive $B \to X\ell$ can be predicted theoretically at the same level of precision as $B \to X_c\ell\bar{\nu}$, so the process of background subtraction can be avoided completely, or at least to a large extend. It is then of interest to compare this local HQE computation with the Monte Carlo data used by Belle and Belle II qualitatively, to see how far the used methods differ from the local HQE. In this way, we can access whether the currently used MC methods underestimate or overestimate the uncertainty related to the $B \to X_u$ contribution. To our knowledge this comparison was never made before.

To this end, we compute the inclusive rate for $B \to X\ell$ by adding the contributions

$$\mathrm{d}\Gamma(B \to X\ell) = \mathrm{d}\Gamma(B \to X_c\ell\bar{\nu}) + \mathrm{d}\Gamma(B \to X_u\ell\bar{\nu}) + \mathrm{d}\Gamma(B \to X_c(\tau \to \ell\bar{\nu}\nu)\bar{\nu}) \quad (6.1)$$

For fully inclusive observables such as (cut) moments each term on the right-hand side can be computed individually in terms of the standard HQE based on the local OPE.

In the following we will use the known results of the HQE for $\mathrm{d}\Gamma(B \to X_u \ell \bar{\nu})$ in the local OPE to compare to generator-level Monte Carlo results, which are used for the background subtraction. In the next section, we compute the five-body contribution $\mathrm{d}\Gamma(B \to X_c(\tau \to \ell \bar{\nu} \nu)\bar{\nu})$.

6.3 Set-up for inclusive decays

The semileptonic $b \to u \ell \bar{\nu}$ decay is described by

$$\mathcal{H}_W = \frac{G_F V_{ub}}{\sqrt{2}} J_L^\alpha J_{H,\alpha} + \text{ h.c.}, \tag{6.2}$$

where $J_L^\alpha = \bar{\ell}\gamma^\alpha(1-\gamma_5)\nu$ and $J_{H,\alpha} = \bar{u}\gamma_\alpha(1-\gamma_5)b$ are the leptonic and hadronic currents, respectively. Equivalent as for the $\bar{B} \to X_c \ell \bar{\nu}_\ell$, we obtain the triple differential decay rate:

$$\frac{\mathrm{d}\Gamma}{\mathrm{d}E_\ell \mathrm{d}q^2 \mathrm{d}E_\nu} = \frac{G_F^2 |V_{ub}|^2}{16\pi^3} L_{\mu\nu} W^{\mu\nu}, \tag{6.3}$$

where $E_{\ell(\nu)}$ is the lepton (neutrino) energy and q^2 is the dilepton invariant mass. Here $L_{\mu\nu}$ is the leptonic tensor and $W^{\mu\nu}$ is the hadronic tensor:

$$W^{\mu\nu} = \frac{1}{4} \sum_{X_u} \frac{1}{2m_B} (2\pi)^3 \left\langle \bar{B} \right| J_H^{\dagger\mu} \left| X_u \right\rangle \left\langle X_u \right| J_H^\nu \left| \bar{B} \right\rangle \delta^{(4)}(p_B - q - p_{X_u}) \,, \tag{6.4}$$

where p_{X_u} is the total partonic momentum. Decomposing (6.4) into Lorentz scalars gives

$$W^{\mu\nu} = -g^{\mu\nu} W_1 + v^\mu v^\nu W_2 - i\epsilon^{\mu\nu\rho\sigma} v_\rho q_\sigma W_3 + q^\mu q^\nu W_4 + (q^\mu v^\nu + v^\mu q^\nu) W_5. \tag{6.5}$$

leading to

$$\begin{aligned} \frac{\mathrm{d}\Gamma}{\mathrm{d}E_\ell \mathrm{d}q^2 \mathrm{d}E_\nu} = \frac{G_F^2 |V_{ub}|^2}{2\pi^3} \Bigg[& q^2 W_1 + (2E_\ell E_\nu - \frac{q^2}{2}) W_2 + q^2 (E_\ell - E_\nu) W_3 \\ & \frac{1}{2} m_\ell^2 \left(-2W_1 + W_2 - 2(E_\nu + E_\ell) W_3 + q^2 W_4 + 4E_\nu W_5 \right) - \frac{1}{2} m_\ell^4 W_4 \Bigg] \,, \end{aligned} \tag{6.6}$$

where we have omitted explicit θ-functions. When considering $\ell = e, \mu$, we set $m_\ell \to 0$, such that $W_{4,5}$ do not contribute. The $W_{1,2,3}$ are now obtained using the HQE.

The HQE has become an well-established tool in the study of inclusive B meson decays, allowing the expression of observables in a double expansion of α_s and $1/m_b$. It is set up by redefining the heavy-quark field by splitting the momentum p_Q of the heavy quark as $p_Q = m_Q v + k$, where v is a time-like vector and k the residual momentum. We can expand the residual momentum $k \sim \mathcal{O}(\Lambda_{\mathrm{QCD}})$ which yields

$m_b^{\rm kin}$	(4.546 ± 0.021) GeV
$\overline{m}_c(3\ {\rm GeV})$	(0.987 ± 0.013) GeV
$(\mu_\pi^2(\mu))_{\rm kin}$	(0.432 ± 0.068) GeV^2
$(\mu_G^2(\mu))_{\rm kin}$	(0.360 ± 0.060) GeV^2
$(\rho_D^3(\mu))_{\rm kin}$	(0.145 ± 0.061) GeV^3
$(\rho_{LS}^3(\mu))_{\rm kin}$	(-0.169 ± 0.097) GeV^3
$\alpha_s(m_b)$	0.223

Table 6.1: Numerical inputs taken from [113]. For the charm mass, we use the $\overline{\rm MS}$ scheme at 3 GeV. All other hadronic parameters are in the kinetic scheme at $\mu = 1$ GeV.

the standard operator-product expansion (OPE), which separates the short-distance physics from non-perturbative forward matrix elements which contain chains of covariant derivatives (see e.g. [103]). This introduces the hadronic matrix elements, μ_G^2 and μ_π^2 at $1/m_b^2$ and ρ_D^3 and $\rho_{\rm LS}^3$ at $1/m_b^3$ which are defined as

$$2m_B\mu_\pi^2 = -\langle B(v)|\,\bar{b}_v(iD)^2 b_v\,|B(v)\rangle\,, \tag{6.7}$$
$$2m_B\mu_G^2 = \langle B(v)|\,\bar{b}_v(iD_\mu)(iD_\nu)(-i\sigma^{\mu\nu})b_v\,|B(v)\rangle\,, \tag{6.8}$$
$$2m_B\rho_D^3 = \langle B(v)|\,\bar{b}_v(iD_\mu)(iv\cdot D)(iD^\mu)b_v\,|B(v)\rangle\,, \tag{6.9}$$
$$2m_B\rho_{LS}^3 = \langle B(v)|\,\bar{b}_v(iD_\mu)(iv\cdot D)(iD_\nu)(-i\sigma^{\mu\nu})b_v\,|B(v)\rangle\,. \tag{6.10}$$

(and a proliferation of matrix elements at higher orders [78, 79, 115]).

In the following, we use this local OPE to compute different moments of the $b \to u\ell\bar{\nu}$ spectrum. The procedure follows closely the standard derivation of the moments in $b \to c\ell\bar{\nu}$.

6.3.1 Definition of the moments

In order to obtain the $b \to u$ local contribution, we calculate different moments of the spectrum. We define normalized moments for a given observable denoted as $\mathcal{O}$:

$$\langle \mathcal{O}^n \rangle_{E_\ell > E_\ell^{\rm cut}} = \frac{\int_{E_\ell > E_\ell^{\rm cut}} {\rm d}\mathcal{O}\, \mathcal{O}^n \frac{{\rm d}\Gamma}{{\rm d}\mathcal{O}}}{\int_{E_\ell > E_\ell^{\rm cut}} {\rm d}\mathcal{O}\, \frac{{\rm d}\Gamma}{{\rm d}\mathcal{O}}}, \tag{6.11}$$

where $E_\ell^{\rm cut}$ is the energy cut of the lepton $\ell = (e,\, \mu)$ and n denotes the n-th order of moment. In addition, we define central moments:

$$\langle (\mathcal{O} - \langle \mathcal{O} \rangle)^n \rangle = \sum_{i=0}^{n} \left(\begin{array}{c} n \\ i \end{array} \right) \langle (\mathcal{O})^i \rangle \, (-\langle \mathcal{O} \rangle)^{n-i}\,, \qquad . \tag{6.12}$$

Specifically, we discuss the lepton energy moments $\langle E_\ell^n \rangle$, hadronic mass moments $\langle M_x^n \rangle$ and q^2 ($q^2 = (p_\ell + p_\nu)^2$) moments $\langle (q^2)^n \rangle$. The moments can be obtained using

Eq. (6.11) and the triple differential rate in Eq. (6.6). For the hadronic invariant mass, this requires its relation to the partonic quantities:

$$\langle M_x^2 \rangle = \langle p_{X_u}^2 \rangle + \bar{\Lambda} m_b \langle z \rangle + \bar{\Lambda}^2 \tag{6.13}$$

where $z \equiv 2(v \cdot p_{X_u})/m_b$ and

$$\bar{\Lambda} = m_B - m_b - \frac{\mu_\pi^2 - \mu_G^2}{2m_b} + \dots \ , \tag{6.14}$$

where the ellipses denote terms of higher orders in the $1/m_b$ expansion. In our HQE calculation, we include power-corrections up to order $\mathcal{O}(1/m_b^3)$ and radiative-corrections of order $\mathcal{O}(\alpha_s)$ to the partonic expression (see also [121]). We note that in the massless limit, the coefficient of ρ_D^3 has a dependence on $X_\mu \equiv 8 \ln m_b^2/\mu_{4q}^2$, where μ_{4q} is a renormalization scale. This scale dependence is compensated by the corresponding scale dependence of the matrix element of four-quark operators (weak annihilation contributions). This has been investigated in detail in [121] (see also [122,123]). For our numerical results, we use the expressions given in Appendix A of [121] assuming $16 < X_\mu < 40$ as was done in that reference. This variation is added as an uncertainty to our local HQE predictions. The numerical input parameters for the computation of the moments are taken from [113] and given in Table 6.1. In order to avoid renormalon ambiguities related to the pole mass, we work in the short-distance kinetic mass scheme (used in [113] to extract V_{cb}). We can relate the pole scheme to the kinetic scheme through a perturbative series, see Appendix A.

6.3.2 Comparison between theory and Monte-Carlo

In order to discuss the reliability of the background-subtraction procedure based on MC simulations we perform a direct comparison of the MC data with the theoretical prediction for the moments. To this end, we compare the moments extracted from MC simulations for the $b \to u$ transition only with the theoretically predicted moments, including again only the $b \to u$ transitions.

In Figs. 6.1, 6.2 and 6.3, we show respectively the E_ℓ, the M_x and q^2-moments. For these observables, we show the first moment ($\langle E_\ell \rangle$), the second moment ($\langle E_\ell^2 \rangle$) and the central moments: ($\langle (E_\ell - \langle E_\ell \rangle)^2 \rangle$) and ($\langle (E_\ell - \langle E_\ell \rangle)^3 \rangle$) (and equivalently for M_x and q^2 moments). For our OPE results we show leading-order (LO), next-to-leading-order (NLO) and NLO plus $1/m_b^2$ and $1/m_b^3$ power-corrections individually. The NLO $+1/m_b^2 + 1/m_b^3$ is our final results, for which the blue band indicates the uncertainty obtained by varying the input parameters in Table 6.1. To account for missing α_s corrections, we vary the scale of $\alpha_s(\mu)$ in the range $m_b/2 < \mu < 2m_b$. In addition, we take into account the correlation between the HQE parameters. As these are not given in [113], we take those obtained in [106] assuming the correlations are the same. We do not attribute an additional uncertainty for missing higher-order terms. These theoretical predictions are then compared to generator-level Monte-Carlo (MC) results used at Belle and Belle II. [1].

[1] We thank F. Bernlochner and L. Cao for providing us these generator-level MC results which were obtained using [124].

The crosses indicate the MC data points from several methods. These data points were obtained by L. Cao by producing the events at the generator level, which were then converted to moments at different cuts using the appropriate weight function. No uncertainties from the Monte Carlo simulations were included. The MC data point labelled BLNP uses the BLNP [125] description of the $B \to X_u \ell\nu$ spectrum where for the input parameters of the shape function $b = 3.95$ and $\Lambda = 0.72$ are used. Besides, we show 5 points labelled DFN which is based on [126]. This DFN model contains α_s corrections convoluted with the non-perturbative shape function in an ad-hoc exponential model [127]. The two parameters of this shape function in the Kagan-Neubert scheme are taken from a fit to $B \to X_c \ell\nu$ and $B \to X_s\gamma$ data [128] (see also [129]). In the figures, the points labelled DFN present the central values of the DFN, while $(\lambda_1^+, \lambda_2^+, \lambda_1^-, \lambda_2^-)$ are obtained by varying $\bar{\Lambda}$ and μ_π^2 within 1σ regions obtained in [128]. These variations can be used to estimate the error of the DFN model. This method, using the variation of the DFN models as an error, is used at Belle (see also the recent Belle analysis of the $\bar{B} \to X_u \ell\bar{\nu}$ [129]). For both the DFN and the BLNP models, resonant contributions are included using a "hybrid Monte Carlo". This method is based on the partonic calculation described above convoluted with a hadronization simulation based on PYTHIA, combined with $\bar{B} \to \pi\ell\bar{\nu}$ and $\bar{B} \to \rho\ell\bar{\nu}$ at small invariant partonic invariant masses (see [130, 131]).

Comparing our results with the MC-generated results, we observe:

- **for energy moments (Fig. 6.1):** MC-results are in good agreement with the HQE results. However, we observe a slight deviation from the central values for the second and third central moments. It is known, that central moments are sensitive to non-perturbative effects, and thus we conclude that this small deviation indicates that the MC does not properly incorporate the non-perturbative effects.

- **for hadronic mass moments (Fig. 6.2):** We observe that the MC results exhibit a large spread which is significantly larger than the uncertainty of the HQE prediction, in particular for small lepton energy cuts. Especially the higher central moments are sensitive to non-perturbative effects, which indicates that the models implemented in the MC do not properly describe the non-perturbative aspects.

- **for q^2 moments (Fig. 6.3):** The DFN models agrees well with the HQE result within the estimated uncertainty. However, the BLNP model agrees well with the HQE up to $\mathcal{O}(\alpha_s)$. Similarly to the central moments of the hadronic invariant mass, the central moments of q^2 are deviating from the OPE result. Especially for the third central moment the BNLP model and DFN models are spreading quite far away showing again that the non-perturbative effects are not properly included.

A few extra comments concerning the Monte Carlo models should be made. The DFN model mainly relies on perturbation theory (up to a smearing corresponding to a shape function, mimicking some non-perturbative effects), and thus it is not surprising that these models have difficulties to capture the non-perturbative contributions that are properly described in the HQE. However, the BLNP approach can

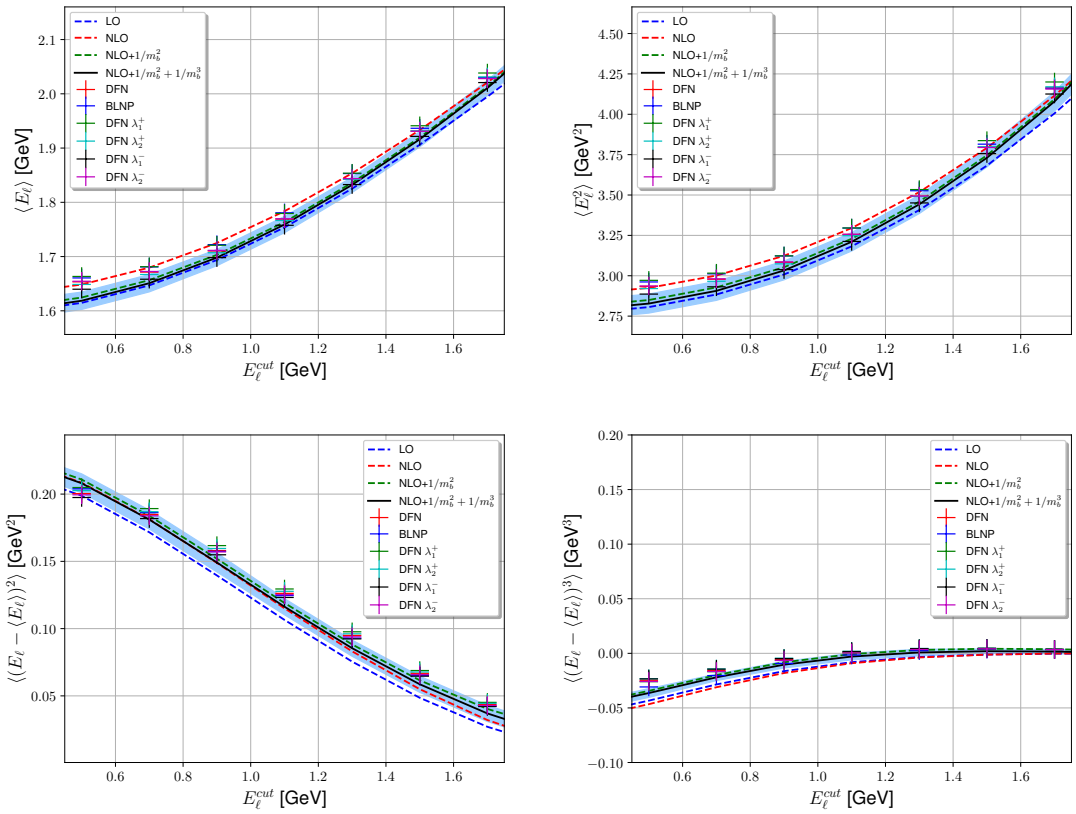

Figure 6.1: HQE results for lepton-energy moments with different energy cuts, showing leading order (LO), next-to-leading-order (NLO) and consecutively added to that $1/m_b^2$ and $1/m_b^3$ terms. In addition, the crosses indicate the MC-results in the BLNP and DFN model as described in the text.

in principle properly describe the results of the HQE, provided that its parameters are adjusted to the local HQE (which we use here). This requires including also the higher moments of the shape-function model as well including subleading shape functions, again with properly adjusted moments. The visible deviation of BLNP from the HQE predictions indicates that the version of BLNP employed in the MC should be updated. In summary, for the energy moment, the MC is in agreement with the HQE predictions, however, especially for the hadronic mass moments in Fig. 6.2, we see that the HQE uncertainty is much smaller than the spread in the MC models. Therefore, we expect our suggested procedure to be more precise for these moments. Studying the full impact of abandoning the MC when dealing with the $B \to X_u$ background requires a full experimental analysis, which should be performed by the experimental collaborations. Such an analysis is clearly beyond the scope of this theoretical paper.

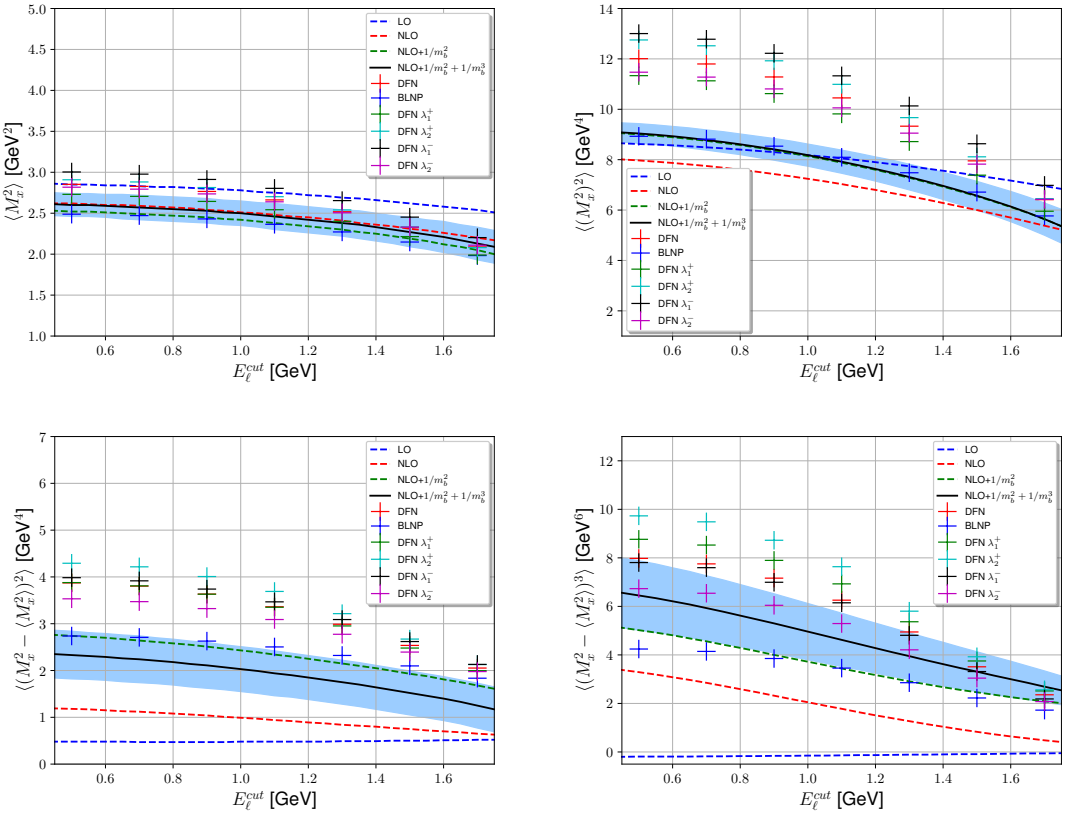

Figure 6.2: HQE results for hadronic-mass moments at different energy cuts compared with MC-results. See text and Fig. 6.1 for explanation.

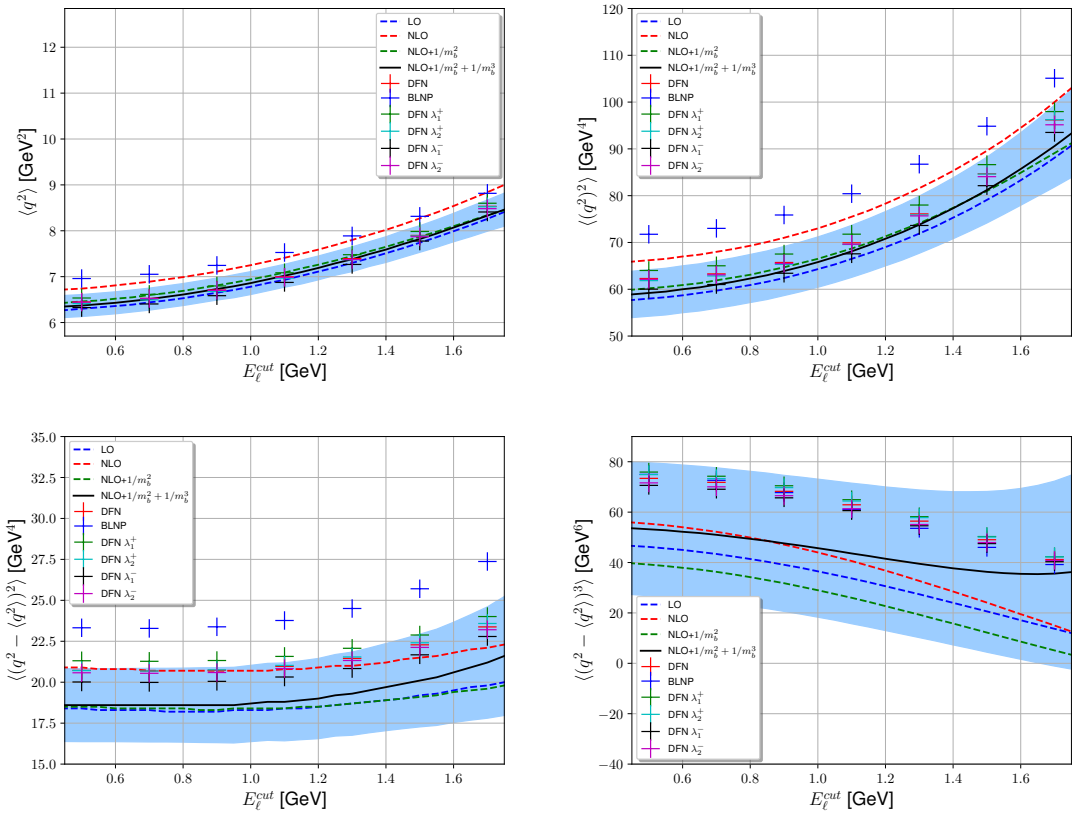

Figure 6.3: HQE results for q^2 moments with different energy cuts compared with MC-results. See text and Fig. 6.1 for explanation.

6.4 Background from the $\bar{B} \to X_c(\tau \to \ell\bar{\nu}_\ell\nu_\tau)\bar{\nu}_\tau$ decay

Next we consider the background contribution of $b \to c\tau(\to \ell\bar{\nu}_\ell\nu_\tau)\bar{\nu}_\tau$. Similar to the $b \to u$ background, this five-body contribution can be calculated exactly within the HQE. Its contribution is expected to be small, due to phase space suppression and the small branching fraction of $\tau \to \ell\bar{\nu}\nu$. Experimentally this five-body contribution can be further reduced by for example cutting on the lepton momentum in the B restframe and by constraining the invariant mass of the B-meson. Due to these extra cuts, it is not as straightforward to compare our exact HQE results with the experimentally used Monte-Carlo data as for the $b \to u$ contamination. In the following, we present our theoretical calculations of this five-body contribution, which may be used to improve the description of this background.

For our HQE calculation, we proceed by following [132] where the τ-contribution to exclusive $B \to D\ell\nu$ decay was studied (see also [133]). To our knowledge, the τ contribution to inclusive decays was never studied. Semitauonic B decays were studied in [134].

In order to obtain lepton energy, hadronic mass and q^2 moments, we construct the differential decay rate of the $B(p_B) \to X_c(p_{X_c})(\tau(q_{[\tau]}) \to \mu(q_{[\mu]})\nu_\mu(q_{[\bar{\nu}_\mu]})\nu_\tau(q_{[\nu_\tau]}))\bar{\nu}_\tau(q_{[\bar{\nu}_\tau]})$:

$$\frac{\mathrm{d}^8\Gamma}{\mathrm{d}q^2\,\mathrm{d}q^2_{[\nu_\tau\bar{\nu}_\mu]}\,\mathrm{d}p^2_{X_c}\,\mathrm{d}^2\Omega\,\mathrm{d}\Omega^*\,\mathrm{d}^2\Omega^{**}} = \\ -\frac{3G_F^2|V_{cb}|^2\sqrt{\lambda}(q^2-m_\tau^2)(m_\tau^2-q^2_{[\nu_\tau\bar{\nu}_\mu]})\mathcal{B}(\tau\to\mu\nu\nu)}{2^{17}\pi^5 m_\tau^8 m_b^3 q^2}W_{\mu\nu}L^{\mu\nu}\,, \tag{6.15}$$

with $q^2_{[\nu_\tau\bar{\nu}_\mu]} = (q_{[\bar{\nu}_\mu]}+q_{[\nu_\tau]})^2$, $\mathrm{d}^2\Omega = \mathrm{d}\cos\theta_{[\tau]}\mathrm{d}\phi$, $\mathrm{d}\Omega^* = \mathrm{d}\cos\theta^*_{[\mu]}$, $\mathrm{d}^2\Omega^{**} = \mathrm{d}\cos\theta^{**}_{[\bar{\nu}_\mu]}\mathrm{d}\phi^{**}$ and $\lambda \equiv \lambda(m_b^2, m_c^2, q^2)$ is the Källén-function. For the different angles we follow the conventions in [132]. The lepton tensor is now given by

$$L^{\mu\nu} = \sum_{\text{spins}} L^\mu L^{\nu *}, \tag{6.16}$$

with

$$L^\mu = \frac{1}{q^2_{[\tau]} - m_\tau^2 + im_\tau\Gamma_\tau}\left[\bar{u}(q_{[\mu]})\gamma_\alpha(1-\gamma_5)v(q_{[\bar{\nu}_\mu]})\right] \\ \times\left[\bar{u}(q_{[\nu_\tau]})\gamma^\alpha(1-\gamma_5)(\not{q}_{[\tau]}+m_\tau)\gamma^\mu(1-\gamma_5)v(q_{[\bar{\nu}_\tau]})\right]. \tag{6.17}$$

For the τ, we use the narrow-width approximation $\Gamma_\tau \ll m_\tau$:

$$\left|\frac{1}{(q^2_{[\tau]} - m_\tau^2 + im_\tau\Gamma_\tau)}\right|^2 \xrightarrow[\Gamma_\tau\ll m_\tau]{} \frac{\pi}{m_\tau\Gamma_\tau}\delta(q^2_{[\tau]}-m_\tau^2)\,, \tag{6.18}$$

where Γ_τ is the total width of the τ lepton. We want to obtain moments of the differential spectrum with cuts on the lepton energy as before. The lepton energy

of the muon E_ℓ can be related to $q^2_{[\nu_\tau \bar{\nu}_\mu]}$ in the following way:

$$E_\ell = \frac{1}{2m_b}\beta_{\nu\bar{\nu}}\Big(\sqrt{\lambda}\sqrt{1-2\beta_\tau}\sin\theta_{[\tau]}\sin\theta^*_{[\mu]}\cos\phi - \sqrt{\lambda}\cos\theta_{[\tau]} \\ \times\Big((1-\beta_\tau)\cos\theta^*_{[\mu]}+\beta_\tau\Big)+\Big(m_b^2-p^2_{X_c}+q^2\Big)\Big(\beta_\tau\cos\theta^*_{[\mu]}-\beta_\tau+1\Big)\Big) \tag{6.19}$$

with

$$\beta_{\nu\bar{\nu}} = \frac{m_\tau^2 - q^2_{[\nu_\tau\bar{\nu}_\mu]}}{2m_\tau^2} \qquad \text{and} \qquad \beta_\tau = \frac{q^2-m_\tau^2}{2q^2}\,. \tag{6.20}$$

The five-body phase-space is similar to the exclusive decay, but the contraction of the hadronic tensor $W_{\mu\nu}$ with the leptonic tensor $L_{\mu\nu}$ differs from the exclusive decay. We discuss the leptonic tensor and definitions of the four-vectors in more detail in our upcoming work [135]. The hadronic tensor $W_{\mu\nu}$ can be constructed following the procedure given in [79] (see Eq. (6.6), where now also $W_{4,5}$ are relevant). Finally, we obtain the eight-fold differential decay rate. We explicitly verified that our differential rate reduces to the total decay rate of $b \to c\tau\bar{\nu}$, i.e.:

$$\Gamma_{\text{tot}}(b\to c\tau(\to \ell\bar{\nu}\nu)\bar{\nu}) = \Gamma_{\text{tot}}(b\to c\tau\bar{\nu})\mathcal{B}(\tau\to\ell\bar{\nu}\nu)\,. \tag{6.21}$$

We note that the branching ratios of $\tau \to \mu\bar{\nu}\nu$ and $\tau \to e\bar{\nu}\nu$ are almost identical. Now we can compute the moments similarly to Sec. 6.2 by integrating the eight differential rate over the appropriate kinematical variables. We do not include radiative corrections for this process.

As we mentioned before, the decay $b \to c\tau(\to \ell\bar{\nu}_\ell\nu_\tau)\bar{\nu}_\tau$ is small compared to $b \to c\ell\bar{\nu}$. Hence, the total decay rate is given as:

$$\frac{\Gamma_{\text{tot}}(b\to c\tau(\to \ell\bar{\nu}_\ell\nu_\tau)\bar{\nu}_\tau)}{\Gamma_{\text{tot}}(b\to c\ell\bar{\nu})} \sim 4.0\% \tag{6.22}$$

In Fig. 6.4, we show for both the five and three-body decay, the total rate with a muon energy cut E_ℓ^{cut} normalized by the corresponding decay rate without cut, i.e. for the five-body decay:

$$\frac{\Gamma_{\text{tot}}(b\to c\tau(\to \ell\bar{\nu}_\ell\nu_\tau)\bar{\nu}_\tau)|_{E_\ell>E_\ell^{\text{cut}}}}{\Gamma_{\text{tot}}(b\to c\tau(\to \ell\bar{\nu}_\ell\nu_\tau)\bar{\nu}_\tau)}\,. \tag{6.23}$$

We find that the five-body decay decreases more rapidly when increasing the lepton energy cut, which is expected as such a lepton-energy cut further reduces the already suppressed phase space.

Finally, we obtain the lepton energy moments (Fig. 6.5), the hadronic mass moments (Fig. 6.6) and the q^2 moments (Fig. 6.7). We note that we have normalized these moments to the corresponding five-body $b \to c(\tau \to \ell\bar{\nu}\nu)\bar{\nu})$ rate. We show both the leading-order (LO, dotted line) and leading-order plus power-corrections of order $\mathcal{O}(1/m_b^2)$ (solid line). In addition, we also plot the lepton energy moments of the inclusive decay $b \to c\ell\nu$ for comparison (red). The band presents an estimate of the uncertainty obtained by varying each input parameter individually and adding

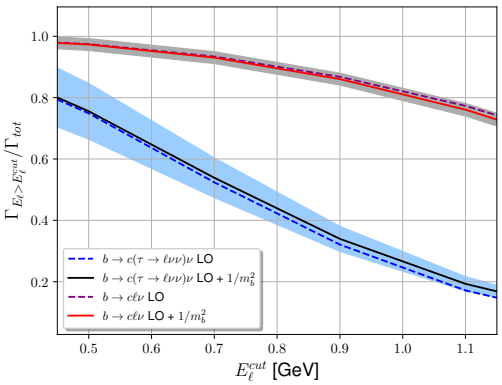

Figure 6.4: Five and three-body decay rates with lepton energy cut ($\Gamma_{E_\ell > E_\ell^{\rm cut}}$) normalized to the corresponding rate without energy cut ($\Gamma_{\rm tot}$). The dotted lines indicate the LO contribution and the solid line includes $1/m_b^2$ corrections for $b \to c(\tau \to \ell\bar{\nu}\nu)\bar{\nu}$ (blue) and $b \to c\ell\bar{\nu}$ (red) and their uncertainty.

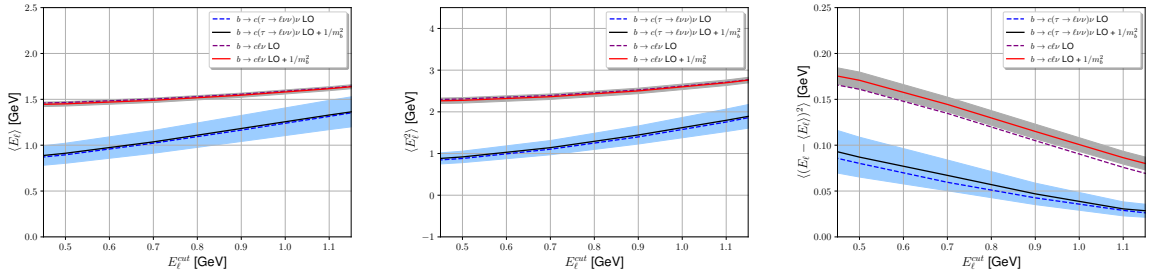

Figure 6.5: E_ℓ moments as a function of $E_\ell^{\rm cut}$ at LO (dotted) and including $1/m_b^2$ corrections (solid) for $b \to c(\tau \to \ell\bar{\nu}\nu)\bar{\nu}$ (blue) and $b \to c\ell\bar{\nu}$ (red) and their uncertainty.

them in quadrature. To compensate for missed higher-order radiative and power-corrections, we added an additional 30% uncertainty. We present these five-body moments in this way, such that they can be compared to Monte-Carlo simulations when this becomes available.

Note that for the five-body decay $q^2 \equiv (p_\tau + p_\nu)^2 = (p_B - p_{X_c})^2$ which obviously is equivalent to the q^2 defined in the three-body $b \to c$ decay. However, in Fig. 6.7 we plot the q^2-moments including a lepton-energy cut which makes the two curves representing the three and five-body decay distinguishable.

In Figs. 6.5 - 6.7, we observe again that the power-correction only give small corrections in the case of lepton energy moments. However, the power-correction are sizable in case of the hadronic invariant mass (Fig. 6.6).

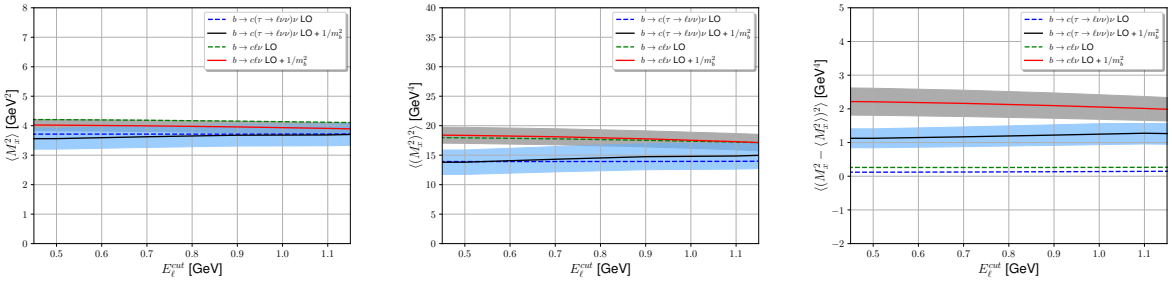

Figure 6.6: M_x^2 moments as a function of E_ℓ^{cut} at LO (dotted) and including $1/m_b^2$ corrections (solid) for $b \to c(\tau \to \ell\bar{\nu}\nu)\bar{\nu}$ (blue) and $b \to c\ell\bar{\nu}$ (red) and their uncertainty.

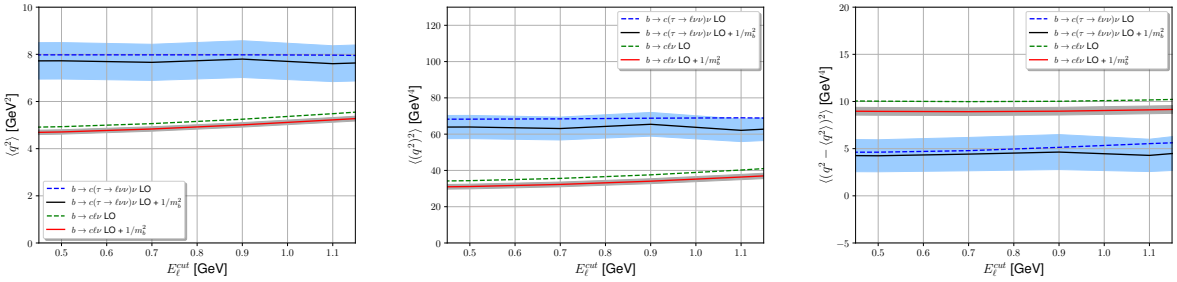

(a) (b) (c)

Figure 6.7: The q^2 moments as a function of E_ℓ^{cut} at LO (dotted) and including $1/m_b^2$ corrections (solid) for $b \to c(\tau \to \ell\bar{\nu}\nu)\bar{\nu}$ (blue) and $b \to c\ell\bar{\nu}$ (red) and their uncertainty.

6.5 Conclusion

The determination of inclusive V_{cb} uses the $\bar{B} \to X_c \ell \bar{\nu}$ rate, which is obtained from the experimentally measured $\bar{B} \to X \ell$ rate by subtracting (among others) the background signals $\bar{B} \to X_u \ell \bar{\nu}$ and $\bar{B} \to X_c(\tau \to \ell \bar{\nu} \nu)\bar{\nu}$. The goal of this note is to stress that these contributions can be exactly obtained within the local OPE/HQE and thus could be included in an analysis of $B \to X \ell$ without the need to subtract these contributions (which induced uncertainties).

To facilitate this new strategy, we computed different moments for $b \to u \ell \bar{\nu}$ at next-to-leading order including power-corrections up to $\mathcal{O}(1/m_b^3)$. We compared our result with generator-level Monte-Carlo data used in Belle and Belle II [124]. Especially, for hadronic invariant mass moments we note sizable difference between Monte-Carlo and HQE, which could be avoided when using the advocated strategy.

In addition, we computed for the first time the contributions of $b \to c(\tau \to \ell \bar{\nu} \nu)\bar{\nu}$, which contributes at the 4% level. In this case we do not have MC results to compare to, but we present our results in such a way that this comparison could be made in the future.

In preparation of the Belle II experimental analysis of inclusive V_{cb}, which will reach an unprecedented precision, we advocate using the full $B \to X \ell$ rate without subtracting the $b \to u$ and $b \to c(\tau \to \ell \bar{\nu} \nu)\bar{\nu}$ contributions. This strategy has the potential to reduce the experimental uncertainties on V_{cb} even further.

Acknowledgements

We thank Danny van Dyk, Marzia Bordone, Florian Bernlochner and Lu Cao for discussions. We specially thank Florian Bernlochner and Lu Cao for providing us the generator level Monte-Carlo data. This research was supported by the Deutsche Forschungsgemeinschaft (DFG, German Research Foundation) under grant 396021762 - TRR 257.

Appendix A Kinetic mass schemes

The relation between the pole mass scheme $m_b(\mu = 0)$ and the kinetic scheme $m_b^{\rm kin}(\mu)$ is [136, 137]

$$m_b(0) = m_b^{\rm pole} = m_b^{\rm kin}(\mu) + \left[\bar{\Lambda}(\mu)\right]_{\rm pert} + \frac{\left[\mu_\pi^2(\mu)\right]_{\rm pert}}{2m_b^{\rm kin}(\mu)} + \dots , \tag{6.24}$$

where μ is the cut-off energy employed in the kinetic mass scheme, which we set $\mu = 1$ GeV (see Table 6.1) and the ellipses represent higher-order terms in the $1/m_b$

expansion. The HQET parameters are now defined as:

$$\mu_\pi^2(0) = \left(\mu_\pi^2(\mu)\right)_{\text{kin}} - \left[\mu_\pi^2(\mu)\right]_{\text{pert}}, \tag{6.25}$$

$$\mu_G^2(0) = \left(\mu_G^2(\mu)\right)_{\text{kin}} - \left[\mu_G^2(\mu)\right]_{\text{pert}}, \tag{6.26}$$

$$\rho_{LS}^3(0) = \left(\rho_{LS}^3(\mu)\right)_{\text{kin}} - \left[\rho_{LS}^3(\mu)\right]_{\text{pert}}, \tag{6.27}$$

$$\rho_D^3(0) = \left(\rho_D^3(\mu)\right)_{\text{kin}} - \left[\rho_D^3(\mu)\right]_{\text{pert}}. \tag{6.28}$$

The quantity $\left[\bar{\Lambda}(\mu)\right]_{\text{pert}}$ describes the binding energy of the heavy meson and $[\mu_\pi^2(\mu)]_{\text{pert}}$ the residual kinetic energy. Their expression are given as:

$$\left[\bar{\Lambda}(\mu)\right]_{\text{pert}} = \frac{4}{3} C_F \frac{\alpha_s(m_b)}{\pi} \mu \left[1 + \frac{\alpha_s(m_b)\beta_0}{2\pi}\left(\log\left(\frac{m_b}{2\mu}\right)\right) + \frac{8}{3}\right], \tag{6.29}$$

$$\begin{aligned}\left[\mu_\pi^2(\mu)\right]_{\text{pert}} &= C_F \frac{\alpha_s(m_b)}{\pi} \mu^2 \left[1 + \frac{\alpha_s(m_b)\beta_0}{2\pi}\left(\log\left(\frac{m_b}{2\mu}\right) + \frac{13}{6}\right)\right. \\ &\quad \left. - \frac{\alpha_s(m_b)}{\pi} C_A \left(\frac{\pi^2}{6} - \frac{13}{12}\right)\right] + \mathcal{O}\left(\frac{\mu^3}{m_b^3}\right),\end{aligned} \tag{6.30}$$

$$\begin{aligned}\left[\rho_D^3(\mu)\right]_{\text{pert}} &= \frac{2}{3} C_F \frac{\alpha_s(m_b)}{\pi} \mu^3 \left[1 + \frac{\alpha_s(m_b)\beta_0}{2\pi}\left(\log\left(\frac{m_b}{2\mu}\right) + 2\right)\right. \\ &\quad \left. - \frac{\alpha_s(m_b)}{\pi} C_A \left(\frac{\pi^2}{6} - \frac{13}{12}\right)\right] + \mathcal{O}\left(\frac{\mu^4}{m_b^4}\right),\end{aligned} \tag{6.31}$$

$$\left[\mu_G^2(\mu)\right]_{\text{pert}} = \mathcal{O}\left(\frac{\mu^3}{m_b^3}\right), \tag{6.32}$$

$$\left[\rho_{LS}^3(\mu)\right]_{\text{pert}} = \mathcal{O}\left(\frac{\mu^4}{m_b^4}\right). \tag{6.33}$$

Here $C_A = 3$ and $\beta_0 = 11 - \frac{2}{3} n_f$ with $n_f = 3$, i.e. three active massless quarks.

Chapter 7

Project II: Standard Model predictions for Lepton Flavour Universality ratios of inclusive semileptonic B decays

Published as an article in:
M. Rahimi, K. K. Vos, JHEP 11 (2022) 007 [4].

Contributions of the authors to the article.
M. Rahimi contributed to the draft and did the analytical derivation and numerical analysis of all expressions obtained in the article. Prof. Dr. Vos performed an independent numerical study and worked on the draft.

Abstract: We present Standard Model predictions for lepton flavour universality ratios of inclusive $B \to X_{(c)}\ell\bar{\nu}_\ell$. For the $\ell = \mu, e$, these ratios are very close to unity as expected. For the τ mode, we update the SM prediction for the branching ratio including power-corrections in the heavy-quark expansion up to $1/m_b^3$. These inclusive ratios serve as an important cross-check of the exclusive $B \to D^{(*)}\ell\bar{\nu}_\ell$ modes, in which tensions exists between the predictions and measurements in those modes.

7.1 Introduction

The inclusive $B \to X_c \ell \bar{\nu}_\ell$ decays, with $\ell = \mu, e$, are by now standard candles in the determination of the CKM element $|V_{cb}|$. Employing the heavy quark expansion (HQE), allows the parametrization of these decays in perturbative Wilson coefficients and non-perturbative HQE elements. Thanks to a combined theoretical and experimental effort, these HQE parameters can be extracted from moments of the decay spectrum giving an impressive 2% uncertainty on the inclusive V_{cb} determinations [14, 15].

The experimental measurements of semileptonic $B \to X_c$ usually combine the muon and electron modes (and B^0 and B^+). Recently, the Belle collaboration also provided the first measurement of q^2 moments, separately for the electron and muon modes [138]. No deviations from lepton flavor universality were found. However, given the discrepancies in the rare $b \to s\ell\ell$ modes, it may be worth measuring the ratio

$$R_{\mu/e}(X_c) \equiv \frac{\Gamma(B \to X_c \mu \bar{\nu}_\mu)}{\Gamma(B \to X_c e \bar{\nu}_e)} \ . \tag{7.1}$$

In the Standard Model (SM), this ratio is expected to be close to one, but more elaborate predictions are not available to our knowledge. In this paper, we provide these predictions by taking into account the masses of the leptons, in light of upcoming measurements. These results are interesting due to the recent inconsistencies in the exclusive $B \to D^*$ forward-backward asymmetry measurements (see [139] for more details). Recently, also the final-state radiation effects in the forward-backward asymmetry were studied in detail [140].

In this work, we do not include structure depend nor ultrasoft QED effects as those are challenging to disentangle from the experimental detector efficiencies (for recent works on QED effects in exclusive semileptonic B decays see e.g. [141–144].).

While the inclusive light-lepton modes have been studied in depth, the situation is very different for the τ mode. Experimentally, only LEP results [145] and a unpublished Belle analysis [146] of the total rate exists, both having large uncertainties. In addition, the LEP measurement requires assumptions about hadronic effects in order to be interpreted. On the theoretical side, SM predictions for this mode exists using the HQE parameters as input. In this paper, we update these predictions to include HQE parameters up to $1/m_b^3$, which have a relatively large impact. These higher-order terms were first studied in [134], but this reference misses some terms in the ρ_D^3 coefficient. Here we correct these results. We point out that numerically, the difference between our results and [134] is small. In light of the tensions in ratios of the exclusive $B \to D^{(*)} \ell \bar{\nu}_\ell$ versus $B \to D^{(*)} \tau \bar{\nu}_\tau$ (see e.g. [147] for a recent review on semileptonic τ modes), we stress the importance of an independent cross-check in the inclusive channel. For this, the SM predictions derived in this short letter are vital. These predictions can be used in the search for new physics, especially in the tau sector where new measurements are expected soon.

7.2 Inclusive decay of $b \to c\ell\bar{\nu}_\ell$ with massive leptons

To calculate the inclusive $b \to c$ semileptonic rate, we employ the standard heavy-quark expansion (HQE). This allows us to perform an operator product expansion (OPE) for the triple differential rate in the lepton (neutrino) energy $E_{\ell(\nu)}$ and the dilepton invariant mass q^2 as

$$\frac{d\Gamma}{dE_\ell dq^2 dE_\nu} = \frac{G_F^2|V_{cb}|^2}{16\pi^3} L_{\mu\nu} W^{\mu\nu} \ . \tag{7.2}$$

Here $L_{\mu\nu}$ is the lepton tensor and $W^{\mu\nu}$ the hadronic tensor as defined in e.g. [2]. Expressing the $W^{\mu\nu}$ tensor in Lorentz scalars as usual then gives

$$\begin{aligned}\frac{\mathrm{d}\Gamma}{\mathrm{d}E_\ell \mathrm{d}q^2 \mathrm{d}E_\nu} = \frac{G_F^2|V_{cb}|^2}{2\pi^3} \Bigg[& q^2 W_1 + (2E_\ell E_\nu - \frac{q^2}{2}) W_2 + q^2(E_\ell - E_\nu) W_3 \\ & \frac{1}{2} m_\ell^2 \left(-2W_1 + W_2 - 2(E_\nu + E_\ell) W_3 + q^2 W_4 + 4E_\nu W_5 \right) - \frac{1}{2} m_\ell^4 W_4 \Bigg] \ ,\end{aligned} \tag{7.3}$$

where we have omitted explicit θ-functions (see [148]).

In general, for $B \to X_c \mu \bar{\nu}_\mu$ and $B \to X_c e \bar{\nu}_e$, lepton masses are neglected. However, for the much heavier decay involving the τ lepton: $B \to X_c \tau \bar{\nu}_\tau$, such an approximation cannot be made. We calculated the total inclusive rate including lepton masses. This calculation differs from the standard case, as now also the structure functions W_4 and W_5 in (7.3) contribute and because the phase space boundaries are affected. We refer to [134, 148] for details.

Considering terms up to $1/m_b^3$, we write the total rate as

$$\Gamma(B \to X_c \ell \bar{\nu}_\ell) = \Gamma_0 \Bigg[C_0^{(0)} + \frac{\alpha_s}{\pi} C_0^{(1)} + C_{\mu_\pi^2}^{\perp} \frac{(\mu_\pi^2)^\perp}{m_b^2} + C_{\mu_G^2}^{\perp} \frac{(\mu_G^2)^\perp}{m_b^2} + C_{\rho_D^3}^{\perp} \frac{(\rho_D^3)^\perp}{m_b^3} + C_{\rho_{LS}^3}^{\perp} \frac{(\rho_{LS}^3)^\perp}{m_b^3} \Bigg] , \tag{7.4}$$

where the coefficients depend on

$$\rho \equiv m_c^2/m_b^2 \ , \qquad \eta \equiv m_\ell^2/m_b^2 \ , \tag{7.5}$$

and

$$\Gamma_0 \equiv \frac{G_F^2|V_{cb}|^2 m_b^5}{192\pi^3} (1 + A_{\mathrm{ew}}), \tag{7.6}$$

which includes the electroweak correction $A_{\mathrm{ew}} = 0.014$ [149].

We define the nonperturbative parameters as (see e.g. [80])

$$2m_B\,(\mu_\pi^2)^\perp \equiv -\langle B|\bar{b}_v(iD_\rho)(iD_\sigma)b_v|B\rangle\Pi^{\rho\sigma}\ , \tag{7.7}$$

$$2m_B\,(\mu_G^2)^\perp \equiv \frac{1}{2}\langle B|\bar{b}_v\,[iD_\rho,iD_\lambda]\,(-i\sigma_{\alpha\beta})b_v|B\rangle\Pi^{\alpha\rho}\Pi^{\beta\lambda}, \tag{7.8}$$

$$2m_B\,(\rho_D^3)^\perp \equiv \frac{1}{2}\langle B|\bar{b}_v\,[iD_\rho,[iD_\sigma,iD_\lambda]]\,b_v|B\rangle\Pi^{\rho\lambda}v^\sigma, \tag{7.9}$$

$$2m_B\,(\rho_{LS}^3)^\perp \equiv \frac{1}{2}\langle B|\bar{b}_v\,\{iD_\rho,[iD_\sigma,iD_\lambda]\}\,(-i\sigma_{\alpha\beta})b_v|B\rangle\Pi^{\alpha\rho}\Pi^{\beta\lambda}v^\sigma\ , \tag{7.10}$$

where

$$\Pi_{\mu\nu} = g_{\mu\nu} - v_\mu v_\nu\ . \tag{7.11}$$

The above definitions differ from e.g. [15,78,115] where the full covariant derivative was used and not only the spatial component as above, linked via $iD_\mu = v_\mu ivD + D_\perp$. To differentiate, we therefore add a $\perp$ superscript to HQE parameters. The relation between the "perped" and full covariant derivative parameters is

$$(\mu_G^2)^\perp = \mu_G^2 + \frac{\rho_D^3+\rho_{LS}^3}{m_b}\ , \tag{7.12}$$

while $(\mu_\pi^2)^\perp = \mu_\pi^2, (\rho_{LS}^3)^\perp = \rho_{LS}^3$ and $(\rho_D^3)^\perp = \rho_D^3$ up to terms of order $1/m_b^3$ (see discussion in Appendix A of [115]).

We list all coefficients, except $C_0^{(1)}$ in Appendix A, for completeness. Setting $\eta \to 0$, reproduces the well-known rate [78, 79, 150]

The coefficients agree with [134] (and previous results in [151, 152] for $C_0, C_{\mu_\pi^2}$ and $C_{\mu_G^2}$) up to a difference in the $C_{\rho_D^3}$. The discrepancy with [134] arises due to the more involved integrations which now contain additional delta functions. For the total rate, where no cut on lepton energy is required, it is easiest to first perform the integration over the lepton energy E_ℓ analytically (as the structure functions W do not depend on E_ℓ.). In the limit $\rho = \eta$, our calculation can be checked and agrees with [153]. We have also contacted the authors of [134], who now agree with our results[1]. Finally, after finalizing this paper, also [155] appeared in which the α_s corrections to the ρ_D^3 coefficient for massive leptons was calculated. At LO, this paper reproduces our results.

We recalculated the perturbative corrections for the partonic rate $C_0^{(1)}$ which agree with [156, 157]. Our analysis does not include α_s^2 corrections, which are known [111] but only available for fixed m_b/m_c. To fully include such effects in a state-of-the-art manner, a new analysis is required. We briefly discuss these corrections in the following. We note that for $\eta = 0$, these corrections are even known up to α_s^3 [158].

[1] After finalizing our paper, we were made aware of [154] which agrees with the calculation in [134]. We assume that the difference with our result arises from the same reasons outlined before. We note that also the recent [155] agrees with our result.

m_b^{kin}	(4.573 ± 0.012) GeV
$\overline{m}_c(2\text{ GeV})$	(1.092 ± 0.008) GeV
$(\mu_\pi^2(\mu))_{\text{kin}}$	(0.477 ± 0.056) GeV^2
$(\mu_G^2(\mu))_{\text{kin}}$	(0.306 ± 0.050) GeV^2
$(\rho_D^3(\mu))_{\text{kin}}$	(0.185 ± 0.031) GeV^3
$(\rho_{LS}^3(\mu))_{\text{kin}}$	(-0.130 ± 0.092) GeV^3
V_{cb}	$(42.16 \pm 0.51) \cdot 10^{-3}$

Table 7.1: Numerical inputs taken from [14], where the HQE parameters are defined in the perp basis. For the charm mass, we use the $\overline{\text{MS}}$ scheme at 2 GeV. All other hadronic parameters are in the kinetic scheme at $\mu = 1$ GeV.

7.3 SM predictions for inclusive rates including masses

With the coefficients C_i for the total rate, we can now in principle predict the branching ratios for semileptonic $b \to c$ decays. However, the light lepton decays and their moments are used to determined the HQE parameters and V_{cb}. Therefore, such predictions are not very instructive for light mesons. For those, we therefore restrict ourselves to ratios of semileptonic modes. For the tau modes, we also discuss the total branching ratio.

As is customary, we work in the kinetic mass scheme, which can be related to the pole mass via a perturbative series [136, 137, 159]. For our numerical analysis, we use the input values listed in Table 7.1 obtained from [14] obtained from leptonic energy and hadronic invariant mass moments. These values can be compared with those obtained from a recent analysis using q^2 moments [15]. In the default analysis of [15], also $1/m_b^4$ terms were included, such that the HQE elements cannot directly be compared. However, Table 6 provides the HQE parameters up to $1/m_b^3$ in the full covariant derivative basis, which can be directly compared. We note that the values for m_b and m_c are similar, as these are used as constraints on the fit in [15]. However, as was discussed in [15], especially the value of $\rho_D^3 = 0.03 \pm 0.02$ GeV^3 differs from the value of [14] quoted in Table 7.1. The difference between the two should be clarified, possibly by performing a combined analysis of lepton energy, hadronic invariant mass and q^2 moments. However, for our current analysis, because the uncertainties on the HQE parameters from the q^2 analysis are somewhat larger than those from [14], we use the latter here as inputs. In the next section, we comment on how our numerical results would differ if the values of [15] were used instead.

	$R_{\tau/\mu}(X_c) \cdot 10^{-2}$	$R_{\tau/e}(X_c) \cdot 10^{-2}$	$R_{\mu/e}(X_c) \cdot 10^{-2}$
ξ_{LO}	23.557	23.429	99.458
ξ_{NLO}	5.446	5.451	0.144
$\xi_{\mu_G^2}$	-2.165	-2.161	-0.0315
$\xi_{\mu_\pi^2}$	0	0	0
$\xi_{\rho_{LS}^3}$	0.4735	0.4726	0.0068
$\xi_{\rho_D^3}$	-6.785	-6.765	-0.0709

Table 7.2: SM predictions for the inclusive LFU ratios. We list the different contributions independently of the value of the HQE parameters and separated according to (7.13).

7.3.1 Lepton Flavour Universality Ratios

We define the ratios $R_{\mu/e}$ as in (7.1) and define equivalently $R_{\tau/\mu}$ and $R_{\tau/e}$. In such ratios, V_{cb} drops out, but the HQE parameters do not completely, due to different mass effects. We split the contributions $R(X_c)$ according to

$$R(X_c) = \xi_{\text{LO}} + \xi_{\text{NLO}} \left(\frac{\alpha_s}{\pi}\right) + \xi_{\mu_G^2} (\mu_G^2)^\perp + \xi_{\mu_\pi^2} (\mu_\pi^2)^\perp + \xi_{\rho_{LS}^3} (\rho_{LS}^3)^\perp + \xi_{\rho_D^3} (\rho_D^3)^\perp \ . \tag{7.13}$$

Using then the input for m_b and m_c as in Table 7.1, we find the SM predictions as listed in Table 7.2. The coefficients ξ can then be used to obtain $R(X_c)$ for any set of HQE parameters. We note that μ_π^2 completely drops out in such ratios, because it can be absorbed into the partonic rate because of reparametrization invariance (see e.g. [78]). The effect of ρ_D^3 is relatively large even though this is a $1/m_b^3$ contribution. We do not include an additional uncertainty for missed higher-order terms of order $1/m_b^4$ and beyond.

Using the HQE parameters as listed in Table 7.1, we find for the light leptons

$$R_{\mu/e}(X_c)|_{\text{NLO}+1/m_b^2+1/m_b^3} = 0.9945 \pm 0.0001 \ . \tag{7.14}$$

The uncertainty is obtained by combining all uncertainties of the input parameters in quadrature. In addition, we vary the scale of $\alpha_s(\mu)$ from $m_b/2 < \mu < 2m_b$.

For the τ modes, we find

$$\begin{aligned} R_{\tau/\mu}(X_c)|_{\text{NLO}+1/m_b^2+1/m_b^3} &= 0.220 \pm 0.004 \\ R_{\tau/e}(X_c)|_{\text{NLO}+1/m_b^2+1/m_b^3} &= 0.218 \pm 0.004 \ . \end{aligned} \tag{7.15}$$

This is in agreement with previous determination in [160], which includes terms up to $1/m_b^2$ in the 1S-scheme:

$$R(X_c)_{\text{FLR}} = 0.223 \pm 0.004 \ . \tag{7.16}$$

In this case, the uncertainty is dominated by m_b and λ_1 (i.e. the HQE element in the infinite mass limit) and includes an additional uncertainty of half of the α_s^2 term. It however does not include an additional uncertainty due the missed $1/m_b^3$ terms.

Finally, also a calculation of only the partonic rates at $\mathcal{O}(\alpha_s^2)$ exists [111]

$$R(X_c)_{\rm BM} = 0.237 \pm 0.031 \ , \tag{7.17}$$

which is based on the on-shell scheme. It was found that α_s^2 effects in the $R_{\tau/\ell}(X_c)$ ratio are very small. While the ratio of leading order decay rates is a rapidly changing function of m_b, m_c and m_τ, radiative corrections to $\mathcal{B}(B \to X_c \tau \nu)$ and $\mathcal{B}(B \to X_c \ell \nu)$ are correlated, so they cancel out in the ratio that is largely independent of the quark masses. Here we do not include these α_s^2 effects as [111] only provides them at fixed m_c/m_b. However, we have verified that the α_s^2 corrections are only 2−3 % of the NLO order contribution. Therefore, our uncertainty estimate obtained by varying α_s accounts for these effects. We also note that our α_s corrections are half of those in [111], due to the switch to the kinetic scheme. In addition, there are α_s corrections to HQE parameters that are not written in (7.13) and not take into account. These corrections are known for massless leptons [**?**,161]. For massive leptons they became available very recently [155], i.e. after finalizing our paper. The corrections of the α_s corrections to the chromomagnetic μ_G^2 and ρ_D^3 coefficients were found to be a the sub-percent level, and thus well within our uncertainty. Given the large dependence on the value of ρ_D^3 discussed below, which first has to be clarified, we leave update these theoretical predictions to a future study.

Finally, we comment on the numerical differences for our predictions if we would have used the inputs [15]. We note that for the q^2 analysis, the extracted μ_π^2 has a large uncertainty [15]. However, as this contribution drops out in the ratios this does not affect our predictions. For the τ modes, we find that the predictions shift by around 1σ. Specifically, we find

$$\begin{aligned} R_{\tau/\mu}(X_c)|^{q^2}_{\rm NLO+1/m_b^2+1/m_b^3} &= 0.225 \pm 0.004 \\ R_{\tau/e}(X_c)|^{q^2}_{\rm NLO+1/m_b^2+1/m_b^3} &= 0.224 \pm 0.004 \ , \end{aligned} \tag{7.18}$$

where we have added a subscript indicating that these predictions use the HQE parameters from the q^2 moments in [15].

7.3.2 Ratios for semileptonic $B \to X$

Experimentally, in order to obtain the semileptonic $B \to X_c$, the $B \to X_u$ background has to be dealt with. On the other hand, as pointed out in [2], this V_{ub}^2/V_{cb}^2 suppressed contribution can also be calculated in the local OPE. Naively taking the $B \to X_c$ rate and setting $\rho \to 0$ works up to $1/m_b^2$, but at order $1/m_b^3$ additional four-quark operators (weak annihilation) have to be introduced that cure the divergence arising in the ρ_D^3 term (see e.g. [162] for references and discussions). For

charm, such effects were studied in [163] using semileptonic D meson data from CLEO [164]. For $B \to X_u$, this issue will be discussed specifically in an upcoming publication [165]. However, at the moment, we can make a reliable estimate for the $R(X)$ ratio by calculating the $B \to X_u$ effects by setting $\rho_D^3 \to 0$. We then have

$$\Gamma(B \to X\ell\bar{\nu}_\ell) = \Gamma(B \to X_c\ell\bar{\nu}_\ell) + \left(\frac{|V_{ub}|}{|V_{cb}|}\right)^2 \Gamma(B \to X_c\ell\bar{\nu}_\ell)|_{\rho\to 0,\rho_D^3\to 0} \,. \tag{7.19}$$

To derive ratios of the $B \to X$ semileptonic rates, we use the exclusive V_{ub} determination from [166]:

$$V_{ub}|_{\text{excl.}} = (3.77 \pm 0.15) \cdot 10^{-3} \,, \tag{7.20}$$

which is in agreement at the $1-2\sigma$ level with the recent inclusive determinations [167]. For V_{cb}, we take the recent inclusive determination in $V_{cb} = (42.16 \pm 0.51) \cdot 10^{-3}$ [14].

We then find

$$R_{\tau/\mu}(X) = 0.221 \pm 0.004 \,, \tag{7.21}$$

$$R_{\tau/e}(X) = 0.220 \pm 0.004 \,, \tag{7.22}$$

$$R_{\mu/e}(X) = 0.994 \pm 0.001 \,. \tag{7.23}$$

We do not quote the $R(X_u)$ as there we do not have the V_{ub}^2 suppression. As such, weak annihilation and ρ_D^3 effects may play a bigger role.

Finally, we note that experimentally, usually a lower cut on the lepton energy E_ℓ employed. Alternatively, also a q^2 cut can be imposed, as suggested first in [115], where q^2 moments of the spectrum are advertised. A q^2 cut is easier to implement for the α_s corrections, therefore we also quote ratios with such a cut. Here we take $q^2_{\text{cut}} = 3$ GeV^2 as a default cut. The full expression with an arbitrary q^2_{cut} can be provide by the authors. We find using the inputs in Table 7.1 of [14]

$$R_{\tau/\mu}(X)_{q^2_{\text{cut}}} = 0.352 \pm 0.004 \,, \tag{7.24}$$

$$R_{\tau/e}(X)_{q^2_{\text{cut}}} = 0.352 \pm 0.004 \,, \tag{7.25}$$

$$R_{\mu/e}(X)_{q^2_{\text{cut}}} = 0.999 \pm 0.001 \,. \tag{7.26}$$

We also explicitly provide the ratios using the masses and HQE parameters listed in Table 6 of [15] and $V_{cb} = (42.69 \pm 0.63) \cdot 10^{-3}$ [15]. We obtain

$$R_{\tau/\mu}(X)_{q^2_{\text{cut}}} = 0.359 \pm 0.005 \,, \tag{7.27}$$

$$R_{\tau/e}(X)_{q^2_{\text{cut}}} = 0.358 \pm 0.005 \,, \tag{7.28}$$

$$R_{\mu/e}(X)_{q^2_{\text{cut}}} = 0.998 \pm 0.002 \,, \tag{7.29}$$

which agrees with the determinations above at the $1-2\sigma$ level as expected, but with larger uncertainties. This is due to the larger relative uncertainty on ρ_D^3.

	$\mathcal{B}(B \to X_c \tau \bar{\nu}_\tau)$ [%]	$\mathcal{B}(B \to X \tau \bar{\nu}_\tau)$ [%]
$\xi_{\rm LO}$	3.042	3.095
$\xi_{\rm NLO}$	-3.064	-3.020
$\xi_{\mu_G^2}$	-0.557	-0.564
$\xi_{\mu_\pi^2}$	-0.0727	-0.074
$\xi_{\rho_{LS}^3}$	0.122	0.123
$\xi_{\rho_D^3}$	-1.408	-1.408

Table 7.3: Predictions for the branching ratio within the local OPE, using $V_{cb} = (42.16 \pm 0.51) \cdot 10^{-3}$ [14] and split according to (7.13). We quote the flavour-averaged rate. Predictions for the charged or neutral B decay can be obtained by multiplying with $\tau_{B^{+,0}}/\tau_B$.

7.3.3 Inclusive decay of $b \to c\tau\bar{\nu}_\tau$

Using (7.4), we update the SM predictions for the branching ratio of the τ-mode. Splitting the branching ratio as in (7.13) and taking $V_{cb} = (42.16 \pm 0.51) \cdot 10^{-3}$ [14], and m_b and m_c from Table 7.1, we find the contributions ξ given in Table 7.3. These results use the averaged decay rate $\tau_B = 1.579$ ps [145], which can be adjusted for the $B^{+,0}$ by multiplying with $\tau_{B^{+,0}}/\tau_B$. As the branching ratio depends V_{cb}^2, predictions using $V_{cb} = (41.69 \pm 0.63) \cdot 10^{-3}$ [15] can be easily obtained by a re-scaling.

Using the inputs for the HQE parameters in Table 7.1, we can calculating the branching ratio directly from the OPE:

$$\begin{aligned}
&\mathcal{B}(B \to X_c \tau \bar{\nu}_\tau)_{\rm OPE} = \\
&\quad \Big(2.34 \pm 0.07|_{m_b} \pm 0.03|_{m_c} \pm 0.02|_{\mu_G^2} + 0.01|_{\rho_{LS}^3} + 0.04|_{\rho_D^3} + 0.06|_{\alpha_s} + 0.05|_{V_{cb}}\Big)\,\% \\
&\quad = (2.34 \pm 0.13)\% \ , \qquad (7.30)
\end{aligned}$$

where we specify the different contributions to the uncertainty and in the last line we summed these in quadrature. Again, we do not include an additional uncertainty due to missed higher-order terms. For completeness we also quote the B^+ and B^0 rates separately

$$\begin{aligned}
\mathcal{B}(B^+ \to X_c^+ \tau \bar{\nu}_\tau) &= (2.43 \pm 0.13)\% \ . \\
\mathcal{B}(B^0 \to X_c^0 \tau \bar{\nu}_\tau) &= (2.25 \pm 0.13)\% \ . \qquad (7.31)
\end{aligned}$$

Our value agrees with [134], despite a missed ρ_D^3 contribution in that paper. Finally, following the procedure outlined in Sec. 7.3.2, we find the $B \to X$ rate as

$$\mathcal{B}(B \to X \tau \bar{\nu}_\tau) = (2.39 \pm 0.13)\,\% \, . \qquad (7.32)$$

These determinations are in agreement with the LEP measurement of the inclusive branching fraction of the admixture of bottom baryons [145]

$$\mathcal{B}(b\text{-admix} \to X\tau\bar{\nu}_\tau) = (2.41 \pm 0.23)\% \,, \tag{7.33}$$

which only to leading order in the HQE can be interpreted as the individual hadron rates.

In addition, there exists an unpublished Belle measurement of the $R_{\tau/(e,\mu)}(X)$ [146]:

$$R(X) \equiv \frac{\mathcal{B}(B \to X\tau\bar{\nu}_\tau)}{\mathcal{B}(B \to X\ell\bar{\nu}_\ell)} = 0.298 \pm 0.022 \,, \tag{7.34}$$

where $\ell = \mu, e$. Comparing this with our estimate in (7.21), we observe a slight tension. Alternatively, we may also estimate the relation between $R(X)$ and $R(X_c)$, by subtracting the theoretically calculated rate. We find

$$R(X) = \begin{cases} R_{\tau/\mu}(X_c) \left(1 + 1.012 \dfrac{|V_{ub}|^2}{|V_{cb}|^2}\right) & \text{for } \ell = \mu \ , \\ R_{\tau/e}(X_c) \left(1 + 1.014 \dfrac{|V_{ub}|^2}{|V_{cb}|^2}\right) & \text{for } \ell = e \ . \end{cases} \tag{7.35}$$

Therefore, we will interpret $R(X) = R(X_c)$. Comparing then (7.34) with our predictions in (7.15), we again observe a slight tension.

Besides calculating the rate directly from the OPE as in (7.30), we may also give predictions of the branching ratio by multiplying them with the measured flavor-averaged light-meson branching ratio. Following the detailed discussion in [147], we take

$$\mathcal{B}(B \to X_c\ell\bar{\nu}_\ell) = (10.48 \pm 0.13)\%, \tag{7.36}$$

which differs slightly from those quoted by [14] and [145]. Averaging our predictions for the muon and electron ratios in (7.15), and multiplying with (7.36), we find

$$\mathcal{B}(B \to X_c\tau\bar{\nu}_\tau)_{\text{Exp+OPE}} \equiv \mathcal{B}(B \to X_c\ell\bar{\nu}_\ell)\, R_{\tau/\ell}(X_c) = (2.30 \pm 0.05)\% \,, \tag{7.37}$$

which is in perfect agreement with, but has a much smaller uncertainty than our direct calculation in (7.30). Using the inputs in [15], and the ratios in (7.18), we find

$$\mathcal{B}(B \to X_c\tau\bar{\nu}_\tau)^{q^2}_{\text{Exp+OPE}} \equiv \mathcal{B}(B \to X_c\ell\bar{\nu}_\ell)\, R_{\tau/\ell}(X_c)|^{q^2} = (2.35 \pm 0.05)\% \,, \tag{7.38}$$

which agrees at 1σ level.

Similarly, we can convert the unpublished Belle measurement in (7.34). In [146], this is multiplied with the measured isospin-average branching fraction $\mathcal{B}(B \to X\ell\bar{\nu}_\ell) = (10.86 \pm 0.16)\%$ to obtain $\mathcal{B}(B \to X\tau\bar{\nu}_\tau) = (3.23 \pm 0.25)\%$. This is in

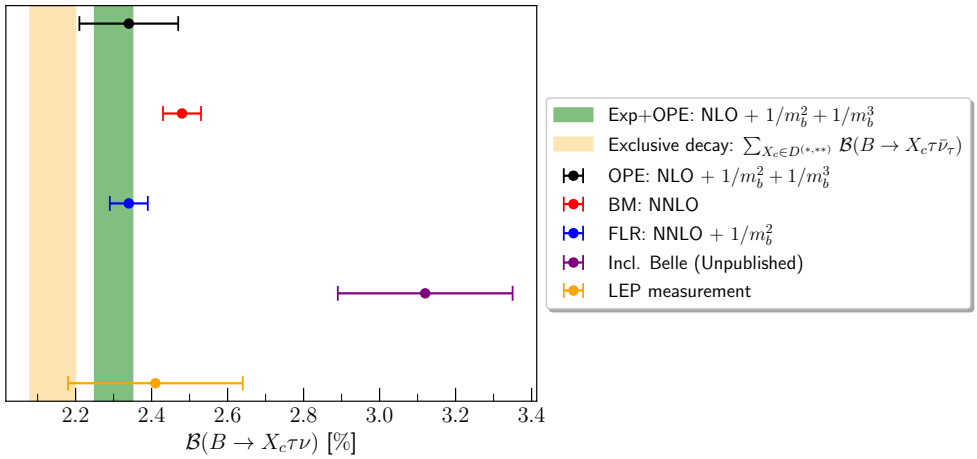

Figure 7.1: Comparison of our predictions for the branching ratio $\mathcal{B}(B \to X_c \tau \nu)$ with previous determinations and with the sum over exclusives from [168]. We also quote the measurements of LEP and the unpublished Belle measurement (see text for details).

tension with the value we find from the direct OPE calculation in (7.32). Using (7.34), we multiply with (7.36) to find

$$\mathcal{B}(B \to X_c \tau \bar{\nu}_\tau)_{\text{Belle}} = (3.12 \pm 0.23)\,\%. \tag{7.39}$$

Multiplying the previous theoretical determination of $R(X_c)$ in (7.16) [160] with with (7.36) gives

$$\mathcal{B}(B \to X_c \tau \bar{\nu}_\tau)_{\text{FLR}} = (2.34 \pm 0.05)\%, \tag{7.40}$$

which is in agreement with the value reported in [168].

Finally, multiplying (7.17) with the branching ratio in (7.36) gives

$$\mathcal{B}(B \to X_c \tau \bar{\nu}_\tau)_{\text{BM}} = (2.47 \pm 0.04)\%. \tag{7.41}$$

It is also interesting to compare our inclusive predictions with a sum over exclusive. To this extend, we follow the recent [168]. Using the HFLAV-averaged SM predictions for $R(D)$ and $R(D^*)$ and the measured rates for the light-modes, combined with the prediction for $\mathcal{B}(B \to D^{**} \ell \bar{\nu}_\ell)$ [169], they find [168]

$$\sum_{X_c \in D^{(*,**)}} \mathcal{B}(B \to X_c \tau \bar{\nu}_\tau) = (2.14 \pm 0.06)\ \%\ . \tag{7.42}$$

Interestingly, this sum over exclusive modes does not saturate our calculated fully inclusive rate. In fact, using the HQE inputs from the q^2 moment analysis predict a larger branching ratio in (7.39) leaving more room for additional states to saturate the rate. We summarize and visualize our findings in Fig. 7.1.

7.4 Conclusion

We calculated the SM predictions for the lepton flavour universality ratios of semileptonic inclusive B decays. In these predictions, we only considered the mass effects, and included HQE parameters up to $1/m_b^3$. We corrected a previous calculation in [134], which missed some terms in the ρ_D^3 contribution.

In addition, we present updated results of the Standard Model for the branching ratio of the $B \to X_c \tau \bar{\nu}_\tau$ decay. Experimentally, for this rate only a LEP measurement and an unpublished Belle analysis are available. In light of the discrepancies between data and experiment in the universality ratios of exclusive semileptonic $B \to D^{(*)}$ update measurements of this observable are highly wanted. A detailed analysis of the effect of new physics operators on inclusive semitauonic decays is in progress [170].

Acknowledgements

We thank Florian Bernlochner for suggesting this project in light of upcoming measurements. Additionally, we thank him, Thomas Mannel and Matteo Fael for their comments. We thank A. Rusov for discussions about [134]. This research was supported by the Deutsche Forschungsgemeinschaft (DFG, German Research Foundation) under grant 396021762 - TRR 257.

Appendix A Total rate

In this Appendix, we explicitly give the coefficients of the rate in (7.4).

We note that all these coefficients except $C_{\rho_D^3}$ agree with [134] when transforming basis from the spatial derivative "perped" basis used here to the full covariant derivative basis via (7.12). Explicitly this means that

$$C_{\mu_\pi^2} = C_{\mu_\pi^2}^\perp \, , C_{\mu_G^2} = C_{\mu_G^2}^\perp \, , C_{\rho_D^3} = C_{\rho_D^3}^\perp + C_{\mu_G^2}^\perp \, , C_{\rho_{LS}^3} = 0 \, . \tag{7.43}$$

We find

$$\begin{aligned} C_0^{(0)} &= R\left[1 - 7\rho - 7\rho^2 + \rho^3 - (7 - 12\rho + 7\rho^2)\eta - 7(1+\rho)\eta^2 + \eta^3\right] \\ &\quad - 12\left[\rho^2 \ln\frac{(1+\rho-\eta-R)^2}{4\rho} - \eta^2 \ln\frac{(1+\eta-\rho+R)^2}{4\eta} - \rho^2\eta^2 \ln\frac{(1-\rho-\eta-R)^2}{4\rho\eta}\right], \end{aligned} \tag{7.44}$$

$$\begin{aligned} C_{\mu_G^2}^\perp &= \frac{R}{2}\left[-3 + 5\rho - 19\rho^2 + 5\rho^3 + (5 + 28\rho - 35\rho^2)\eta - (19 + 35\rho)\eta^2 + 5\eta^3\right] \\ &\quad - 6\left[\rho^2 \ln\frac{(1+\rho-\eta-R)^2}{4\rho} - \eta^2 \ln\frac{(1+\eta-\rho+R)^2}{4\eta} - 5\rho^2\eta^2 \ln\frac{(1-\rho-\eta-R)^2}{4\rho\eta}\right], \end{aligned} \tag{7.45}$$

In addition, we have

$$C^{\perp}_{\mu^2_\pi} = -\frac{C_0}{2}\ , \qquad C^{\perp}_{\rho^3_{LS}} = -C^{\perp}_{\mu^2_G} \tag{7.46}$$

$$C^{\perp}_{\rho^3_D} = \frac{R}{6}\Big\{77 + 5\rho^3 + \rho^2(13 - 35\eta) + 13\eta - 59\eta^2 + 5\eta^3 - \rho(11 + 12\eta + 35\eta^2)\Big\} \tag{7.47}$$

$$+\ \left\{\eta^2(10\rho^2 + 8\eta - 2)\ \ln\left[\frac{(1-\rho-\eta-R)^2}{4\eta\rho}\right] + (8 + 6\rho^2 - 8\eta - 6\eta^2)\ \ln\left[\frac{(1+\rho-\eta-R)^2}{4\rho}\right]\right\},$$

where $R = \sqrt{\rho^2 + (-1+\eta)^2 - 2\rho(1+\eta)}$.

Chapter 8

Project III: New physics contributions to moments of inclusive $b \to c$ semileptonic decays

Published as a preprint in:
M. Fael, M. Rahimi, K. K. Vos [6].
At the time of writing, this work is being prepared for publication in a peer-reviewed journal.

Contributions of the authors to the article.
M. Rahimi contributed to the draft and did the analytical derivation and numerical analysis of all expressions obtained in the article. Dr. Fael and Prof. Dr. Vos performed an independent numerical study and worked on the draft.

Abstract: Inclusive semileptonic $B \to X_c \ell \bar{\nu}_\ell$ decays, where $\ell = \mu, e$, are by now standard candles in the determination of the CKM element $|V_{cb}|$. These determinations rely on the heavy-quark expansion and use moments of decay spectra to extract the non-perturbative parameters directly from data under the standard model assumption. At the same time, new physics could influence the moments of the inclusive decay. In this paper, we compute power-corrections and next-to-leading order corrections in the strong coupling constant using the full basis of dimension-six new physics operators for the inclusive $B \to X_c \ell \bar{\nu}$ decay. We provide predictions for lepton energy, hadronic and leptonic invariant mass moments, and perform a phenomenological study to show the possible impact of new physics. Our results could be used to perform a global fit including new physics contributions.

8.1 Introduction

Semileptonic $b \to c$ decays provide important tests of the Standard Model (SM) of particle physics as they are mediated by a tree-level weak transition. As such, both the inclusive $B \to X_c \ell \bar{\nu}_\ell$ and exclusive $B \to D^{(*)} \ell \bar{\nu}_\ell$ decays, where $\ell = \mu, e$, are clean probes of the CKM element $|V_{cb}|$. For the exclusive decays, this requires information on the $B \to D^{(*)}$ form factors, while the inclusive decay relies fully on the heavy quark expansion (HQE) and the extraction of non-perturbative parameters from data. Thanks to a combined theoretical and experimental effort, the inclusive determination of $|V_{cb}|$ has reached an impressive $1.2 - 1.5\%$ relative uncertainty [14, 15].

Despite this progress, the puzzling tension between the exclusive and inclusive determination of V_{cb} persists and has received quite some attention recently (see e.g. [119, 139, 171–175]). At the same time the possible New Physics (NP) origin of this discrepancy has been investigated (see [176–178]). The search for such NP has been boosted by the recent finding of the B anomalies, discrepancies between experimental data and theoretical SM predictions in both the neutral ($b \to s\ell\ell$) and charged ($b \to c\tau\bar{\nu}_\tau$) current decay of B mesons.

In this paper, we consider the effect of possible new physics interactions on moments of the inclusive $B \to X_c \ell \bar{\nu}_\ell$ decay, for light leptons. The effect of NP on the moments of the $b \to c$ spectrum have so far only been studied in [134, 179], where a subset of possible NP operators was included. NP contributions to the total inclusive rate were included in the analysis of Ref. [177], while new tensor interactions were discussed in [176].

Using the framework of the HQE, we consider the $B \to X_c \ell \bar{\nu}_\ell$ spectra including the full set of NP dimension-six operators appearing in the weak effective theory (WET) below the electroweak (EW) scale. We provide predictions for lepton energy (E_ℓ), hadronic (M_X^2) and leptonic (q^2) invariant mass moments. Moreover we study also NP effects in forward-backward asymmetries which were proposed in [82] and recently reconsidered in [140]. When considering the most general effective Hamiltonian for $b \to c\ell\bar{\nu}_\ell$ transition with dimension-six operators, we have three expansion parameters in the HQE: the inverse of the EW scale $G_F = 1/(\sqrt{2}v^2)$, $1/m_b$ and $\alpha_s(m_b)$. In order to properly catch the leading effects in the various moments, we compute the following kind of contributions:

- NP contributions at tree level in the free-quark approximation. These terms scale like $G_F^2 \times \alpha_s^0 \times (\frac{1}{m_b})^0$ in the prediction for the differential rate. Note that the interference between SM and NP operators vanishes for scalar and tensor currents when the leptons are considered massless.

- Power suppressed contributions up to order $1/m_b^3$ also for the NP operator contributions. These corrections scale like $G_F^2 \times \alpha_s^0 \times (\frac{1}{m_b})^{2,3}$. Since the prediction for q^2 and M_X^2 central moments receive large contributions from power

corrections, it is important to consider also the power suppressed terms for the NP effects.

- Perturbative QCD NLO corrections to the NP effective interactions in the free quark approximation, which scale like $G_F^2 \times \alpha_s^1 \times (\frac{1}{m_b})^0$. For the second and third central moments of M_X^2, the α_s corrections are effectively a leading-order contribution since the partonic invariant mass differs from m_c only starting at $\mathcal{O}(\alpha_s)$.

In the end, our results could be included in a fit to the experimental data to constrain possible NP contributions. We plan to implement this in the EOS software [180]. In the mean time, to show the impact of such an analysis, we illustrate the effect of different NP scenarios with some phenomenological studies. Finally, we present a toy fit to show the effect on the V_{cb} extraction, as the HQE parameters could mimic the effect of NP.

This work is organised as follows. In Section 8.2 we introduce the set of dimension-six operators which can contribute to the inclusive semileptonic B decay and discuss the derivation of the NLO corrections for the NP operators. In Sec. 8.3 we present the results for the NP contributions to moments, illustrate their effects using three benchmark scenarios and study their impact on the extraction of the HQE parameters in global fits via a toy fit. In Sec. 8.4 we discuss the effects of NP in the forward-backward asymmetries. We conclude in Sec. 8.5. In Appendix A, we give the contribution to the total rate, while in Appendix B we give our results for the different contributions to the moments.

8.2 Effective NP contributions to $b \to c\ell\bar{\nu}_\ell$

We consider NP effects in $b \to c\ell\bar{\nu}_\ell$ decays arising from

$$\mathcal{H}_{\text{eff}} = \frac{4G_F V_{cb}}{\sqrt{2}} \left[(1 + C_{V_L})\, O_{V_L} + \sum_{i=V_R,S_L,S_R,T} C_i\, O_i \right], \tag{8.1}$$

where the effective dimension-six operators are

$$O_{V_{L(R)}} = \left(\bar{c}\gamma_\mu P_{L(R)} b\right) \left(\bar{\ell}\gamma^\mu P_L \nu_\ell\right), \tag{8.2}$$

$$O_{S_{L(R)}} = \left(\bar{c} P_{L(R)} b\right) \left(\bar{\ell} P_L \nu_\ell\right) \tag{8.3}$$

$$O_T = \left(\bar{c}\,\sigma_{\mu\nu} P_L b\right) \left(\bar{\ell}\,\sigma^{\mu\nu} P_L \nu_\ell\right). \tag{8.4}$$

with $P_{L(R)} = 1/2\,(1 \mp \gamma_5)$ and $\sigma^{\mu\nu} = \frac{i}{2}[\gamma^\mu, \gamma^\nu]$. In the SM only O_{V_L} contributes. We have written out this contribution explicitly, such that all Wilson coefficients C_i are zero in the SM. We do not consider interactions with right handed neutrinos (see e.g. [181] for a discussion of these effects on exclusive $B \to D^{(*)}\ell\bar{\nu}_\ell$ decays).

Note that if one would consider NP effects in the SMEFT framework [182], there would be an additional expansion in powers of $1/\Lambda$, where Λ corresponds to the NP scale above the EW scale. The tree-level matching of SMEFT operators onto the effective Hamiltonian can be obtained from [183]. In the WET the expansion parameter is $1/v$, therefore from the SMEFT point of view the Wilson coefficients in Eq. (8.1) would be further suppressed by the small ratio $(v/\Lambda)^2$.

To study the effects of the NP operators on moments of the spectrum, we calculate the triple differential decay rate in terms of the lepton (neutrino) energy $E_{\ell(\nu)}$ and the dilepton invariant mass $q^2 = (p_\ell + p_\nu)^2$. We write

$$\frac{\mathrm{d}\Gamma_{\mathrm{SM+NP}}}{\mathrm{d}E_\ell \mathrm{d}q^2 \mathrm{d}E_\nu} = \frac{G_F^2 |V_{cb}|^2}{16\pi^3} \tilde{W} \otimes \tilde{L} \ , \tag{8.5}$$

where

$$\begin{aligned}
\tilde{W} \otimes \tilde{L} \equiv\ & |1 + C_{V_L}|^2 \left(W_{\mu\nu} L^{\mu\nu}\right)_{V_L,V_L} + |C_{V_R}|^2 \left(W_{\mu\nu} L^{\mu\nu}\right)_{V_R,V_R} + |C_{S_L}|^2 \left(WL\right)_{S_L,S_L} \\
& + |C_{S_R}|^2 \left(WL\right)_{S_R,S_R} + |C_T|^2 \left(W_{\mu\nu\rho\sigma} L^{\mu\nu\rho\sigma}\right)_{T,T} + \mathrm{Re}((1 + C_{V_L}) C_{V_R}^*) \left(W_{\mu\nu} L^{\mu\nu}\right)_{V_L,V_R} \\
& + \mathrm{Re}(C_{S_L} C_{S_R}^*) \left(WL\right)_{S_L,S_R} + \mathrm{Re}(C_{S_L} C_T^*) (W_{\mu\nu} L^{\mu\nu})_{S_L,T} \\
& + \mathrm{Re}(C_{S_R} C_T^*) (W_{\mu\nu} L^{\mu\nu})_{S_R,T} \ .
\end{aligned} \tag{8.6}$$

We split the contributions into the lepton (L) and hadronic (W) tensors. We define

$$L = \sum_{\text{lepton spin}} \langle 0 | \, J_L^\dagger \, | \ell \bar{\nu}_\ell \rangle \, \langle \ell \bar{\nu}_\ell | \, J_{L'} \, | 0 \rangle \ , \tag{8.7}$$

where we suppressed the Lorenz indices in the leptonic tensor. The indices L and L' can take the values $S_{L,R}, V_{L,R}$ and T with

$$J_{S_{L,R}} = (\bar{\ell} P_L \nu_\ell), \qquad J^\mu_{V_{L,R}} = (\bar{\ell} \gamma^\mu P_L \nu_\ell), \qquad J^{\mu\alpha}_T = (\bar{\ell} \sigma^{\mu\alpha} P_L \nu_\ell). \tag{8.8}$$

We define the hadronic tensor in the following way:

$$W = \sum_{X_c} \frac{1}{2m_B} (2\pi)^3 \, \langle \bar{B} | \, J_H^\dagger \, | X_c \rangle \, \langle X_c | \, J_{H'} \, | \bar{B} \rangle \, \delta^{(4)}(p_B - q - p_{X_c}), \tag{8.9}$$

where p_{X_c} is the total momentum of the X_c state and also in this case we suppressed the Lorenz indices. In the presence of NP interactions, the index H and H' can take the values $S_{L,R}, V_{L,R}$ and T where

$$J_{S_{L(R)}} = (\bar{c} P_{L(R)} b) \ , \qquad J^\mu_{V_{L(R)}} = (\bar{c} \gamma^\mu P_{L(R)} b) \ , \qquad J^{\mu\alpha}_T = (\bar{c} \sigma^{\mu\alpha} P_L b) \ . \tag{8.10}$$

In Eq. (8.6) we neglected combinations of the form $\left(W_\mu L^\mu\right)_{V_{L(R)},S_{L(R)}}$ and $\left(W_{\mu\rho\sigma} L^{\mu\rho\sigma}\right)_{V_{L(R)},T}$ since they do not contribute in the limit $m_\ell \to 0$ considered in this work. The

hadronic tensors W can now be calculated using the heavy quark expansion (HQE) (see e.g. [103]), expressing them in pertubatively calculable coefficients and hadronic matrix elements scaling with inverse powers of m_b. The number of matrix elements proliferates at each higher order in $1/m_b$ (see [78, 79, 115]). Here we only consider terms up to $1/m_b^3$ defined as: (see e.g. [80])

$$
\begin{aligned}
2m_B\,(\mu_\pi^2) &\overset{\perp}{=\!=} -\langle B|\bar{b}_v (iD_\rho)(iD_\sigma) b_v|B\rangle \Pi^{\rho\sigma}\ , \\
2m_B\,(\mu_G^2) &\overset{\perp}{=\!=} \frac{1}{2}\langle B|\bar{b}_v \left[iD_\rho, iD_\lambda\right](-i\sigma_{\alpha\beta}) b_v|B\rangle \Pi^{\alpha\rho}\Pi^{\beta\lambda}, \\
2m_B\,(\rho_D^3) &\overset{\perp}{=\!=} \frac{1}{2}\langle B|\bar{b}_v \left[iD_\rho, [iD_\sigma, iD_\lambda]\right] b_v|B\rangle \Pi^{\rho\lambda} v^\sigma, \\
2m_B\,(\rho_{LS}^3) &\overset{\perp}{=\!=} \frac{1}{2}\langle B|\bar{b}_v \left\{iD_\rho, [iD_\sigma, iD_\lambda]\right\}(-i\sigma_{\alpha\beta}) b_v|B\rangle \Pi^{\alpha\rho}\Pi^{\beta\lambda} v^\sigma\ ,
\end{aligned}
\tag{8.11}
$$

where $v^\mu = p_B^\mu / m_B$ is the velocity of the B meson and

$$
\Pi_{\mu\nu} = g_{\mu\nu} - v_\mu v_\nu\ . \tag{8.12}
$$

In the following, we drop the "perp" superscript for simplicity. Alternative, the HQE parameters can be defined with the full covariant derivative, related to the spatial component via $iD^\mu = v^\mu (iv\cdot D) + D_\perp^\mu$. These definitions were used in Refs. [15, 78, 115] as, in the reparametrization invariant (RPI) basis, it is beneficial to use the full derivative (see discussion in Appendix A of [115] for the relation between these two bases). In principle, the $1/m_b^4$ terms can be included as recently done for the q^2 moment analysis [15]. The two $1/m_b^4$ parameter extracted were found to be consistent with zero. These higher-order corrections were also studied in [113] using the lowest-lying state approximation. Therefore, for this study of NP effects, we only consider terms up to $1/m_b^3$.

8.2.1 Next-to-leading order corrections

Besides these power-corrections, we also compute the NLO corrections to the triple differential rate for the full NP operator basis in (8.1). For scalar NP interactions, the NLO corrections to the q^2 spectrum are already given in [184], using results from [185]. The NLO corrections for the SM are well known for both the massive and massless leptons in the semileptonic decay $b \to c\ell\bar{\nu}_\ell$ [108, 121, 126, 157, 186, 187].

We compute the $\mathcal{O}(\alpha_s)$ for the structure functions of the hadronic tensor W for the different currents which enter the fully differential decay width. We note that it turns out to be more convenient to express the triple differential rate with respect to $u \equiv p_{X_c}^2 - m_c^2$ instead of E_ν as in [187]. We then extract the predictions for the various moments and forward-backward asymmetries with arbitrary cuts via numerical integration of the differential rate over the allowed phase space, following the approach described in [188].

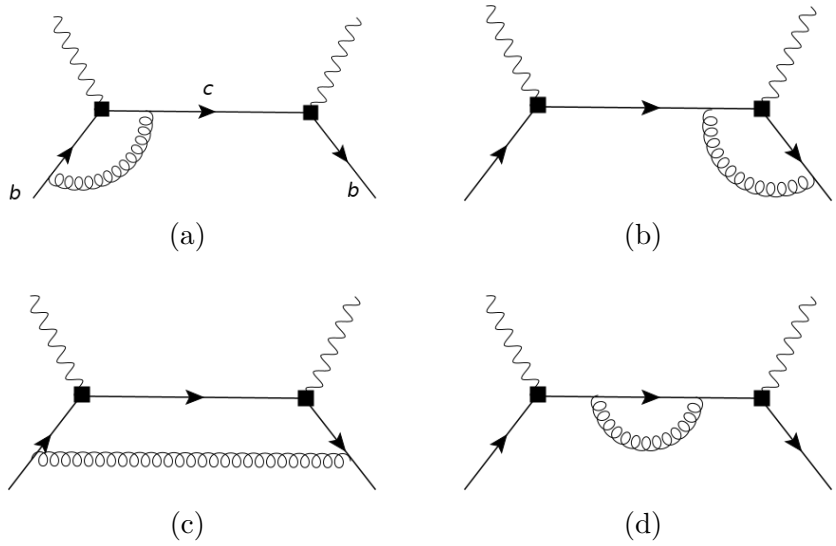

Figure 8.1: One-loop forward scattering diagrams which contribute to the $b \to X_c \ell \bar{\nu}_\ell$ differential rate at NLO. The black boxes represents one of the currents J_H defined in (8.10). Solid lines represent the quarks, curly lines the gluons and wavy lines the color-singlet external current mediating the weak decay.

In general we can express the structure functions as:

$$W_{HH'}(q^2,(v\cdot q)) = W^{(0)}_{HH'}(q^2,(v\cdot q)) + \frac{\alpha_s(\mu)}{\pi}\Big[W^{(1)}_{HH',\text{virt}}(q^2,(v\cdot q)) + W^{(1)}_{HH',\text{real}}(q^2,(v\cdot q))\Big], \tag{8.13}$$

where "virt" and "real" stand for virtual and real contributions, respectively. The indices HH' run over all possible pairs of NP interactions, e.g. $V_L V_R, S_L S_R$, etc.

For the ultraviolet and infrared divergences, we use dimensional regularization and define $\epsilon = (4-d)/2$, where d is the space-time dimensions. For the calculation we use the Mathematica package `FeynCalc` [189]. The ultraviolet divergences in the one-loop virtual diagrams are removed by using on-shell quark mass and wave function renormalization. Furthermore, there are additional ultraviolet divergences for the scalar and tensor currents. We therefore apply a renormalization of these currents according to their one-loop anomalous dimension (see e.g. [190]). For the computation of real emission we employed the inverse unitarity approach [191]. This method allows us to rewrite the real emission diagram integrated over the gluon phase-space as a multi-loop integral with cut propagators. We can then apply the usual IBP reduction to reduce the real emission contribution to phase-space master integrals which are then calculated explicitly. In the process of the reduction to master integrals we take into account the cut in the gluon and charm intermediate

state. For the real emission we encounter the following integral family:

$$I(a,b,c) = \left(4\pi\, e^{-\gamma_E}\right)^{-\epsilon} \mathrm{Disc} \int \frac{\mathrm{d}^d k}{(2\pi)^d} \frac{1}{[k^2]^a [(p_b-k)^2-m_b^2]^b [(p_b-q-k)^2-m_c^2]^c} \tag{8.14}$$

By applying the Cutkosky's rules for the gluon and charm intermediate state:

$$\frac{1}{k^2} \to (-2\pi i)\,\delta(k^2)\,,$$

$$\frac{1}{(p_b-q-k)^2-m_c^2} \to (-2\pi i)\,\delta((p_b-q-k)^2-m_c^2)\,, \tag{8.15}$$

we obtain the following master integrals:

$$\begin{aligned} I(1,0,1) &= \left(4\pi\, e^{-\gamma_E}\right)^{-\epsilon} \int \frac{\mathrm{d}^d k}{(2\pi)^d} (-2\pi i)^2 \delta(k^2)\delta((p_b-q-k)^2-m_c^2)\Theta(k_0) \\ &= -\frac{\hat{u}}{4\pi\hat{s}} \left(\frac{\hat{u}}{\sqrt{\hat{s}}}\right)^{-2\epsilon} \left(\frac{1}{2}+\epsilon+\mathcal{O}(\epsilon^2)\right), \end{aligned} \tag{8.16}$$

$$\begin{aligned} I(1,1,1) &= \left(4\pi\, e^{-\gamma_E}\right)^{-\epsilon} \int \frac{\mathrm{d}^d k}{(2\pi)^d} \frac{1}{(p_b+k)^2-m_b^2} (-2\pi i)^2 \delta(k^2)\delta((p_b-q-k)^2-m_c^2)\Theta(k_0) \\ &= \left(\frac{\hat{u}}{\sqrt{\hat{s}}}\right)^{-2\epsilon} \left\{ \frac{1}{8\pi\sqrt{\lambda}} \log\left(\frac{1-\hat{q}^2+\hat{s}+\sqrt{\lambda}}{1-\hat{q}^2+\hat{s}-\sqrt{\lambda}}\right) \right. \\ &\left. + \frac{\epsilon}{4\pi\sqrt{\lambda}} \left[\mathrm{Li}_2\left(\frac{2\sqrt{\lambda}}{1-\hat{q}^2+\hat{s}+\sqrt{\lambda}}\right) + \frac{1}{4}\log^2\left(\frac{1-\hat{q}^2+\hat{s}+\sqrt{\lambda}}{1-\hat{q}^2+\hat{s}-\sqrt{\lambda}}\right)\right] + \mathcal{O}(\epsilon^2) \right\}, \end{aligned} \tag{8.17}$$

where $\hat{s} = \rho + \hat{u}$, $\lambda = \lambda(1,\hat{q}^2,\hat{s})$ and $\lambda(x,y,z) = x^2+y^2+z^2-2xy-2xz-2yz$ is the Källen function. The singularities of the real emissions are located at $\hat{u}=0$ with:

$$\hat{u} = (1-\hat{q})^2 - \rho\,, \qquad 0 \le \hat{u} \le \hat{u}_{\max} = (1-\sqrt{\hat{q}^2})^2 - \rho\,. \tag{8.18}$$

We have to extract the singular behavior of the master integrals around $\hat{u}=0$ before expanding in ϵ. The infrared divergences are extracted explicitly by using the plus distribution:

$$\hat{u}^{-1+a\epsilon} = \frac{1}{a\epsilon}\delta(\hat{u})\,\hat{u}_{\max} + \left[\frac{1}{\hat{u}}\right]_+ + \mathcal{O}(\epsilon)\,. \tag{8.19}$$

The integration of the plus distribution over a test function is defined as:

$$\int_0^{\hat{u}_{\max}} f(\hat{u}) \left[\frac{1}{\hat{u}}\right]_+ \mathrm{d}\hat{u} = \int_0^{\hat{u}_{\max}} \frac{f(\hat{u})-f(0)}{\hat{u}} \mathrm{d}\hat{u}\,. \tag{8.20}$$

In the sum between real and virtual corrections all the infrared divergences cancel. For the γ_5 definition in dimensional regularization we use the Larin prescription [192], i.e.

$$\gamma_5 = \frac{i}{12}\epsilon_{\mu_1\mu_2\mu_3\mu_4}\gamma^{\mu_1}\gamma^{\mu_2}\gamma^{\mu_3}\gamma^{\mu_4}, \tag{8.21}$$

which requires an additional finite renormalization constant in order to restore the correct Ward identity.

Note that, our method to compute the one-loop diagrams differs from [187] where they regularize IR divergences via a finite gluon mass. Ref. [187] presented also the corrections of $\mathcal{O}(\alpha_s^n\beta_0^{n-1})$ (the so-called large-β_0 limit). This can be also done in our approach, however, we do not include them in this analysis. To summarize, in this work we consider leading order, power-corrections up to $\mathcal{O}(1/m_b^3)$ and next-to-leading order corrections. Schematically:

$$\frac{\mathrm{d}\Gamma_{\rm SM+NP}}{\mathrm{d}E_\ell \mathrm{d}q^2 \mathrm{d}E_\nu} = \frac{\mathrm{d}\Gamma^{\rm LO}_{\rm SM+NP}}{\mathrm{d}E_\ell \mathrm{d}q^2 \mathrm{d}E_\nu} + \frac{\mathrm{d}\Gamma^{\rm Pow}_{\rm SM+NP}}{\mathrm{d}E_\ell \mathrm{d}q^2 \mathrm{d}E_\nu} + \left(\frac{\alpha_s}{\pi}\right)\frac{\mathrm{d}\Gamma^{\rm NLO}_{\rm SM+NP}}{\mathrm{d}E_\ell \mathrm{d}q^2 \mathrm{d}E_\nu}\,. \tag{8.22}$$

8.2.2 Moments of the spectrum

In the following, we consider the lepton energy moments, dilepton invariant mass (q^2) moments and hadronic invariant mass moments of the $b \to c$ spectrum. The first two can be easily obtained from the triple differential rate defined as in (8.5). The hadronic invariant mass is related to these variables via

$$M_X^2 \equiv (p_B - q)^2 = (m_B^2 + q^2 - 2m_B(v\cdot q))\ . \tag{8.23}$$

The normalized moments for observable $\mathcal{M}$ are then defined

$$\langle \mathcal{M}^n \rangle_{E_\ell > E_\ell^{\rm cut}} = \frac{\int_{E_\ell > E_\ell^{\rm cut}} \mathrm{d}\mathcal{M}\, \mathcal{M}^n \frac{\mathrm{d}\Gamma}{\mathrm{d}\mathcal{M}}}{\int_{E_\ell > E_\ell^{\rm cut}} \mathrm{d}\mathcal{M}\, \frac{\mathrm{d}\Gamma}{\mathrm{d}\mathcal{M}}}, \tag{8.24}$$

where $E_\ell^{\rm cut}$ is the energy cut of the lepton $\ell = (e,\, \mu)$ and n denotes the n-th order of moment. Similarly, for q^2 moments, we consider moments with minimum cut $q^2_{\rm cut}$ on the value of q^2. As is customary, we also calculate central moments defined as

$$\langle (\mathcal{M} - \langle \mathcal{M} \rangle)^n \rangle = \sum_{i=0}^{n} \binom{n}{i} \langle (\mathcal{M})^i \rangle \, (-\langle \mathcal{M} \rangle)^{n-i}\,. \tag{8.25}$$

The moments can be obtained using Eq. (8.24) and by integrating the triple differential rate over the allowed phase space.

8.3 New physics in moments of $B \to X_c \ell \bar{\nu}_\ell$

The moments can now be obtained from the triple differential rate in (8.5). We write

$$\begin{aligned}\langle \mathcal{M} \rangle = \xi_{\rm SM} &+ |C_{V_R}|^2\, \xi_{\rm NP}^{\langle V_R, V_R\rangle} + |C_{S_L}|^2\, \xi_{\rm NP}^{\langle S_L, S_L\rangle} + |C_{S_R}|^2\, \xi_{\rm NP}^{\langle S_R, S_R\rangle} + |C_T|^2\, \xi_{\rm NP}^{\langle T, T\rangle} \\ &+ {\rm Re}((C_{V_L}-1)C_{V_R}^*)\, \xi_{\rm NP}^{\langle V_L, V_R\rangle} + {\rm Re}(C_{S_L} C_{S_R}^*)\, \xi_{\rm NP}^{\langle S_L, S_R\rangle} + {\rm Re}(C_{S_L} C_T^*)\, \xi_{\rm NP}^{\langle S_L, T\rangle} \\ &+ {\rm Re}(C_{S_R} C_T^*)\, \xi_{\rm NP}^{\langle S_R, T\rangle}\ , \end{aligned} \tag{8.26}$$

where we assume that the NP Wilson coefficients are smaller than one so that we can expand the ratios in Eq. (8.24) up to quadratic NP couplings. The contribution $C_{V_L}\xi_{\rm NP}^{\langle V_L\rangle}$ drops out for normalized moments and in the branching ratio it is equivalent to a rescaling of V_{cb}. The coefficients denoted by ξ depend on the bottom and charm quark masses, the HQE parameters and the lepton energy cut or the q^2 cut. For $\xi_{\rm SM}$, we agree with the numerical results at $\mathcal{O}(\alpha_s)$ given in [112] for the electron energy and M_X moments. The NP coefficients with NLO corrections are lengthy and require numerical integration depending on the lepton energy (or q^2) cut. Therefore, we do not report explicitly our results. They can be obtained in Mathematica format from the authors. However, to illustrate the effect of the NP contributions, we report our predictions for the various central moments for benchmark values of the cuts. We consider $E_\ell^{\rm cut} = 1$ GeV in case of the lepton energy and hadronic invariant mass moments. For the q^2 moments, we present results for $q^2_{\rm cut} = 4$ GeV^2. In the next section, we also illustrate the lepton energy or q^2 cut dependence for specific NP scenarios.

In Appendix B we report our predictions for the different moments. We work in the kinetic scheme [159, 185, 193, 194]. We fix the value of the scale μ in $m_b^{\rm kin}(\mu)$ at 1 GeV. For the charm quark mass we use the $\overline{\rm MS}$ scheme and fix $\overline{m}_c(2\ {\rm GeV})$. For the strong coupling constant we use $\alpha_s(m_b^{\rm kin}) = 0.2184$ [195]. In addition, we use the input values in Table 8.1. These are obtained from a global fit to lepton energy and hadronic invariant mass moments of the $B \to X_c \ell \bar{\nu}_\ell$ spectra in [14] (which updates the fit of [113]). Interestingly, the value of ρ_D^3 in Table 8.1 differs from the determination of $\rho_D^3 = (0.03 \pm 0.02)$ GeV^3 found in [15]. The latter uses q^2 moments, which depend on a reduced RPI basis of HQE elements. Specifically, ρ_{LS}^3 does not enter into the prediction of RPI quantities and the dependence on μ_π^2 is very much reduced for normalized q^2 moments. The difference between the values for ρ_D^3 obtained from these two data sets requires further study, preferably via a combined fit to all available data. These studies are in progress. On the contrary, the lepton and hadronic mass moments depends on ρ_{LS}^3 and μ_π^2, so we cannot use the HQE parameter values from [15] for these moments. However, for the q^2 moments both determinations of HQE parameters can be used. We comment on this in the next section.

$m_b^{\rm kin}$	(4.573 ± 0.012) GeV
$\overline{m}_c(2\ {\rm GeV})$	(1.092 ± 0.008) GeV
$(\mu_\pi^2(\mu))_{\rm kin}$	(0.477 ± 0.056) GeV^2
$(\mu_G^2(\mu))_{\rm kin}$	(0.306 ± 0.050) GeV^2
$(\rho_D^3(\mu))_{\rm kin}$	(0.185 ± 0.031) GeV^3
$(\rho_{LS}^3(\mu))_{\rm kin}$	(-0.130 ± 0.092) GeV^3

Table 8.1: Numerical inputs from [14]. The HQE parameters and the b-quark mass are given in the kinetic scheme at $\mu = 1$ GeV.

Our results in Appendix B show the impact of different NP contributions. As stated already in the introduction, especially for the M_X and q^2 moments, the inclusion of $1/m_b$ power corrections is crucial, while in addition for the former also α_s numerically plays an important role. In principle, the coefficients have an uncertainty stemming from the input parameters. However, here we refrain from giving those. We include them in the next section when discussing different NP scenarios.

From our results, we observe that for all moments the contribution proportional to C_T^2 is sizable compared to $\xi_{\rm SM}$. Especially for the third E_ℓ and q^2 moments, tensor contributions can be as large as ten times the SM prediction or more (for order one coefficients). Therefore, a moment analysis is expected to be able to strongly constrain such contributions. It is also interesting to consider the case of contributions from both C_{S_L} and C_T, because due to RGE running (see e.g. [196, 197]), tensor interactions always generate left-handed scalar interactions. We note that q^2 moments are only sensitive to the quadratic contributions, while lepton and hadronic mass moments are also sensitive to interference. Assuming real couplings and $C_{S_L} > C_T$ (see discussion in [177]), we observe that the q^2 moments mainly constrain C_{S_L}, while the lepton moments constrain the tensor part. Clearly, the situation for the inclusive decay is not as straightforward as for the exclusive case, because our current "SM prediction" depends on the input of the HQE elements that are extracted from data. Nevertheless, we can visualize and investigate the potential NP bounds for different scenarios by assuming that the SM prediction is known (namely $\xi_{\rm SM}$). We then define

$$\delta\langle\mathcal{M}\rangle \equiv \frac{\langle\mathcal{M}\rangle - \langle\mathcal{M}\rangle_{\rm SM}}{\langle\mathcal{M}\rangle_{\rm SM}} \tag{8.27}$$

where $\mathcal{M}_{\rm SM} = \xi_{\rm SM}$ for the specific moment under consideration. Considering then a 10% measurement of the moments, i.e. $\delta\langle\mathcal{M}\rangle = \pm 0.1$, leads to a constraint on the NP parameters. Specifically, for the $S_L - T$ contributions we obtain

$$-0.1 < |C_{S_L}|^2 \hat{\xi}_{\rm NP}^{\langle S_L, S_L\rangle} + |C_T|^2 \hat{\xi}_{\rm NP}^{\langle T,T\rangle} + {\rm Re}(C_{S_L} C_T^*) \hat{\xi}_{\rm NP}^{\langle S_L, T\rangle} < 0.1\ , \tag{8.28}$$

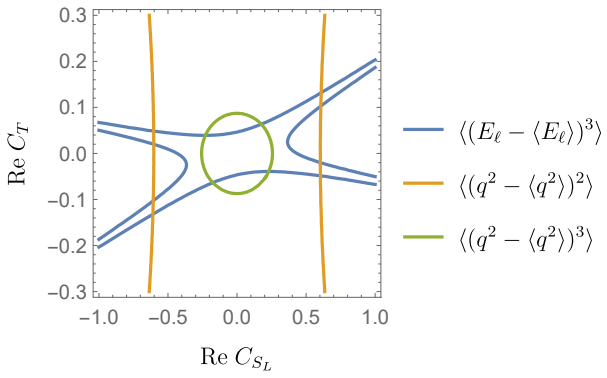

Figure 8.2: Illustration of complementarity of constraints on C_{S_L} and C_T from lepton energy moments and q^2 moments, assuming $\delta\langle\mathcal{M}\rangle = \pm 0.1$.

where

$$\hat{\xi}_i \equiv \frac{\xi_i}{\xi_{\rm SM}} \,, \tag{8.29}$$

and the ξ_i can be found in Appendix B for the different moments and NP scenarios. In order to illustrate the effects, we use these ξ's, which are re-expanded in the Wilson coefficients. The constraints obtained from (8.28) are illustrated in Fig. 8.2. Interestingly, we see that the different moments give complementary bounds on NP, similar as the $B \to D$ versus $B \to D^*$ constraints in the exclusive case (for the latter see [177]).

Similarly, in Fig. 8.3, we illustrate the possible bounds on C_{V_L} and C_{V_R} (left) and C_{S_L} and C_{S_R} (right). In these cases, we see that the M_X moments give much weaker constraints than the lepton energy and q^2 moments. We should stress that the uncertainties on the M_X moments are in general also larger as they are more sensitive to higher-order HQE corrections. Comparing with the exclusive constraints on C_{S_L} versus C_{S_R} in [177], we observe that such a SM measurement would constrain NP along the $C_{S_L} = -C_{S_R}$ plane, similar as the $B \to D$ exclusive mode, while $B \to D^*$ gives constraints orthogonal to that.

Finally, we note that the $C_{S_{L,R}} C_T$ coefficient vanishes for q^2 moments because the differential rate has only a parity-odd contribution while q^2 moments with a cut on q^2 are parity even observables. For lepton energy and hadronic mass moments, the contribution proportional to $C_{S_R} C_T$ is non-zero only due to power corrections. Therefore, the sensitivity to these types of NP is limited.

8.3.1 Illustration for specific NP scenarios

To visualize the effect of possible NP in the moments of the $B \to X_c \ell \bar{\nu}_\ell$ spectrum as a function of the lepton energy cut (or q^2 cut), we consider three NP scenarios specified in Table 8.2 allowing for either new scalar interactions (Scen. I), new tensor and scalar interactions interactions (Scen. II) and new vector interactions (Scen. III).

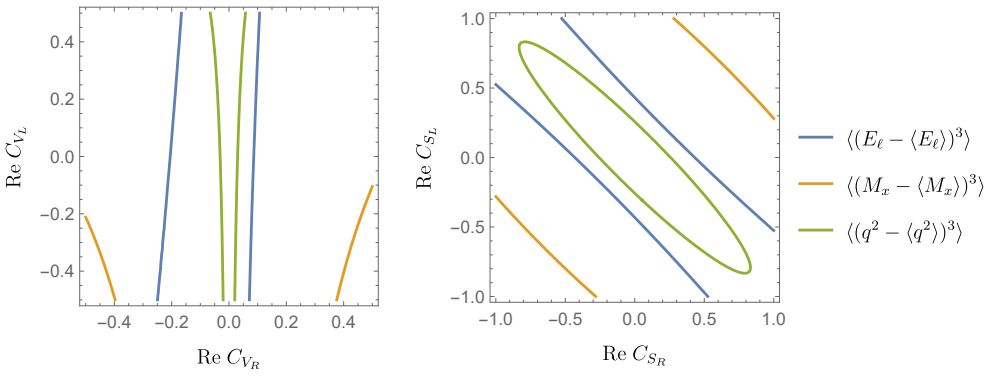

Figure 8.3: Illustration of the possible bounds on (left) C_{V_L} versus C_{V_R} and (right) C_{S_L} versus C_{S_R} assuming a 10% SM measurement.

NP Scenarios	C_{V_L}	C_{V_R}	C_{S_R}	C_{S_L}	C_T
I	0	0	1	1	0
II	0	0	0	-1	0.5
III	-1	0.5	0	0	0

Table 8.2: Three NP scenarios that we consider to visualize the effect of the NP parameters in the moments. All Wilson coefficients are defined at the scale $\mu = m_b$.

These scenarios are just to illustrate how the NP contributions depend on the cut and to the SM uncertainty. We stress that these scenarios may not be realistic in light of current data on exclusive $B \to D^{(*)}$ decays, were the same NP operators would contribute. Specifically Scenario II, where we allow for a rather large tensor contribution, may be already excluded by the exclusive decays (see [177]). For the scalar contributions, we pick $C_{S_R} = C_{S_L}$, based on Fig. 8.3 as we see that this would give a large effect on the spectrum. Finally, as here we consider rather large Wilson coefficients we do not re-expand the expression for the moments in the Wilson coefficients. We observe in Figs. 8.4, 8.5 and 8.6 that the prediction for all central moments are modified by the presence of NP contributions, but that the cut-dependence remains similar as that of the SM prediction. For all cases, we observe that the third central moment is most sensitive to NP effects.

Electron energy moments:

Figure 8.4 shows the lepton energy moments as a function of the lepton energy cut for the SM and the three NP scenarios. In order to qualitatively understand the sensitivity on possible NP effects, we show in these plots the experimental results from Belle [198] and BaBar [199]. On the right-hand side, we show the impact of

the NP scenarios by showing the absolute value of $\delta\langle\mathcal{M}\rangle$ defined in (8.27).

For simplicity, we only show an uncertainty band for the SM prediction obtained by varying the inputs in Table 8.1 within their 1σ ranges. To account for missing α_s corrections, we vary the scale of $\alpha_s(\mu)$ in the range $m_b/2 < \mu < 2\,m_b$. We observe for electron energy moments, Scen. I is rather close to the SM, while Scen. II and III cause a shift much larger than the SM uncertainty. These lepton energy moments therefore seem rather sensitive to NP effects and it would be potentially able to constrain NP via a full global analysis of these moments. Note also that the contribution from power corrections are in general small for this kind of moments, reducing the dependence on the value of the HQE parameters.

M_X^2 moments:

Results for the hadronic invariant mass moments are shown in Fig. 8.5. We observe that these moments are sensitive to new scalar couplings, as Scen. I shows the largest deviation from the SM prediction. On the other hand, both Scen. II and III lie within the uncertainty of the SM error band, which is rather large. This happens because for the M_X moments the contribution from power corrections is very important and the α_s corrections are much larger compared to the partonic LO. The dependence of the M_X moments on the scale of α_s is therefore much larger compared for instance to the electron energy moments and so prevents a precise SM determination of these kind of observables.

For the experimental data points we use the results of CLEO [200], Belle [201] and BaBar [202]. The latter does not provide the central moments but only $\langle(M_X^2)^{i=1,2,3}\rangle$. We have calculated the central moments using (8.25). We do not show the recent results of Belle II [203] since the uncertainties are still rather large.

q^2 moments:

For the q^2 moments, we consider the SM and NP predictions at different values of the q^2 cut shown in Figure 8.6. For the plots on the left-hand side, we used the HQE parameters from Table 8.1 from [14]. Comparing with the experimental data points of Belle [138] and Belle II [204], we find large deviations. Interestingly, these deviations cannot be accommodated by the three NP scenarios we consider. As mentioned before, in [15], where these data were used to extract the HQE parameters and V_{cb}, a value of ρ_D^3 incompatible with that in Table 8.1 was found. The mismatch in Fig. 8.6 is a consequence of this: the q^2 data pull ρ_D^3 to much smaller value. To illustrate this, we show on the right-hand side of Fig. 8.6 the SM predictions using the HQE parameters obtained in [15]. We observe good agreement with the data points. In addition, the uncertainty of the SM prediction is rather large, reflecting that these moments are more sensitive to the power corrections than the lepton energy moments. This was already observed in [158]. Note that the ξ coefficients in Appendix B are obtained using Table 8.1. As the goal of these scenarios is merely to demonstrate the effect of different NP parameters, we do not present ξ's using

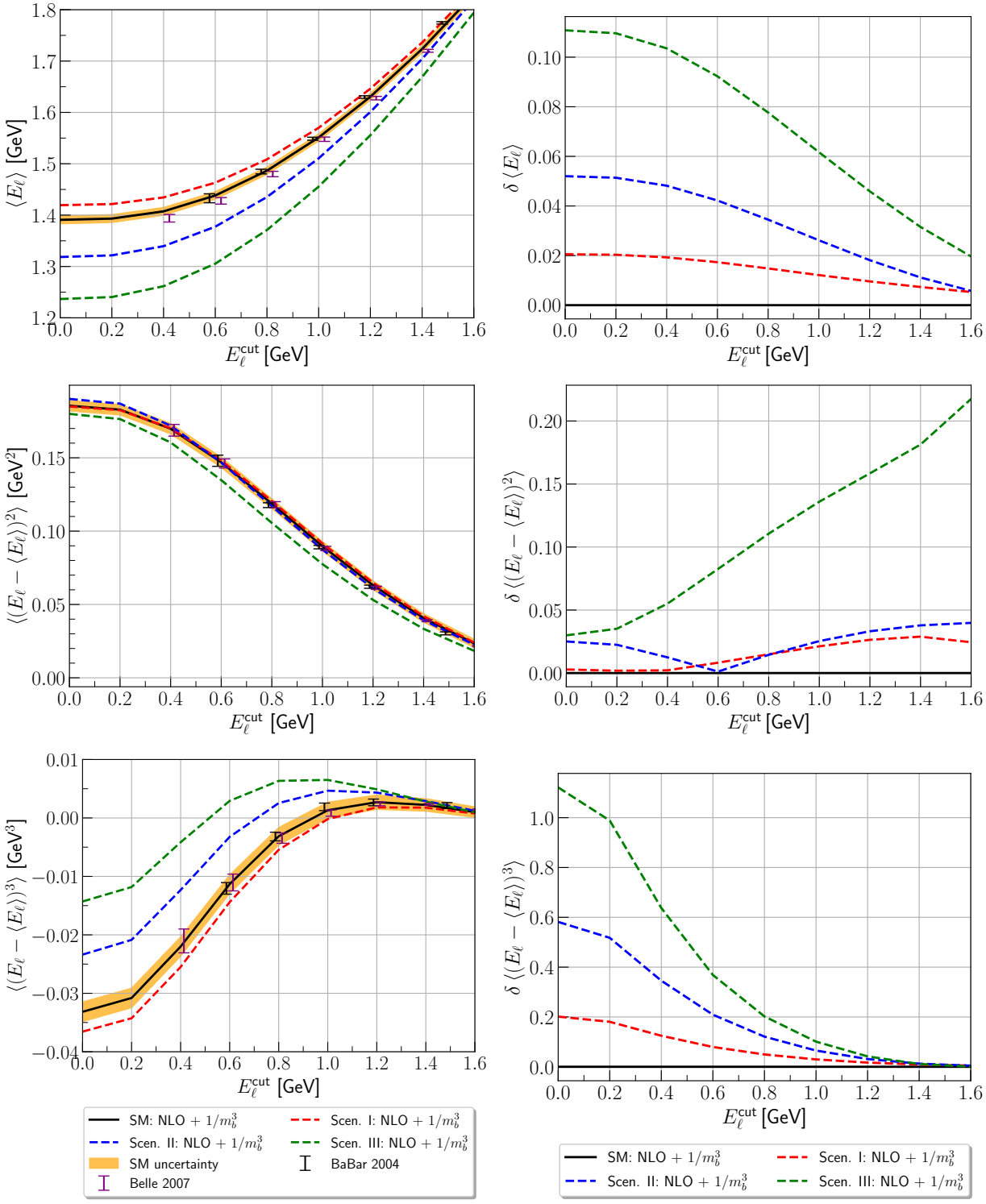

Figure 8.4: Lepton energy moments for the $B \to X_c \ell \bar{\nu}_\ell$ decay for the different NP scenarios (see Tab. 8.2). The experimental results of BaBar is taken from [199] and Belle from [198].

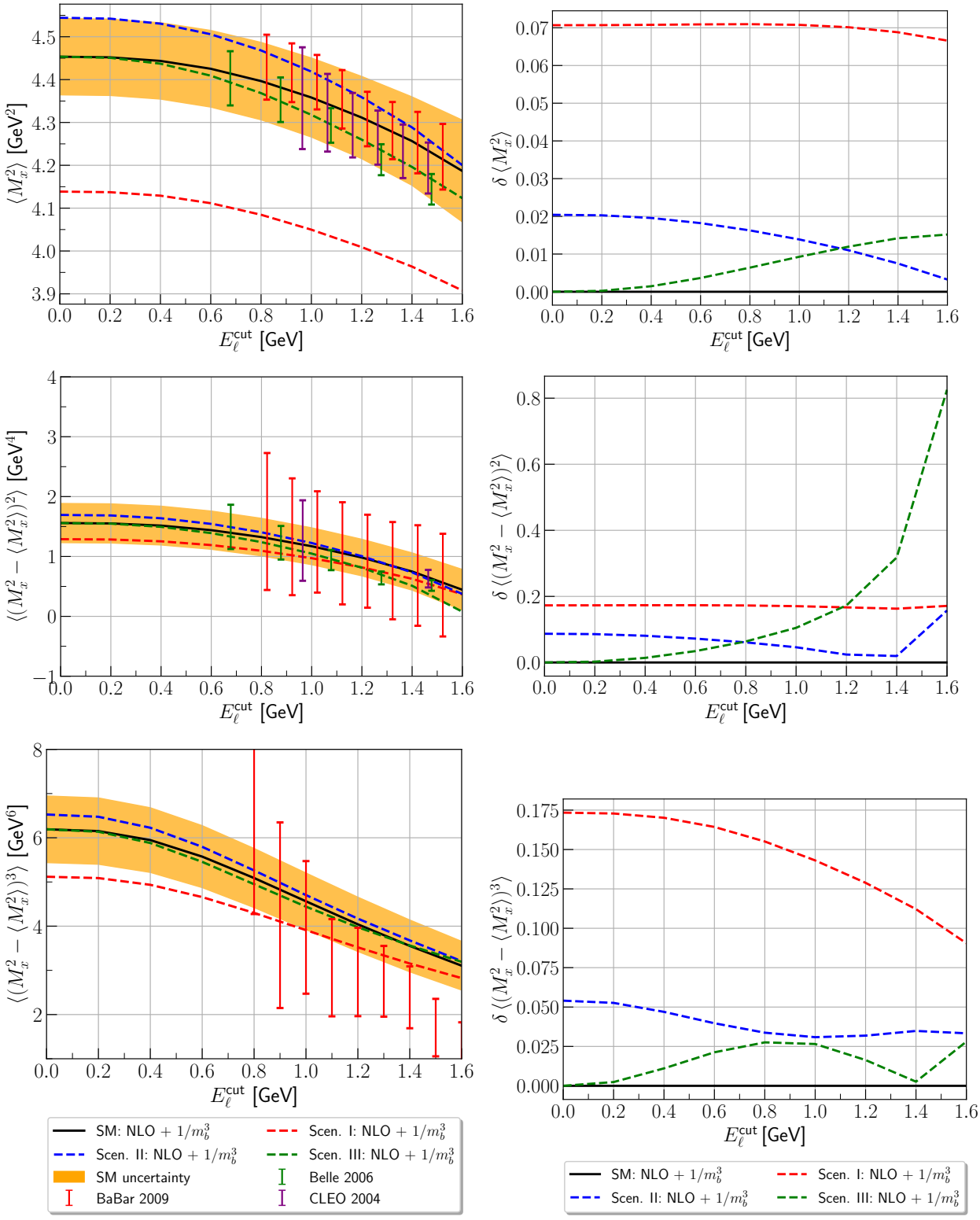

Figure 8.5: Hadronic invariant mass moments for the $B \to X_c \ell \bar{\nu}_\ell$ decay different NP scenarios (see Tab. 8.2). The experimental values of BaBar is taken from [202], CLEO [200], Belle [201].

	$\mathcal{B}(B \to X_c \ell \bar{\nu})$ in %
$\xi_{\rm SM}$	$12.983\vert_{\rm LO} - 0.962\vert_{\rm pow} - \left(\frac{\alpha_s}{\pi}\right) 16.101$
$\xi_{\rm NP}^{\langle V_R, V_R\rangle}$	$12.983\vert_{\rm LO} - 0.962\vert_{\rm pow} - \left(\frac{\alpha_s}{\pi}\right) 16.101$
$\xi_{\rm NP}^{\langle S_L, S_L\rangle}$	$3.245\vert_{\rm LO} + 0.067\vert_{\rm pow} + \left(\frac{\alpha_s}{\pi}\right) 2.783$
$\xi_{\rm NP}^{\langle S_R, S_R\rangle}$	$3.245\vert_{\rm LO} + 0.067\vert_{\rm pow} + \left(\frac{\alpha_s}{\pi}\right) 2.783$
$\xi_{\rm NP}^{\langle T, T\rangle}$	$155.802\vert_{\rm LO} - 16.493\vert_{\rm pow} - \left(\frac{\alpha_s}{\pi}\right) 163.665$
$\xi_{\rm NP}^{\langle V_L, V_R\rangle}$	$-8.453\vert_{\rm LO} + 1.332\vert_{\rm pow} + \left(\frac{\alpha_s}{\pi}\right) 13.375$
$\xi_{\rm NP}^{\langle S_L, S_R\rangle}$	$4.226\vert_{\rm LO} + 0.380\vert_{\rm pow} + \left(\frac{\alpha_s}{\pi}\right) 4.550$
$\xi_{\rm NP}^{\langle S_L, T\rangle}$	0
$\xi_{\rm NP}^{\langle S_R, T\rangle}$	0

Table 8.3: Numerical values of the parameters for the branching ratio without lepton energy cut for fixed B meson lifetime.

the HQE parameters from [15]. We observed the q^2 moments are most sensitive to Scen. I, while Scen. III has basically no effect. This is because for this scenario there is a cancellation between the Wilson coefficients, rendering the effect almost unobservable. For smaller values of C_{V_L}, there is an effect on the moments and in fact the q^2 moments can put rather strong constraints as seen in Fig. 8.3.

8.3.2 Lepton Flavor Universality Ratios

In order to study NP in Lepton Flavor Universality Ratios of light leptons, we give the analytic expression for the total rate in Appendix A.

For completeness, we also give the numerical coefficients including NLO correction. Writing the branching ratio in terms of ξ_i as in (8.26), with the only difference that the $\xi_{\rm SM}$ term gets multiplied with $|1 + C_{V_L}|^2$, we find the coefficients listed in Table 8.3. We used the iputs in Table 8.1 and a fixed value for the B meson lifetime $\tau_B = 1.579$ ps [205] and $|V_{cb}| = (42.16 \pm 0.51) \cdot 10^{-3}$ [14]. However, we note that NP would also affect the total lifetime of the B meson.

The expressions in the Appendix and our numerical results can be used to study ratios of electron versus muon rates under the assumption of lepton-flavour universality violating new physics. Note that a lepton-flavour universal and diagonal NP effect in C_L can in principle be absorbed by a shift in V_{cb}. Recently, the SM predictions for lepton-flavour universality ratios were studied [4]. Because the current data (see for example the q^2 moments split up for electron and muon contributions in [138]) do not indicate any deviation from lepton universality in the charged light modes, we do not study these effects here further.

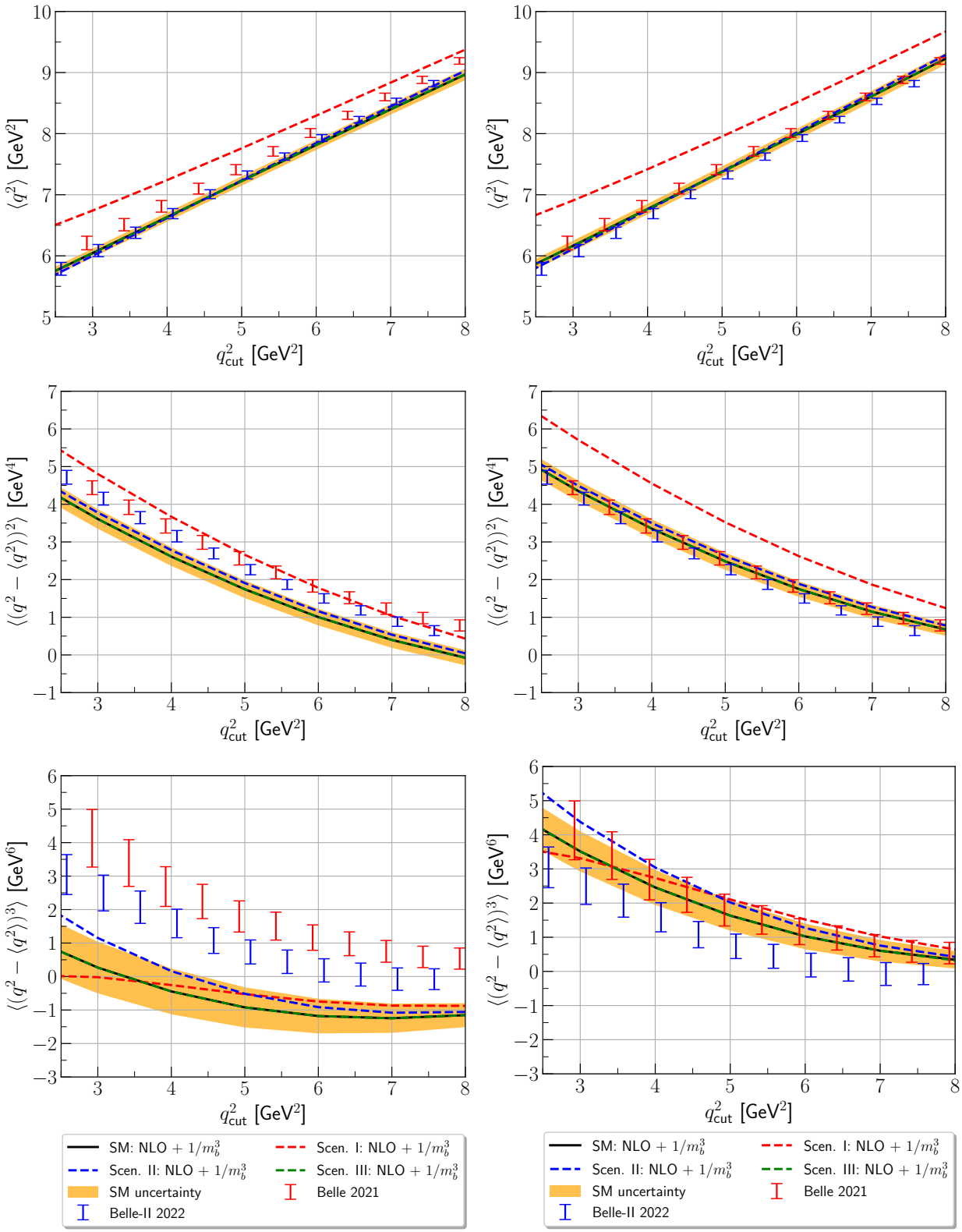

Figure 8.6: Dilepton invariant mass moments (q^2) for the $B \to X_c \ell \bar{\nu}_\ell$ decay in comparison with Belle [138] and Belle II data [204]. (Left) Using the inputs in Table 8.1 from [14](Right) using the inputs from [15].

8.3.3 HQE parameters versus NP

The HQE parameters are extracted from moments of the $b \to c$ spectrum under the assumption of the SM. However, it can be that NP mimics the effect of the HQE parameters shifting the spectrum up or down. In fact, Fig. 8.6 shows that shifting ρ_D^3 seems to be able to mimic the effect that NP may have on the spectrum. It would therefore be interesting to perform a full analysis of the moments including NP. Such an analysis lies beyond the scope of the current paper. However, we can illustrate the possible effect with a simplified toy fit. To this extend, we generate pseudo data points for the three NP scenarios in Table 8.2 for lepton energy and hadronic invariant mass moments at different lepton energy cuts as well as q^2 moments with $q^2_{\rm cut}$. For this, we use the HQE parameters in Table 8.1. We generate 9 data points per scenario: the first, second and third central moments with $E_\ell^{\rm cut} = 1.0$ GeV for the lepton energy and hadronic invariant mass moments and with $q^2_{\rm cut} = 4$ GeV^2 for q^2 moments. For the uncertainty on these points, we vary the contribution of ρ_D^3 by 30%, μ_G^2 by 20% and α_s between its value at $\mu = m_b/2$ and $\mu = m_b$, based on [14, 15]. As this render the uncertainty for the lepton energy moments rather small, we add an additional uncertainty based on the current experimental uncertainty. In addition, we also include the current experimental uncertainty for the third q^2 and M_X moments as these are rather large.

In principle, these pseudo data points can then be used to fit for the HQE parameters $\mu_G^2, \mu_\pi^2, \rho_{LS}^3, \rho_D^3$ using the SM expressions. In this way, our toy fit mimics a situation that may happen in reality: i.e. NP is present but the extraction of HQE parameters is done assuming the SM. We observe that for the three NP scenarios in Table 8.2, our simple toy fit yields large χ^2. The reason for this is that it is challenging to accommodate the third moments, which are sensitive to NP, and first lepton energy moments, which drives the fit due to its small uncertainty, at the same time. Turning the argumentation around this may indicate that a full simultaneous fit of the HQE parameters and NP parameters would give rather good constraints on NP. In this endeavour, it seems crucial to improve the experimental inputs especially on the third moments.

Finally, we may also consider a more realistic scenario taken from the analysis of [177]: $C_T = 0.05$ and $C_{S_L} = -0.5$. Assuming no correlations between the pseudo data points, we obtain a $\chi^2/d.o.f. \simeq 2.4$ and

$$\mu_G^2|_{\rm toy} = 0.40 \text{ GeV}^2, \;\; \mu_\pi^2|_{\rm toy} = 0.45 \text{ GeV}^2, \;\; \rho_{LS}^3|_{\rm toy} = 0.09 \text{ GeV}^3, \;\; \rho_D^3|_{\rm toy} = 0.11 \text{ GeV}^3. \tag{8.30}$$

Comparing with the values in Table 8.1, we find $1-2\sigma$ shifts, with a rather poor fit quality. We note that this toy fit merely serves to illustrate how NP could be hidden in the HQE extraction, because the fit is rather flexible in accounting for such variations. Strong conclusions should not be made from this fit, except that it may be worth performing a full analysis on data. On the other hand, we also note that this may be challenging due to the large number of extra parameters.

8.4 Forward-backward asymmetry

In this section, we consider the forward-backward asymmetry discussed in [82] and more recently in [140]. The asymmetry is defined as

$$A_{FB} \equiv \frac{\displaystyle\int_{-1}^{0} \mathrm{d}z \frac{\mathrm{d}\Gamma}{\mathrm{d}z} - \int_{0}^{1} \mathrm{d}z \frac{\mathrm{d}\Gamma}{\mathrm{d}z}}{\displaystyle\int_{-1}^{1} \mathrm{d}z \frac{\mathrm{d}\Gamma}{\mathrm{d}z}} \,, \tag{8.31}$$

where

$$z \equiv \cos\theta = \frac{v \cdot p_{\bar{\nu}_\ell} - v \cdot p_\ell}{\sqrt{(v \cdot q)^2 - q^2}} \,, \tag{8.32}$$

and θ is the angle between spacial momenta of the lepton and the B meson in the rest-frame of the dilepton pair.

As discussed in [140], including a lepton energy cut E_ℓ^{cut} in the A_{FB} definition leads to a cusp in the differential spectrum in the variable z, which can be problematic in experimental analysis. To circumvent this issue, Ref. [140] proposed to study A_{FB} with a minimum cut on q^2 instead of E_ℓ. We therefore consider only q^2 cuts, which also considerably simplifies the calculation. We refer to [140] for details of the calculation.

Writing our results as in (8.26), we find the ξ's listed in Table 8.4. We consider for the first time the α_s-corrections, both for the SM and for NP scenarios. In the upper part of Fig. 8.7, we show the differential distribution in z normalized to $1/\Gamma_0$ as defined in Appendix A for the SM and our three NP scenarios in Table 8.2. Our normalization, i.e. using only $1/\Gamma_0$, differs from that used by [82,140], but our results for the SM are in agreement. In the lower panel of Fig. 8.7, we show the prediction for A_{FB} as a function of q^2_{cut} where we plot the different SM contributions for illustration. The plots shows that forward-backward asymmetry and the differential distribution are sensitive the NP contributions and can distinguish among our three different scenarios. The forward-backward asymmetry has not been measured so far, but our analysis shows the potential for understanding the SM and possibly to constrain NP contributions.

	$A_{FB} \cdot 10^{-2}$
$\xi_{\rm SM}$	$24.603\vert_{\rm LO} - 2.928\vert_{\rm pow} - \left(\frac{\alpha_s}{\pi}\right) 6.63$
$\xi_{\rm NP}^{\langle V_R, V_R\rangle}$	$-25.387\vert_{\rm LO} + 0.769\vert_{\rm pow} + \left(\frac{\alpha_s}{\pi}\right) 4.47$
$\xi_{\rm NP}^{\langle S_L, S_L\rangle}$	$-8.683\vert_{\rm LO} - 0.333\vert_{\rm pow} - \left(\frac{\alpha_s}{\pi}\right) 15.91$
$\xi_{\rm NP}^{\langle S_R, S_R\rangle}$	$-8.683\vert_{\rm LO} - 0.333\vert_{\rm pow} - \left(\frac{\alpha_s}{\pi}\right) 15.91$
$\xi_{\rm NP}^{\langle T, T\rangle}$	$-254.730\vert_{\rm LO} + 40.911\vert_{\rm pow} + \left(\frac{\alpha_s}{\pi}\right) 2.13$
$\xi_{\rm NP}^{\langle V_L, V_R\rangle}$	$-24.208\vert_{\rm LO} + 4.025\vert_{\rm pow} + \left(\frac{\alpha_s}{\pi}\right) 7.53$
$\xi_{\rm NP}^{\langle S_L, S_R\rangle}$	$12.104\vert_{\rm LO} - 1.415\vert_{\rm pow} - \left(\frac{\alpha_s}{\pi}\right) 24.67$
$\xi_{\rm NP}^{\langle S_L, T\rangle}$	$49.207\vert_{\rm LO} + 0.954\vert_{\rm pow} + \left(\frac{\alpha_s}{\pi}\right) 51.17$
$\xi_{\rm NP}^{\langle S_R, T\rangle}$	$2.20\vert_{\rm pow}$

Table 8.4: Numerical values of the parameters for the A_{FB} given in Eq. (8.26). We consider $q^2_{\rm cut} = 4$ GeV^2.

8.5 Conclusion

We investigated New Physics effects on the semileptonic channel $B \to X_c \ell \bar{\nu}_\ell$. For the first time, we compute power-corrections up to $\mathcal{O}(1/m_b^3)$ and α_s-corrections for the full basis of the New Physics operators in the WET over the full differential decay width. These corrections are necessary to properly describe the dominant NP contributions to central moments of dilepton invariant mass q^2 and hadronic invariant mass M_X^2.

We compared SM predictions, using HQE parameters obtained from experimental data, and experimental measurements to the moments of lepton energy, hadronic invariant mass and dilepton momentum for different toy New Physics scenarios. In addition, we also computed the forward-backward asymmetry. The main goal of this work is to pave the way for a global fit analysis, which includes the full base of NP operators. To further constrain such global fit, one may take advantage of lattice results for the HQE parameters, extracted from meson mass calculations at different quark mass values [206], and scattering matrix for $B \to X_c \ell \bar{\nu}_\ell$ [207, 208]. Such results, even if preliminary, could enhance the predictive power of the HQE by better assessing the non-perturbative inputs. We aim to perform such a fit using the EOS software [180].

Acknowledgements

We thank T. Mannel and M. Bordone for discussion and correspondence. This research was supported by the Deutsche Forschungsgemeinschaft (DFG, German Research Foundation) under grant 396021762 - TRR 257.

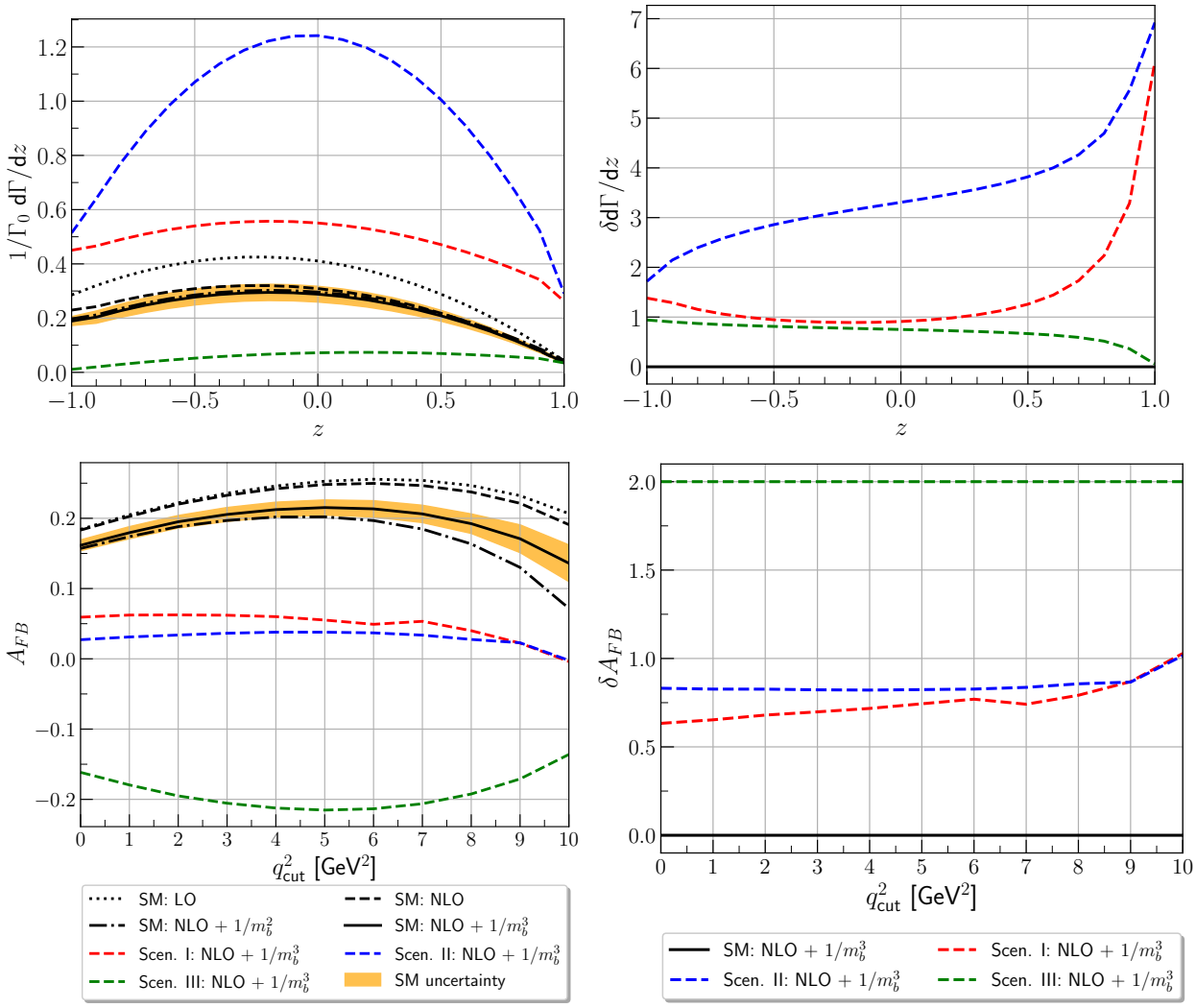

Figure 8.7: (Upper part) The differential rate for $B \to X_c \ell \bar{\nu}_\ell$ as a function of z without lepton energy cut and relative size of the NP scenarios w.r.t. the SM prediction. (Lower part) Forward-backward asymmetry as a function of the q^2 cut for the three NP scenarios in Table 8.2 and their relative size w.r.t. the SM.

Appendix A NP contributions to the total rate

We decompose the prediction of the total rate in two parts:

$$\Gamma(B \to X_c \ell \bar{\nu}) = \Gamma_0 \left(\Gamma^{\text{LO}}_{\text{NP}}(B \to X_c \ell \bar{\nu}) + \Gamma^{\text{Pow}}_{\text{NP}}(B \to X_c \ell \bar{\nu}) \right) \tag{8.33}$$

where

$$\Gamma_0 = \frac{G_F^2 |V_{cb}|^2 m_b^5}{192\pi^3} (1 + A_{\text{ew}}) \tag{8.34}$$

and $A_{\rm ew} = 0.014$ [149]. The LO result in the free quark approximation is given by

$$\Gamma^{\rm LO}_{\rm NP}(B \to X_c \ell \bar{\nu}) = \Gamma^{\rm LO}_{\rm SM}(B \to X_c \ell \bar{\nu}) \left(|1 + C_{V_L}|^2 + |C_{V_R}|^2 + \frac{1}{4} \left(|C_{S_L}|^2 + |C_{S_R}|^2 \right) + 12 |C_T|^2 \right)$$
$$+ \Gamma^{\rm LO}_{\rm mix}(B \to X_c \ell \bar{\nu}) \left({\rm Re}((1 + C_{V_L}) C_{V_R}) - \frac{1}{2} {\rm Re}(C_{S_L} C_{S_R}) \right) , \quad (8.35)$$

with

$$\Gamma^{\rm LO}_{\rm SM} = (1 - 8\rho - 12\rho^2 \log(\rho) + 8\rho^3 - \rho^4) , \quad (8.36)$$

$$\Gamma^{\rm LO}_{\rm mix} = -4\sqrt{\rho} \, (1 + 9\rho + 6\rho(1 + \rho) \log(\rho) - 9\rho^2 - \rho^3) . \quad (8.37)$$

Our result agrees with the leading-order (LO) results from [177]. The contribution from the power corrections is

$$\Gamma^{\rm Pow}_{\rm NP}(B \to X_c \ell \bar{\nu}) = \frac{\mu_\pi^2}{m_b^2} \Gamma^{\mu_\pi^2}_{\rm SM} \Big(|1 + C_{V_L}|^2 + |C_{V_R}|^2 + \frac{1}{4} (|C_{S_L}|^2 + |C_{S_R}|^2) + 12 |C_T|^2$$
$$- 2\sqrt{\rho} \Big(\rho^3 + 9\rho^2 - 9\rho - 6(\rho + 1)\rho \log(\rho) - 1 \Big) \Big({\rm Re}((1 + C_{V_L}) C^*_{V_R})$$
$$- \frac{1}{2} {\rm Re}(C_{S_L} C^*_{S_R}) \Big) \Big) + \left(\frac{\mu_G^2}{m_b^2} - \frac{\rho_{LS}^3}{m_b^3} \right) \left(\Gamma^{\mu_G^2}_{\rm SM} \left(|1 + C_{V_L}|^2 + |C_{V_R}|^2 \right) \right.$$
$$- \frac{1}{8} \Big(5\rho^4 - 32\rho^3 + 72\rho^2 - 32\rho + 12(\rho - 4)\rho \log(\rho) - 13 \Big) (|C_{S_L}|^2 + |C_{S_R}|^2)$$
$$- 2 \Big(15\rho^4 - 64\rho^3 + 24\rho^2 + 12(3\rho + 4)\rho \log(\rho) + 25 \Big) |C_T|^2$$
$$+ \frac{2\sqrt{\rho}}{3} \Big(13\rho^3 - 27\rho^2 - 6(3\rho^2 - 3\rho + 2) \log(\rho) + 27\rho - 13 \Big) {\rm Re}((1 + C_{V_L}) C^*_{V_R})$$
$$- 3\sqrt{\rho} \Big(\rho^3 - 3\rho^2 - 2(\rho^2 - 5\rho - 2) \log(\rho) - 9\rho + 11 \Big) {\rm Re}(C_{S_L} C^*_{S_R}) \Big)$$
$$+ \frac{\rho_D^3}{m_b^3} \left(\Gamma^{\rho_D^3}_{\rm SM} \left(|1 + C_{V_L}|^2 + |C_{V_R}|^2 \right) + \frac{1}{24} \Big(- 5\rho^4 - 8\rho^3 + 12(3\rho^2 + 8\rho + 8) \log(\rho) \right.$$
$$\left. - 184\rho + 197 \Big) \left(|C_{S_L}|^2 + |C_{S_R}|^2 \right) + 2 \Big(- 5\rho^4 - 8\rho^3 + 32\rho^2 + 4(9\rho^2 - 8\rho + 8) \log(\rho) \right.$$
$$\left. - 56\rho + 37 \Big) |C_T|^2 + 2 \left(\rho^3 - 15\rho^2 + 6(\rho^2 - \rho - 2) \log(\rho) + 39\rho - 25 \right) \right.$$
$$\times {\rm Re}((1 + C_{V_L}) C^*_{V_R}) + \frac{2\sqrt{\rho}}{6} \Big(\rho^3 + 9\rho^2 + (-18\rho^2 + 90\rho + 60) \log(\rho)$$
$$\left. - 153\rho + 143 \Big) {\rm Re}(C_{S_L} C^*_{S_R}) \Big) \quad (8.38)$$

with

$$\Gamma_{\rm SM}^{\mu_\pi^2} = -\frac{1}{2}\Gamma_{\rm SM}^{\rm LO}\,, \tag{8.39}$$

$$\Gamma_{\rm SM}^{\mu_G^2} = -\frac{1}{2}(5\rho^4 - 24\rho^3 + 24\rho^2 + 12\rho^2\log(\rho) - 8\rho + 3)\,, \tag{8.40}$$

$$\Gamma_{\rm SM}^{\rho_{LS}^3} = \frac{1}{2}\left(5\rho^4 - 24\rho^3 + 24\rho^2 + 12\rho^2\log(\rho) - 8\rho + 3\right)\,, \tag{8.41}$$

$$\Gamma_{\rm SM}^{\rho_D^3} = \frac{1}{6}\left(-5\rho^4 - 8\rho^3 + 24\rho^2 + 12(3\rho^2+4)\log(\rho) - 88\rho + 77\right)\,. \tag{8.42}$$

For the power-corrections $\mathcal{O}(1/m_b^2)$ of $(1+C_{V_L})C_{V_R}$ our result agrees with [179] $c_L c_R$ term.

Appendix B NP effects on the moments

In this Appendix, we list the coefficients ξ defined in 8.26. We categorize the contributions of leading-order, power-corrections and α_s corrections.

	$\langle E_\ell \rangle \cdot 10^{-2}$	$\langle (E_\ell - \langle E_\ell \rangle)^2 \rangle \cdot 10^{-2}$	$\langle (E_\ell - \langle E_\ell \rangle)^3 \rangle \cdot 10^{-3}$
$\xi_{\rm SM}$	$157.23\vert_{\rm LO} - 1.78\vert_{\rm pow} - \left(\frac{\alpha_s}{\pi}\right) 4.608$	$8.715\vert_{\rm LO} + 0.291\vert_{\rm pow} - \left(\frac{\alpha_s}{\pi}\right) 1.970$	$-3.076\vert_{\rm LO} + 3.399\vert_{\rm pow} + \left(\frac{\alpha_s}{\pi}\right) 14.388$
$\xi_{\rm NP}^{\langle V_R, V_R\rangle}$	$-10.00\vert_{\rm LO} + 1.63\vert_{\rm pow} + \left(\frac{\alpha_s}{\pi}\right) 1.172$	$0.188\vert_{\rm LO} - 0.242\vert_{\rm pow} + \left(\frac{\alpha_s}{\pi}\right) 0.531$	$9.394\vert_{\rm LO} - 1.555\vert_{\rm pow} - \left(\frac{\alpha_s}{\pi}\right) 5.711$
$\xi_{\rm NP}^{\langle S_L, S_L\rangle}$	$0.849\vert_{\rm pow} + \left(\frac{\alpha_s}{\pi}\right) 0.414$	$0.128\vert_{\rm pow} - \left(\frac{\alpha_s}{\pi}\right) 0.161$	$-0.712\vert_{\rm pow} + \left(\frac{\alpha_s}{\pi}\right) 0.0365$
$\xi_{\rm NP}^{\langle S_R, S_R\rangle}$	$0.849\vert_{\rm pow} + \left(\frac{\alpha_s}{\pi}\right) 0.414$	$0.128\vert_{\rm pow} - \left(\frac{\alpha_s}{\pi}\right) 0.161$	$-0.712\vert_{\rm pow} + \left(\frac{\alpha_s}{\pi}\right) 0.0365$
$\xi_{\rm NP}^{\langle T, T\rangle}$	$-77.960\vert_{\rm LO} + 9.734\vert_{\rm pow} + \left(\frac{\alpha_s}{\pi}\right) 15.260$	$0.023\vert_{\rm LO} - 1.120\vert_{\rm pow} + \left(\frac{\alpha_s}{\pi}\right) 6.887$	$71.831\vert_{\rm LO} - 7.041\vert_{\rm pow} - \left(\frac{\alpha_s}{\pi}\right) 49.633$
$\xi_{\rm NP}^{\langle V_L, V_R\rangle}$	$0.364\vert_{\rm LO} - 0.660\vert_{\rm pow} + \left(\frac{\alpha_s}{\pi}\right) 2.864$	$-0.278\vert_{\rm LO} - 0.119\vert_{\rm pow} - \left(\frac{\alpha_s}{\pi}\right) 0.462$	$-0.572\vert_{\rm LO} - 0.266\vert_{\rm pow} - \left(\frac{\alpha_s}{\pi}\right) 0.672$
$\xi_{\rm NP}^{\langle S_L, S_R\rangle}$	$0.182\vert_{\rm LO} + 1.503\vert_{\rm pow} + \left(\frac{\alpha_s}{\pi}\right) 0.553$	$-0.139\vert_{\rm LO} + 0.234\vert_{\rm pow} - \left(\frac{\alpha_s}{\pi}\right) 0.657$	$-0.286\vert_{\rm LO} - 1.208\vert_{\rm pow} + \left(\frac{\alpha_s}{\pi}\right) 0.315$
$\xi_{\rm NP}^{\langle S_L, T\rangle}$	$9.745\vert_{\rm LO} + 0.575\vert_{\rm pow} + \left(\frac{\alpha_s}{\pi}\right) 9.652$	$-0.0029\vert_{\rm LO} + 0.739\vert_{\rm pow} - \left(\frac{\alpha_s}{\pi}\right) 0.279$	$-8.978\vert_{\rm LO} + 1.011\vert_{\rm pow} - \left(\frac{\alpha_s}{\pi}\right) 5.528$
$\xi_{\rm NP}^{\langle S_R, T\rangle}$	$0.624\vert_{\rm pow}$	$0.348\vert_{\rm pow}$	$0.780\vert_{\rm pow}$

Table 8.5: Numerical values of the coefficients ξ in Eq. 8.26 for the lepton energy moments. We consider $E_\ell^{\rm cut} = 1$ GeV.

	$\langle M_X \rangle \cdot 10^{-1}$	$\langle (M_X - \langle M_X \rangle)^2 \rangle \cdot 10^{-1}$	$\langle (M_X - \langle M_X \rangle)^3 \rangle \cdot 10^{-1}$
$\xi_{\rm SM}$	$43.016\vert_{\rm LO} + 0.0648\vert_{\rm pow} + (\frac{\alpha_s}{\pi}) 7.219$	$2.232\vert_{\rm LO} + 7.417\vert_{\rm pow} + (\frac{\alpha_s}{\pi}) 29.666$	$-0.211\vert_{\rm LO} + 49.523\vert_{\rm pow} - (\frac{\alpha_s}{\pi}) 53.141$
$\xi_{\rm NP}^{\langle V_R, V_R\rangle}$	$1.221\vert_{\rm LO} - 1.680\vert_{\rm pow} - (\frac{\alpha_s}{\pi}) 0.925$	$-0.554\vert_{\rm LO} + 3.466\vert_{\rm pow} - (\frac{\alpha_s}{\pi}) 0.747$	$0.019\vert_{\rm LO} + 1.586\vert_{\rm pow} - (\frac{\alpha_s}{\pi}) 11.023$
$\xi_{\rm NP}^{\langle S_L, S_L\rangle}$	$-0.600\vert_{\rm LO} - 0.7916\vert_{\rm pow} - (\frac{\alpha_s}{\pi}) 2.041$	$0.0421\vert_{\rm LO} - 0.853\vert_{\rm pow} - (\frac{\alpha_s}{\pi}) 0.947$	$0.130\vert_{\rm LO} - 2.751\vert_{\rm pow} - (\frac{\alpha_s}{\pi}) 5.180$
$\xi_{\rm NP}^{\langle S_R, S_R\rangle}$	$-0.600\vert_{\rm LO} - 0.7916\vert_{\rm pow} - (\frac{\alpha_s}{\pi}) 2.041$	$0.042\vert_{\rm LO} - 0.853\vert_{\rm pow} - (\frac{\alpha_s}{\pi}) 0.947$	$0.130\vert_{\rm LO} - 2.751\vert_{\rm pow} - (\frac{\alpha_s}{\pi}) 5.180$
$\xi_{\rm NP}^{\langle T, T\rangle}$	$7.911\vert_{\rm LO} + 7.594\vert_{\rm pow} + (\frac{\alpha_s}{\pi}) 1.926$	$0.492\vert_{\rm LO} + 12.059\vert_{\rm pow} + (\frac{\alpha_s}{\pi}) 10.068$	$-1.620\vert_{\rm LO} + 39.365\vert_{\rm pow} + (\frac{\alpha_s}{\pi}) 20.575$
$\xi_{\rm NP}^{\langle V_L, V_R\rangle}$	$-2.134\vert_{\rm LO} + 2.182\vert_{\rm pow} - (\frac{\alpha_s}{\pi}) 0.274$	$0.364\vert_{\rm LO} - 5.449\vert_{\rm pow} - (\frac{\alpha_s}{\pi}) 0.137$	$0.404\vert_{\rm LO} - 8.685\vert_{\rm pow} + (\frac{\alpha_s}{\pi}) 5.821$
$\xi_{\rm NP}^{\langle S_L, S_R\rangle}$	$-1.067\vert_{\rm LO} - 1.616\vert_{\rm pow} - (\frac{\alpha_s}{\pi}) 3.189$	$0.182\vert_{\rm LO} - 0.811\vert_{\rm pow} - (\frac{\alpha_s}{\pi}) 1.786$	$0.202\vert_{\rm LO} - 4.346\vert_{\rm pow} - (\frac{\alpha_s}{\pi}) 9.340$
$\xi_{\rm NP}^{\langle S_L, T\rangle}$	$0.213\vert_{\rm LO} - 0.215\vert_{\rm pow} + (\frac{\alpha_s}{\pi}) 0.890$	$-0.145\vert_{\rm LO} + 1.040\vert_{\rm pow} + (\frac{\alpha_s}{\pi}) 0.018$	$-0.058\vert_{\rm LO} + 0.656\vert_{\rm pow} + (\frac{\alpha_s}{\pi}) 3.876$
$\xi_{\rm NP}^{\langle S_R, T\rangle}$	$-0.081\vert_{\rm pow}$	$0.327\vert_{\rm pow}$	$0.193\vert_{\rm pow}$

Table 8.6: Numerical values of the coefficients ξ in 8.26 for the hadronic invariant mass moments. We consider $E_\ell^{\rm cut} = 1$ GeV.

	$\langle q^2 \rangle$	$\langle (q^2 - \langle q^2 \rangle)^2 \rangle$	$\langle (q^2 - \langle q^2 \rangle)^3 \rangle$
$\xi_{\rm SM}$	$7.072\vert_{\rm LO} - 0.449\vert_{\rm pow} + (\frac{\alpha_s}{\pi})\, 0.168$	$4.278\vert_{\rm LO} - 1.727\vert_{\rm pow} + (\frac{\alpha_s}{\pi})\, 0.854$	$3.773\vert_{\rm LO} - 4.695\vert_{\rm pow} + (\frac{\alpha_s}{\pi})\, 6.879$
$\xi_{\rm NP}^{\langle V_R, V_R \rangle}$	$-0.681\vert_{\rm LO} + 0.138\vert_{\rm pow} + (\frac{\alpha_s}{\pi})\, 0.121$	$-1.231\vert_{\rm LO} + 0.429\vert_{\rm pow} + (\frac{\alpha_s}{\pi})\, 1.467$	$0.486\vert_{\rm LO} - 0.136\vert_{\rm pow} + (\frac{\alpha_s}{\pi})\, 5.182$
$\xi_{\rm NP}^{\langle S_L, S_L \rangle}$	$0.135\vert_{\rm LO} + 0.182\vert_{\rm pow} + (\frac{\alpha_s}{\pi})\, 0.373$	$0.099\vert_{\rm LO} + 0.592\vert_{\rm pow} + (\frac{\alpha_s}{\pi})\, 0.379$	$-0.512\vert_{\rm LO} + 1.236\vert_{\rm pow} - (\frac{\alpha_s}{\pi})\, 0.789$
$\xi_{\rm NP}^{\langle S_R, S_R \rangle}$	$0.135\vert_{\rm LO} + 0.182\vert_{\rm pow} + (\frac{\alpha_s}{\pi})\, 0.373$	$0.099\vert_{\rm LO} + 0.592\vert_{\rm pow} + (\frac{\alpha_s}{\pi})\, 0.379$	$-0.512\vert_{\rm LO} + 1.236\vert_{\rm pow} - (\frac{\alpha_s}{\pi})\, 0.789$
$\xi_{\rm NP}^{\langle T, T \rangle}$	$-2.174\vert_{\rm LO} + 0.510\vert_{\rm pow} + (\frac{\alpha_s}{\pi})\, 0.535$	$-1.591\vert_{\rm LO} + 1.290\vert_{\rm pow} - (\frac{\alpha_s}{\pi})\, 0.275$	$8.200\vert_{\rm LO} - 1.716\vert_{\rm pow} - (\frac{\alpha_s}{\pi})\, 10.168$
$\xi_{\rm NP}^{\langle V_L, V_R \rangle}$	$0.692\vert_{\rm LO} - 0.108\vert_{\rm pow} - (\frac{\alpha_s}{\pi})\, 0.090$	$0.765\vert_{\rm LO} - 0.248\vert_{\rm pow} - (\frac{\alpha_s}{\pi})\, 1.327$	$-2.109\vert_{\rm LO} + 0.814\vert_{\rm pow} - (\frac{\alpha_s}{\pi})\, 2.351$
$\xi_{\rm NP}^{\langle S_L, S_R \rangle}$	$0.346\vert_{\rm LO} + 0.359\vert_{\rm pow} + (\frac{\alpha_s}{\pi})\, 0.759$	$0.382\vert_{\rm LO} + 1.152\vert_{\rm pow} + (\frac{\alpha_s}{\pi})\, 0.557$	$-1.05\vert_{\rm LO} + 2.492\vert_{\rm pow} - (\frac{\alpha_s}{\pi})\, 2.439$
$\xi_{\rm NP}^{\langle S_L, T \rangle}$	0	0	0
$\xi_{\rm NP}^{\langle S_R, T \rangle}$	0	0	0

Table 8.7: Numerical values of the coefficients ξ in Eq. 8.26 for the q^2 moments. We consider $q^2_{\rm cut} = 4$ GeV^2.

Chapter 9

Project IV: Lepton flavour violation in rare Λ_b decays

Published as an article in:
M. Bordone, M. Rahimi, K. K. Vos, Eur.Phys.J.C 81 (2021) 8, 756 [3].

Contributions of the authors to the article.
M. Rahimi contributed to the draft and did the analytical derivation and numerical analysis of all expressions obtained in the article. Dr. Bordone and Prof. Dr. Vos performed an independent numerical study and worked on the draft.

Abstract: Lepton flavour violation (LFV) naturally occurs in many new physics models, specifically in those explaining the B anomalies. While LFV has already been studied for mesonic decays, it is important to consider also baryonic decays mediated by the same quark transition. In this paper, we study LFV in the baryonic $\Lambda_b \to \Lambda \ell_1 \ell_2$ using for the first time a full basis of New Physics operators. We present expected bounds on the branching ratio in a model-independent framework and using two specific new physics models. Finally, we point out the interplay and orthogonality between the baryonic and mesonic LFV searches.

9.1 Introduction

The incredible joint theoretical and experimental effort carried out in the last years allows us to probe the Standard Model (SM) of particle physics with an unprecedented precision. This brought to light some deviations between theoretical predictions and experimental measurements in semileptonic B meson decays [209–223]. These discrepancies, the so-called B anomalies, hint at Lepton Flavour Universality (LFU) violation. This is quite surprising, as LFU is one of the foundation of the SM.

The B anomalies can be split into two classes: *i*) deviations in μ/e universality in $b \to s\ell^+\ell^-$ and *ii*) deviations in τ vs. light leptons universality in the $b \to c\ell\bar{\nu}$ transitions. These exciting findings may indicate the presence of New Physics (NP) particles, and have inspired a plethora of theoretical and experimental work. The NP explanations for B anomalies span a broad class of new heavy particles, from vectors to scalars states [224–268]. However, a common feature in all of these models is the prediction of sizeable effects for Lepton Flavour Violating (LFV) B, τ and μ decays. Current upper bounds on these modes largely constrain the allowed parameter space for NP models, and upcoming experimental analyses will be fundamental to corroborate or falsify these NP hypotheses.

When searching for LFV decays mediated by $b \to s\ell_1\ell_2$ transitions, it is crucial to consider both mesonic and baryonic decays. Although mediated by the same underlying partonic transition, these two types of decays provide orthogonal information on possible NP models. A striking example of this is the NP analysis of $\Lambda_b \to \Lambda\mu^+\mu^-$ decays [269], which shows that even though $B \to K\mu^+\mu^-$ angular distribution seems to be affected by some short-distance NP [270–273], the latter is not visible in the $\Lambda_b \to \Lambda\mu^+\mu^-$ angular observables. It is therefore natural to assume that $\Lambda_b \to \Lambda\ell_1^-\ell_2^+$ decays provide complementary information compared to their mesonic counterparts $B^+ \to K^+\ell_1\ell_2$ or $\bar{B}_s \to \ell_1\ell_2$ decays. More precisely, the spin structure of the $\Lambda_b \to \Lambda$ decays induces a richer set of hadronic matrix elements. Therefore, $\Lambda_b \to \Lambda$ decays probe different parameter space than their mesonic counter parts. In addition, the Λ_b baryon is copiously produced at LHCb and the dataset collected with Run 1 and Run 2 allow to make precision measurement of observables constructed from Λ_b decays (see e.g. [274]).

In this paper, we calculate for the first time the angular distribution of $\Lambda_b \to \Lambda\ell_1^-\ell_2^+$ decays using a full base of NP operators (partial results are available in [275, 276]). To achieve this, we use the decomposition of the $\Lambda_b \to \Lambda$ hadronic matrix elements in [277] and the lattice QCD determination of the corresponding form factors [278]. We then use model independent constraints to derive upper bounds for the branching ratio of $\Lambda_b \to \Lambda\ell_1^-\ell_2^+$ decays and specific models to provide predictions in a few scenarios [252, 253].

This paper is organised as follows: in Sect. 9.2 we highlight the main steps of our calculation and provide numerical results in a generic scenario. In Sect. 9.3 we use constraints on various LFV mesonic decays to put bounds on the branching ratio of

$\Lambda_b \to \Lambda \ell_1^- \ell_2^+$, for different choices of leptons in the final state and make predictions for specific models. We conclude in Sect. 9.4.

9.2 The angular distribution of $\Lambda_b \to \Lambda\, \ell_1^- \ell_2^+$

In this Section, we introduce the concepts that we need for the study of phenomenological aspects in Sect. 9.3.

We consider the following effective Hamiltonian for LFV $b \to s\ell_1^-\ell_2^+$ transitions:

$$\mathcal{H}_{\text{eff}} = -\frac{4G_F}{\sqrt{2}} V_{tb}V_{ts}^* \frac{\alpha_{\text{em}}}{4\pi} \sum_{i=9,10,S,P} \left(C_i^{\ell_1\ell_2}(\mu)\mathcal{O}_i^{\ell_1\ell_2}(\mu) + C_i^{\prime\ell_1\ell_2}(\mu)\mathcal{O}_i^{\prime\ell_1\ell_2}(\mu) \right), \quad (9.1)$$

where the relevant operators are defined by

$$\begin{aligned}
\mathcal{O}_9^{\ell_1\ell_2} &= (\bar{s}\gamma_\mu P_L b)(\bar{\ell}_1\gamma^\mu \ell_2), & \mathcal{O}_{10}^{\ell_1\ell_2} &= (\bar{s}\gamma_\mu P_L b)(\bar{\ell}_1\gamma^\mu\gamma^5 \ell_2), \\
\mathcal{O}_S^{\ell_1\ell_2} &= (\bar{s}P_R b)(\bar{\ell}_1 \ell_2), & \mathcal{O}_P^{\ell_1\ell_2} &= (\bar{s}P_R b)(\bar{\ell}_1\gamma_5 \ell_2)\,, \\
\mathcal{O}_T^{\ell_1\ell_2} &= (\bar{s}\sigma^{\mu\nu} b)(\bar{\ell}_1\sigma_{\mu\nu} \ell_2)\,, & \mathcal{O}_{T5}^{\ell_1\ell_2} &= (\bar{s}\sigma^{\mu\nu} b)(\bar{\ell}_1\sigma_{\mu\nu}\gamma_5 \ell_2)\,,
\end{aligned} \quad (9.2)$$

and the operators with flipped chirality $\mathcal{O}_i^{\prime\ell_1\ell_2}$ are obtained from $\mathcal{O}_i^{\ell_1\ell_2}$ by replacing $P_L \leftrightarrow P_R$, where $P_{L/R} = \frac{1}{2}(1 \mp \gamma_5)$. Notice that the operator $\mathcal{O}_7$:

$$\mathcal{O}_7 = \frac{m_b}{e}(\bar{s}\sigma_{\mu\nu}P_R b)F^{\mu\nu} \quad (9.3)$$

cannot generate LFV contributions due to the universality of electromagnetic interactions. We parametrise the hadronic matrix elements for $\Lambda_b(p, s_{\Lambda_b}) \to \Lambda(k, s_\Lambda)$

decays using an helicity decomposition [277–280]:

$$\begin{aligned}\langle\Lambda(k,s_\Lambda)|\bar{s}\,\gamma^\mu\,b|\Lambda_b(p,s_{\Lambda_b})\rangle = &+\bar{u}_\Lambda(k,s_\Lambda)\Bigg[f_0(q^2)\,(m_{\Lambda_b}-m_\Lambda)\frac{q^\mu}{q^2}\\ &+f_+(q^2)\frac{m_{\Lambda_b}+m_\Lambda}{s_+}\left(p^\mu+k^\mu-(m^2_{\Lambda_b}-m^2_\Lambda)\frac{q^\mu}{q^2}\right)\\ &+f_\perp(q^2)\left(\gamma^\mu-\frac{2m_\Lambda}{s_+}p^\mu-\frac{2m_{\Lambda_b}}{s_+}k^\mu\right)\Bigg]u_{\Lambda_b}(p,s_{\Lambda_b}),\end{aligned}\tag{9.4}$$

$$\begin{aligned}\langle\Lambda(k,s_\Lambda)|\bar{s}\,\gamma^\mu\gamma_5\,b|\Lambda_b(p,s_{\Lambda_b})\rangle = &-\bar{u}_\Lambda(k,s_\Lambda)\,\gamma_5\Bigg[g_0(q^2)\,(m_{\Lambda_b}+m_\Lambda)\frac{q^\mu}{q^2}\\ &+g_+(q^2)\frac{m_{\Lambda_b}-m_\Lambda}{s_-}\left(p^\mu+k^\mu-(m^2_{\Lambda_b}-m^2_\Lambda)\frac{q^\mu}{q^2}\right)\\ &+g_\perp(q^2)\left(\gamma^\mu+\frac{2m_\Lambda}{s_-}p^\mu-\frac{2m_{\Lambda_b}}{s_-}k^\mu\right)\Bigg]u_{\Lambda_b}(p,s_{\Lambda_b})\,,\end{aligned}\tag{9.5}$$

$$\begin{aligned}\langle\Lambda(k,s_\Lambda)|\,\bar{s}i\sigma^{\mu\nu}b\,|\Lambda_b(p,s_{\Lambda_b})\rangle = &+\bar{u}_\Lambda(k,s_\Lambda)\Bigg\{2h_+(q^2)\frac{p^\mu k^\nu-p^\nu k^\mu}{s_+}\\ &+h_\perp(q^2)\Big[\frac{m_{\Lambda_b}+m_\Lambda}{q^2}(q^\mu\gamma^\nu-q^\nu\gamma^\mu)-2\left(\frac{1}{q^2}+\frac{1}{s_+}\right)(p^\mu k^\nu-p^\nu k^\mu)\Big]\\ &+\widetilde{h}_+(q^2)\Big[i\sigma^{\mu\nu}-\frac{2}{s_-}(m_{\Lambda_b}(k^\mu\gamma^\nu-k^\nu\gamma^\mu)\\ &-m_\Lambda(p^\mu\gamma^\nu-p^\nu\gamma^\mu)+p^\mu k^\nu-p^\nu k^\mu)\Big]\\ &+\widetilde{h}_\perp(q^2)\frac{m_{\Lambda_b}-m_\Lambda}{q^2 s_-}\Big[(m^2_{\Lambda_b}-m^2_\Lambda-q^2)(\gamma^\mu p^\nu-\gamma^\nu p^\mu)\\ &-(m^2_{\Lambda_b}-m^2_\Lambda+q^2)(\gamma^\mu k^\nu-\gamma^\nu k^\mu)\\ &+2(m_{\Lambda_b}-m_\Lambda)(p^\mu k^\nu-p^\nu k^\mu)\Big]\Bigg\}u_{\Lambda_b}(p,s_{\Lambda_b})\end{aligned}\tag{9.6}$$

with $q = p - k$, $s_\pm = (m_{\Lambda_b} \pm m_\Lambda)^2 - q^2$, and s_{Λ_b} and s_Λ are the spin of the Λ_b and Λ baryons, respectively. Applying equations of motion to Eqs. (9.4)–(9.6), we obtain the following matrix elements for scalar and pseudoscalar operators:

$$\langle \Lambda(k, s_\Lambda)|\bar{s}\, b|\Lambda_b(p, s_{\Lambda_b})\rangle = \frac{m_{\Lambda_b} - m_\Lambda}{m_b(\mu) - m_s(\mu)} f_0 \bar{u}_\Lambda(k, s_\Lambda) u_{\Lambda_b}(p, s_{\Lambda_b})\,, \tag{9.7}$$

$$\langle \Lambda(k, s_\Lambda)|\bar{s}\gamma_5 b|\Lambda_b(p, s_{\Lambda_b})\rangle = \frac{m_{\Lambda_b} + m_\Lambda}{m_b(\mu) + m_s(\mu)} g_0 \bar{u}_\Lambda(k, s_\Lambda)\gamma_5 u_{\Lambda_b}(p, s_{\Lambda_b})\,, \tag{9.8}$$

which agree with the expressions in Ref. [277]. In the following, we take the masses in $\overline{\text{MS}}$ using $\overline{m}_b(\overline{m}_b) = 4180$ MeV [281] and $\overline{m}_s(\overline{m}_b) = 78\,\text{MeV}$ [282].

9.2.1 Differential decay width and numerical analysis

We decompose the spin-independent double-differential decay width as

$$\frac{1}{\Gamma^{(0)}} \frac{d\Gamma(\Lambda_b(p, s_{\Lambda_b}) \to \Lambda(k, s_\Lambda)\ell_1^-(p_1)\ell_2^+(p_2))}{d\cos\theta dq^2} = a + b\cos\theta_\ell + c\cos^2\theta_\ell\,, \tag{9.9}$$

with $\Gamma^{(0)} = \frac{\alpha_{\text{em}}^2 G_{\text{F}}^2 |V_{tb}V_{ts}^*|^2}{2048\pi^5 m_{\Lambda_b}^3 q^2}\sqrt{\lambda_H}\sqrt{\lambda_L}$. We define $\lambda_H \equiv \lambda(m_{\Lambda_b}^2, m_\Lambda^2, q^2)$ and $\lambda_L \equiv \lambda(q^2, m_{\ell_1}^2, m_{\ell_2}^2)$, where λ is the usual Källén function defined as $\lambda(a, b, c) = a^2 + b^2 + c^2 - 2a(b + c) - 2bc$. Here $\cos\theta_\ell$ is the helicity angle in the dilepton frame as defined in Appendix A. The coefficients a, b and c are one of the main result of this work and have been calculated using the operator base in Eq. (9.1) and the

decomposition for the hadronic matrix elements in Eqs. (9.4)–(9.6). We find:

$$
\begin{aligned}
a = &-\frac{1}{q^2}\Bigg\{|f_0|^2\frac{(m_{\Lambda_b}-m_\Lambda)^2}{q^2}s_+[|C_{10+}^{\ell_1\ell_2}|^2(m_{\ell_1}+m_{\ell_2})^2q_- + |C_{9+}^{\ell_1\ell_2}|^2(m_{\ell_1}-m_{\ell_2})^2q_+] \\
&+ |f_\perp|^2 s_-[|C_{10+}^{\ell_1\ell_2}|^2(\lambda_L+2q^2q_+) + |C_{9+}^{\ell_1\ell_2}|^2(\lambda_L+2q^2q_-)] \\
&+ |f_+|^2(m_{\Lambda_b}+m_\Lambda)^2 s_-[|C_{10+}^{\ell_1\ell_2}|^2\, q_+ + |C_{9+}^{\ell_1\ell_2}|^2\, q_-] \\
&+ |g_0|^2\frac{(m_{\Lambda_b}+m_\Lambda)^2}{q^2}s_-[|C_{10-}^{\ell_1\ell_2}|^2(m_{\ell_1}+m_{\ell_2})^2q_- + |C_{9-}^{\ell_1\ell_2}|^2(m_{\ell_1}-m_{\ell_2})^2q_+] \\
&+ |g_\perp|^2 s_+[|C_{10-}^{\ell_1\ell_2}|^2(\lambda_L+2q^2q_+) + |C_{9-}^{\ell_1\ell_2}|^2(\lambda_L+2q^2q_-)] \\
&+ |g_+|^2(m_{\Lambda_b}-m_\Lambda)^2 s_+[|C_{10-}^{\ell_1\ell_2}|^2 q_+ + |C_{9-}^{\ell_1\ell_2}|^2 q_-] \\
&+ 16|h_+|^2 s_-[(m_{\ell_1}+m_{\ell_2})^2q_-|C_T^{\ell_1\ell_2}|^2 + (m_{\ell_1}-m_{\ell_2})^2q_+|C_{T5}^{\ell_1\ell_2}|^2] \\
&+ 16|\tilde{h}_+|^2 s_+[(m_{\ell_1}-m_{\ell_2})^2q_-|C_T^{\ell_1\ell_2}|^2 + (m_{\ell_1}+m_{\ell_2})^2q_+|C_{T5}^{\ell_1\ell_2}|^2] \\
&+ 16|h_\perp|^2\frac{s_-}{q^2}(m_{\Lambda_b}+m_\Lambda)^2[q_-((m_{\ell_1}+m_{\ell_2})^2+q^2)|C_T^{\ell_1\ell_2}|^2 + q_+((m_{\ell_1}+m_{\ell_2})^2+q^2)|C_{T5}^{\ell_1\ell_2}|^2] \\
&+ 16|\tilde{h}_\perp|^2\frac{s_+}{q^2}(m_{\Lambda_b}-m_\Lambda)^2[q_+((m_{\ell_1}-m_{\ell_2})^2+q^2)|C_T^{\ell_1\ell_2}|^2 + q_-((m_{\ell_1}+m_{\ell_2})^2+q^2)|C_{T5}^{\ell_1\ell_2}|^2]\Bigg\} \\
&- (q_-|C_{P-}^{\ell_1\ell_2}|^2 + q_+|C_{S-}^{\ell_1\ell_2}|^2)\frac{s_-(m_{\Lambda_b}+m_\Lambda)^2}{(m_b+m_s)^2}|g_0|^2 - (q_-|C_{P+}^{\ell_1\ell_2}|^2 + q_+|C_{S+}^{\ell_1\ell_2}|^2)\frac{s_+(m_{\Lambda_b}-m_\Lambda)^2}{(m_b-m_s)^2}|f_0|^2 \\
&- \frac{2s_+}{q^2}\frac{(m_{\Lambda_b}-m_\Lambda)^2}{m_b-m_s}[\mathrm{Re}(C_{10+}^{\ell_1\ell_2}C_{P+}^{*\ell_1\ell_2})(m_{\ell_1}+m_{\ell_2})q_- + \mathrm{Re}(C_{9+}^{\ell_1\ell_2}C_{S+}^{*\ell_1\ell_2})(m_{\ell_1}-m_{\ell_2})q_+]|f_0|^2 \\
&- \frac{2s_-}{q^2}\frac{(m_{\Lambda_b}+m_\Lambda)^2}{m_b+m_s}[\mathrm{Re}(C_{10-}^{\ell_1\ell_2}C_{P-}^{*\ell_1\ell_2})(m_{\ell_1}+m_{\ell_2})q_- + \mathrm{Re}(C_{9-}^{\ell_1\ell_2}C_{S-}^{*\ell_1\ell_2})(m_{\ell_1}-m_{\ell_2})q_+]|g_0|^2 \\
&- \frac{8}{q^2}\Bigg\{(m_{\ell_1}+m_{\ell_2})(m_{\Lambda_b}+m_\Lambda)s_-q_-\mathrm{Re}(C_{9+}^{\ell_1\ell_2}\,C_T^{*\ell_1\ell_2})\Big[\mathrm{Re}(f_+\,h_+^*) + 2\mathrm{Re}(f_\perp\,h_\perp^*)\Big] \\
&+ (m_{\ell_1}-m_{\ell_2})(m_{\Lambda_b}-m_\Lambda)s_+q_+\mathrm{Re}(C_{10-}^{\ell_1\ell_2}\,C_T^{*\ell_1\ell_2})\Big[\mathrm{Re}(g_+\,\tilde{h}_+^*) + 2\mathrm{Re}(g_\perp\,\tilde{h}_\perp^*)\Big] \\
&+ (m_{\ell_1}+m_{\ell_2})(m_{\Lambda_b}-m_\Lambda)s_+q_-\mathrm{Re}(C_{9-}^{\ell_1\ell_2}\,C_T^{*\ell_1\ell_2})\Big[\mathrm{Re}(g_+\,\tilde{h}_+^* + 2\mathrm{Re}(g_\perp\,\tilde{h}_\perp^*))\Big] \\
&+ (m_{\ell_1}-m_{\ell_2})(m_{\Lambda_b}+m_\Lambda)s_-q_+\mathrm{Re}(C_{10+}^{\ell_1\ell_2}\,C_{T5}^{*\ell_1\ell_2})\Big[\mathrm{Re}(f_+\,\tilde{h}_+^* + 2\mathrm{Re}(f_\perp\,\tilde{h}_\perp^*))\Big]\Bigg\},
\end{aligned}
\tag{9.10}
$$

$$
\begin{aligned}
b =& \frac{2}{q^4}\Big[\mathrm{Re}(f_0 f_+^*)(|C_{9+}^{\ell_1\ell_2}|^2+|C_{10+}^{\ell_1\ell_2}|^2)+\mathrm{Re}(g_0 g_+^*)(|C_{9-}^{\ell_1\ell_2}|^2+|C_{10-}^{\ell_1\ell_2}|^2)\Big]\sqrt{\lambda_H\lambda_L}(m_{\ell_2}^2-m_{\ell_1}^2)(m_{\Lambda_b}^2-m_\Lambda^2)\\
&-4[\mathrm{Re}(C_{9-}^{\ell_1\ell_2}C_{10+}^{*\ell_1\ell_2})+\mathrm{Re}(C_{9+}^{\ell_1\ell_2}C_{10-}^{*\ell_1\ell_2})]\mathrm{Re}(f_\perp g_\perp^*)\sqrt{\lambda_H\lambda_L}\\
&-\frac{2(m_{\Lambda_b}^2-m_\Lambda^2)}{q^2(m_b-m_s)}\sqrt{\lambda_H\lambda_L}[\mathrm{Re}(C_{10+}^{\ell_1\ell_2}C_{P+}^{*\ell_1\ell_2})(m_{\ell_1}-m_{\ell_2})+\mathrm{Re}(C_{9+}^{\ell_1\ell_2}C_{S+}^{*\ell_1\ell_2})(m_{\ell_1}+m_{\ell_2})]\mathrm{Re}(f_0 f_+^*)\\
&-\frac{2(m_{\Lambda_b}^2-m_\Lambda^2)}{q^2(m_b+m_s)}\sqrt{\lambda_H\lambda_L}[\mathrm{Re}(C_{10-}^{\ell_1\ell_2}C_{P-}^{*\ell_1\ell_2})(m_{\ell_1}-m_{\ell_2})+\mathrm{Re}(C_{9-}^{\ell_1\ell_2}C_{S-}^{*\ell_1\ell_2})(m_{\ell_1}+m_{\ell_2})]\mathrm{Re}(g_0 g_+^*)\\
&+\frac{64}{q^4}(|C_T^{\ell_1\ell_2}|^2+|C_{T5}^{\ell_1\ell_2}|^2)(m_{\ell_2}^2-m_{\ell_1}^2)(m_{\Lambda_b}^2-m_\Lambda^2)\sqrt{\lambda_H\lambda_L}\mathrm{Re}(h_\perp\tilde{h}_\perp^*)\\
&-\frac{8}{q^2}\Bigg\{\mathrm{Re}(C_{9+}^{\ell_1\ell_2}\,C_T^{*\ell_1\ell_2})(m_{\ell_1}-m_{\ell_2})(m_{\Lambda_b}-m_\Lambda)\sqrt{\lambda_H\lambda_L}\Big[\mathrm{Re}(f_0 h_+^*)+2\mathrm{Re}(f_\perp\tilde{h}_\perp^*)\Big]\\
&+\mathrm{Re}(C_{10-}^{\ell_1\ell_2}\,C_T^{*\ell_1\ell_2})(m_{\ell_1}+m_{\ell_2})(m_{\Lambda_b}+m_\Lambda)\sqrt{\lambda_H\lambda_L}\Big[\mathrm{Re}(g_0\tilde{h}_+^*)+2\mathrm{Re}(g_\perp h_\perp^*)\Big]\\
&+q^2\frac{(m_{\Lambda_b}-m_\Lambda)}{(m_b-m_s)}\mathrm{Re}(C_{S+}^{\ell_1\ell_2}\,C_T^{*\ell_1\ell_2})\sqrt{\lambda_H\lambda_L}\mathrm{Re}(f_0\,h_+^*)+q^2\frac{(m_{\Lambda_b}+m_\Lambda)}{(m_b+m_s)}\mathrm{Re}(C_{P-}^{\ell_1\ell_2}\,C_T^{*\ell_1\ell_2}) \qquad (9.11)\\
&\times\sqrt{\lambda_H\lambda_L}\mathrm{Re}(g_0\,\tilde{h}_+^*)+\mathrm{Re}(C_{9-}^{\ell_1\ell_2}\,C_{T5}^{*\ell_1\ell_2})(m_{\ell_1}-m_{\ell_2})(m_{\Lambda_b}+m_\Lambda)\sqrt{\lambda_H\lambda_L}\Big[\mathrm{Re}(g_0\tilde{h}_+^*)+2\mathrm{Re}(g_\perp h_\perp^*)\Big]\\
&+\mathrm{Re}(C_{10+}^{\ell_1\ell_2}\,C_{T5}^{*\ell_1\ell_2})(m_{\ell_1}+m_{\ell_2})(m_{\Lambda_b}-m_\Lambda)\sqrt{\lambda_H\lambda_L}\Big[\mathrm{Re}(f_0 h_+^*)+2\mathrm{Re}(f_\perp\tilde{h}_\perp^*)\Big]\\
&+q^2\frac{(m_{\Lambda_b}+m_\Lambda)}{(m_b+m_s)}\mathrm{Re}(C_{S-}^{\ell_1\ell_2}C_{T5}^{*\ell_1\ell_2})\sqrt{\lambda_H\lambda_L}\mathrm{Re}(g_0\tilde{h}_+^*)+q^2\frac{(m_{\Lambda_b}-m_\Lambda)}{(m_b-m_s)}\mathrm{Re}(C_{P+}^{\ell_1\ell_2}C_{T5}^{*\ell_1\ell_2})\sqrt{\lambda_H\lambda_L}\mathrm{Re}(f_0 h_+^*)\Bigg\} \qquad (9.12)
\end{aligned}
$$

$$
\begin{aligned}
c =& +(|C_{9+}^{\ell_1\ell_2}|^2+|C_{10+}^{\ell_1\ell_2}|^2)\frac{\lambda_L\lambda_H}{q^2 s_+}\Bigg[-|f_+|^2\frac{(m_{\Lambda_b}+m_\Lambda)^2}{q^2}+|f_\perp|^2\Bigg]\\
&+(|C_{9-}^{\ell_1\ell_2}|^2+|C_{10-}^{\ell_1\ell_2}|^2)\frac{\lambda_L\lambda_H}{q^2 s_-}\Bigg[-|g_+|^2\frac{(m_{\Lambda_b}-m_\Lambda)^2}{q^2}+|g_\perp|^2\Bigg]\\
&+(|C_T^{\ell_1\ell_2}|^2+|C_{T5}^{\ell_1\ell_2}|^2)\frac{4\lambda_L}{q^2}\Bigg[s_-|h_+|^2+s_+|\tilde{h}_+|^2-\frac{(m_{\Lambda_b}+m_\Lambda)^2 s_-}{q^2}|h_\perp|^2-\frac{(m_{\Lambda_b}-m_\Lambda)^2 s_+}{q^2}|\tilde{h}_\perp|^2\Bigg], \qquad (9.13)
\end{aligned}
$$

with $C_{X\pm}^{\ell_1\ell_2} = (C_X^{\ell_1\ell_2} \pm C_X^{\prime\ell_1\ell_2})$, $q_\pm = (m_{\ell_1} \pm m_{\ell_2})^2 - q^2$ and $\sigma^{\mu\nu} = i/2[\gamma^\mu, \gamma^\nu]$. Our results agree with [280] when setting $m_{\ell_1} = m_{\ell_2} = 0$ and with [283] for $m_{\ell_1} = m_{\ell_2}$. However, we note that our convention for the helicity angle $\cos\theta_\ell$ has the opposite sign that the one in [280] . We also note that our formulae above disagree with Ref. [276], in the specific in terms proportional to $(m_{\ell_1} - m_{\ell_2})^2|C_{9+}^{\ell_1\ell_2}|^2|f_0|^2$ and $(m_{\ell_1} - m_{\ell_2})^2|C_{9+}^{\ell_1\ell_2}|^2|g_0|^2$. We ascribe these differences to an incorrect treatment of mass effects in [276]. Our formulae for the angular coefficients a, b, c also hold for $\Lambda_b \to \Lambda^* \ell_1^- \ell_2^+$ decays, when setting the additional perpendicular $\Lambda_b \to \Lambda^*$ form factor to zero. This is a reasonable approximation as in the Heavy-Quark-Expansion, this form factor is suppressed by $\Lambda_{\rm QCD}/m_b$ [284–286].
In the following, we focus on the branching ratio and forward-backward asymmetry:

$$\frac{d\mathcal{B}^{\ell_1\ell_2}}{dq^2} = 2\Gamma^{(0)}\tau_{\Lambda_b}\left(a + \frac{c}{3}\right), \tag{9.14}$$

$$\frac{dA_{\rm FB}^{\ell_1\ell_2}}{dq^2} = \frac{\int_0^1 d\cos\theta \frac{d\Gamma}{d\cos\theta dq^2} - \int_{-1}^0 d\cos\theta \frac{d\Gamma}{d\cos\theta dq^2}}{\int_0^1 d\cos\theta \frac{d\Gamma}{d\cos\theta dq^2} + \int_{-1}^0 d\cos\theta \frac{d\Gamma}{d\cos\theta dq^2}} = \frac{b}{2\left(a + \frac{c}{3}\right)}, \tag{9.15}$$

where the branching ratio $\mathcal{B} = \tau_{\Lambda_b}\Gamma$, where τ_{Λ_b} is the mean life of the Λ_b baryon [287] and Γ the total width. To evaluate the size of LFV $\Lambda_b \to \Lambda\ell_1^-\ell_2^+$ decay, we provide the q^2-integrated quantities of Eqs. (9.14)–(9.15). For simplicity, we set $C_i^{\prime\ell_1\ell_2} = 0$. We further set $C_{T(5)}^{\ell_1\ell_2} = 0$. This choice is discussed at the beginning of Sect. 9.3. Using the values for the masses from PDG [281], CKM factors from the UT-fit collaboration [288] and lattice QCD inputs for the form factors [278], we obtain

$$\begin{aligned} 10^8 \cdot \mathcal{B}^{\ell_1\ell_2} = {} & \xi_9^{\ell_1\ell_2}|C_9^{\ell_1\ell_2}|^2 + \xi_{10}^{\ell_1\ell_2}|C_{10}^{\ell_1\ell_2}|^2 + \xi_S^{\ell_1\ell_2}|C_S^{\ell_1\ell_2}|^2 + \xi_P^{\ell_1\ell_2}|C_P^{\ell_1\ell_2}|^2 \\ & + \xi_{9S}^{\ell_1\ell_2}{\rm Re}(C_9^{\ell_1\ell_2}C_S^{*\ell_1\ell_2}) + \xi_{10P}^{\ell_1\ell_2}\,{\rm Re}(C_{10}^{\ell_1\ell_2}C_P^{*\ell_1\ell_2}), \end{aligned} \tag{9.16}$$

$$\begin{aligned} A_{\rm FB}^{\ell_1\ell_2} = {} & \Big[\rho^{\ell_1\ell_2}(|C_{10}^{\ell_1\ell_2}|^2 + |C_9^{\ell_1\ell_2}|^2) + \rho_{910}^{\ell_1\ell_2}{\rm Re}(C_9^{\ell_1\ell_2}C_{10}^{*\ell_1\ell_2}) \\ & + \rho_{9S}^{\ell_1\ell_2}{\rm Re}(C_9^{\ell_1\ell_2}C_S^{*\ell_1\ell_2}) + \rho_{10P}^{\ell_1\ell_2}{\rm Re}(C_{10}^{\ell_1\ell_2}C_P^{*\ell_1\ell_2})\Big] \Big/ \Gamma^{\ell_1\ell_2}, \end{aligned} \tag{9.17}$$

with the numerical values for the coefficients $\xi_i^{\ell_1\ell_2}$ and $\rho_i^{\ell_1\ell_2}$ listed in Tables 9.1–9.2 and $\Gamma^{\ell_1\ell_2}$ is the integrated width. We present only explicit results for the final states $\tau^\pm\mu^\mp$ and $\mu^\pm e^\mp$. The results for $\tau^\pm e^\mp$ can easily be obtained from the above results and agree within 1σ with those of $\tau^\pm\mu^\mp$. The quoted uncertainties only include those from the form factors, which are the dominant ones. The correlation matrices between the two sets of $\{\xi_i^{\ell_1\ell_2}, \rho_i^{\ell_1\ell_2}\}$ coefficients are given in Appendix B. The $\xi_i^{\ell_1\ell_2}$ coefficients in Table 9.1 do not depend on the charges of the final state

	$\ell_1 = \mu,\ \ell_2 = \tau$	$\ell_1 = \mu,\ \ell_2 = e$
$\xi_9^{\ell_1\ell_2}$	2.15 ± 0.11	3.13 ± 0.20
$\xi_{10}^{\ell_1\ell_2}$	2.08 ± 0.10	3.13 ± 0.20
$\xi_S^{\ell_1\ell_2}$	0.980 ± 0.057	1.83 ± 0.11
$\xi_P^{\ell_1\ell_2}$	1.06 ± 0.06	1.83 ± 0.11
$\xi_{9S}^{\ell_1\ell_2}$	-0.973 ± 0.059	0.142 ± 0.013
$\xi_{10P}^{\ell_1\ell_2}$	1.20 ± 0.07	0.144 ± 0.013

Table 9.1: Numerical values for the parameters of Eq. (9.16). The coefficients do not depend on the charges of the final state leptons, except for $\xi_{9S}^{\ell_1\ell_2}$ which changes sign when switching the charges of the leptons, i.e. $\xi_{9S}^{\tau\mu} = -\xi_{9S}^{\mu\tau}$ and $\xi_{9S}^{e\mu} = -\xi_{9S}^{\mu e}$. The uncertainties only include those from the form factor which are the dominant ones.

	$\ell_1 = \mu,\ \ell_2 = \tau$	$\ell_1 = \tau,\ \ell_2 = \mu$	$\ell_1 = \mu,\ \ell_2 = e$	$\ell_1 = e,\ \ell_2 = \mu$
$\rho^{\ell_1\ell_2}$	1.26 ± 0.08	-1.26 ± 0.08	-0.025 ± 0.005	0.025 ± 0.005
$\rho_{910}^{\ell_1\ell_2}$	-5.09 ± 0.24	-5.09 ± 0.24	-9.16 ± 0.55	-9.16 ± 0.55
$\rho_{9S}^{\ell_1\ell_2}$	-2.23 ± 0.12	-2.23 ± 0.12	-0.283 ± 0.023	-0.283 ± 0.023
$\rho_{10P}^{\ell_1\ell_2}$	1.99 ± 0.11	-1.96 ± 0.11	-0.280 ± 0.023	0.280 ± 0.023

Table 9.2: Coefficients for the numerator of $A_{\rm FB}^{\ell_1\ell_2}$. We give the values in units of 10^{-21} GeV^{-1}. This factor is compensated by the size of the decay width in Eq. (9.17).

leptons, except for $\xi_{9S}^{\mu\tau}$ which depends on $(m_{\ell_1} - m_{\ell_2})$ and thus switches sign when switching the charges of the final state leptons, i.e. $\xi_{9S}^{\tau\mu} = -\xi_{9S}^{\mu\tau}$. Besides, we note that for μe final states, $\xi_9^{\ell_1\ell_2} = \xi_{10}^{\ell_1\ell_2}$ and $\xi_S^{\ell_1\ell_2} = \xi_P^{\ell_1\ell_2}$, such that only the combination $|C_9^{\ell_1\ell_2}|^2 + |C_{10}^{\ell_1\ell_2}|^2$ and $|C_P^{\ell_1\ell_2}|^2 + |C_S^{\ell_1\ell_2}|^2$ can be constrained. The coefficients $\rho_i^{\ell_1\ell_2}$ in Table 9.2 are reported in units of 10^{-21} GeV^{-1}, which is then compensated in $A_{\rm FB}^{\ell_1\ell_2}$ by the size of the decay width.

9.3 Phenomenological implications

In the following, we discuss the implications of the available constraints on LFV B-meson decays and which bounds they imply on the observables in the baryonic modes. In order to do so, we need to choose which NP operators are present. Since no NP particles have been observed so far above the electroweak scale, we choose to

work with the SMEFT:

$$\mathcal{L}_{\text{eff}} = \mathcal{L}_{\text{SM}} - \frac{1}{M^2}\Big\{[\mathcal{C}_{lq}^{(3)}]^{ij\alpha\beta}(\bar{Q}^i\gamma^\mu\sigma^a Q^j)(\bar{L}^\alpha\gamma_\mu\sigma^a L^\beta) + [\mathcal{C}_{lq}^{(1)}]^{ij\alpha\beta}(\bar{Q}^i\gamma^\mu Q^j)(\bar{L}^\alpha\gamma_\mu L^\beta)$$

$$+[\mathcal{C}_{ledq}]^{ij\alpha\beta}(\bar{Q}^i d_R^j)(\bar{e}_R^\alpha L^\beta)\Big\}\,, \tag{9.18}$$

where we adopt the so-called Warsaw basis [182]. Here we denote with Q and L the left-handed quark and lepton doublets, respectively, and with e_R and d_R the right-handed charged leptons and down-type quarks, respectively. We further denote $\epsilon = i\sigma_2$ and M is the effective scale which can be associated with the mass of the heavy NP degrees of freedom.
The operators in Eq. (9.18) are the complete set of dimension-6 semileptonic operators that can contribute to $b \to s\ell_1\ell_2$ transitions. We note that none of these operators contain a tensor current; nonetheless, at low energy, the operator $\mathcal{O}_{T(5)}^{\ell_1\ell_2}$ defined in Eq. (9.2) could be generated through effective operators containing a covariant derivative [289]. However, as tensor operators provide a poor explanation for B anomalies (see e.g. [290]), we do not consider them in our analysis.

The Wilson coefficients of the operators in Eq. (9.18) can be constrained from low-energy processes as well as high-p_T data, and in general a flavour structure has to be assumed to reduce the number of independent NP parameters. In the following, we choose to consider only constraints from low-energy data and first do not to assume any hierarchy for the NP couplings. In Sect. 9.3.2 we then study particular scenarios, where a more complex structure for NP couplings in flavour space is assumed. For the $b \to s\ell_1\ell_2$ transition we are interested in, we set $i = 2$ and $j = 3$ and generic $\alpha = \ell_1$ and $\beta = \ell_2$ in Eq. (9.18). Performing now the tree-level matching onto Eq. (9.1), we have

$$\begin{aligned}
C_9^{\ell_1\ell_2} &= -\,C_{10}^{\ell_1\ell_2} = +\,\frac{v^2}{\Lambda^2}\frac{\pi}{\alpha_{\text{em}}|V_{tb}V_{ts}^*|}\left([\mathcal{C}_{lq}^{(3)}]^{23\ell_1\ell_2} + [\mathcal{C}_{lq}^{(1)}]^{23\ell_1\ell_2}\right)\,,\\
C_9'^{\ell_1\ell_2} &= +\,C_{10}'^{\ell_1\ell_2} = +\,\frac{v^2}{\Lambda^2}\frac{\pi}{\alpha_{\text{em}}|V_{tb}V_{ts}^*|}[\mathcal{C}_{ld}]^{23\ell_1\ell_2}\,,\\
C_S^{\ell_1\ell_2} &= -\,C_P^{\ell_1\ell_2} = +\,\frac{v^2}{\Lambda^2}\frac{\pi}{\alpha_{\text{em}}|V_{tb}V_{ts}^*|}[\mathcal{C}_{leqd}]^{23\ell_1\ell_2}\,,\\
C_S'^{\ell_1\ell_2} &= +\,C_P'^{\ell_1\ell_2} = +\,\frac{v^2}{\Lambda^2}\frac{\pi}{\alpha_{\text{em}}|V_{tb}V_{ts}^*|}[\mathcal{C}_{leqd}^*]^{32\ell_1\ell_2}\,.
\end{aligned} \tag{9.19}$$

Observable	Upper Bound
$\mathcal{B}(\bar{B}_s \to \mu^\pm \tau^\mp)$	$3.5 \cdot 10^{-5}$ [291]
$\mathcal{B}(\bar{B}_s \to \mu^\pm e^\mp)$	$5.4 \cdot 10^{-9}$ [292]
$\mathcal{B}(B^+ \to K^+ \tau^- \mu^+)$	$4.5 \cdot 10^{-5}$ [293]
$\mathcal{B}(B^+ \to K^+ \mu^- \tau^+)$	$3.9 \cdot 10^{-5}$ [294]
$\mathcal{B}(B^+ \to K^+ \mu^- e^+)$	$7.0 \cdot 10^{-9}$ [295]
$\mathcal{B}(B^+ \to K^+ e^- \mu^+)$	$6.4 \cdot 10^{-9}$ [295]

Table 9.3: Experimental upper limits for LFV B decays at 90% C.L..

	$\ell_1^- = \mu^-$, $\ell_2^+ = \tau^+$	$\ell_1^- = \mu^-$, $\ell_2^+ = e^+$
$c^{9+}_{\ell_1\ell_2}$	1.09	1.75
$c^{10+}_{\ell_1\ell_2}$	1.14	1.75
$c^{S}_{\ell_1\ell_2}$	1.47	2.68
$c^{P}_{\ell_1\ell_2}$	1.58	2.68
$c^{S9}_{\ell_1\ell_2}$	-1.35	0.21
$c^{P10}_{\ell_1\ell_2}$	1.66	0.21

Table 9.4: Predictions for the coefficients describing $B^+ \to K^+ \ell_1^- \ell_2^+$ decays using the hardonic form factors from Ref. [83, 296]. We note that these coefficients are independent of the charges of the leptons, except for $c^{S9}_{\ell_1\ell_2}$ which changes sign depending on the charge of the heavier lepton.

9.3.1 Model-independent approach

First, we consider the constraints on several combinations of Wilson coefficients from measurements of mesonic LFV decays. We consider the branching ratios of the decay modes $\bar{B}_s \to \ell_1^- \ell_2^+$ and $B \to K \ell_1^- \ell_2^+$, for which the experimental upper

limits at 90% C.L. are reported in Table 9.4. Using Eq. (9.1), we have:

$$\mathcal{B}(\bar{B}_s \to \ell_1^- \ell_2^+) = \frac{\tau_{B_s}}{64\pi^3} \frac{\alpha_{\rm em}^2 G_F^2 |V_{tb} V_{ts}^*|^2}{m_{B_s}^3} f_{B_s}^2 \, \lambda^{1/2}(m_{B_s}^2, m_{\ell_1}^2, m_{\ell_2}^2) \times$$

$$\times \left\{ [m_{B_s}^2 - (m_{\ell_1} - m_{\ell_2})^2] \left| (m_{\ell_1} + m_{\ell_2}) C_{10-}^{\ell_1\ell_2} + \frac{m_{B_s}^2}{m_b + m_s} C_{P-}^{\ell_1\ell_2} \right|^2 \right.$$

$$\left. + [m_{B_s}^2 - (m_{\ell_1} + m_{\ell_2})^2] \left| (m_{\ell_1} - m_{\ell_2})(C_{9-}^{\ell_1\ell_2}) + \frac{m_{B_s}^2}{m_b + m_s} (C_{S-}^{\ell_1\ell_2}) \right|^2 \right\} , \tag{9.20}$$

and

$$\mathcal{B}(B^+ \to K^+ \ell_1^- \ell_2^+) = 10^{-8} \left\{ c_{\ell_1\ell_2}^{9+} \left| C_{9+}^{\ell_1\ell_2} \right|^2 + c_{\ell_1\ell_2}^{10+} \left| C_{10+}^{\ell_1\ell_2} \right|^2 + c_{\ell_1\ell_2}^{S} \left| C_{S+}^{\ell_1\ell_2} \right|^2 \right.$$

$$\left. + c_{\ell_1\ell_2}^{P} \left| C_{P+}^{\ell_1\ell_2} \right|^2 + c_{\ell_1\ell_2}^{S9} \, \mathrm{Re}[C_{S+}^{*\ell_1\ell_2} C_{9+}^{\ell_1\ell_2}] + c_{\ell_1\ell_2}^{P10} \, \mathrm{Re}[C_{P+}^{*\ell_1\ell_2} C_{10+}^{\ell_1\ell_2}] \right\} , \tag{9.21}$$

Both Eqs. (9.20)–(9.21) agree with previous results in the literature [297,298]. Using again the values for the masses from PDG [281], CKM factors from the UT-fit collaboration [288], $f_{B_s} = 215\,\mathrm{MeV}$ [299] and Lattice QCD/Light Cone Sum Rule results in Refs. [83, 296], we find the coefficients $c_{\ell_1\ell_2}^i$ in Eq. (9.21) as listed in Table 9.4. Similar as for ξ_{9S}, the coefficient $c_{\ell_1\ell_2}^{S9}$ is proportional to $m_{\ell_1} - m_{\ell_2}$ and thus changes sign depending on charge of the heavier lepton. We stress that the numbers in Table 9.4 are strongly dependent on the choice for $\alpha_{\rm em}$. Here we take $\alpha_{\rm em} = 1/133$. A different choice can be implemented by rescaling the $c_{\ell_1\ell_2}^i$ coefficients.

Finally, we use the experimental upper bounds listed in Table 9.3 and Eqs. (9.20)–(9.21) to constrain different combinations of couplings $C_i^{\ell_1,\ell_2}$. As stated before, we do not consider τe decays as the constraints coming from these decays are similar to those from the $\tau\mu$ channel. Furthermore, for simplicity we also do not consider the $\mathcal{O}_i'^{\ell_1\ell_2}$ operators. This choice is motivated by the fact that these operators are unappealing when trying to fit $b \to s\ell\ell$ data [270–273, 300]. Nevertheless, we stress that the baryonic channels have a different dependence on the primed operators with respect to the mesonic ones, which may be interesting to consider once scenarios involving these operators become more interesting to explain the B anomalies.

The obtained bounds for $\tau\mu$ and μe finals states are given in Fig. 9.1 and in Fig. 9.2, respectively. We consider three 2-dimensional scenarios, in which we allow only some combinations of NP Wilson coefficients to be non-zero: $C_9^{\ell_1\ell_2}$ and $C_{10}^{\ell_1\ell_2}$, $C_S^{\ell_1\ell_2}$ and $C_P^{\ell_1\ell_2}$ and the SMEFT inspired one, where $C_9^{\ell_1\ell_2} = -C_{10}^{\ell_1\ell_2}$ and $C_S^{\ell_1\ell_2} = -C_P^{\ell_1\ell_2}$. For the $C_9^{\ell_1\ell_2} - C_{10}^{\ell_1\ell_2}$ and $C_S^{\ell_1\ell_2} - C_P^{\ell_1\ell_2}$ scenarios, which are independent

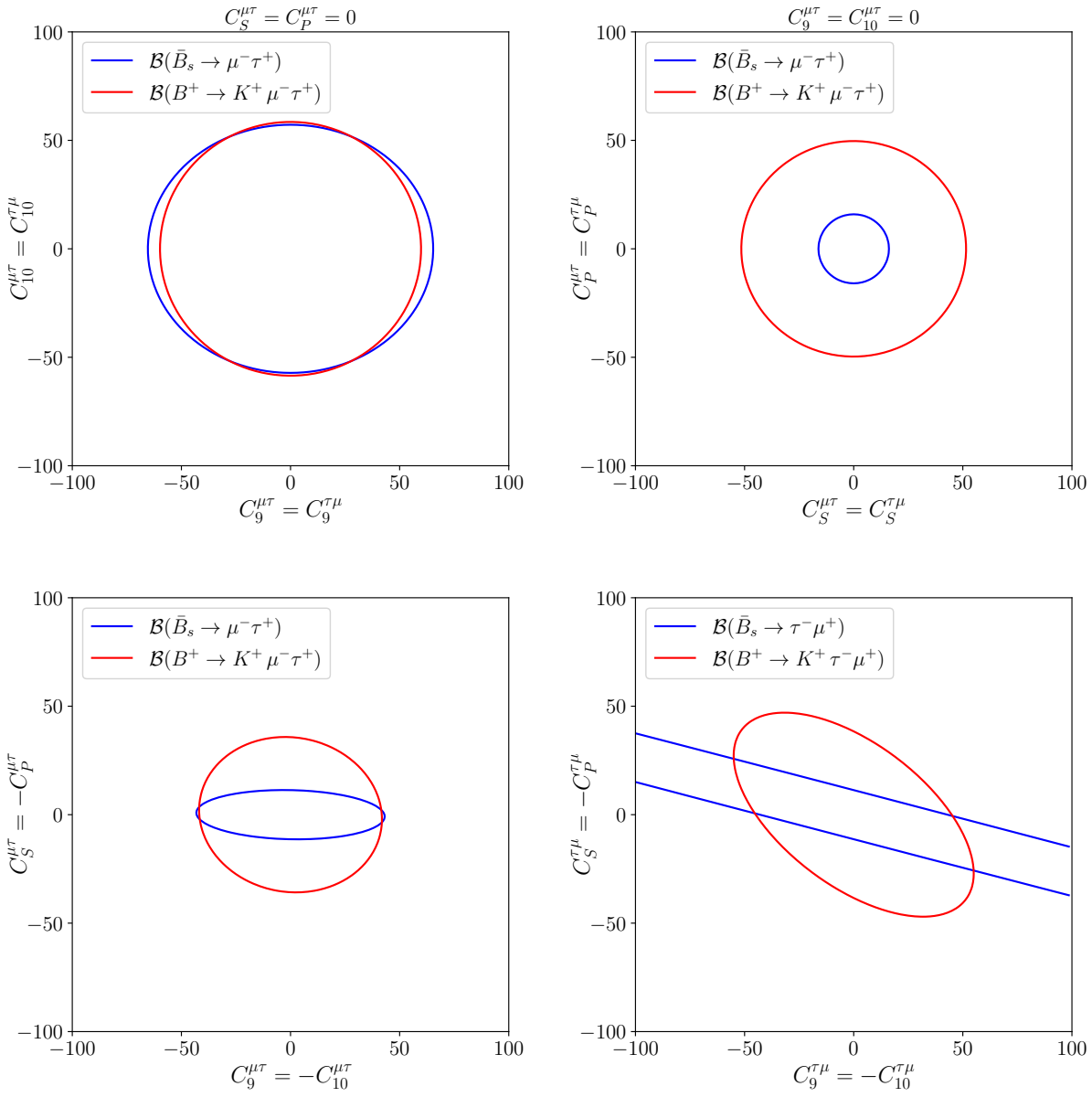

Figure 9.1: Model independent constrains on different combinations of Wilson coefficients obtained from the 90% C.L. upper limits on meson $b \to s\mu^{\pm}\tau^{\mp}$ transitions.

of the charge configuration in the final state, we only consider the strongest bound in Table 9.3. As the interference between $C_9^{\ell_1\ell_2}$ and $C_S^{\ell_1\ell_2}$ depends on the charge configuration of the leptons in the final state, we present plots for both the $\tau^+\mu^-$ and $\tau^-\mu^+$ final states. We note that the $\bar{B}_s \to \tau^-\tau^+$ decay only gives a very weak constraint in the $C_9^{\ell_1\ell_2} = -C_{10}^{\ell_1\ell_2}$ plane ranging from -200 to 200. From comparison of the plots in Fig. 9.1, we find large differences between the $\tau^+\mu^-$ and the $\tau^-\mu^+$. Hence, we stress that it is important to analyse these final states separately. For the

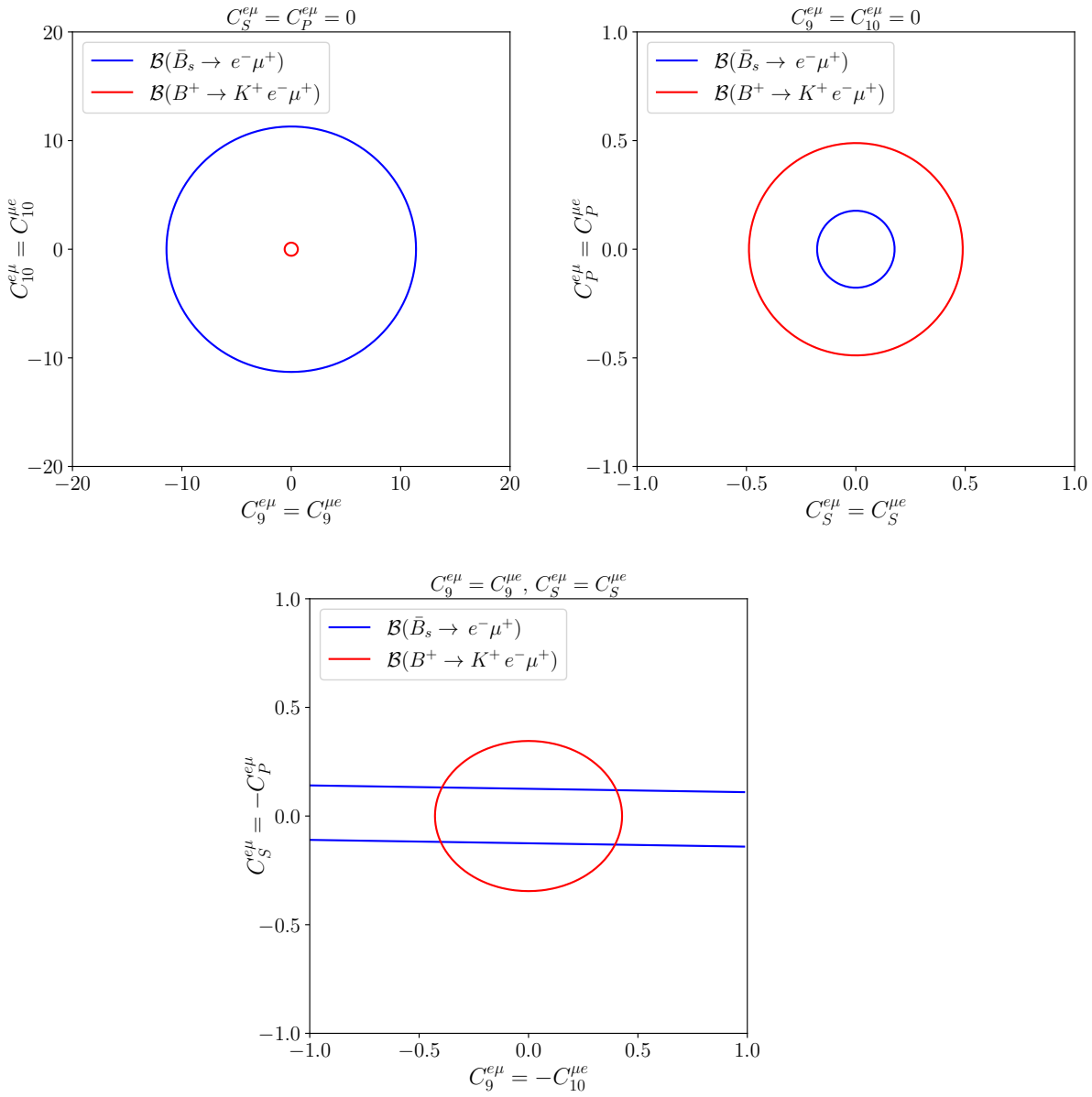

Figure 9.2: Model independent constrains on different combinations of Wilson coefficients obtained from the 90% C.L. upper limits on meson $b \to s\mu^{\pm}e^{\mp}$ transitions.

electron, the differences between $\mu^- e^+$ and $\mu^+ e^-$ are negligible and we only present one figure.

As the mesonic $B^+ \to K^+\ell_1\ell_2$ and $\bar{B}_s \to \ell_1\ell_2$ are mediated by the same quark level transition, we can use the obtained upper limits on combinations of Wilson coefficients and convert those into upper limit on the branching ratio and forward-backward asymmetry for $\Lambda_b \to \Lambda\ell_1\ell_2$ decays using Eq. (9.17). When allowing for only one NP Wilson coefficient to be nonzero at a time, for example allowing only

	$\mathcal{B}^{\mu\tau}$ ($\mathcal{B}^{\tau\mu}$) $\times 10^{-5}$	$\mathcal{B}^{e\mu} = \mathcal{B}^{\mu e} \times 10^{-8}$
$C_9^{\ell_1\ell_2} \neq 0, C_{10}^{\ell_1\ell_2} \neq 0, C_S^{\ell_1\ell_2} = C_P^{\ell_1\ell_2} = 0$	< 7.7 (7.7)	< 1.1
$C_S^{\ell_1\ell_2} \neq 0, C_P^{\ell_1\ell_2} \neq 0, C_9^{\ell_1\ell_2} = C_{10}^{\ell_1\ell_2} = 0$	< 2.7 (2.7)	< 0.06
$C_9^{\ell_1\ell_2} = -C_{10}^{\ell_1\ell_2}, C_S^{\ell_1\ell_2} = -C_P^{\ell_1\ell_2}$	< 7.4 (11)	< 1.1

Table 9.5: Upper limits for the branching ratio of $\Lambda_b \to \Lambda$ LFV decays obtained in a model independent way by considering their mesonic counter parts. Bounds are at 90% C.L.. For the first two scenarios, the branching ratios are independent of the charge configuration. However for the SMEFT scenario this is not the case anymore, hence we present both branching ratios for $\mu^-\tau^+$ and in brackets $\tau^-\mu^+$.

$C_9^{\ell_1\ell_2} \neq 0$, the corresponding bounds can be easily obtained by calculating the scale factor between $c^i_{\ell_1\ell_2}$ of the meson $B \to K$ LFV decay and $\xi_i^{\ell_1\ell_2}$ of the baryon $\Lambda_b \to \Lambda$ decay using Table 9.1 and Table 9.4 and re-scaling the upper limit of the mesonic decay accordingly. In addition, comparing the coefficients in these Tables, we observe that the ratios $c^i_{\ell_1\ell_2}/c^j_{\ell_1\ell_2}$ and $\xi_i^{\ell_1\ell_2}/\xi_j^{\ell_1\ell_2}$ are very similar for $i, j = 9, 10$ and $i, j = S, P$. Therefore, the sensitivities for LFV $B \to K$ and $\Lambda_b \to \Lambda$ decays are rather similar when considering the $C_9^{\ell_1\ell_2} - C_{10}^{\ell_1\ell_2}$ only and $C_S^{\ell_1\ell_2} - C_P^{\ell_1\ell_2}$ only scenarios. Upper limits (at 90% C.L.) for the branching ratio of $\Lambda_b \to \Lambda\ell_1\ell_2$ derived from their mesonic counter parts for the three scenarios are presented in Table 9.5. These values should be interpreted as follows: any future experimental upper limit on the baryonic mode below the quoted value gives stronger constraints on the Wilson coefficients than those obtained from the current mesonic upper limits.

The complementarity of the mesonic and the baryonic LFV channels specifically arises when considering both (axial)vector and (pseudo)scalar operators. This complementarity is caused the difference between the ratios $c^i_{\ell_1\ell_2}/c^j_{\ell_1\ell_2}$ and $\xi_i^{\ell_1\ell_2}/\xi_j^{\ell_1\ell_2}$ for $i = S9, P10$ and $j = S, P, 9, 10$. We expect a similar complementarity also when both tensor operators and (axial)vector operators are present. We illustrate quantitatively this in Fig. 9.3 for the SMEFT scenario where $C_9^{\ell_1\ell_2} = -C_{10}^{\ell_1\ell_2}, C_S^{\ell_1\ell_2} = -C_P^{\ell_1\ell_2}$. We present the current meson constraints combined with two possible constraints on the $\Lambda_b \to \Lambda\mu^-\tau^+$ branching ratio and observe that the mesonic modes place strong constraints on scalar/pseudoscalar interactions while the baryonic channel is more sensitive to $C_9^{\mu\tau}$ and $C_{10}^{\mu\tau}$.

Finally, we consider the integrated forward-backward asymmetry $A_{\rm FB}^{\ell_1\ell_2}$ which provides orthogonal information compared to the branching ratio. From Eq. (9.17) we note the following properties: $A_{\rm FB}^{\ell_1\ell_2}$ is identically zero if $C_9^{\ell_1\ell_2} = C_{10}^{\ell_1\ell_2} = 0$, and in the case in which only $C_9^{\ell_1\ell_2} = -C_{10}^{\ell_1\ell_2} \neq 0$ $A_{\rm FB}^{\ell_1\ell_2}$ is independent on the values of $C_9^{\ell_1\ell_2}$ and $C_{10}^{\ell_1\ell_2}$. In the latter scenario, we find for $C_9^{\ell_1\ell_2} = -C_{10}^{\ell_1\ell_2}$ and $C_S^{\ell_1\ell_2} = C_P^{\ell_1\ell_2} = 0$

$$A_{\rm FB}^{\tau\mu} = 0.14 \pm 0.01 \ , \qquad A_{\rm FB}^{\mu\tau} = 0.40 \pm 0.03 \ , \qquad A_{\rm FB}^{e\mu} = A_{\rm FB}^{\mu e} = 0.33 \pm 0.04 \ . \tag{9.22}$$

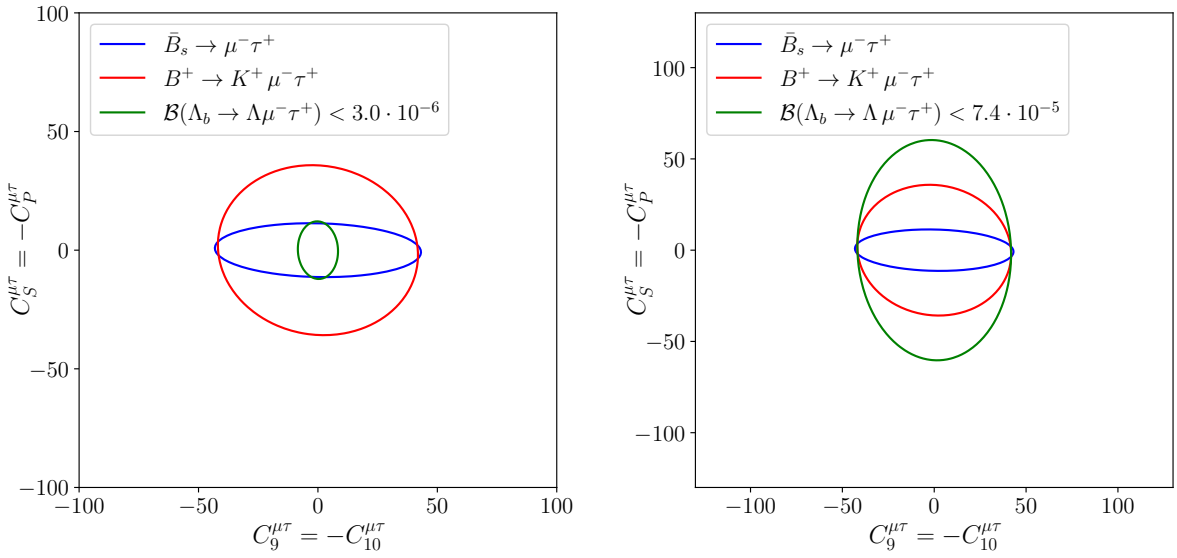

Figure 9.3: Illustration of the orthogonality between current mesonic and possible future baryonic constraints.

A measurement or an upper limit different from these values provides interesting complementary information. This is illustrated in Fig. 9.4, where we consider for the $\mu^-\tau^+$ final state a future scenario in which an upper limit of $A_{\rm FB}^{\mu\tau} < 0.3$ and $\mathcal{B}^{\mu\tau} < 7.7 \cdot 10^{-5}$ are considered. As we can see from Fig. 9.4, the information on $A_{\rm FB}^{\tau\mu}$ helps to rule out a large part of the allowed space in the $C_9^{\ell_1\ell_2} - C_{10}^{\ell_1\ell_2}$ plane.

9.3.2 Explicit models

As mentioned, in many models that explain LFU violation, also LFV naturally occurs. Since our aim is not to perform a detailed analysis of all the observables in low-energy phenomenology, we choose to focus here on two specific models that explain the B anomalies. We choose two interesting solutions, which are the most favourite in the literature: the combination of the scalar leptoquarks S_1 and S_3 and the vector leptoquark U_1. For these models we provide predictions for observables in $\Lambda_b \to \Lambda \ell_1^- \ell_2^+$ decays.

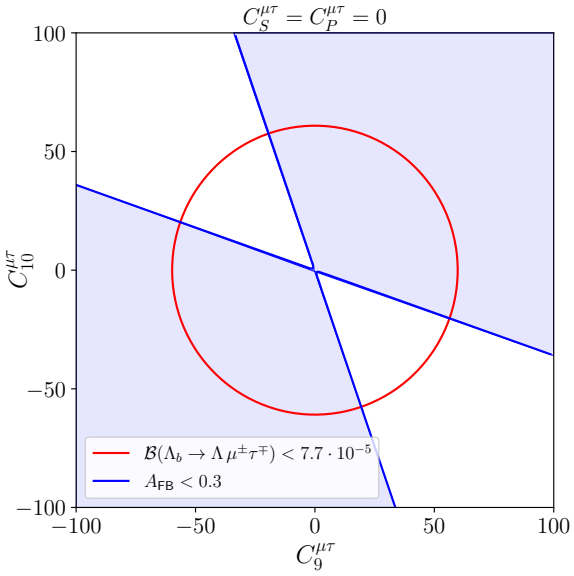

Figure 9.4: Illustration of how the forward-backward asymmetry provides orthogonal constraints to the branching ratio of $\Lambda_b \to \Lambda\mu^-\tau^+$. The shaded area present the allowed region for an upper limit $A_{\rm FB}^{\mu\tau} < 0.3$, compared to an upper limit for the branching ratio of $7.7 \cdot 10^{-5}$.

The $S_1 + S_3$ scalar leptoquarks scenario [252]

Here we focus on the $S_1 + S_3$ scenario, following the analysis in Ref. [252][1]. The main idea there is to apply the Froggatt-Nielsen mechanism [301], that explains the hierarchies of quark masses, as a power counting for NP operators, and thereby providing simultaneously an explanation for the B-anomalies and the flavour puzzle. Converting the formalism of Ref. [252] to the Wilson coefficients defined in Eq. (9.1), we find:

$$C_9^{\ell_1\ell_2} = -C_{10}^{\ell_1\ell_2} = \frac{v^2}{M^2}\frac{\pi}{\alpha_{\rm em}|V_{tb}V_{ts}^*|}|g_3|^2 \tilde{S}_{QL}^{3\ell_2}\tilde{S}_{QL}^{*2\ell_1} \tag{9.23}$$

where M is the mass of the heavy scalar leptoquarks, $\tilde{S}_{QL}^{i\ell_i}$ is the spurion associated with the S_3 scalar leptoquark and encodes the Froggatt-Nielsen power counting, and g_3 is an overall coupling which is expected to be of $\mathcal{O}(1)$. Notice that the scalar leptoquark S_1 does not contribute to $b \to s\ell_1^-\ell_2^+$ transitions. With this, we find

$$\begin{aligned} C_9^{\mu\tau} &= -C_{10}^{\mu\tau} = -\left(0.41 \pm 0.07\right), \\ C_9^{\tau\mu} &= -C_{10}^{\tau\mu} = \quad \left(10 \pm 2\right). \end{aligned} \tag{9.24}$$

For the modes with electrons and muons in the final states, we find $C_9^{e\mu} \propto 10^{-3}$ and

[1]The analysis Ref. [252] provides qualitatively the same results as Ref. [248].

a even lower value for $C_9^{\mu e}$. Therefore, we conclude that the corresponding branching ratios are too small to be measured by any experiment in the near future.
Focusing then on the final states with muons and taus, using the Wilson coefficients in (9.24) and our results in Sect. 9.2 gives

$$\begin{aligned} \mathcal{B}^{\mu\tau} &= (7.1 \pm 2.5) \cdot 10^{-9} \,, \\ \mathcal{B}^{\tau\mu} &= (4.2 \pm 1.7) \cdot 10^{-6} \,, \end{aligned} \tag{9.25}$$

where the errors are dominated by the ones on the NP Wilson coefficients. Note that since this model predicts $C_9^{\ell_1\ell_2} = -C_{10}^{\ell_1\ell_2}$, $A_{\rm FB}^{\ell_1\ell_2}$ is independent from any Wilson coefficients and assumes the value in Eq. (9.22). From Fig. 9.4 we can conclude that the $C_9^{\ell_1\ell_2} = -C_{10}^{\ell_1\ell_2}$ scenario would be excluded by the measurement of $A_{\rm FB}^{\ell_1\ell_2}$. Hence, this stresses the importance of obtaining experimental constraints on this observable.

The U_1 vector leptoquark scenario [253]
Other interesting NP models are those with a vector leptoquark, usually denoted U_1. In fact, this NP particle is the only one able to accommodate both classes of B anomalies on its own. Among the various possibilities available in the literature, we focus on [253], where the vector leptoquark is a massive state originating from the Spontaneus Symmetry Breaking of a gauge groupe larger than the SM one. As a consequence of the gauge representation of the U_1 vector leptoquark, not only vector and axial vector couplings, but also scalar and pseudoscalar couplings are generated. In particular, the latter are very useful in explaining the large discrepancies in $b \to c\tau\bar{\nu}$ data and as a consequence, generate sizeable $b \to s\ell_1\ell_2$ interactions. Therefore, we expect very different signatures for the U_1 model than the ones in the scalar leptoquark case. In Ref. [253] several cases are taken into account, where the flavour structure of the NP couplings has a $U(2)^5$ flavour symmetry [302] or not, and where (pseudo-)scalar couplings are present or not. In the following we report results for the case in which no $U(2)^5$ flavour symmetry is assumed. We note that using the scenario based on th $U(2)^5$ flavour symmetry yields very similar results. We also note that given the flavour structure assumed in Ref. [253], the couplings of the vector leptoquark to electrons is zero, hence no effect is predicted for $\Lambda_b \to \Lambda e^{\pm}\mu^{\mp}$. In the notation of Ref. [253] we have

$$\begin{aligned} C_9^{\ell_1\ell_2} &= -C_{10}^{\ell_1\ell_2} = + \frac{2\pi}{\alpha_{\rm em}|V_{tb}V_{ts}^*|} C_U \beta_L^{2\ell_1} (\beta_L^{3\ell_2})^* \,, \\ C_S^{\ell_1\ell_2} &= -C_P^{\ell_1\ell_2} = + \frac{4\pi}{\alpha_{\rm em}|V_{tb}V_{ts}^*|} C_U \beta_L^{2\ell_1} (\beta_R^{3\ell_2})^* \,, \end{aligned} \tag{9.26}$$

where C_U is a normalisation constant which contains the mass of the vector leptoquark normalised to the electroweak vacuum-expectation value and the gauge coupling of the leptoquark. The factor $\beta_{L(R)}^{j\beta}$ represents the coupling in flavour space to

left(right)-handed fermions. In the following we neglect the uncertainties on the fitted parameters obtained from [253] due to their large and asymmetric distributions. Either way, this scenario provides a useful benchmark that allows us to predict the size of LFV $\Lambda_b \to \Lambda$ decays. We first look at the case $\beta_R^{3\beta} = 0$. We find

$$\begin{aligned} C_9^{\tau\mu} &= -C_{10}^{\tau\mu} = -\,5.93\,, \\ C_9^{\mu\tau} &= -C_{10}^{\mu\tau} = +\,2.90\,. \end{aligned} \tag{9.27}$$

The predictions for $A_{\rm FB}^{\ell_1\ell_2}$ in this case are the same as in Eq. (9.22). The corresponding integrated branching ratios are:

$$\begin{aligned} \mathcal{B}^{\tau\mu} &= 1.5 \times 10^{-6} \\ \mathcal{B}^{\mu\tau} &= 3.6 \times 10^{-7}\,. \end{aligned} \tag{9.28}$$

In the case where $\beta_R^{3\beta} \neq 0$, we find

$$\begin{aligned} C_9^{\tau\mu} &= -C_{10}^{\tau\mu} = -\,4.47\,, \quad C_S^{\tau\mu} = -C_P^{\tau\mu} = \;\; 0\,, \\ C_9^{\mu\tau} &= -C_{10}^{\mu\tau} = \;\; 2.03\,, \quad\;\; C_S^{\mu\tau} = -C_P^{\mu\tau} = \;\; 4.06\,, \end{aligned} \tag{9.29}$$

which yields

$$\begin{aligned} \mathcal{B}^{\tau\mu} &= \;\; 8.5 \times 10^{-7} \quad \text{and} \qquad A_{\rm FB}^{\tau\mu} = \;\; 0.14\,, \\ \mathcal{B}^{\mu\tau} &= \;\; 5.3 \times 10^{-7} \quad \text{and} \qquad A_{\rm FB}^{\mu\tau} = \;\; 0.12\,. \end{aligned} \tag{9.30}$$

Some comments are in order. In the scenario where $C_{S(P)}^{\ell_1\ell_2} = 0$, $A_{\rm FB}^{\ell_1\ell_2}$ is independent from the Wilson coefficients and its value is given in Eq. (9.22). We find that $\mathcal{B}^{\tau\mu} > \mathcal{B}^{\mu\tau}$ due to a factor of two between the respective NP couplings. In the case where we have also $C_S^{\mu\tau} = -C_P^{\mu\tau} \neq 0$, we find that $\mathcal{B}^{\mu\tau}$ is surprisingly small due to the negative interference between $C_S^{\mu\tau}$ and $C_P^{\mu\tau}$. On the other hand, $A_{\rm FB}^{\mu\tau}$ is found to be smaller than $A_{\rm FB}^{\tau\mu}$, hence providing a possible way to distinguish the different scenarios.

9.3.3 LHCb prospects

The results found in the above Sections indicate that $\Lambda_b \to \Lambda\ell_1\ell_2$ decays are very good probes of physics beyond the SM and provide in certain scenarios complementary bounds with respect to the ones from $\bar{B} \to \ell_1\ell_2$ and $B^+ \to K^+\ell_1\ell_2$ decays. Here we want to comment on the prospective for measurement of $\Lambda_b \to \Lambda\ell_1\ell_2$ decays at the LHCb experiment.

If we consider measurement carried out with the same dataset, we expect for the measured yields:

$$\frac{\mathcal{N}(\Lambda_b \to \Lambda(\to p\pi)\ell_1\ell_2)}{\mathcal{N}(B^+ \to K^+\ell_1\ell_2)} = \frac{\mathcal{B}(\Lambda_b \to \Lambda(\to p\pi)\ell_1\ell_2)|_{\rm theory}}{\mathcal{B}(B^+ \to K^+\ell_1\ell_2)|_{\rm theory}} \frac{f_{\Lambda_b}}{f_{B^+}} r_{\Lambda_b/B^+}\,, \tag{9.31}$$

where f_{Λ_b}/f_{B^+} is the ratios of the fragmentation functions for the Λ_b and the B^+ modes, respectively, and r_{Λ_b/B^+} is a correction factor due to different reconstruction efficiencies. In Ref. [303], the ratio $f_{\Lambda_b}/(f_u + f_d)$ is measured. Using isospin relations, we can write $f_{\Lambda_b}/f_{B^+} = 2f_{\Lambda_b}/(f_u + f_d) = (0.518 \pm 0.036)$. The ratio of the predicted values of the theoretical branching ratios depends on the NP model and final state leptons. However, as we noted already in Sect. 9.3.1, the branching ratios for the baryon and the meson case are very similar in size: therefore, for an order of magnitude estimate, we consider them to be equal. The last piece of information needed is the ratio r_{Λ_b/B^+}, that is difficult to estimate without a thorough simulation of the LHCb detector. However, in order to give an estimate, we use the information in Refs. [214, 304], that are based on the same integrated luminosity. From these papers we extract

$$\frac{\mathcal{N}(\Lambda_b \to \Lambda(\to p\pi)\mu^-\mu^+)}{\mathcal{N}(B^+ \to K^+\mu^-\mu^+)} \approx 0.31\,. \tag{9.32}$$

This means that we expect the efficiency for the reconstruction of the Λ_b to be roughly 1.67 times less than that of the B^+, when also taking into account the fragmentation fractions effect. Hence we set $r_{\Lambda_b/B^+} = 1.67$. We expect that all the other correction factors due to the reconstruction of the leptons in the final state cancel out since we are comparing the same leptonic final states in both decays. This yields

$$\mathcal{B}(\Lambda_b \to \Lambda(\to p\pi)\ell_1\ell_2) \approx 1.67\frac{f_{\Lambda_b}}{f_{B^+}}\mathcal{B}(B^+ \to K^+\ell_1\ell_2)\,. \tag{9.33}$$

Using the current upper limit on $\mathcal{B}(B^+ \to K^+\tau^+\mu^-)$, we thus expect that LHCb can reach the following sensitivity:

$$\mathcal{B}(\Lambda_b \to \Lambda(\to p\pi)\mu^-\tau^+) \lesssim 6.5 \cdot 10^{-5}\,, \tag{9.34}$$

for Run 1 and 2 datasets. In the above estimate, we have not included any correction for the trigger efficiency, which can be different for the baryonic and mesonic mode. The estimate in Eq. (9.34) can be compared to the model dependent and model independent bounds on $\mathcal{B}(\Lambda_b \to \Lambda\tau^+\mu^-)$ found in the previous Sections. In particular, the expected upper bound from LHCb would already give better constraints than the corresponding ones from the mesonic decays, as illustrated in Fig. 9.3. We also stress that future runs will improve the upper limit in Eq. (9.34) of at least a factor of roughly two with Run 3 and a factor of three with further runs [274].

9.4 Conclusions

In this paper, we present the first full analysis of $\Lambda_b \to \Lambda\ell_1^-\ell_2^+$ lepton flavour violating (LFV) decays in terms of possible new physics operators. The main results of this paper are Eqs. (9.10)–(9.13), where the coefficients of the angular distributions for $\Lambda_b \to \Lambda\ell_1^-\ell_2^+$ decays are given. We study the interplay between the baryonic and

mesonic searches for LFV, where for the latter upper limits are already available. We convert these upper limits into constraints on the branching ratio and forward-backward asymmetry for $\Lambda_b \to \Lambda \ell_1^- \ell_2^+$ decays. We find that the $\Lambda_b \to \Lambda \ell_1^- \ell_2^+$ decays provide different constraints on the new physics Wilson coefficients than $\bar{B}_s \to \ell_1^- \ell_2^+$ and $B^+ \to K^+ \ell_1^- \ell_2^+$ decays, and have the potential to reduce the allowed parameter space for new physics models. We then analyse quantitatively the size of $\Lambda_b \to \Lambda \ell_1^- \ell_2^+$ decays in specific scenarios that can address B anomalies, using as a reference [252] and [253]. Our findings indicate that the predicted branching ratio for $\Lambda_b \to \Lambda \ell_1^- \ell_2^+$ for these scenarios are such that they can further constrain the new physics couplings. As a final prospective, we estimate the reach of LHCb for $\Lambda_b \to \Lambda \ell_1^- \ell_2^+$ decays, finding that an upper limit of $\mathcal{B}(\Lambda_b \to \Lambda \mu^- \tau^+) \lesssim 6.5 \cdot 10^{-5}$ can be reached with Run 1 and Run 2 data.

Acknowledgements

We thank Yasmine Amhis, Flavio Archilli, Lex Greeven and Mick Mulder for insightful discussion on experimental prospects. The work of MB is supported by the Italian Ministry of Research (MIUR) under grant PRIN 20172LNEEZ. The work of MR is supported by the Deutsche Forschungsgemeinschaft (DFG, German Research Foundation) under grant 396021762 - TRR 257.

Appendix A Details on kinematics

In the Λ_b rest frame ($\Lambda_b - \mathrm{RF}$), the momenta are defined as

$$q^\mu|_{\Lambda_b-\mathrm{RF}} = (q^0, 0, 0, -|\vec{q}|)\,, \tag{9.35}$$

$$k^\mu|_{\Lambda_b-\mathrm{RF}} = (m_{\Lambda_b} - q^0, 0, 0, |\vec{q}|)\,. \tag{9.36}$$

where

$$q^0|_{\Lambda_b-\mathrm{RF}} = \frac{m_{\Lambda_b}^2 - m_\Lambda^2 + q^2}{2m_{\Lambda_b}}\,, \quad \text{and} \quad |\vec{q}|_{\Lambda_b-\mathrm{RF}} = \frac{\sqrt{\lambda(m_{\Lambda_b}^2, m_\Lambda^2, q^2)}}{2m_{\Lambda_b}}\,, \tag{9.37}$$

where λ is the usual Källen function defined as $\lambda(a,b,c) = a^2+b^2+c^2-2a(b+c)-2bc$. In the dilepton rest frame we have that $q^\mu|_{2\ell-\mathrm{RF}} = \sqrt{q^2}(1,0,0,0)$, and

$$p_1^\mu|_{2\ell-\mathrm{RF}} = (E_{\ell_1}, -|\vec{p}_2||_{2\ell-\mathrm{RF}} \sin\theta_\ell, 0, -|\vec{p}_2||_{2\ell-\mathrm{RF}} \cos\theta_\ell)\,, \tag{9.38}$$

$$p_2^\mu|_{2\ell-\mathrm{RF}} = (E_{\ell_2}, +|\vec{p}_2||_{2\ell-\mathrm{RF}} \sin\theta_\ell, 0, +|\vec{p}_2||_{2\ell-\mathrm{RF}} \cos\theta_\ell)\,, \tag{9.39}$$

where

$$|\vec{p}_2||_{2\ell-\mathrm{RF}} = \frac{\sqrt{\lambda(q^2, m_{\ell_1}^2, m_{\ell_2}^2)}}{2\sqrt{q^2}}\,, \quad \text{and} \quad E_{\ell_{1,2}} = \frac{q^2 + m_{\ell_{1,2}}^2 - m_{\ell_{2,1}}^2}{2\sqrt{q^2}}. \tag{9.40}$$

The two reference systems are connected by the following relation for any vector:

$$x^{\mu}||_{\Lambda_b-\mathrm{RF}} = \Lambda_{\mu\nu} x^{T\mu}\,, \qquad \Lambda = \begin{pmatrix} \gamma & 0 & 0 & -\beta\gamma \\ 0 & 1 & 0 & 0 \\ 0 & 0 & 1 & 0 \\ -\beta\gamma & 0 & 0 & \gamma \end{pmatrix} \tag{9.41}$$

where $\Lambda_{\mu\nu}$ is a Lorentz transformation along the z axis. It's parameters are:

$$\gamma = \frac{q^0|_{\Lambda_b-\mathrm{RF}}}{\sqrt{q^2}}\,, \quad \text{and} \quad \beta = \frac{|\vec{q}||_{\Lambda_b-\mathrm{RF}}}{q^0|_{\Lambda_b-\mathrm{RF}}} \tag{9.42}$$

Appendix B Correlations

We present correlation matrices for the set of coefficients $\{\xi_i^{\ell_1\ell_2}, \rho_i^{\ell_1\ell_2}\}$, with the same ordering as in Tables 9.1–9.2. In Table 9.6 we present the correlations for μe final states and in Table 9.7 the ones for $\mu\tau$ final states.

1	1	0.617	0.617	0.643	0.643	-0.728	0.820	-0.839	-0.839
1	1	0.617	0.617	0.643	0.643	-0.728	0.820	-0.839	-0.839
0.617	0.617	1	1	0.885	0.885	-0.559	0.451	-0.778	-0.778
0.617	0.617	1	1	0.885	0.885	-0.559	0.451	-0.778	-0.778
0.643	0.643	0.885	0.885	1	1	-0.835	0.438	-0.911	-0.911
0.643	0.643	0.885	0.885	1	1	-0.835	0.437	-0.911	-0.911
-0.728	-0.728	-0.559	-0.559	-0.835	-0.835	1	-0.434	0.932	0.932
0.820	0.820	0.451	0.451	0.438	0.438	-0.434	1	-0.517	-0.517
-0.839	-0.839	-0.778	-0.778	-0.911	-0.911	0.932	-0.517	1	1
-0.839	-0.839	-0.778	-0.778	-0.911	-0.911	0.932	-0.517	1	1

Table 9.6: Correlation matrix for the $\Lambda_b \to \Lambda\mu^- e^+$ parameters.

1	0.997	0.709	0.716	-0.742	0.742	0.835	0.857	-0.877	0.877
0.997	1	0.747	0.755	-0.787	0.788	0.858	0.838	-0.900	0.900
0.709	0.747	1.00	0.999	-0.962	0.947	0.715	0.466	-0.835	0.835
0.716	0.755	0.999	1	-0.971	0.958	0.734	0.470	-0.846	0.846
-0.742	-0.787	-0.962	-0.971	1	-0.999	-0.841	-0.481	0.899	-0.899
0.742	0.788	0.947	0.958	-0.999	1	0.857	0.480	-0.903	0.903
0.835	0.858	0.715	0.734	-0.841	0.857	1	0.519	-0.964	0.964
0.857	0.838	0.466	0.470	-0.481	0.480	0.519	1	-0.544	0.544
-0.877	-0.900	-0.835	-0.846	0.899	-0.903	-0.964	-0.544	1	-1
0.877	0.900	0.835	0.846	-0.899	0.903	0.964	0.544	-1	1

Table 9.7: Correlation matrix for the $\Lambda_b \to \Lambda \mu^- \tau^+$ parameters.

Chapter 10

Project V: Dispersive bounds for local form factors in $\Lambda_b \to \Lambda$ transitions

Published as a preprint in:
T. Blake, S. Meinel, M. Rahimi, D. van Dyk [5].
At the time of writing, this work is being prepared for publication in a peer-reviewed journal.

Contributions of the authors to the article.
M. Rahimi contributed to the draft and did the analytical derivation and numerical analysis of all expressions obtained in the article. Dr. van Dyk performed an independent numerical study and worked on the draft. Dr. Meinel provided the lattice-QCD data and along with Dr. Blake, discussed the results and worked on the draft.

Abstract: We investigate the ten independent local form factors relevant to the b-baryon decay $\Lambda_b \to \Lambda\ell^+\ell^-$, combining information of lattice QCD and dispersive bounds. We propose a novel parametrization of the form factors in terms of orthonormal polynomials that diagonalizes the form factor contributions to the dispersive bounds. This is a generalization of the unitarity bounds developed for meson-to-meson form factors. In contrast to ad-hoc parametrizations of these form factors, our parametrization provides a degree of control of the form-factor uncertainties at large hadronic recoil. This is of phenomenological interest for theoretical predictions of, *e.g.*, $\Lambda_b \to \Lambda\gamma$ and $\Lambda_b \to \Lambda\ell^+\ell^-$ decay processes.

10.1 Introduction

For the last decade, decays involving $b \to s\mu^+\mu^-$ transitions have been a focus of flavour physics community due to the substantial number of so-called "b anomalies". These anomalies are a pattern of deviations between theoretical expectations, within the Standard Model of particle physics (SM), and experimental measurements, chiefly by the LHCb experiment [305–310]. Compatible experimental results, for many of these measurements, have since been obtained by the ATLAS [311,312], CMS [313–315], and Belle [316] experiments.

There is substantial interest in corroborating the b anomalies through decay channels that feature complementary sources of theoretical systematic uncertainties *and* complementary sensitivity to effects beyond the SM. The decay $\Lambda_b \to \Lambda(\to p\pi^-)\mu^+\mu^-$ is a prime candidate for this task [280]. In contrast to $B \to K^*(\to K\pi)\mu^+\mu^-$ decays, the local form factors for $\Lambda_b \to \Lambda\mu^+\mu^-$ decays correspond to transition matrix elements between stable single-hadron states in QCD. This allows precise lattice QCD calculations using standard methods, and results for the $\Lambda_b \to \Lambda$ form factors have been available for some time [278]. Measurements of $\Lambda_b \to \Lambda(\to p\pi^-)\mu^+\mu^-$ observables [317,318] have been included in global fits of the $b \to s\mu^+\mu^-$ couplings [269,271,319,320], and dedicated analyses for effects beyond the SM, even accounting for production polarization of the Λ_b, have been performed in recent years [269, 321]. Lepton-flavor universality violation in baryonic $b \to s\ell^+\ell^-$ decay modes has also been studied theoretically; in Ref. [3] the angular distribution of $\Lambda_b \to \Lambda\ell^+\ell^-$ has been computed for the full base of New Physics operator (partial results are available in Ref. [275, 276]). Measurements by LHCb are also available for the branching fraction of the $\Lambda_b \to \Lambda\gamma$ decay [318].

In this work, we investigate one of the two main sources of theoretical uncertainties that arise in the predictions of $\Lambda_b \to \Lambda\ell^+\ell^-$ and $\Lambda_b \to \Lambda\gamma$ transitions; the hadronic form factors of local $\bar{s}\Gamma\, b$ currents of mass dimension three. The complete set of scalar-valued hadronic form factors describing these currents is comprised of ten independent functions of the dilepton invariant mass squared, q^2. A convenient Lorentz decomposition of the hadronic matrix elements is achieved in terms of helicity amplitudes [277]. Here, we set out to improve the description of the form factors as functions of q^2 across the whole kinematic phase space available to the $\Lambda_b \to \Lambda\ell^+\ell^-$ decay. To that end, we derive dispersive bounds for the form factors in the six $\bar{s}\Gamma b$ currents: the (pseudo)scalar, the (axial)vector, and the two tensor currents. We demonstrate that previous analyses of dispersive bounds for baryon-to-baryon form factors [322–325] overestimate the saturation of the bounds (see also the discussion in Ref. [173]). Our formulation of the bounds uses polynomials that are orthonormal on an arc of the unit circle in the variable z (see Sec. 10.2.4 for the definition). As a consequence, benefits inherent to meson-to-meson form-factor parametrizations with dispersive bounds now also apply to our approach. We illustrate the usefulness of our formulation of the dispersive bounds for the form factor parameters for $\Lambda_b \to \Lambda$, but note that it applies similarly to other ground-state

baryon to ground-state baryon form factors (*e.g.* $\Lambda_b \to \Lambda_c$ transitions). As inputs, we use lattice QCD determinations of the form factors at up to three different points in q^2. Our analysis also paves the way for the application of the bounds directly, through a modified z-expansion, within future lattice QCD studies. This is likely to increase the precision of future form-factor predictions, especially at large hadronic recoil where $q^2 \simeq 0$.

In Sec. 10.2, we briefly recap the theory of the local form factors for baryon-to-baryon transitions and their dispersive bounds. We then propose a new parametrization for the full set of form factors in $\Lambda_b \to \Lambda$ transitions, which diagonalizes the dispersive bound. In Sec. 10.3, we illustrate the power of our parametrization based on lattice QCD constraints for the $\Lambda_b \to \Lambda$ form factors. We highlight how the form-factor uncertainties in the low momentum transfer region are affected by our parametrization and the different types of bounds we apply. We conclude in Sec. 10.4.

10.2 Derivation of the dispersive Bounds

We begin with a review of the Lorentz decomposition of the hadronic matrix elements in Sec. 10.2.1. We then introduce the two-point correlation functions responsible for the dispersive bound and their theoretical predictions within an operator product expansion in Sec. 10.2.2. The hadronic representation of the correlation functions is discussed in Sec. 10.2.3. Our proposed parametrization is introduced in Sec. 10.2.4.

10.2.1 Lorentz decomposition in terms of helicity form factors

A convenient definition of the form factors is achieved when each helicity amplitude corresponds to a single form factor:

$$\langle \Lambda(k)| \, \bar{s}\Gamma^\mu b \, |\Lambda_b(p)\rangle \; \varepsilon^*_\mu(\lambda) \propto f^\Gamma_\lambda(q^2) \,, \tag{10.1}$$

where $q^2 = (p-k)^2$, and ε is the polarization vector of a fictitious vector mediator with polarization λ. For $1/2^+ \to 1/2^+$ transitions, this definition is achieved by the

Lorentz decomposition [277]:

$$\langle \Lambda(k,s_\Lambda)|\,\overline{s}\,\gamma^\mu\,b\,|\Lambda_b(p,s_{\Lambda_b})\rangle = \overline{u}_\Lambda(k,s_\Lambda)\Bigg[f_t^V(q^2)\,(m_{\Lambda_b}-m_\Lambda)\frac{q^\mu}{q^2} \tag{10.2}$$

$$+ f_0^V(q^2)\frac{m_{\Lambda_b}+m_\Lambda}{s_+}\left(p^\mu+k^\mu-(m_{\Lambda_b}^2-m_\Lambda^2)\frac{q^\mu}{q^2}\right)$$

$$+ f_\perp^V(q^2)\left(\gamma^\mu-\frac{2m_\Lambda}{s_+}p^\mu-\frac{2m_{\Lambda_b}}{s_+}k^\mu\right)\Bigg]u_{\Lambda_b}(p,s_{\Lambda_b})\,,$$

$$\langle \Lambda(k,s_\Lambda)|\,\overline{s}\,\gamma^\mu\gamma_5\,b\,|\Lambda_b(p,s_{\Lambda_b})\rangle = -\overline{u}_\Lambda(k,s_\Lambda)\,\gamma_5\Bigg[f_t^A(q^2)\,(m_{\Lambda_b}+m_\Lambda)\frac{q^\mu}{q^2} \tag{10.3}$$

$$+ f_0^A(q^2)\frac{m_{\Lambda_b}-m_\Lambda}{s_-}\left(p^\mu+k^\mu-(m_{\Lambda_b}^2-m_\Lambda^2)\frac{q^\mu}{q^2}\right)$$

$$+ f_\perp^A(q^2)\left(\gamma^\mu+\frac{2m_\Lambda}{s_-}p^\mu-\frac{2m_{\Lambda_b}}{s_-}k^\mu\right)\Bigg]u_{\Lambda_b}(p_{\Lambda_b},s_{\Lambda_b}),$$

$$\langle \Lambda(k,s_\Lambda)|\,\overline{s}\,i\sigma^{\mu\nu}q_\nu\,b\,|\Lambda_b(p,s_{\Lambda_b})\rangle = -\overline{u}_\Lambda(k,s_\Lambda)\Bigg[f_0^T(q^2)\frac{q^2}{s_+}\left(p^\mu+k^\mu-(m_{\Lambda_b}^2-m_\Lambda^2)\frac{q^\mu}{q^2}\right) \tag{10.4}$$

$$+ f_\perp^T(q^2)\,(m_{\Lambda_b}+m_\Lambda)\left(\gamma^\mu-\frac{2m_\Lambda}{s_+}\,p^\mu-\frac{2m_{\Lambda_b}}{s_+}\,k^\mu\right)\Bigg]u_{\Lambda_b}(p,s_{\Lambda_b})\,,$$

$$\langle \Lambda(k,s_\Lambda)|\,\overline{s}\,i\sigma^{\mu\nu}q_\nu\gamma_5\,b\,|\Lambda_b(p,s_{\Lambda_b})\rangle = -\overline{u}_\Lambda(k,s_\Lambda)\,\gamma_5\Bigg[f_0^{T5}(q^2)\,\frac{q^2}{s_-}\left(p^\mu+k^\mu-(m_{\Lambda_b}^2-m_\Lambda^2)\frac{q^\mu}{q^2}\right) \tag{10.5}$$

$$+ f_\perp^{T5}(q^2)\,(m_{\Lambda_b}-m_\Lambda)\left(\gamma^\mu+\frac{2m_\Lambda}{s_-}\,p^\mu-\frac{2m_{\Lambda_b}}{s_-}\,k^\mu\right)\Bigg]u_{\Lambda_b}(p,s_{\Lambda_b})\,,$$

where we abbreviate $\sigma^{\mu\nu}=\frac{i}{2}[\gamma^\mu,\gamma^\nu]$ and $s_\pm=(m_{\Lambda_b}\pm m_\Lambda)-q^2$. The labelling of the ten form factors follows the conventions of Ref. [280]. Each form factor, f_λ^Γ, arises in the current $\bar{s}\Gamma b$ in a helicity amplitude with polarization $\lambda=t,0,\perp$. We refer to Ref. [280] for details and the relations between the form factors and the helicity amplitudes. Note that the matrix elements for the scalar and pseudo-scalar current can be related to the vector and axial-vector current of the timelike-polarized form

factors f_t^V and f_t^A via the equations of motion:

$$\langle \Lambda(k,s_\Lambda)|\,\overline{s}\,b\,|\Lambda_b(p,s_{\Lambda_b})\rangle = \frac{q^\mu}{m_b-m_s}\,\langle \Lambda(k,s_\Lambda)|\,\overline{s}\,\gamma_\mu\,b\,|\Lambda_b(p,s_{\Lambda_b})\rangle$$

$$= f_t^V(q^2)\frac{m_{\Lambda_b}-m_\Lambda}{m_b-m_s}\overline{u}_\Lambda(k,s_\Lambda)\,u_{\Lambda_b}(p,s_{\Lambda_b})\,, \tag{10.6}$$

$$\langle \Lambda(k,s_\Lambda)|\,\overline{s}\,\gamma_5\,b\,|\Lambda_b(p,s_{\Lambda_b})\rangle = -\frac{q^\mu}{m_b+m_s}\,\langle \Lambda(k,s_\Lambda)|\,\overline{s}\,\gamma_\mu\gamma_5\,b\,|\Lambda_b(p,s_{\Lambda_b})\rangle$$

$$= f_t^A(q^2)\frac{m_{\Lambda_b}+m_\Lambda}{m_b+m_s}\overline{u}_\Lambda(k,s_\Lambda)\,\gamma_5\,u_{\Lambda_b}(p,s_{\Lambda_b})\,. \tag{10.7}$$

Although the ten functions, $f_\lambda^\Gamma(q^2)$, are a-priori independent, some relations exist at specific points in q^2. These so-called endpoint relations arise due to two different mechanisms. First, the hadronic matrix elements on the left-hand sides of Eq. (10.2) to Eq. (10.5) must be free of kinematic singularities. Two such singularities can arise, as spurious poles at $q^2=0$ and $q^2=q^2_{\rm max}\equiv(m_{\Lambda_b}-m_\Lambda)^2$. They are removed by the following identities:

$$f_t^V(0)=f_0^V(0)\,, \qquad\qquad f_t^A(0)=f_0^A(0)\,, \tag{10.8}$$

$$f_\perp^A(q^2_{\rm max})=f_0^A(q^2_{\rm max})\,, \qquad\qquad f_\perp^{T5}(q^2_{\rm max})=f_0^{T5}(q^2_{\rm max})\,. \tag{10.9}$$

In addition to the above, an algebraic relation between $\sigma^{\mu\nu}$ and $\sigma^{\mu\nu}\gamma_5$ ensures that

$$f_\perp^{T5}(0)=f_\perp^T(0)\,. \tag{10.10}$$

See also Ref. [326] for additional discussion of endpoint relations for baryon transition form factors.

10.2.2 Two-point correlation functions and OPE representation

Dispersive bounds for local form factors have a successful history. They were first used for the kaon form factor [327–329] and have also successfully been applied to exclusive $B\to\pi$ [330, 331] and $B\to D^{(*)}$ [322, 332, 333] form factors[1]. In the latter case, the heavy-quark expansion renders the bounds phenomenologically more useful due to relations between all form factors of transitions between doublets under heavy-quark spin symmetry [340], see Refs. [117, 118, 120] for recent phenomenological updates and analyses up to order $1/m^2$ in the heavy-quark expansion, respectively. The application of the bound to form factors arising in baryon-to-baryon

[1] See also applications [334–338] of the dispersive matrix method [339].

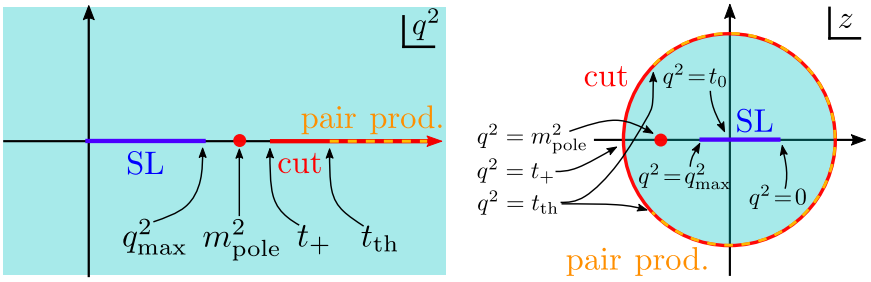

Figure 10.1: Sketch of the analytic structure of the baryon-to-baryon form factors in the variable q^2 (left) and the variable z (right). The q^2 range of semileptonic decays is marked "SL". The baryon/antibaryon pair production is marked "pair prod.". The form factors develop a branch cut below the baryon/antibaryon pair production threshold due to rescattering of virtual baryon/antibaryon pairs into, *e.g.*, $\bar{B}K^{(*)}$ pairs.

transitions is more complicated [173, 323], chiefly due to the fact that for any form factor, F, its first branch point, t_+^F, does not coincide with the threshold for baryon/antibaryon pair production, $t_{\rm th}^F$. Instead, the branch points lay to the left of the pair production points, at the pair production threshold for the corresponding ground-state meson/antimeson pair. We show a sketch of this structure in the left-hand side of Figure 10.1.

The dispersive bounds connect a theoretical computation of a suitably-chosen two-point function with weighted integrals of the squared hadronic form factors. For concreteness and brevity we derive the dispersive bound for the vector current J_V^μ and its hadronic form factors. The generalization to the currents

$$J_V^\mu = \bar{s}\gamma^\mu b\,, \qquad\qquad J_A^\mu = \bar{s}\gamma^\mu\gamma_5 b\,, \tag{10.11}$$

$$J_T^\mu = \bar{s}\sigma^{\mu\nu}q_\nu b\,, \qquad\qquad J_{T5}^\mu = \bar{s}\sigma^{\mu\nu}q_\nu\gamma_5\, b \tag{10.12}$$

is straight-forward following the same prescription as J_V^μ. As we will see below, the results for scalar and pseudo-scalar currents can be obtained from the vector and axial currents, respectively.

We define $\Pi_V^{\mu\nu}$ to be the vacuum matrix elements of the two point function with two insertions of J_V:

$$\Pi_V^{\mu\nu}(Q) = i\int \mathrm{d}^4x\; e^{iQ\cdot x}\,\langle 0|\,\mathcal{T}\{J_V^\mu(x), J_V^{\nu\dagger}(0)\}\,|0\rangle\;, \tag{10.13}$$

where Q^μ is the four-momentum flowing through the two-point function. This tensor-valued function can be expressed in terms of two scalar-valued functions:

$$\Pi_V^{\mu\nu}(Q) = P_{J=0}^{\mu\nu}(Q)\Pi_V^{J=0}(Q^2) + P_{J=1}^{\mu\nu}(Q)\Pi_V^{J=1}(Q^2)\,, \tag{10.14}$$

Γ	J	form factors	$\chi^J_\Gamma\vert_{\rm OPE}$ $[10^{-2}]$	n
V	0	f_t^V	1.42	1
V	1	f_0^V, $f_\perp^V$	$1.20\,/\,m_b^2$	2
A	0	f_t^A	1.57	1
A	1	f_0^A, $f_\perp^A$	$1.13\,/\,m_b^2$	2
T	1	f_0^T, $f_\perp^T$	$0.803\,/\,m_b^2$	3
$T5$	1	f_0^{T5}, $f_\perp^{T5}$	$0.748\,/\,m_b^2$	3

Table 10.1: The values of $\chi^J_\Gamma(Q^2=0)|_{\rm OPE}$ as taken from Ref. [341], which include terms at next-to-leading order in α_s and subleading power corrections. The number of derivatives for each current $\Gamma = V, A, S, P, T, T5$ is provided as n. Note that the results for χ in the rows for $\Gamma = T, T5$ differ from those given in Ref. [341] by a factor of $\frac{1}{4}$, which is due to differences in convention for the tensor current. The value of the b-quark mass is taken as $m_b = 4.2$ GeV.

using the two projectors

$$P^{\mu\nu}_{J=0}(p) = \frac{p^\mu p^\nu}{p^2}\,, \qquad\qquad P^{\mu\nu}_{J=1}(p) = \frac{1}{3}\left(\frac{p^\mu p^\nu}{p^2} - g^{\mu\nu}\right). \tag{10.15}$$

Note that the two tensor currents do not feature a $J = 0$ component, *i.e.*, the coefficients of the projectors $P_{J=0}$ vanish for these currents.

The functions $\Pi_V^{J=0}(Q^2)$ and $\Pi_V^{J=1}(Q^2)$ feature singularities along the real Q^2 axis, which will be discussed below. These singularities are captured by the discontinuities of $\Pi_V^{J=0}$ and $\Pi_V^{J=1}$. It is now convenient to define a new function, χ_V^J, which is completely described in terms of the discontinuities of the functions $\Pi_V^{J=1}$:

$$\chi_V^{J=1}(Q^2) = \frac{1}{n!}\left(\frac{d}{dQ^2}\right)^n \Pi_V^{J=1}(Q^2) = \frac{1}{2\pi i}\int_0^\infty \mathrm{d}t\,\frac{\mathrm{Disc}\,\Pi_V^{J=1}(t)}{(t-Q^2)^{n+1}}\,. \tag{10.16}$$

Here, the number of derivatives n (also known as the number of "subtractions") is chosen to be the smallest number that yields a convergent integral. Note that in general the functions χ for the scalar and pseudo-scalar currents require a different value of n than the functions for the vector and axial currents, respectively, despite the fact that they can be extracted from the vector and axial two-point correlators.

The dispersive bound is constructed by equating two different representation of χ_V with each other, based on the assumption of global *quark hadron duality*:

$$\chi_V^J\Big|_{\rm OPE} = \chi_V^J\Big|_{\rm hadr}\,. \tag{10.17}$$

The left-hand side representation is obtained from an operator product expansion (OPE) of the time-ordered product that gives rise to $\Pi_V^{\mu\nu}(Q)$. For $\bar{s}\Gamma b$ currents, the most recent analysis of these OPE results, including subleading contributions, has been presented in Ref. [341] for all the dimension-three currents considered in this work. We summarize results of the analysis for $Q^2 = 0$ in Table 10.1, where we also list the values for n on a per-current basis.
The right-hand side representation is obtained from the hadronic matrix elements of on-shell intermediate states. We will discuss this representation and its individual terms in the next section.

10.2.3 Hadronic representation of the bound

We continue to discuss the bounds for the case of the vector current, and concretely, the scalar-valued two-point function $\Pi_V^{J=1}$,

$$\Pi_V^{J=1} = [P_{J=1}]_{\mu\nu}\, \Pi_V^{\mu\nu} \,. \tag{10.18}$$

Its discontinuity due to a hadronic intermediate state, $H_{\bar{s}b}$, with flavour quantum numbers $B = -S = 1$ can be obtained using

$$\begin{aligned}\operatorname{Disc} \Pi_\Gamma^J = i \sum_{\text{spin}} \int \mathrm{d}\rho\, (2\pi)^4 \delta^{(4)} \left(q - \sum_i^n p_i \right) P_J^{\mu\nu}(q) \left\langle 0 \right| J_\Gamma^\mu \left| H_{b\bar{s}}(p_1, \ldots, p_n) \right\rangle \\ \times \left\langle H_{b\bar{s}}(p_1, \ldots, p_n) \right| J_\Gamma^{\nu\dagger} \left| 0 \right\rangle \,,\end{aligned} \tag{10.19}$$

where the $\mathrm{d}\rho$ is the phase-space element of the n-particle intermediate state. Below we consider the cases of one- and two-particle intermediate states, with:

$$\int \mathrm{d}\rho = \begin{cases} \displaystyle\int \frac{\mathrm{d}^3 p}{(2\pi)^3 2E_{\vec{p}}} & \text{for one-particle states,} \\ \displaystyle\int \frac{\mathrm{d}^3 p_1}{(2\pi)^3 2E_{\vec{p}_1}} \int \frac{\mathrm{d}^3 p_2}{(2\pi)^3 2E_{\vec{p}_2}} & \text{for two-particle states.} \end{cases} \tag{10.20}$$

One-particle contributions

Here, we discuss contributions due to a single asymptotic on-shell state $H_{b\bar{s}}$ with flavour quantum numbers $B = -S = 1$, which excludes states that strongly decay such as radially excited states. We continue to use the case $\Gamma = V$ as an example,

with $J = 1$. In that case, the discontinuity receives a single contribution:

$$\text{Disc}\,\Pi_V^{J=1}(q^2)\Big|_{1\text{pt}} = i\int \mathrm{d}\rho\,(2\pi)^4\delta^{(4)}(q-p)\sum_\lambda [P_{J=1}]_{\mu\nu}\,\langle 0|\,J_V^\mu\,|\bar{B}_s^*(p,\lambda)\rangle\,\langle \bar{B}_s^*(p,\lambda)|\,J_V^{\nu\dagger}\,|0\rangle \tag{10.21}$$

$$= i\int \mathrm{d}\rho\,(2\pi)^4\delta^{(4)}(q-p) m_{B_s^*}^2 f_{B_s^*}^2 \tag{10.22}$$

$$= 2\pi\delta(q^2 - m_{B_s^*}^2)\theta(q^0) m_{B_s^*}^2 f_{B_s^*}^2\,, \tag{10.23}$$

where λ is the polarization of the $\bar{B}_s^*$ meson and $m_{B_s^*}$ its mass. States other than the B_s^* do not contribute, since either their matrix elements with the $\Gamma = V$ current vanish; their projection onto the $J = 1$ state vanish; or they decay strongly. The generalization to $\Gamma = A$ and $J = 0$ is straightforward:

$$\text{Disc}\,\Pi_V^{J=0}(q^2)\Big|_{1\text{pt}} = 2\pi\delta(q^2 - m_{B_{s,0}^*}^2)\theta(q^0) m_{B_{s,0}^*}^2 f_{B_{s,0}^*}^2\,, \tag{10.24}$$

$$\text{Disc}\,\Pi_A^{J=0}(q^2)\Big|_{1\text{pt}} = 2\pi\delta(q^2 - m_{B_s}^2)\theta(q^0) m_{B_s}^2 f_{B_s}^2\,, \tag{10.25}$$

$$\text{Disc}\,\Pi_A^{J=1}(q^2)\Big|_{1\text{pt}} = 2\pi\delta(q^2 - m_{B_{s,1}}^2)\theta(q^0) m_{B_{s,1}}^2 f_{B_{s,1}}^2\,. \tag{10.26}$$

Here B_s is the ground-state pseudoscalar meson with a very well-known decay constant $f_{B_s} = 230.7 \pm 1.3$ MeV [342], $B_{s,1}$ is the axial vector meson, and $B_{s,0}^*$ is the scalar meson. In brief, the (pseudo)scalar current receives a contribution from a (pseudo)scalar on-shell state, and the axialvector current receives a contribution from an axialvector on-shell state. Although sub-BK-threshold $B_{s,1}$ or $B_{s,0}^*$ states have not yet been seen in the experiment, there are indications in lattice QCD analyses that such sub-threshold states exist [343]. However, the values of their respective decay constants are presently not very well known; estimates have been obtained, via QCD sum rule at next-to-leading order, in Ref. [344, 345]. Nevertheless, these states produce a pole both in the two-point functions Π_Γ^J and in their associated form factors, which is a necessary information for the formulation of the dispersive bounds and the form factor parametrization. From this point forward, we assume the presence of a single pole due to a $J^P = \{0^+, 1^-, 0^-, 1^+\}$ state contributing to form factors with $(\Gamma, J) = \{(V,0),(V,1),(A,0),(A,1)\}$, respectively.

The cases for currents with $\Gamma = T$ and $\Gamma = T5$ benefit from further explanation. For these currents one might assume that tensor, *i.e.*, $J^P = 2^\pm$, states play a leading role. However, these states do not contribute at all, since their matrix elements vanish:

$$\langle 0|\,\bar{s}\sigma^{\mu\nu}(\gamma_5)b\,|B_s(J^P = 2^\pm)\rangle = 0\,. \tag{10.27}$$

This can readily be understood, since the above matrix elements are antisymmetric in the indices μ and ν, while the polarization tensors of $J^P = 2^\pm$ mesons are symmetric quantities. Nevertheless, the currents $\Gamma = T$ and $\Gamma = T5$ do feature poles due to one-particle contributions, which arise from states with $J^P = 1^\pm$. We obtain:

$$\text{Disc}\,\Pi_T^{J=1}(q^2)\Big|_{\text{1pt}} = 2\pi\delta(q^2 - m_{B_s^*}^2)\theta(q^0)m_{B_s^*}^4(f_{B_s^*}^T)^2\,, \tag{10.28}$$

$$\text{Disc}\,\Pi_{T5}^{J=1}(q^2)\Big|_{\text{1pt}} = 2\pi\delta(q^2 - m_{B_{s,1}}^2)\theta(q^0)m_{B_{s,1}}^4(f_{B_{s,1}}^T)^2. \tag{10.29}$$

where $f_{B_s^*,T}$ and $f_{B_{s,1},T}$ are the decay constants of the respective state for a tensor current:

$$\langle 0|\, J_T^\mu\, |\bar{B}_s^*(p)\rangle = im_{B_s^*}^2 f_{B_s^*}^T\epsilon^\mu \qquad \langle 0|\, J_{T5}^\mu\, |\bar{B}_{s,1}(p)\rangle = -im_{B_{s,1}}^2 f_{B_{s,1}}^T\epsilon^\mu\,. \tag{10.30}$$

Plugging the results for the discontinuities into Eq. (10.23) we obtain:

$$\chi_V^{J=1}(Q^2)\Big|_{\text{1pt}} = \frac{m_{B_s^*}^2 f_{B_s^*}^2}{(m_{B_s^*}^2 - Q^2)^{n+1}}\,, \qquad \chi_V^{J=0}(Q^2)\Big|_{\text{1pt}} = \frac{m_{B_{s,0}^*}^2 f_{B_{s,0}^*}^2}{(m_{B_{s,0}^*}^2 - Q^2)^{n+1}}\,, \tag{10.31}$$

$$\chi_A^{J=1}(Q^2)\Big|_{\text{1pt}} = \frac{m_{B_{s,1}}^2 f_{B_{s,1}}^2}{(m_{B_{s,1}}^2 - Q^2)^{n+1}}\,, \qquad \chi_A^{J=0}(Q^2)\Big|_{\text{1pt}} = \frac{m_{B_s}^2 f_{B_s}^2}{(m_{B_s}^2 - Q^2)^{n+1}}\,, \tag{10.32}$$

$$\chi_T^{J=1}(Q^2)\Big|_{\text{1pt}} = \frac{m_{B_s^*}^4 (f_{B_s^*}^T)^2}{(m_{B_s^*}^2 - Q^2)^{n+1}}\,, \qquad \chi_{T5}^{J=1}(Q^2)\Big|_{\text{1pt}} = \frac{m_{B_{s,1}}^4 (f_{B_{s,1}}^T)^2}{(m_{B_{s,1}}^2 - Q^2)^{n+1}}\,. \tag{10.33}$$

The one-particle contributions each amount to about 10% of the respective OPE result.

Two-particle contributions

Here, we focus on the contributions to χ due to an intermediate $\Lambda_b\bar{\Lambda}$ state. By means of unitarity we can express the discontinuity of the two-particle correlator $\Pi_\Gamma^J(t)$ as a sum of intermediate $H_{b\bar{s}}$ states with flavour quantum numbers $B = -S = 1$:

$$\text{Disc}\,\Pi_\Gamma^J = i\sum_{\text{spins}}\int \text{d}\rho\,(2\pi)^4\delta^{(4)}(q - (p_1 + p_2))[P_J]_{\mu\nu}\,\langle 0|\, J_\Gamma^\mu\, |\Lambda_b(p_1, s_{\Lambda_b})\bar{\Lambda}(-p_2, s_\Lambda)\rangle$$

$$\times\,\langle\bar{\Lambda}(-p_2, s_\Lambda)\Lambda_b(p_1, s_{\Lambda_b})|\, J_\Gamma^{\nu\dagger}\, |0\rangle + \text{further positive terms}\,. \tag{10.34}$$

Note that further two-particle contributions for which dispersive bounds have been applied include $\bar{B}K, \bar{B}K^*$ and $\bar{B}_s\phi$ [341]. The effect of each of those two-particle

contributions would decrease the upper bound only by 1–4% [341], *i.e.*, by a smaller amount than the one-particle contributions.

We can evaluate the phase-space integration in the rest frame of the two-particle system as

$$\int \mathrm{d}\rho\,(2\pi)^4\delta^{(4)}(q-(p_1+p_2)) = \frac{1}{8\pi}\frac{\sqrt{\lambda(m_{\Lambda_b}^2,m_\Lambda^2,q^2)}}{q^2}\theta(q^2-s_{\Lambda_b\Lambda}), \tag{10.35}$$

with $s_{\Lambda_b\Lambda}=(m_{\Lambda_b}+m_\Lambda)^2$. From this we obtain

$$\mathrm{Disc}\,\Pi_\Gamma^J = \frac{i}{8\pi}\frac{\sqrt{\lambda(m_{\Lambda_b}^2,m_\Lambda^2,q^2)}}{q^2}\theta(q^2-s_{\Lambda_b\Lambda})[P_J]_{\mu\nu}\langle 0|\,J_\Gamma^\mu\,|\Lambda_b\bar\Lambda\rangle\,\langle\bar\Lambda\Lambda_b|\,J_\Gamma^{\nu\dagger}\,|0\rangle \tag{10.36}$$

where in the last line we dropped all further positive terms. In the following we summarize the contraction between helicity operators and matrix elements that can be expressed via local form factors.

$$[P_J]_{\mu\nu}\langle 0|\,J_V^\mu\,|\bar\Lambda\Lambda_b\rangle\,\langle\bar\Lambda\Lambda_b|\,J_V^{\nu\dagger}\,|0\rangle = \begin{cases} \dfrac{2(m_{\Lambda_b}-m_\Lambda)^2}{q^2}s_+(q^2)|f_t^V|^2 & \text{for } J=0,\\ \dfrac{2s_-(q^2)}{3q^2}\Big((m_{\Lambda_b}+m_\Lambda)^2|f_0^V|^2+2q^2\,|f_\perp^V|^2\Big) & \text{for } J=1, \end{cases} \tag{10.37}$$

$$[P_J]_{\mu\nu}\langle 0|\,J_A^\mu\,|\bar\Lambda\Lambda_b\rangle\,\langle\bar\Lambda\Lambda_b|\,J_A^{\nu\dagger}\,|0\rangle = \begin{cases} \dfrac{2s_-(q^2)}{q^2}(m_{\Lambda_b}+m_\Lambda)^2|f_t^A|^2 & \text{for } J=0,\\ \dfrac{2s_+(q^2)}{3q^2}\Big((m_{\Lambda_b}-m_\Lambda)^2|f_0^A|^2+2q^2\,|f_\perp^A|^2\Big) & \text{for } J=1, \end{cases} \tag{10.38}$$

$$[P_J]_{\mu\nu}\langle 0|\,J_T^\mu\,|\bar\Lambda\Lambda_b\rangle\,\langle\bar\Lambda\Lambda_b|\,J_T^{\nu\dagger}\,|0\rangle = \begin{cases} 0 & \text{for } J=0,\\ \dfrac{2s_-(q^2)}{3}\Big(2(m_{\Lambda_b}+m_\Lambda)^2|f_\perp^T|^2+q^2\,|f_0^T|^2\Big) & \text{for } J=1, \end{cases} \tag{10.39}$$

$$[P_J]_{\mu\nu}\langle 0|\,J_{T5}^\mu\,|\bar\Lambda\Lambda_b\rangle\,\langle\bar\Lambda\Lambda_b|\,J_{T5}^{\nu\dagger}\,|0\rangle = \begin{cases} 0 & \text{for } J=0,\\ \dfrac{2s_+(q^2)}{3}\Big(2(m_{\Lambda_b}-m_\Lambda)^2|f_\perp^{T5}|^2+q^2\,|f_0^{T5}|^2\Big) & \text{for } J=1, \end{cases} \tag{10.40}$$

where the sum over the baryon spins is implied.

10.2.4 Parametrization

We relate the OPE representation to the hadronic representation of the functions χ_Γ^J through Eq. (10.17). Using $\Gamma = V$ and $J = 1$ again as an example, the dispersive bound takes the form

$$\chi_V^{J=1}(Q^2)\Big|_{\text{OPE}} \geq \chi_V^{J=1}(Q^2)\Big|_{\text{1pt}} + \int_{s_{\Lambda_b\Lambda}}^{\infty} \mathrm{d}t\, \frac{1}{24\pi^2} \frac{\sqrt{\lambda(m_{\Lambda_b}^2, m_\Lambda^2, t)}}{t^2(t-Q^2)^{n+1}} s_-(t) \tag{10.41}$$

$$\times \Big((m_{\Lambda_b} + m_\Lambda)^2 |f_0^V(t)|^2 + 2t|f_\perp^V(t)|^2\Big)\,,$$

where the last term is the two-particle contribution due to the ground-state baryons. Our intent is now to parametrize the $\Lambda_b \to \Lambda$ form factors (here: $f_0^V, f_\perp^V$) in such a way that their parameters enter the two-particle contributions to χ_Γ in a simple form. Concretely, we envisage a contribution that enters as the 2-norm of the vector of parameters.

In general, the bounds are best represented by transforming the variable t to the new variable z, defined as

$$z(t; t_0, t_+) = \frac{\sqrt{t_+ - t} - \sqrt{t_+ - t_0}}{\sqrt{t_+ - t} + \sqrt{t_+ - t_0}}\,. \tag{10.42}$$

In the above, t_0 corresponds to the zero of $z(t)$ and is a free parameter that can be chosen, and t_+ corresponds to lowest branch point of the form factors. The mapping from $t = q^2$ to z is illustrated in Figure 10.1. The integral comprising the two-particle contribution starts at the pair-production threshold t_{th}.

When discussing the dispersive bounds for e.g. $B \to D$ or $B \to \pi$ form factors, one has $t_{\text{th}} = t_+$. The integral of the discontinuity along the real t axis in the mesonic analogue of Eq. (10.41) then becomes a contour integral along the unit circle $|z| = 1$. For an arbitrary function g,

$$\begin{aligned}\int_{t_{\text{th}}=t_+}^{\infty} \mathrm{d}t\, \text{Disc}\, g(t) &= \frac{1}{2} \oint_{|z|=1} \mathrm{d}z \left|\frac{\mathrm{d}t(z)}{\mathrm{d}z}\right| \text{Disc}\, g(t(z)) \\ &= \frac{i}{2} \int_{-\pi}^{+\pi} \mathrm{d}\alpha \left|\frac{\mathrm{d}t(z)}{\mathrm{d}z}\right| e^{i\alpha}\, \text{Disc}\, g(t(e^{i\alpha}))\,. \end{aligned} \tag{10.43}$$

The contribution to the integrand from a form factor F is then written as $|\phi_F|^2|F|^2$, where the *outer function* ϕ_F is constructed such that the product $\phi_F F$ is free of kinematic singularities on the unit disk $|z| < 1$ [330, 332, 333, 340, 346]. The product of outer function and form factor is then commonly expressed as a power series in

z, which is bounded in the semileptonic region. Powers of z are orthonormal with respect to the scalar product

$$\langle z^n | z^m \rangle \equiv \oint_{|z|=1} \frac{\mathrm{d}z}{iz}\, z^{n,*} z^m = \int_{-\pi}^{+\pi} \mathrm{d}\alpha\, z^{n,*} z^m \Big|_{z=e^{i\alpha}} = 2\pi\delta_{nm}\,, \tag{10.44}$$

that is, when integrated over the entire unit circle. As a consequence, for an analytic function on the z unit disk that is square-integrable on the z unit circle, the Fourier coefficients exist only for positive index n and coincide with the Taylor coefficients for an expansion in $z = 0$. The contribution to the dispersive bound can then be expressed as the 2-norm of the Taylor coefficients. For more details of the derivation, we refer the reader to Ref. [339].

For $b \to s$ transitions, $\bar{B}_s\pi$ intermediate states produce the lowest-lying branch cut. However, production of a $\bar{B}_s\pi$ state from the vacuum through a $\bar{s}b$ current violates isospin symmetry and is therefore strongly suppressed. For the purpose of this analysis we set t_+ to the first branch point that contributes in the isospin symmetry limit:

$$t_+ \equiv (m_B + m_K)^2\,. \tag{10.45}$$

The integral contribution for $\bar{B}K$ intermediate states can then be mapped onto the entire unit circle in z as discussed above, and their contributions to the dispersive bound can be expressed as the 2-norm of their Taylor coefficients. However, intermediate states with larger pair-production thresholds cover only successively smaller *arcs of the unit circle*, and the correspondence of the 2-norm of the Taylor coefficients and their contributions to the dispersive bound does not hold any longer. The branch point at t_+ arises from scattering into on-shell $\bar{B}K$ intermediate states.

In the following, we discuss the application of the series expansion to baryon-to-baryon form factors in the presence of a dispersive bound. The main difference between our approach and other parametrizations is that we do not assume the lowest branch point t_+ to coincide with the baryon/antibaryon threshold $t_{\mathrm{th}} > t_+$. As a consequence, the contour integral representing the form factor's contribution to its bound is supported only on the arc of the unit circle with opening angle $2\alpha_{\Lambda_b\Lambda}$, where

$$\alpha_{\Lambda_b\Lambda} = \arg z((m_\Lambda + m_{\Lambda_b})^2)\,. \tag{10.46}$$

Specifically, Eq. (10.41) becomes

$$\begin{aligned} 1 \geq{}& \frac{1}{48\pi^2 \chi_V^{J=1}(Q^2)\big|_{\mathrm{OPE}}} \int_{-\alpha_{\Lambda_b\Lambda}}^{+\alpha_{\Lambda_b\Lambda}} \mathrm{d}\alpha \left| \frac{\mathrm{d}z(\alpha)}{\mathrm{d}\alpha} \frac{\mathrm{d}t(z)}{\mathrm{d}z} \right| \frac{\sqrt{\lambda(m_{\Lambda_b}^2, m_\Lambda^2, t)}}{t^2(t-Q^2)^{n+1}} s_-(t) \\ &\times \Big((m_{\Lambda_b} + m_\Lambda)^2 |f_0^V(t)|^2 + 2t |f_\perp^V(t)|^2 \Big) \qquad (10.47) \\ \equiv{}& \int_{-\alpha_{\Lambda_b\Lambda}}^{+\alpha_{\Lambda_b\Lambda}} \mathrm{d}\alpha \, \Big(|\phi_{f_0^V}(z)|^2 |f_0^V(z)|^2 + |\phi_{f_\perp^V}(z)|^2 |f_\perp^V(z)|^2 \Big)_{z=e^{i\alpha}}\,, \qquad (10.48) \end{aligned}$$

where $t = t(z(\alpha))$, and we dropped the one-particle contributions for legibility. Here, $\phi_{f_0^V}(z), \phi_{f_\perp^V}(z)$ are the outer functions for the form factors f_0^V and $f_\perp^V$. The full list of expressions for the outer functions of all baryon-to-baryon form factors is compiled in Appendix B.

A form factor's contribution to the bound is expressed in terms of an integral with a positive definite integrand. Hence, we immediately find that a parametrization that assumes integration over the full unit circle rather than the relevant pair production arc $|\alpha| < \alpha_{\Lambda_b\Lambda}$ *overestimates* the saturation of the dispersive bound due to that form factor. To express the level of saturation due to each term in Eq. (10.48) as a 2-norm of some coefficient sequence, we expand the form factors in a basis of polynomials $p_n(z)$. These polynomials must be orthonormal with respect to the scalar product

$$\langle p_n | p_m \rangle \equiv \oint_{\substack{|z|=1 \\ |\arg z| \leq \alpha_{\Lambda_b\Lambda}}} \frac{\mathrm{d}z}{iz}\, p_n^*(z)\, p_m(z) = \int_{-\alpha_{\Lambda_b\Lambda}}^{+\alpha_{\Lambda_b\Lambda}} \mathrm{d}\alpha\, p_n^*(z)\, p_m(z)\Big|_{z=e^{i\alpha}} = \delta_{nm}\,. \tag{10.49}$$

The polynomials $p_n(z)$ are the Szegő polynomials [347], which can be derived via the the Gram-Schmidt procedure; see details in Appendix A. A computationally efficient and numerically stable evaluation of the polynomials can be achieved using the Szegő recurrence relation [347], which we use in the reference implementation of our parametrization as part of the `EOS` software. The first five so-called Verblunsky coefficients that uniquely generate the polynomials are listed in Append A.

Our series expansion for the parametrization of the local form factors now takes the form

$$f_\lambda^\Gamma(q^2) = \frac{1}{\mathcal{P}(q^2)\,\phi_{f_\lambda^\Gamma}(z)} \sum_{i=0}^{\infty} a_{f_\lambda^\Gamma}^i\; p_i(z), \tag{10.50}$$

where $\mathcal{P}(q^2) = z(q^2; t_0 = m_{\text{pole}}^2, t_+)$ is the Blaschke factor, $\phi_{f_\lambda^\Gamma}(z)$ is the outer function and $p_i(z)$ are the orthonormal polynomials. The Blaschke factor takes into account bound-state poles below the lowest branch point t_+ without changing the contribution to the dispersive bound [339]. Here, we assume each form factor to have a single bound-state pole, with the masses given in Table 10.2. For our parametrization, we choose $t_0 = q_{\text{max}}^2 = (m_{\Lambda_b} - m_\Lambda)^2$. The rationale as is as follows: at negative values of z, the Szegő polynomials oscillate as functions of their index n. Our choice of t_0 means that the entire semileptonic phase is mapped onto the *positive* real z axis. Given that the lattice data does not show any oscillatory pattern, this choice appears to be the most appropriate. While our parametrization appears to feature all of the benefits inherent to the BGL parametrization for meson-to-meson form factors [332], this is not the case. The BGL parametrization uses the z^n monomials, which are bounded on the open unit disk. As a consequence, the form factor parametrization for processes such as $\bar{B} \to D$ are an *absolutely convergent* series [339]. This benefit

does not translate to the baryon-to-baryon form factors.[2] The polynomials p_n are not bounded on the open unit disk. In fact, the Szegő recurrence relation combined with the Szegő condition provide that $p_n(z=0)$ increase exponentially with n for large n. Nevertheless, our proposed parametrization proves to be useful to limit the truncation error, as demonstrated in Sec. 10.3.

Based on Eq. (10.37)–(10.40), we arrive at *strong unitarity bounds* on the form-factor coefficients:

$$\sum_{i=0}^{\infty} |a^i_{f_t^V}|^2 \leq 1 - \frac{\chi_V^{J=0}\big|_{\rm 1pt}}{\chi_V^{J=0}\big|_{\rm OPE}}\,, \qquad \sum_{i=0}^{\infty} |a^i_{f_t^A}|^2 \leq 1 - \frac{\chi_A^{J=0}\big|_{\rm 1pt}}{\chi_A^{J=0}\big|_{\rm OPE}}\,, \tag{10.51}$$

$$\sum_{i=0}^{\infty} \left\{|a^i_{f_0^V}|^2 + |a^i_{f_\perp^V}|^2\right\} \leq 1 - \frac{\chi_V^{J=1}\big|_{\rm 1pt}}{\chi_V^{J=1}\big|_{\rm OPE}}\,, \quad \sum_{i=0}^{\infty} \left\{|a^i_{f_0^A}|^2 + |a^i_{f_\perp^A}|^2\right\} \leq 1 - \frac{\chi_A^{J=1}\big|_{\rm 1pt}}{\chi_A^{J=1}\big|_{\rm OPE}}\,, \tag{10.52}$$

$$\sum_{i=0}^{\infty} \left\{|a^i_{f_0^T}|^2 + |a^i_{f_\perp^T}|^2\right\} \leq 1 - \frac{\chi_T^{J=1}\big|_{\rm 1pt}}{\chi_T^{J=1}\big|_{\rm OPE}}\,, \quad \sum_{i=0}^{\infty} \left\{|a^i_{f_0^{T5}}|^2 + |a^i_{f_\perp^{T5}}|^2\right\} \leq 1 - \frac{\chi_{T5}^{J=1}\big|_{\rm 1pt}}{\chi_{T5}^{J=1}\big|_{\rm OPE}}\,. \tag{10.53}$$

Note that here we also subtracted the one-particle contributions, which are discussed in Sec. 10.2.3. However, this subtraction decreases the bound by only $\sim 10\%$. In our statistical analysis of only $\Lambda_b \to \Lambda$ form factors, we find that this subtraction is not yet numerically significant. Nevertheless, we advocate to include the one-particle contributions in global fits of the known local $b \to s$ form factors, where their impact will likely be numerically relevant.

At this point, we have not yet employed the endpoint relations given in Eq. (10.8) - (10.10). By using the endpoint relations, we can express the zeroth coefficient of $f_t^V, f_t^A, f_\perp^A, f_\perp^T, f_0^{T5}$ in terms of coefficients of other form factors.

Our proposed parametrization has two tangible benefits. First, each form factor parameter a_k is bounded in magnitude, $|a_k| \leq 1$. The N dimensional parameter space is therefore restricted to the hypercube $[-1,+1]^N$. We refer to this type of parameter bound as the *weak bound*[3]. It facilitates fits to theoretical or phenomenological inputs on the form factors, since the choice of a prior is not subjective.

[2] It also does not transfer to form factors for processes such as $\bar{B}_s \to D_s$ or $\bar{B}_s \to \bar{K}$, which suffer from the same problem: branch cuts below their respective pair-production thresholds. Our approach can be adjusted for these form factors.

[3] Our definitions of *weak* and *strong* bounds differ from the definitions proposed in Ref. [120]. There, what we call the *weak bound* is not considered in isolation, and what we call the *strong bound* is labelled a "weak bound", in contrast to a "strong bound" that affects more than one decay process.

Form factor	Pole spin-parity J^P	m_{pole} in GeV
$f_0^V, f_\perp^V, f_0^T, f_\perp^T$	1^-	5.416
f_t^V	0^+	5.711
$f_0^A, f_\perp^A, f_0^{T5}, f_\perp^{T5}$	1^+	5.750
f_t^A	0^-	5.367

Table 10.2: List of B_s meson pole masses appearing in the different form factors. The values are taken from Refs. [343, 348].

Second, the form factor parameters are restricted by the *strong bounds* Eq. (10.51) to Eq. (10.53). In the absence of the small number of exact relations between the form factors that we discussed earlier, this strong bound is in fact an upper bound on the sum of the squares of the form-factor parameters. As a consequence, the parameter space is further restricted to the combination of four hyperspheres, one per bound.[4] The strong bounds imply that the sequence of form factor parameters asymptotically falls off faster than $1/\sqrt{k}$. This behaviour does not prove absolute convergence of the series expansion of the form factors, which would require a fall off that compensates the exponential growth of the polynomials. Nevertheless, we will assume sufficient convergence of the form factors from this point on. Below, we check empirically if the strong bound suffices to provide bounded uncertainties for the form factors in truncated expansions.

10.3 Statistical Analysis

10.3.1 Data Sets

To illustrate the power of our proposed parametrization, we carry out a number of Bayesian analyses to the lattice QCD results for the full set of $\Lambda_b \to \Lambda$ form factors as provided in Ref. [278]. These analyses are all carried out using the `EOS` software [349], which has been modified for this purpose. Our proposed parametrization for the $\Lambda_b \to \Lambda$ form factors is implemented as of `EOS` version 1.0.2 [350]. The form factors are constrained by a multivariate Gaussian likelihood that jointly describes synthetic data points of the form factors, up to three per form factor. Each data point is generated for one of three possible values of the momentum transfer q^2: $q_i^2 \in \{13, 16, 19\}$ GeV^2. The overall q^2 range is chosen based on the availability of lattice

[4]The form factor relations mix the parameters of form factors that belong to different strong bounds, thereby making a geometric interpretation less intuitive.

QCD data points in Ref. [278]. The synthetic data points are illustrated by black crosses in Figs. 10.2–10.3.

Reference [278] provides two sets of parametrizations of the form factors in the continuum limit and for physical quark masses, obtained from one "nominal" and one "higher-order" fit to the lattice data. The nominal fit uses first-order z expansions, which are modified with correction terms that describe the dependence on the lattice spacing and quark masses. The higher-order fit uses second-order z expansions and also includes higher-order lattice-spacing and quark-mass corrections. The parameters that only appear in the higher-order fit are additionally constrained with Gaussian priors. In the case of lattice spacing and quark masses, these priors are well motivated by effective field theory considerations [278]. In the higher-order fit, the coefficients $a^2_{f^\Gamma_\lambda}$ of the z expansion are also constrained with Gaussian priors, centered around zero and widths equal to twice the magnitude for the corresponding coefficients $a^1_{f^\Gamma_\lambda}$ obtained within the nominal fit. This choice of prior was less well motivated but has little effect in the high-q^2 region. Ref. [278] recommends to use the following procedure for evaluating the form factors in phenomenological applications: the nominal-fit results should be used to evaluate the central values and statistical uncertainties, while a combination of the higher order-fit and nominal-fit results should be used to estimate systematic uncertainties as explained in Eqs. (50)–(56) in Ref. [278].

To generate the synthetic data points for the present work, we first updated both the nominal and the higher-order fits of Ref. [278] with minor modifications: we now enforce the endpoint relations among the form factors at $q^2 = 0$ *exactly*, rather than approximately as done in Ref. [278], and we include one additional endpoint relation $f_\perp^{T5}(0) = f_\perp^T(0)$, which is not used in Ref. [278].

The synthetic data points for f_0^V, f_0^A and $f_\perp^T$ at $q^2 = 13\ \text{GeV}^2$, and f_0^A and f_0^{T5} at $19\ \text{GeV}^2$, have strong correlation with other data points. This can be understood, since five exact relations hold for these form factors either at $q^2 = 0$ or $q^2 = (m_{\Lambda_b} - m_\Lambda)^2$ between pairs of form factors. We remove the synthetic data points listed above, which renders the covariance matrix regular and positive definite. We arrive at a 25 dimensional multivariate Gaussian likelihood. The likelihood is accessible under the name

`Lambda_b->Lambda::f_time+long+perp^V+A+T+T5[nominal,no-prior]DM:2016A`

as part of the constraints available within the `EOS` software.

10.3.2 Models

In this analysis, we consider a variety of statistical models. First, we truncate the series shown in Eq. (10.50) at $N = 2$, 3 or 4. The number of form factor parameters is $10(N + 1)$, due to a total of ten form factors under consideration. Since we implement the five form factors relations *exactly*, the number of fit parameters is smaller than the number of form factor parameters by five. Hence, we arrive at

between $P = 25$ and $P = 45$ fit parameters. We use three different types of priors in our analyses. An analysis labelled "w/o bound" uses a uniform prior, which is chosen to contain at least 99% of the integrated posterior probability. An analysis labelled "w/ weak bound" uses a uniform prior on the hypercube $[-1, +1]^P$, thereby applying the weak bound for all fit parameters. An analysis labelled "w/ strong bound" uses the same prior as the weak bound. In addition, we modify the posterior to include the following element, which can be interpreted either as an informative non-linear prior or a factor of the likelihood. For each of the six bounds $B(\{a_n\})$, we add the penalty term [117]

$$\begin{cases} 0 & \rho_B < 1, \\ 100(\rho_B - 1)^2 & \text{otherwise} \end{cases} \tag{10.54}$$

to $-2 \ln \text{Posterior}$. Here, $\rho_B = \sum_n |a_n|^2$, and the sum includes only the parameters affected by the given bound B. The additional terms penalize parameter points that violate any of the bounds with a one-sided χ^2-like term. The factor of 100 corresponds to the inverse square of the relative theory uncertainty on the bound, which we assume to be 10%. This uncertainty is compatible with the results obtained in Ref. [341]. In the above, we use unity as the largest allowed saturation of each bound. As discussed in Sec. 10.2.3, one-body and mesonic two-body contributions to the bounds are known. They could be subtracted from the upper bounds. However, we suggest here to include these contributions on the left-hand side of the bound in a global analysis of the available $b \to s$ form factor data. A global analysis clearly benefits from this treatment, which induces non-trivial theory correlations among the form factor parameters across different processes. It also clearly goes beyond the scope of the present work.

For $N = 2$, the number of parameters is equal to the number of data points, and we arrive at zero degrees of freedom. For $N > 2$, the number of parameters exceeds the number of data points. Hence, a frequentist statistical interpretation is not possible in these cases. Within our analyses, we instead explore whether the weak or strong bounds suffice to limit the a-posteriori uncertainty on the form factors, despite having zero or negative degrees of freedom.

10.3.3 Results

We begin with three analyses at truncation $N = 2$, using each of the three types of priors defined above. In all three analyses, we arrive at the same best-fit point. This indicates clearly that the best-fit point not only fulfills the weak bound, but also the strong bound. We explicitly confirm this by predicting the saturation of the individual bounds at the best-fit point. These range between 12% (for the 1^- bound) and 33% (for the 1^+ bound), which renders the point *well within* the region allowed by the strong bound. Accounting for the known one-particle contributions does not change this conclusion. At the maximum-likelihood point, the χ^2 value arising from

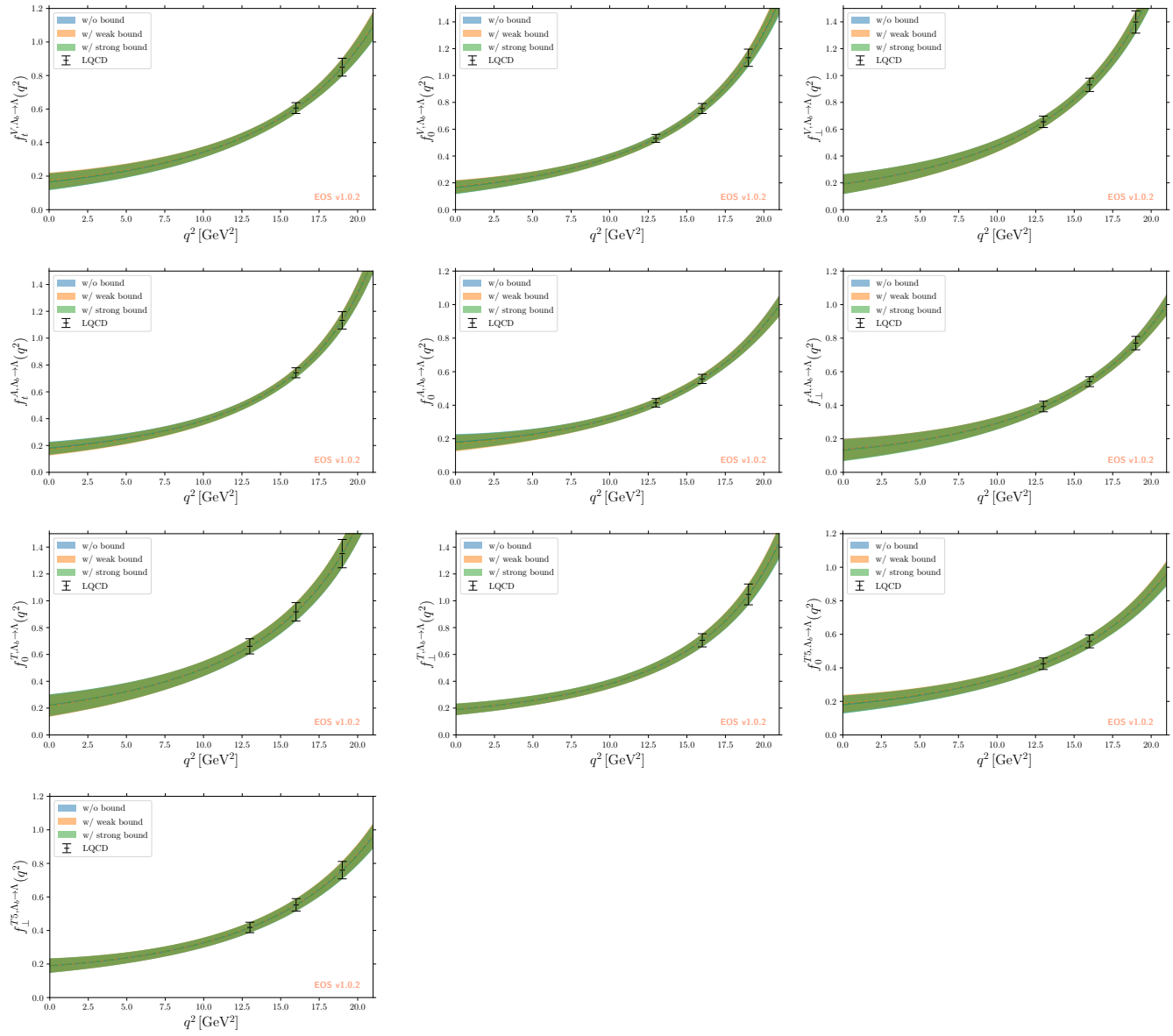

Figure 10.2: Uncertainty bands for the a-posteriori form-factor predictions of the ten form factors. The bands comprise the central 68% probability interval at every point in q^2. We show the form factor results at $N = 2$ in the absence of any bounds, using weak bounds $|a^i_{V,\lambda}| < 1$, and using the strong bounds (see text), respectively. The markers indicate the synthetic lattice data points.

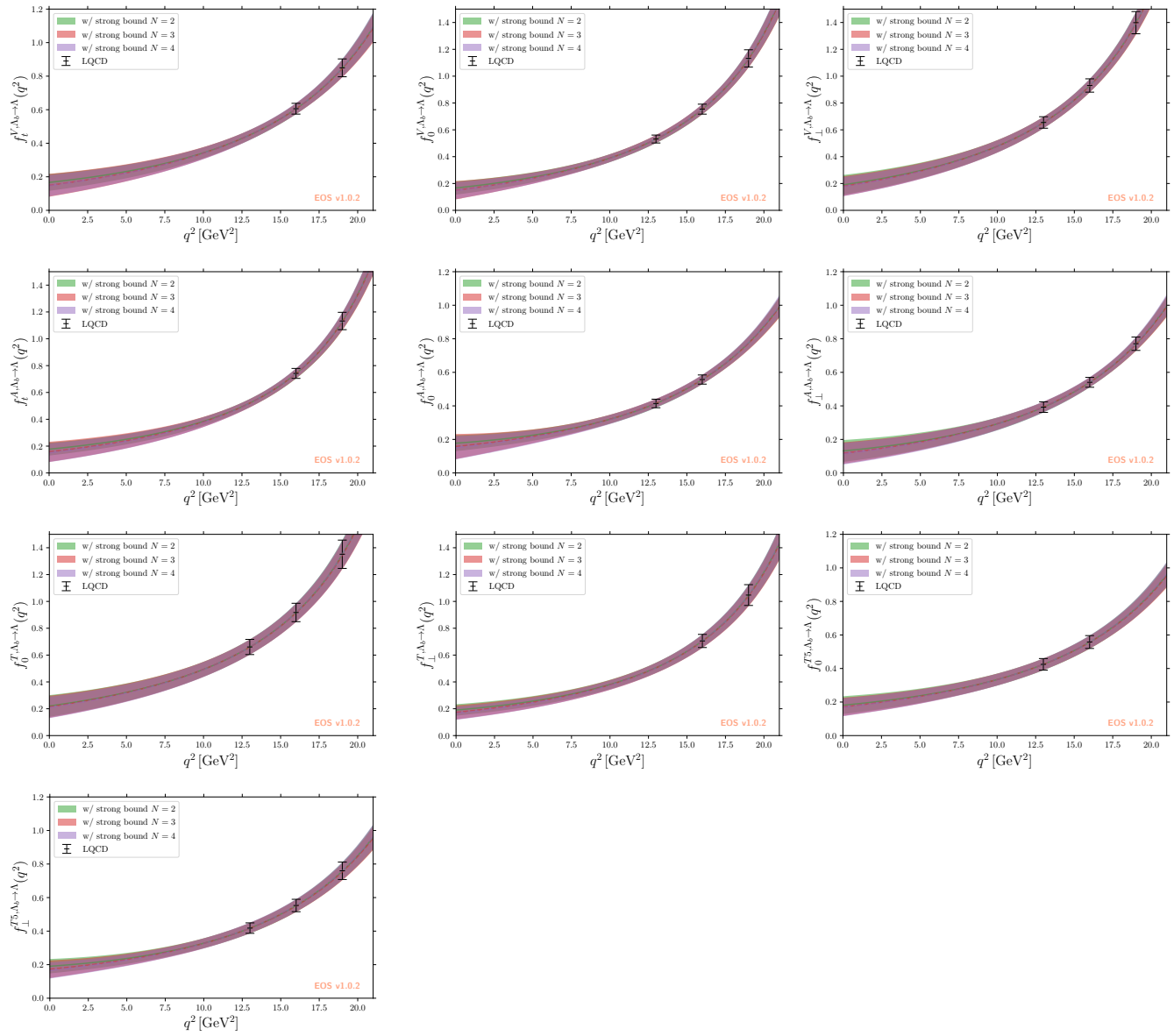

Figure 10.3: Uncertainty bands for the a-posteriori form-factor predictions of the ten form factors. The bands comprise the central 68% probability interval at every point in q^2. We show the form factor results at $N \in \{2, 3, 4\}$ when using the strong bound. Note that for $N > 2$ we have more parameters than data points. Finite uncertainty envelopes are enforced by the bound. The markers indicate the synthetic lattice data points.

the likelihood is compatible with zero at a precision of 10^{-5} or better. For each of the three analyses, we obtain a unimodal posterior and sample from the posterior using multiple Markov chains and the Metropolis-Hastings algorithm [351, 352]. We use these samples to produce posterior-predictive distributions for each of the form factors, which are shown in Figures 10.2–10.3 on the left-hand side. We observe that the strong bound has some impact on the form factor uncertainties, chiefly far away from the region where synthetic data points are available. For $N = 2$, we do not find a significant reduction of the uncertainties due to the application of the strong bound. Rather, it influences the shape of the form factors and suppresses the appearance of local minima in the form factors close to $q^2 = 0$, which become visible when extrapolating to negative q^2. The modified shape aligns better with the naive expectation that the form factors rise monotonically with increasing q^2 below the first subthreshold pole. It also provides confidence that, with more precise lattice QCD results, analyses of the nonlocal form factors at negative q^2 can be undertaken. This opens the door toward analysis in the spirit of what has been proposed in Refs. [353, 354].

We continue with three analyses using the strong bound, for $N = 2$, $N = 3$, and $N = 4$. Due to the nature of the orthonormal polynomials, the best-fit point for $N = 2$ is not expected to be nested within the $N = 3$ and $N = 4$ solutions. Similarly, the $N = 3$ best-fit point is not nested within the $N = 4$ solution. In all three cases, we find a single point that maximizes the posterior. For all three points we find that the bounds are fulfilled and consequently we obtain χ^2 values consistent with zero. The form-factor shapes are compatible between the $N = 2$, 3 and 4 solutions. We show the a-posteriori form factor envelopes at 68% probability together with the median values in Figure 10.3. A clear advantage of our proposed parameterization is that the uncertainties in the large recoil region, *i.e.* away from the synthetic data points, do not increase dramatically when N increases. This is in stark contrast with a scenario without any bounds on the coefficients a_n, where the a-posteriori uncertainty for the form factors would be divergent for negative degrees of freedom. This indicates that the bounds are able to constrain the parameterization even in an underconstrained analysis and gives confidence that the series can be reliably truncated in practical applications of this method. Figure 10.4 shows the saturation of the strong bound for the different form factors with $N = 2$, 3 and 4. For $N = 2$, the bounds are saturated between $10 - 30\%$. This is as large or even larger than the one-particle contributions, which saturate the bounds to $\sim 10\%$ and much larger than the two-particle mesonic contributions, which saturate the bounds by only 1–4% [341]. As N increases, the average saturation of the bounds increases. This is expected as additional parameters have to be included in the bound. The observed behaviour of the bound saturation provides further motivation for a global analysis of all $b \to s$ form factor data.

Based on the updated analysis of the lattice data of Ref. [278], we produce a-posteriori prediction obtain for the tensor form factor $f_\perp^T$ at $q^2 = 0$ from our analyses. We use this form factor as an example due to its phenomenological rel-

evance in predictions of $\Lambda_b \to \Lambda\gamma$ observables. Moreover, its location at $q^2 = 0$ provides the maximal distance between a phenomenologically relevant quantity and the synthetic lattice QCD data points, thereby maximizing the parametrization's systematic uncertainty. Applying the strong bound, we obtain

$$\begin{aligned} f_\perp^T(q^2=0)\Big|_{N=2} &= 0.190 \pm 0.043\,, \\ f_\perp^T(q^2=0)\Big|_{N=3} &= 0.173 \pm 0.053\,, \\ f_\perp^T(q^2=0)\Big|_{N=4} &= 0.166 \pm 0.049\,. \end{aligned} \tag{10.55}$$

We observe a small downward trend in the central value and stable parametric uncertainties. The individual bands are compatible with each other within their uncertainties. We remind the reader that our results are obtained for negative degrees of freedom and should therefore not be compared with the behaviour of a regular fit. Our results should be compared with

$$f_\perp^T(q^2=0)\Big|_{[278]} = 0.166 \pm 0.072\,. \tag{10.56}$$

This value and its uncertainty is obtained from the data and method described in Ref. [278], however, includes the exact form factor relation Eq. (10.10), which has not been previously used. Our parametrization exhibits a considerably smaller parametric uncertainty.

10.4 Conclusion

In this work we have introduced a new parametrization for the ten independent local $\Lambda_b \to \Lambda$ form factors. Our parametrization has the advantage that the parameters are bounded, due to the use of orthonormal polynomials that diagonalize the form factors' contribution within their respective dispersive bounds. Using a Bayesian analysis of the available lattice QCD results for the $\Lambda_b \to \Lambda$ form factors, we illustrate that our parametrization provides excellent control of systematic uncertainties when extrapolating from low to large hadronic recoil. To that end, we investigate our parametrization for different truncations and observe that the extrapolation uncertainty does not increase significantly within the kinematic phase space of $\Lambda_b \to \Lambda\ell^+\ell^-$ decays. We point out that the dispersive bounds are able to constrain the form factor uncertainties to such an extent that a massively underconstrained analyses still exhibit stable uncertainty estimates. This is a clear benefit compared to other parametrizations.

For future improvements of the proposed parametrization, one can insert the framework of dispersive bounds directly into the lattice-QCD analysis. Moreover, by including the one-particle contributions, as discussed in Sec. 10.2.3, and other

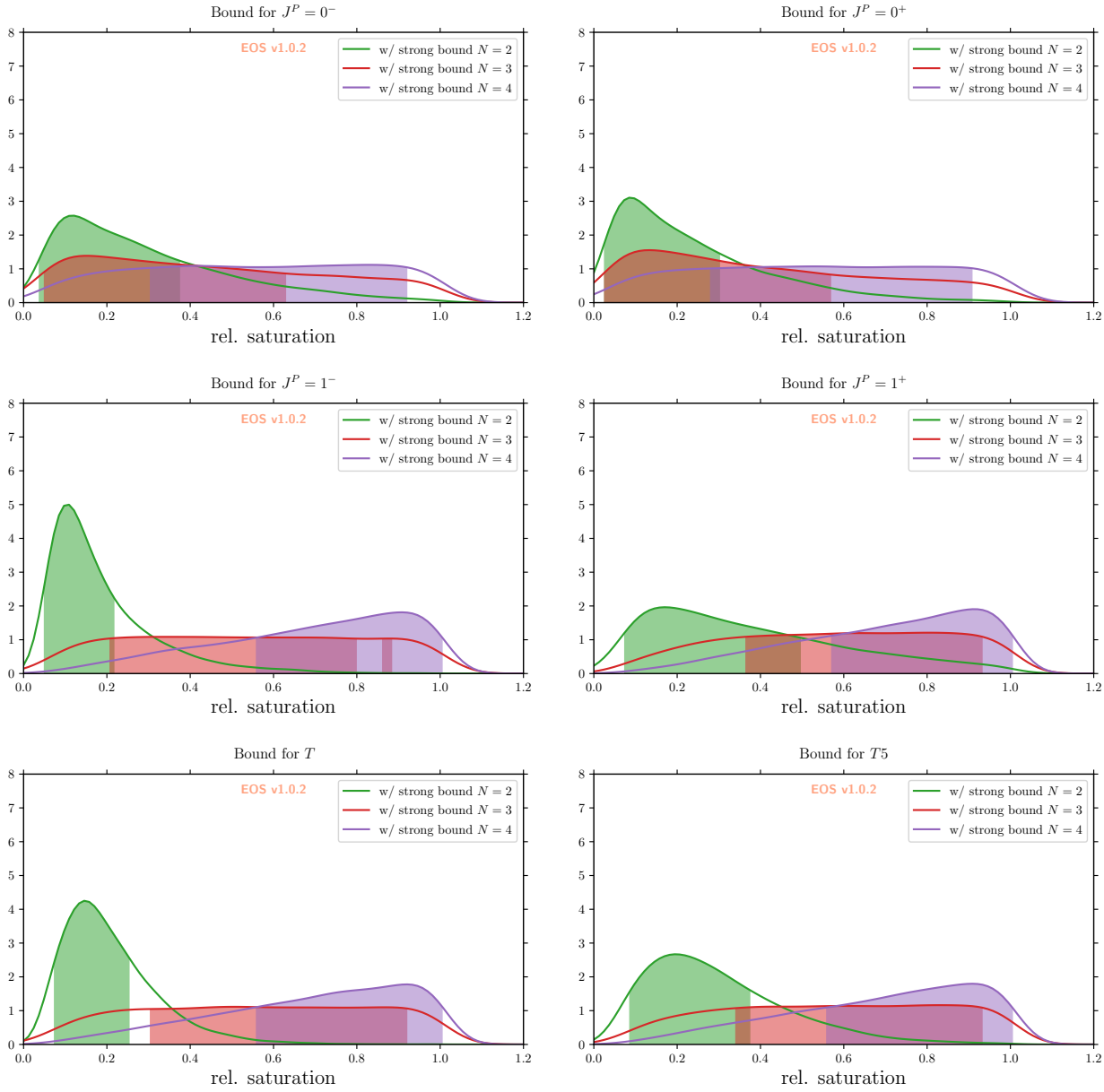

Figure 10.4: Relative saturation of the form factors with their respective spin-parity number J^P obtained from posterior samples. The saturation's are shown for different truncation's of N, where the coefficients are constrained through the strong unitarity bound. The vertical bands comprise the central 68% probability interval.

two-particle contributions, as discussed in Sec. 10.2.3, in a global analysis of the available $b \to s$ form factor data, we would expect even more precise results to be obtained for the form factors as the upper bound would be even more saturated.

Acknowledgements

We would like to thank Marzia Bordone, Nico Gubernari, Martin Jung, and Méril Reboud for helpful discussions. The work of TB is supported by the Royal Society (UK). The work of SM is supported by the U.S. Department of Energy, Office of Science, Office of High Energy Physics under Award Number DE-SC0009913. The work of MR is supported by the Deutsche Forschungsgemeinschaft (DFG, German Research Foundation) under grant 396021762 - TRR 257. The work of DvD is supported by the DFG within the Emmy Noether Programme under grant DY-130/1-1 and the Sino-German Collaborative Research Center TRR110 "Symmetries and the Emergence of Structure in QCD" (DFG Project-ID 196253076, NSFC Grant No. 12070131001, TRR 110). DvD was supported in the final phase of this work by the Munich Institute for Astro- and Particle Physics (MIAPP), which is funded by the DFG under Germany's Excellence Strategy – EXC-2094 – 390783311.

Appendix A Orthonormal polynomials

In this section we discuss briefly how to obtain the orthonormal polynomials $p_N(z)$, which enter the series expansion in Eq. (10.50) to parameterize the form factors of the $\Lambda_b \to \Lambda$ transition. The functions can be derived with the Gram-Schmidt orthogonalization process in the basis $\{1, z, \ldots, z^N\}$ and fulfill Eq. (10.49). The orthonormal functions are defined on the arc of the unit circle that covers the angle between $-\alpha_{\Lambda_b\Lambda}$ and $+\alpha_{\Lambda_b\Lambda}$, see Eq. (10.46). The orthonormal polynomials are given by

$$p_n(z) = \frac{p_n'(z)}{\sqrt{\langle p_n'(z)|p_n'(z)\rangle}}\,, \tag{10.57}$$

where

$$p_n'(z) = z^n - \sum_{j=0}^{n-1} \langle p_j'(z)|z^n\rangle \cdot p_j'(z)\,, \qquad p_0'(z) = 1\,. \tag{10.58}$$

The orthonormal polynomials for $\Lambda_b \to \Lambda$ can be evaluated efficiently using the orthogonal Szegő polynomials via a recurrence relation [347]. We use

$$\begin{aligned} &\Phi_0(z) = 1\,, && \Phi_0^*(z) = 1\,, \\ &\Phi_n(z) = z\Phi_{n-1} - \rho_{n-1}\Phi_{n-1}^*\,, && \Phi_n^*(z) = \Phi_{n-1}^* - \rho_{n-1} z\Phi_{n-1}\,, \end{aligned} \tag{10.59}$$

which holds for real z. The orthonormal polynomials then follow from

$$p_n(z) = \frac{\Phi_n(z)}{N_n}\,, \quad N_n = \left[2\alpha_{\Lambda_b\Lambda}\prod_{i=0}^{n-1}\left(1-\rho_i^2\right)\right]^{1/2}\,, \tag{10.60}$$

where $2\alpha_{\Lambda_b\Lambda} = 3.22198$ and the Verblunsky coefficients are

$$\{\rho_0, \ldots \rho_4\} = \{+0.62023, -0.66570, +0.68072, -0.68631, +0.68877\}\,, \tag{10.61}$$

as obtained from the Gram-Schmidt procedure.

Appendix B Outer functions

The modulus squares of the outer functions for the different form factors are

$$|\phi_{f_t^V}(z)|^2 = \frac{(m_{\Lambda_b}-m_\Lambda)^2}{16\pi^2\chi_V^{J=0}(Q^2)\big|_{\text{OPE}}}\left(\frac{\sqrt{\lambda(m_{\Lambda_b}^2,m_\Lambda^2,t)}}{t^2(t-Q^2)^{n+1}}s_+(t)\right)_{t=t(z(\alpha))}\left|\frac{\mathrm{d}z(\alpha)}{\mathrm{d}\alpha}\frac{\mathrm{d}t(z)}{\mathrm{d}z}\right|, \tag{10.62}$$

$$|\phi_{f_0^V}(z)|^2 = \frac{(m_{\Lambda_b}+m_\Lambda)^2}{48\pi^2\chi_V^{J=1}(Q^2)\big|_{\text{OPE}}}\left(\frac{\sqrt{\lambda(m_{\Lambda_b}^2,m_\Lambda^2,t)}}{t^2(t-Q^2)^{n+1}}s_-(t)\right)_{t=t(z(\alpha))}\left|\frac{\mathrm{d}z(\alpha)}{\mathrm{d}\alpha}\frac{\mathrm{d}t(z)}{\mathrm{d}z}\right|, \tag{10.63}$$

$$|\phi_{f_\perp^V}(z)|^2 = \frac{1}{24\pi^2\chi_V^{J=1}(Q^2)\big|_{\text{OPE}}}\left(\frac{\sqrt{\lambda(m_{\Lambda_b}^2,m_\Lambda^2,t)}}{t(t-Q^2)^{n+1}}s_-(t)\right)_{t=t(z(\alpha))}\left|\frac{\mathrm{d}z(\alpha)}{\mathrm{d}\alpha}\frac{\mathrm{d}t(z)}{\mathrm{d}z}\right|, \tag{10.64}$$

$$|\phi_{f_t^A}(z)|^2 = 3\,|\phi_{f_0^V}(z)|^2 \quad \text{with replacement} \quad \chi_V^{J=1}(Q^2)\big|_{\text{OPE}} \to \chi_A^{J=0}(Q^2)\big|_{\text{OPE}}, \tag{10.65}$$

$$|\phi_{f_0^A}(z)|^2 = \frac{1}{3}\,|\phi_{f_t^V}(z)|^2 \quad \text{with replacement} \quad \chi_V^{J=0}(Q^2)\big|_{\text{OPE}} \to \chi_A^{J=1}(Q^2)\big|_{\text{OPE}}, \tag{10.66}$$

$$|\phi_{f_\perp^A}(z)|^2 = \frac{1}{24\pi^2\chi_A^{J=1}(Q^2)\big|_{\text{OPE}}}\left(\frac{\sqrt{\lambda(m_{\Lambda_b}^2,m_\Lambda^2,t)}}{t(t-Q^2)^{n+1}}s_+(t)\right)_{t=t(z(\alpha))}\left|\frac{\mathrm{d}z(\alpha)}{\mathrm{d}\alpha}\frac{\mathrm{d}s(z)}{\mathrm{d}z}\right|, \tag{10.67}$$

$$|\phi_{f_\perp^T}(z)|^2 = \frac{(m_{\Lambda_b}+m_\Lambda)^2}{24\pi^2\chi_T^{J=1}(Q^2)\big|_{\text{OPE}}}\left(\frac{\sqrt{\lambda(m_{\Lambda_b}^2,m_\Lambda^2,t)}}{t(t-Q^2)^{n+1}}s_-(t)\right)_{t=t(z(\alpha))}\left|\frac{\mathrm{d}z(\alpha)}{\mathrm{d}\alpha}\frac{\mathrm{d}t(z)}{\mathrm{d}z}\right| \tag{10.68}$$

$$|\phi_{f_0^T}(z)|^2 = \frac{1}{48\pi^2\chi_T^{J=1}(Q^2)\big|_{\text{OPE}}}\left(\frac{\sqrt{\lambda(m_{\Lambda_b}^2,m_\Lambda^2,t)}}{(t-Q^2)^{n+1}}s_-(t)\right)_{t=t(z(\alpha))}\left|\frac{\mathrm{d}z(\alpha)}{\mathrm{d}\alpha}\frac{\mathrm{d}t(z)}{\mathrm{d}z}\right|, \tag{10.69}$$

$$|\phi_{f_\perp^{T5}}(z)|^2 = \frac{(m_{\Lambda_b} - m_\Lambda)^2}{24\pi^2 \chi_{T5}^{J=1}(Q^2)\Big|_{\text{OPE}}} \left(\frac{\sqrt{\lambda(m_{\Lambda_b}^2, m_\Lambda^2, t)}}{t(t-Q^2)^{n+1}} s_+(t) \right)_{t=t(z(\alpha))} \left| \frac{\mathrm{d}z(\alpha)}{\mathrm{d}\alpha} \frac{\mathrm{d}t(z)}{\mathrm{d}z} \right| , \tag{10.70}$$

$$|\phi_{f_0^{T5}}(z)|^2 = \frac{1}{48\pi^2 \chi_{T5}^{J=1}(Q^2)\Big|_{\text{OPE}}} \left(\frac{\sqrt{\lambda(m_{\Lambda_b}^2, m_\Lambda^2, t)}}{(t-Q^2)^{n+1}} s_+(t) \right)_{t=t(z(\alpha))} \left| \frac{\mathrm{d}z(\alpha)}{\mathrm{d}\alpha} \frac{\mathrm{d}t(z)}{\mathrm{d}z} \right| , \tag{10.71}$$

where the value of $\chi_\Gamma^J(Q^2)\Big|_{\text{OPE}}$ can be found in Table 10.1. We can re-express the Källen function as $\lambda(m_{\Lambda_b}^2, m_\Lambda^2, t) = s_-(t)s_+(t)$. Our choice of outer functions $\phi_{f_\lambda^\Gamma}(z)$ must satisfy Eq. (10.62) - (10.71) and must be analytical within the open unit disk $|z| < 1$. This can be achieved by replacing poles within the unit disk with

$$\left(\frac{1}{t-X}\right)^m \to \left(-\frac{z(t,X)}{t-X}\right)^m . \tag{10.72}$$

Note that any poles of $1/s_+(t)$ are at $t = (m_{\Lambda_b} + m_\Lambda)^2$, which is mapped by the z transformation to the boundary of the unit disk. Hence, we do not require any modification to these terms.

Following Ref. [333, 339], we compactly express the outer functions of the form factors in a general form:

$$\phi_{f_\lambda^\Gamma}(z) = \frac{\mathcal{N}}{\sqrt{(16 + 8\cdot c)\cdot d \cdot \pi^2 \chi_\Gamma^J\Big|_{\text{OPE}}}} \phi_1(z)^{e/4} \phi_2(z)^{f/4} \phi_3(z)^{(n+g)/2} \phi_4(z) \tag{10.73}$$

with $\mathcal{N} = (m_{\Lambda_b} + m_\Lambda)^a (m_{\Lambda_b} - m_\Lambda)^b$ and

$$\phi_1(z) = \left(\frac{s_-(t)}{z(t, (m_{\Lambda_b} - m_\Lambda)^2)} \right) , \tag{10.74}$$

$$\phi_2(z) = s_+(t) , \tag{10.75}$$

$$\phi_3(z) = \left(-\frac{z(t,0)}{t} \right) , \tag{10.76}$$

$$\phi_4(z) = \sqrt{4(t_+ - t_0)} (1+z)^{1/2} (1-z)^{-3/2} . \tag{10.77}$$

The coefficient a–g are listed in Table 10.3.

Outer function	a	b	c	d	e	f	g
$\phi_{f_t^V}$	0	1	0	1	1	3	3
$\phi_{f_0^V}$	1	0	1	2	3	1	3
$\phi_{f_\perp^V}$	0	0	1	1	3	1	2
$\phi_{f_t^A}$	1	0	1	$\frac{2}{3}$	3	1	3
$\phi_{f_0^A}$	0	1	0	3	1	3	3
$\phi_{f_\perp^A}$	0	0	1	1	1	3	2
$\phi_{f_0^T}$	0	0	1	2	3	1	1
$\phi_{f_\perp^T}$	1	0	1	1	3	1	2
$\phi_{f_0^{T5}}$	0	0	1	2	1	3	1
$\phi_{f_\perp^{T5}}$	0	1	1	1	1	3	2

Table 10.3: Summary of the outer functions for each form factor, in terms of the parameters for the general decomposition of all outer functions in Eq. (10.73).

Chapter 11

Project VI: QCD sum rules for parameters of the B-meson distribution amplitudes

Published as an article in:
M. Rahimi, M. Wald, Phys.Rev.D 104 (2021) 1, 016027 [1].

Contributions of the authors to the article.
M. Rahimi and M. Wald contributed to the draft and did the analytical derivation and numerical analysis of all expressions obtained in the article.

Abstract: We obtain new estimates for the parameters λ_E^2, λ_H^2 and their ratio $\mathcal{R} = \lambda_E^2/\lambda_H^2$, which appear in the second moments of the B-meson light-cone distribution amplitudes defined in the heavy-quark effective field theory. The computation is based on two-point QCD sum rules for the diagonal correlation function and includes all contributions up to mass dimension seven in the operator-product expansion. For the ratio we get $\mathcal{R} = (0.1 \pm 0.1)$ with $\lambda_H^2 = (0.15 \pm 0.05)\,\text{GeV}^2$ and $\lambda_E^2 = (0.01 \pm 0.01)\,\text{GeV}^2$.

11.1 Introduction

Light-cone distribution amplitudes (LCDAs) are of great importance in exclusive B-meson decays like $B \to \pi\pi$ or $B \to \pi K$ in the heavy quark limit and allow for the study of CP-violation in weak interactions. They parametrize matrix elements of nonlocal heavy-light currents separated along the light-cone at leading order in the heavy-quark effective theory (HQET) [69] in terms of expansions in wave functions of increasing twist [355, 356]. In particular, LCDAs appear in factorization theorems such as QCD factorization [355, 357, 358], since these amplitudes encode the nonperturbative nature of the strong interactions and are crucial in B-meson decay form factor computations. General definitions have been obtained in [355, 356]. Contrary to light-meson distribution amplitudes, which also appear in factorization theorems, the properties of the B-meson distribution amplitudes are less known. However, they have been extensively studied recently. Their evolution equations have been investigated for the leading twist two-particle LCDA in [359–363] and for higher twist amplitudes in [364]. Moreover, the decay $B \to \gamma\ell\nu$ is of particular interest, because it provides a simple example to probe the light-cone structure of the B-meson. Here, the photon has a large energy compared to the strong interaction scale Λ, so QCD factorization can be used to study parameters like the inverse moment λ_B [365–371].

Three-particle LCDAs have also been investigated e.g. in [356, 372], where the corresponding Mellin moments have been defined and identities between two-particle and three-particle LCDAs have been found. In general, these three-particle LCDAs occur in higher dimensional vacuum to meson matrix elements including nonlocal quark operators. But in the case of local quark operators, these matrix elements can be expressed in terms of the parameters $\lambda^2_{E,H}$, which also contribute to the second Mellin moments of the three-particle B-meson distribution amplitudes.

These are the parameters of particular interest in this work. They have been first investigated by Grozin and Neubert [356] within the framework of QCD sum rules [89,373,374]. All contributions to the operator-product expansion (OPE) [375] in local vacuum condensates up to mass dimension five have been considered there. Up to mass dimension four, the leading order contribution is of $\mathcal{O}(\alpha_s)$, while the leading order of the mass dimension five condensate contributes at $\mathcal{O}(\alpha_s^0)$.

The extraction of these parameters is connected to a rather large uncertainty, because the sum rules turn out to be unstable with respect to the variation of the Borel parameter. Notice that such a dependence is not unexpected, since it is well known [376–378] that higher dimensional condensates tend to give large contributions to correlation functions including higher dimensional operators.

Further study by Nishikawa and Tanaka [378] lead to deviations from the original values for $\lambda^2_{E,H}$. These authors argued in their work that a consistent treatment of all $\mathcal{O}(\alpha_s)$ contributions should resolve the stability problem, which is related to the fact that the OPE does not converge for the parameters $\lambda^2_{E,H}$ in [356]. For this analysis, they included the $\mathcal{O}(\alpha_s)$ corrections of the coupling constant $F(\mu)$ as well, which,

albeit leading to good convergence of the OPE, obey large higher order perturbative corrections [379, 380]. Moreover, they included as an additional nonperturbative correction the dimension six diagram of $\mathcal{O}(\alpha_s)$ in order to check the convergence of the OPE beyond mass dimension five and calculated the $\mathcal{O}(\alpha_s)$ corrections for the dimension five condensate. After performing a resummation of the large logarithmic contributions, which results into more stable sum rules and into a more convergent OPE compared to [356], they obtained new estimates for the parameters $\lambda^2_{E,H}$. If we compare the estimates from [356] and [378] in Table 11.3, we see that the values for $\lambda^2_{E,H}$ differ by approximately a factor of three, although the ratio λ^2_E/λ^2_H gives nearly the same value.

It is therefore timely to investigate new alternative sum rules which also allow for the predictions of $\lambda^2_{E,H}$. Instead of analysing a correlation function with a three-particle and a two-particle current, we consider sum rules based on a diagonal correlation function of two quark-antiquark-gluon three-particle currents. We include all leading order contributions up to mass dimension seven. The advantage of this sum rule is that it is positive definite and hence we expect that the quark-hadron duality is more accurate compared to [356, 378]. But due to the high mass dimension of the correlation function, we see that the OPE does not show better convergence than in the nondiagonal case. Moreover, the continuum and higher excited states are dominating the sum rule. This problem will be resolved by considering combinations of the parameters $\lambda^2_{E,H}$, in particular the $\mathcal{R}$-ratio $\mathcal{R} = \lambda^2_E/\lambda^2_H$.

The paper is organized as follows: In Sec. 11.2 we derive the sum rules for the parameters $\lambda^2_{E,H}$ and the sum $(\lambda^2_H + \lambda^2_E)$. Sec. 11.3 is devoted to the computation of the OPE contributions which enter the sum rules. In Sec. 11.4 we present the numerical analysis of the sum rules and state our final results for the parameters $\lambda^2_{E,H}$. Additionally, we investigate the ratio given by the quotient of these parameters. Finally, we conclude in Section 11.5.

11.2 Derivation of the QCD Sum Rules in HQET

In this chapter we derive the sum rules for the diagonal quark-antiquark-gluon three-particle correlation function. Before we start, the definition of the HQET parameter $\lambda^2_{E,H}$ is in order [356]:

$$\langle 0|\, g_s \bar{q}\, \vec{\alpha}\cdot\vec{E}\, \gamma_5 h_v\, |\bar{B}(v)\rangle = F(\mu)\, \lambda^2_E\,, \tag{11.1}$$

$$\langle 0|\, g_s \bar{q}\, \vec{\sigma}\cdot\vec{H}\, \gamma_5 h_v\, |\bar{B}(v)\rangle = iF(\mu)\, \lambda^2_H. \tag{11.2}$$

From a physical point of view, these quantities parametrize the local vacuum to $\bar{B}$-meson matrix elements, which contain the chromoelectric and chromomagnetic fields in HQET. The chromoelectric field is given by $E^i = G^{0i}$ and $H^i = -\frac{1}{2}\epsilon^{ijk}G^{jk}$ denotes

the chromomagnetic field, with $G_{\mu\nu} = G^a_{\mu\nu} T^a$. Here, the tensor $G^{\mu\nu} = \frac{i}{g_s}[D^\mu, D^\nu]$ is the field strength tensor, while g_s corresponds to the strong coupling constant. Furthermore, the fields $\bar{q}$ in Eq. (11.1) and (11.2) indicate light quark fields, whereas the field h_v denotes the HQET heavy quark field. Moreover, v is the velocity of the heavy $\bar{B}$-meson. The Dirac matrices α^i are given by $\gamma^0\gamma^i$ and $\sigma^i = \gamma^i\gamma^5$. In addition to that the HQET decay constant $F(\mu)$ is defined via the matrix element

$$\langle 0|\, \bar{q}\gamma_\mu\gamma_5 h_v\, |\bar{B}(v)\rangle = iF(\mu)v_\mu \tag{11.3}$$

and can be related to the $B(\bar{B})$-meson decay constant in QCD up to one loop order [381]:

$$f_B\sqrt{m_B} = F(\mu)K(\mu) = F(\mu)\Big[1 + \frac{C_F\alpha_s}{4\pi}\Big(3\cdot\ln\frac{m_b}{\mu} - 2\Big) + ...\Big] + \mathcal{O}\Big(\frac{1}{m_b}\Big). \tag{11.4}$$

Its explicit scale dependence has to cancel with the one of the matching prefactor in order to lead to the constant f_B. Values for f_B can be found in [382] and estimate this decay constant to be:

$$f_B = (192.0 \pm 4.3)\ \text{MeV}\,. \tag{11.5}$$

The coupling constant $F(\mu)$ will be of particular importance for the derivation of the relevant low-energy parameters in the following QCD sum rule analysis. But since we are investigating the sum rules at leading order accuracy, corrections of the order $\mathcal{O}(\alpha_s)$ and $\mathcal{O}\Big(\frac{1}{m_b}\Big)$ will be neglected.

As already discussed before, Grozin and Neubert [356] introduced the parameters $\lambda^2_{E,H}$. For this, they considered the correlation function shown in Eq. (11.6). The starting point for our calculation is the correlation function given in Eq. (11.7).

$$\Pi_{\text{GN}} = i\int \mathrm{d}^d x e^{-i\omega v\cdot x}\,\langle 0|\, T\{\bar{q}(0)\Gamma_1^{\mu\nu} g_s G_{\mu\nu}(0) h_v(0) \times \bar{h}_v(x)\gamma_5 q(x)\}\,|0\rangle\ , \tag{11.6}$$

$$\Pi_{\text{diag}} = i\int \mathrm{d}^d x\ e^{-i\omega v\cdot x}\,\langle 0|\, T\{\bar{q}(0)\Gamma_1^{\mu\nu} g_s G_{\mu\nu}(0) h_v(0) \times \bar{h}_v(x)\Gamma_2^{\rho\sigma} g_s G_{\rho\sigma}(x) q(x)\}\,|0\rangle\ . \tag{11.7}$$

Notice that at this point we do not require a specific choice of the quantities $\Gamma_1^{\mu\nu}$ and $\Gamma_2^{\rho\sigma}$, which indicate an arbitrary combination of Dirac γ-matrices, but in the

following steps it is convenient to choose these matrices such that combinations of the HQET parameters $\lambda_{E,H}^2$ are projected out. This requires that the perturbative and nonperturbative contributions to the OPE in Sec. 11.3 are computed for general $\Gamma_1^{\mu\nu}$ and $\Gamma_2^{\rho\sigma}$. Since we are considering a diagonal Greens function, the structure of $\Gamma_2^{\rho\sigma}$ is directly related to $\Gamma_1^{\mu\nu}$ by replacing indices. From now on we use the notation:

$$\Gamma_1 \equiv \Gamma_1^{\mu\nu}\,, \tag{11.8}$$

$$\Gamma_2 \equiv \Gamma_2^{\rho\sigma}\,. \tag{11.9}$$

Moreover, we are working in the $\bar{B}$-meson rest frame, where $v = (1, \vec{0})^T$, in order to simplify the calculations.

The next step in the derivation of the sum rules will be to exploit the unitary condition, where the ground state $\bar{B}$-meson is separated from the continuum and excited states:

$$\begin{aligned}
\frac{1}{\pi}\mathrm{Im}\Pi_{\mathrm{diag}}(\omega) =& \sum_n (2\pi)^3 \delta(\omega - p_n) \langle 0|\, \bar{q}(0)\Gamma_1 g_s G_{\mu\nu}(0) h_v(0)\, |n\rangle \\
& \times \langle n|\, \bar{h}_v(x)\Gamma_2 g_s G_{\rho\sigma}(x) q(x)\, |0\rangle \, \mathrm{d}\Phi_n \\
=\ & \delta(\omega - \bar{\Lambda}) \langle 0|\, \bar{q}(0)\Gamma_1 g_s G_{\mu\nu}(0) h_v(0)\, |\bar{B}\rangle \langle \bar{B}|\, \bar{h}_v(0)\Gamma_2 g_s G_{\rho\sigma}(0) q(0)\, |0\rangle \\
& + \rho^{\mathrm{hadr.}}(\omega)\Theta(\omega - \omega^{th})\,.
\end{aligned} \tag{11.10}$$

In Eq. (11.10), we introduced the binding energy $\bar{\Lambda} = m_B - m_b$, which is one of the important low-energy parameters in this formalism. Furthermore, we separated the full n-particle contribution in the first line into a ground state contribution, which will be the dominant contribution in our chosen stability window, and a continuum contribution including broad higher resonances. In the case of QCD correlation functions, the exponential in Eq. (11.7) would generally take the form e^{-iqx} with q denoting the external momentum. Due to the fact that there is no spatial component in the B-meson rest frame, transitions from the ground state to the excited states in Eq. (11.10) are possible by injecting energy q^0 into the system. In this work we explicitly chose $q = \omega \cdot v$ such that we end up with the correlation function shown in Eq. (11.7).

The matrix elements occurring in (11.10) can be decomposed in the following

way [356, 378]:

$$\langle 0|\,\bar{q}(0)\Gamma_1 g_s G_{\mu\nu}(0) h_v(0)\,|\bar{B}\rangle = \frac{-i}{6}F(\mu)\{\lambda_H^2(\mu)$$

$$\times \mathrm{Tr}[\Gamma_1 P_+ \gamma_5 \sigma_{\mu\nu}] + [\lambda_H^2(\mu) - \lambda_E^2(\mu)]$$

$$\times \mathrm{Tr}[\Gamma_1 P_+ \gamma_5 (iv_\mu \gamma_\nu - iv_\nu \gamma_\mu)]\}. \tag{11.11}$$

Notice that the second decomposition is indeed valid since the B-meson ground state explicitly depends on the velocity v and $\sigma_{\mu\nu} = \frac{i}{2}[\gamma_\mu, \gamma_\nu]$ corresponds to the usual antisymmetric Dirac tensor. In (11.11) we made use of the covariant trace formalism, further investigated in [356, 383].

The next step will be to use the standard dispersion relation, after using the residue theorem and the Schwartz reflection principle [1]:

$$\Pi_{\mathrm{diag}}(\omega) = \frac{1}{\pi}\int_0^\infty \mathrm{d}s \frac{\mathrm{Im}\Pi_{\mathrm{diag}}(s)}{s - \omega - i0^+}$$

$$= \frac{1}{\bar{\Lambda} - \omega - i0^+}\,\langle 0|\,\bar{q}(0)\Gamma_1 g_s G_{\mu\nu}(0) h_v(0)\,|\bar{B}\rangle$$

$$\times \langle \bar{B}|\,\bar{h}_v(0)\Gamma_2 g_s G_{\rho\sigma}(0) q(0)\,|0\rangle + \int_{s^{th}}^\infty \mathrm{d}s \frac{\rho^{\mathrm{hadr.}}(s)}{s - \omega - i0^+}\,. \tag{11.12}$$

In Eq. (11.12) we introduce the threshold parameter s^{th}, which is another relevant low-energy parameter that separates the ground state contribution from higher resonances and continuum contributions.

We can now move on and evaluate the ground state contribution:

$$\langle 0|\,\bar{q}(0)\Gamma_1 g_s G_{\mu\nu}(0) h_v(0)\,|\bar{B}\rangle\,\langle \bar{B}|\,\bar{h}_v(0)\Gamma_2 g_s G_{\rho\sigma}(0) q(0)\,|0\rangle = \frac{-i}{6}F(\mu)\Big[\lambda_H^2(\mu)\mathrm{Tr}[\Gamma_1 P_+ \gamma_5 \sigma_{\mu\nu}]$$

$$+ [\lambda_H^2(\mu) - \lambda_E^2(\mu)]\mathrm{Tr}[\Gamma_1 P_+ \gamma_5 (iv_\mu \gamma_\nu - iv_\nu \gamma_\mu)]\Big] \tag{11.13}$$

$$\times \frac{-i}{6}F^\dagger(\mu)\Big[\lambda_H^2(\mu)\mathrm{Tr}[\gamma_5 P_+ \Gamma_2 \sigma_{\rho\sigma}]$$

$$- [\lambda_H^2(\mu) - \lambda_E^2(\mu)]\mathrm{Tr}[\gamma_5 P_+ \Gamma_2 (iv_\rho \gamma_\sigma - iv_\sigma \gamma_\rho)]\Big]\,.$$

[1] For more details on QCD sum rules or HQET sum rules, see [95, 384]

Notice that the term involving the difference of both HQET parameter $(\lambda_H^2 - \lambda_E^2)$ does not change its sign under complex conjugation.

In order to derive the sum rules which ultimately determine the parameters $\lambda_{E,H}^2$, we make an explicit choice for the matrices Γ_1 and Γ_2 [356]. Following the same approach as [356], we choose our gamma matrices $\Gamma_{1,2}$ as:

$$\Gamma_1 = \frac{i}{2}\sigma_{\mu\nu}\gamma_5 \tag{11.14}$$

to obtain the $(\lambda_H^2 + \lambda_E^2)^2$ sum rule. Furthermore, for the projection of the λ_H^4 sum rule we choose

$$\Gamma_1 = i\left(\frac{1}{2}\delta_\alpha^{\ \nu} - v_\nu v^\alpha\right)\sigma_{\mu\alpha}\gamma_5 \tag{11.15}$$

and for λ_E^4:

$$\Gamma_1 = i v_\nu v^\alpha \sigma_{\mu\alpha}\gamma_5\,. \tag{11.16}$$

Notice that these choices are Lorentz covariant in comparison to Eq. (11.1) and (11.2). The corresponding expressions for Γ_2 can be obtained from Γ_1 by replacing $\mu \to \rho$, $\nu \to \sigma$.
Using the relation in Eq. (11.13), we can obtain expressions for $\Pi_{E,H}$ and Π_{HE}:

$$\Pi_{E,H}(\omega) = F(\mu)^2 \cdot \lambda_{E,H}^4 \cdot \frac{1}{\bar{\Lambda} - \omega - i0^+} + \int_{s^{th}}^{\infty} \mathrm{d}s \frac{\rho_{E,H}^{\text{hadr.}}(s)}{s - \omega - i0^+} \tag{11.17}$$

$$\Pi_{HE}(\omega) = F(\mu)^2 \cdot (\lambda_H^2 + \lambda_E^2)^2 \cdot \frac{1}{\bar{\Lambda} - \omega - i0^+} + \int_{s^{\text{th}}}^{\infty} \mathrm{d}s \frac{\rho_{HE}^{\text{hadr.}}(s)}{s - \omega - i0^+} \tag{11.18}$$

Note that the threshold parameter s^{th} in Eq. (11.17) does not necessarily coincide with the threshold parameter in Eq. (11.18).

To parametrize the hadronic spectral density, we make use of the global and semilocal quark-hadron duality (QHD) [100, 385] in order to connect the hadronic spectral density with the spectral density which is described by the OPE [95, 373, 375, 381]. This is the essential idea of this formalism. However, power suppressed nonperturbative effects become dominant in comparison to the perturbative contribution for $-|\omega| \approx \Lambda_{\text{QCD}}$. In the QCD sum rule approach [373], these effects are parametrized in terms of a power series of local condensates as a consequence of the non-trivial QCD vacuum structure. These condensates carry the quantum numbers of the QCD vacuum. For convenience, we show explicitly in Appendix A the expansion and averaging of the vacuum matrix element (11.7) in order to obtain the quark condensate $\langle 0|\,\bar{q}q\,|0\rangle$, the gluon condensate $\langle 0|\,G_{\mu\nu}^a G_{\rho\sigma}^a\,|0\rangle$, the quark-gluon condensate $\langle 0|\,\bar{q}g_s\sigma\cdot Gq\,|0\rangle$ and the triple-gluon condensate $\langle 0|\,g_s^3 f^{abc} G_{\mu\nu}^a G_{\rho\sigma}^b G_{\alpha\lambda}^c\,|0\rangle$.

Although we can handle the Euclidean region, the physical states described by the spectral function in Eq. (11.17) and (11.18) are defined for $\omega \in \mathbb{R}$. But since there is no estimate for the hadronic spectral density $\rho_X^{\text{hadr.}}(s)$, we need to make use of two statements. First, we exploit that for $\omega \ll 0$ the hadronic and the OPE spectral functions coincide at the global level:

$$\Pi_X^{\text{hadr.}} = \Pi_X^{\text{OPE}} \quad \text{for } X \in \{H, E, HE\}. \tag{11.19}$$

Asymptotic freedom guarantees that this equality holds. Moreover, we need to employ the semilocal quark-hadron duality, which connects the spectral densities:

$$\int_{s_X^{th}}^{\infty} \mathrm{d}s \frac{\rho_X^{\text{hadr.}}(s)}{s - \omega - i0^+} = \int_{s_X^{th}}^{\infty} \mathrm{d}s \frac{\rho_X^{\text{OPE}}(s)}{s - \omega - i0^+}, \tag{11.20}$$

where X needs be chosen according to (11.19). In the low-energy region, where nonperturbative effects dominate, the duality relation is largely violated due to strong resonance peaks, while in the high-energy region these peaks become broad and overlapping. Once a sum rule is obtained, the approximations made by QHD are consistent (see Section 11.4 for more details). So it is necessary to work in the transition region where the condensates are important, but still small and local enough such that perturbative methods can be applied.

Based on the relations in Eq. (11.19), (11.20), we separate the integral over the OPE spectral density by introducing the threshold parameter s^{th}. Hence, we end up with the following form for the sum rules:

$$F(\mu)^2 \cdot \lambda_{E,H}^4 \frac{1}{\bar{\Lambda} - \omega - i0^+} = \int_0^{s^{th}} \mathrm{d}s \frac{\rho_{E,H}^{\text{OPE}}(s)}{s - \omega - i0^+}\,, \tag{11.21}$$

$$F(\mu)^2 \cdot (\lambda_H^2 + \lambda_E^2)^2 \frac{1}{\bar{\Lambda} - \omega - i0^+} = \int_0^{s^{th}} \mathrm{d}s \frac{\rho_{HE}^{\text{OPE}}(s)}{s - \omega - i0^+}. \tag{11.22}$$

Finally, we perform a Borel transformation, which removes possible subtraction terms and leads further to an exponential suppression of higher resonances and the continuum. In addition to that, the convergence of our sum rule is improved. Generally, the Borel transform can be defined in the following way [95, 384]:

$$\mathcal{B}_M f(\omega) = \lim_{n \to \infty, -\omega \to \infty} \frac{(-\omega)^{n+1}}{\Gamma(n+1)} \left(\frac{\mathrm{d}}{\mathrm{d}\omega} \right)^n f(\omega), \tag{11.23}$$

where $f(\omega)$ illustrates an arbitrary test function. Furthermore, we keep the ratio $M = \frac{-\omega}{n}$ fixed, M denotes the Borel parameter.

After applying this transformation, we derive the final form of our sum rule

expressions:

$$F(\mu)^2 \cdot \lambda_{E,H}^4 \cdot e^{-\bar{\Lambda}/M} = \int_0^{\omega_{th}} \mathrm{d}\omega \; \rho_{E,H}^{\mathrm{OPE}}(\omega) \; e^{-\omega/M}$$

$$= \int_0^{\omega_{\mathrm{th}}} \mathrm{d}\omega \; \frac{1}{\pi} \mathrm{Im}\Pi_{E,H}^{\mathrm{OPE}}(\omega) \; e^{-\omega/M} \,, \tag{11.24}$$

$$F(\mu)^2 \cdot (\lambda_H^2 + \lambda_E^2)^2 \cdot e^{-\bar{\Lambda}/M} = \int_0^{\omega_{th}} \mathrm{d}\omega \; \rho_{HE}^{\mathrm{OPE}}(\omega) \; e^{-\omega/M}$$

$$= \int_0^{\omega_{\mathrm{th}}} \mathrm{d}\omega \; \frac{1}{\pi} \mathrm{Im}\Pi_{HE}^{\mathrm{OPE}}(\omega) \; e^{-\omega/M} \,. \tag{11.25}$$

These are the QCD sum rules presented in the paper. In order to obtain reliable values for the parameters $\lambda_{E,H}^2$ from the sum rules in Eq. (11.24) and (11.25), the Borel parameter M needs to be chosen accordingly together with the threshold parameter ω_{th}. The next step will be to determine the spectral function $\Pi_X^{\mathrm{OPE}}(s)$, which is given by the OPE:

$$\Pi_{\mathrm{X}}^{\mathrm{OPE}}(\omega) = C_{\mathrm{pert}}^{\mathrm{X}}(\omega) + C_{\bar{q}q}^{\mathrm{X}} \langle \bar{q}q \rangle + C_{G^2}^{\mathrm{X}} \langle \frac{\alpha_s}{\pi} G^2 \rangle$$

$$+ C_{\bar{q}Gq}^{\mathrm{X}} \langle \bar{q} g_s \sigma \cdot G q \rangle + C_{G^3}^{\mathrm{X}} \langle g_s^3 f^{abc} G^a G^b G^c \rangle$$

$$+ C_{\bar{q}qG^2}^{\mathrm{X}} \langle \bar{q}q \rangle \langle \frac{\alpha_s}{\pi} G^2 \rangle + ... \tag{11.26}$$

The Wilson coefficients C in Eq. (11.26) will be discussed in Sec. 11.3. Moreover, we define a more convenient notation for the condensate contributions:

$$\langle \bar{q}q \rangle := \langle 0 | \, \bar{q}q \, | 0 \rangle \,, \langle G^2 \rangle := \langle 0 | \, G_{\mu\nu}^a G^{a,\mu\nu} \, | 0 \rangle \,,$$

$$\langle \bar{q} g_s \sigma \cdot G q \rangle := \langle 0 | \, \bar{q} g_s G^{\mu\nu} \sigma_{\mu\nu} q \, | 0 \rangle \,,$$

$$\langle g_s^3 f^{abc} G^a G^b G^c \rangle := \langle 0 | \, g_s^3 f^{abc} G_{\mu\nu}^a G^{b,\nu\rho} G_\rho^{c,\mu} \, | 0 \rangle \,. \tag{11.27}$$

As previously mentioned, the condensates are uniquely parametrized up to mass dimension five. Starting at dimension six and higher, there occur many different possible contributions, but some of them are related by QCD equations of motions and Fierz identities [386] to each other [2]. Note that in the power expansion of Eq. (11.26) we have only stated the dimension six and seven condensates, which give a leading order contribution to the parameters $\lambda_{E,H}^2$.

[2] A list is given for example in the review [98].

Moreover, there are many estimates for the values of the condensates given in the literature, which have been obtained from e.g. lattice QCD, sum rules [98], but obtaining values for condensates of dimension six and higher is an ongoing task due to the mixing with lower dimensional condensates. Because of the lack of these values, the vacuum saturation approximation [89] is exploited in many cases, where a full set of intermediate states is introduced into the higher dimensional condensate and the assumption is used that only the ground state gives a dominant contribution. Thus, the higher dimensional condensate will be effectively reduced to a combination of lower dimensional condensates [3].

11.3 Computation of the Wilson Coefficients

In this chapter, the leading perturbative and nonperturbative contributions to the correlation function in (11.17) and (11.18) are calculated up to dimension seven. Since the leading order of the diagonal correlator of two three-particle currents is of $\mathcal{O}(\alpha_s)$ in the strong coupling constant, we only investigate contributions up to this order in perturbation theory. For the perturbative contribution we choose the Feynman gauge for the background field, while the nonperturbative contributions to the OPE are evaluated in the fixed-point or Fock-Schwinger (FS) gauge [387, 388]:

$$x_\mu A^\mu(x) = 0 \quad \text{and} \quad A_\mu(x) = \int_0^1 \mathrm{d}u \, u x^\nu G_{\nu\mu}(ux). \tag{11.28}$$

In the FS gauge, we set the reference point to $x_0 = 0$. This reference point would occur in all intermediate steps of the calculation and cancel in the end of the calculation. It is well known that this gauge is particularly useful in QCD sum rule computations.

Within the framework of QCD sum rules, the long-distance effects are encoded in local vacuum matrix elements of increasing mass dimension. In order to obtain these local condensates, the gluon field strength tensor is expanded in its spacetime coordinate x, which results in a simple relation between the gluon field A_μ and the field strength tensor $G_{\mu\nu}$. Additionally, gluon fields do not interact with the heavy quark in HQET, which can be easily seen by considering the heavy-quark propagator in position space [378]:

$$\begin{aligned} \overbrace{h_v(0)\bar{h}_v(x)} &= \Theta(-v\cdot x)\,\delta^{(d-1)}(x_\perp)\,P_+\,\mathcal{P} \\ &\quad \times \exp\left(ig_s\int_{v\cdot x}^0 \mathrm{d}s\, v\cdot A(sv)\right). \end{aligned} \tag{11.29}$$

[3] This has already been done for the dimension seven condensate in Eq. (11.26).

Here, $x_\perp^\mu = x^\mu - (v\cdot x)v^\mu$, $P_+ = (1+\not{v})/2$ denotes the projection operator and $\mathcal{P}$ illustrates the path ordering operator. Besides these simplifications, there are three additional vanishing subdiagrams depicted in Fig. 11.5 due to the FS gauge.

Generally, all diagrams can be evaluated in position space like in [356, 378], but in this work we choose to work in momentum space. We make use of dimensional regularization for the loop integrals with the convention $d = 4 - 2\epsilon$. Fig. 11.1-11.5 [4] show the diagrams which need to be computed in order to obtain the Wilson coefficients in Eq. (11.26). The calculation of these coefficients proceeds in the following way: First, we use FeynCalc [189] to decompose tensor integrals to scalar integrals. In the next step, these scalar integrals are reduced to master integrals by integration-by-parts identities using LiteRed [390]

We start by considering the perturbative contribution and the contribution from the quark condensate in Fig. 11.1:

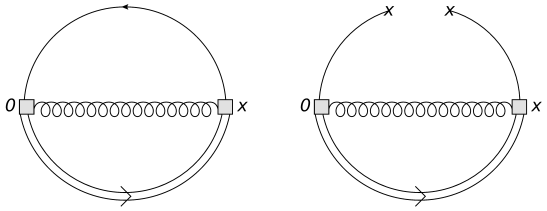

(a) (b)

Figure 11.1: Feynman diagrams for the perturbative and $\langle\bar{q}q\rangle$ condensate contribution. The double line denotes the heavy quark propagator. The solid line denotes the light quark propagator and the curly line denotes the gluon propagator.

$$C^{\mathrm{X}}_{\mathrm{pert}}(\omega) = \frac{2\alpha_s}{\pi^3}\cdot C_F N_c \cdot \mathrm{Tr}[\Gamma_1 P_+ \Gamma_2 \not{v}]\cdot \bar{\mu}^{4\epsilon}$$
$$\times\, \Gamma(-6+4\epsilon)\cdot\Gamma(2-\epsilon)\cdot\omega^{6-4\epsilon}e^{4i\pi\epsilon}$$
$$\times \left[\Gamma(2-\epsilon)\cdot T^1_{\mu\rho\nu\sigma} + \Gamma(3-\epsilon)\cdot T^2_{\mu\rho\nu\sigma}\right], \tag{11.30}$$

$$C^{\mathrm{X}}_{\bar{q}q}(\omega) = -\frac{\alpha_s}{\pi}\cdot C_F \cdot \mathrm{Tr}[\Gamma_1 P_+ \Gamma_2]\cdot\bar{\mu}^{2\epsilon}\cdot\Gamma(-3+2\epsilon)$$
$$\times\,\omega^{3-2\epsilon}e^{2i\pi\epsilon}\left[\Gamma(2-\epsilon)\cdot T^1_{\mu\rho\nu\sigma} + \Gamma(3-\epsilon)\cdot T^2_{\mu\rho\nu\sigma}\right], \tag{11.31}$$

[4] All diagrams in this work have been created with JaxoDraw [389].

with

$$\bar{\mu}^2 := \frac{\mu^2 e^{\gamma_E}}{4}\,, \tag{11.32}$$

$$T^1_{\mu\rho\nu\sigma} := g_{\mu\rho}g_{\nu\sigma} - g_{\mu\sigma}g_{\nu\rho}\,, \tag{11.33}$$

$$T^2_{\mu\rho\nu\sigma} := -g_{\nu\sigma}v_\mu v_\rho + g_{\mu\sigma}v_\nu v_\rho + g_{\nu\rho}v_\mu v_\sigma - g_{\mu\rho}v_\nu v_\sigma\,. \tag{11.34}$$

Notice that the tensor structures of $T^{1,2}_{\mu\rho\nu\sigma}$ satisfy the symmetries imposed by the field strength tensors $G_{\mu\nu}$ and $G_{\rho\sigma}$. In particular, the expressions are anti-symmetric under the exchange of $\{\mu \leftrightarrow \nu\}$, $\{\rho \leftrightarrow \sigma\}$ and symmetric under the combined exchanges $\{\mu \leftrightarrow \rho, \nu \leftrightarrow \sigma\}$ and $\{\mu \leftrightarrow \nu, \rho \leftrightarrow \sigma\}$. The Wilson coefficient for the gluon condensate and higher mass dimension correction for the quark condensate share the same tensor structure as the coefficients stated in Eq. (11.30) and (11.31). Furthermore, the mass dimension five contribution with the non-Abelian vertex in Eq. (11.39) and the dimension seven contribution in Eq. (11.41) make use of these tensor structures as well.

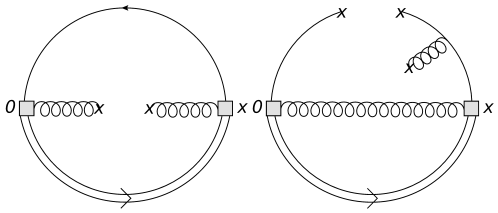

(a) (b)

Figure 11.2: (a) shows the Feynman diagram for the dimension four contribution, (b) a schematic illustration of the dimension five condensate originating from the higher order expansion of the dimension three contribution in Fig. 11.1.

The Wilson coefficient of the gluon condensate, which corresponds to Fig. 11.2 (a) can be expressed as:

$$C^{\mathrm{X}}_{G^2}(\omega) = \mathrm{Tr}[\Gamma_1 P_+ \Gamma_2 \not{v}] \cdot \frac{\bar{\mu}^{2\epsilon}}{(4-2\epsilon)(3-2\epsilon)}$$
$$\times \Gamma(-2+2\epsilon)\cdot\Gamma(2-\epsilon)\cdot\omega^{2-2\epsilon}e^{2i\pi\epsilon}\cdot T^1_{\mu\rho\nu\sigma}\,. \tag{11.35}$$

The mass dimension five contributions are given as:

$$C^{\mathrm{X}}_{\bar{q}Gq,1}(\omega) = -\frac{\alpha_s}{\pi}\cdot C_F \cdot \mathrm{Tr}[\Gamma_1 P_+ \Gamma_2]\cdot\frac{\bar{\mu}^{2\epsilon}}{(4-2\epsilon)}$$
$$\times \Gamma(-3+2\epsilon)\cdot\Gamma(3-\epsilon)\cdot\omega^{1-2\epsilon}e^{2i\pi\epsilon}\cdot T^1_{\mu\rho\nu\sigma}\,, \tag{11.36}$$

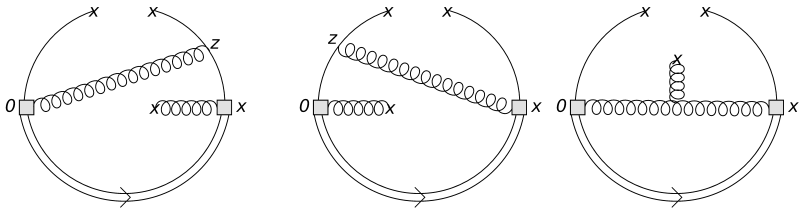

(a) (b) (c)

Figure 11.3: Feynman diagrams for dimension five condensate contributions.

$$C^{\mathrm{X}}_{\bar{q}Gq,2}(\omega) = \frac{\alpha_s}{4\pi} \cdot \frac{C_F \cdot \bar{\mu}^{2\epsilon}}{(4-2\epsilon)(3-2\epsilon)} \cdot \Gamma(-1+2\epsilon) \cdot \Gamma(1-\epsilon)$$

$$\times\, \omega^{1-2\epsilon} e^{2i\pi\epsilon} \cdot \Big[\mathrm{Tr}[\Gamma_1 P_+ \Gamma_2 \sigma_{\mu\nu} \sigma_{\rho\sigma}]$$

$$- (1-\epsilon) \cdot \mathrm{Tr}[\Gamma_1 P_+ \Gamma_2 \not{v} \mathrm{i}(v_\mu \gamma_\nu - v_\nu \gamma_\mu) \sigma_{\rho\sigma}] \Big] , \tag{11.37}$$

$$C^{\mathrm{X}}_{\bar{q}Gq,3}(\omega) = \frac{\alpha_s}{4\pi} \cdot \frac{C_F \cdot \bar{\mu}^{2\epsilon}}{(4-2\epsilon)(3-2\epsilon)} \Gamma(-1+2\epsilon) \cdot \Gamma(1-\epsilon)$$

$$\times\, \omega^{1-2\epsilon} e^{2i\pi\epsilon} \cdot \Big[\mathrm{Tr}[\Gamma_1 P_+ \Gamma_2 \sigma_{\mu\nu} \sigma_{\rho\sigma}]$$

$$+ (1-\epsilon) \cdot \mathrm{Tr}[\Gamma_1 P_+ \Gamma_2 \sigma_{\mu\nu} \mathrm{i}(v_\rho \gamma_\sigma - v_\sigma \gamma_\rho) \not{v}] \Big] , \tag{11.38}$$

$$C^{\mathrm{X}}_{\bar{q}Gq,4}(\omega) = \frac{i\alpha_s}{32\pi} \cdot \frac{C_A C_F \cdot \bar{\mu}^{2\epsilon}}{(2-\epsilon)(3-2\epsilon)} \cdot \mathrm{Tr}[\Gamma_1 P_+ \Gamma_2 \sigma^{\chi\beta}]$$

$$\times\, \Gamma(-1+2\epsilon) \cdot \Gamma(1-\epsilon) \cdot \omega^{1-2\epsilon} e^{2i\pi\epsilon} \cdot$$

$$\Big[\{ g_{\mu\chi} T^1_{\nu\rho\beta\sigma} - (\beta \leftrightarrow \chi) \} + (1-\epsilon)$$

$$\times \Big(\{ v_\beta g_{\mu\rho} (v_\sigma g_{\nu\chi} - v_\nu g_{\sigma\chi}) - (\rho \leftrightarrow \sigma) \} +$$

$$\{ v_\nu g_{\mu\chi} (v_\sigma g_{\beta\rho} - v_\rho g_{\beta\sigma}) - (\beta \leftrightarrow \chi) \} \Big) \Big] - (\mu \leftrightarrow \nu) , \tag{11.39}$$

Although the other contributions for the mass dimension five condensate (Fig. 11.3) possess a more complicated tensor structure, all symmetries described before are still satisfied. We obtain the total Wilson coefficient for the mass dimension five condensate if we sum up all four previous contributions, namely $C^{\mathrm{X}}_{\bar{q}Gq} = \sum_{k=1}^{4} C^{\mathrm{X}}_{\bar{q}Gq,k}$. The

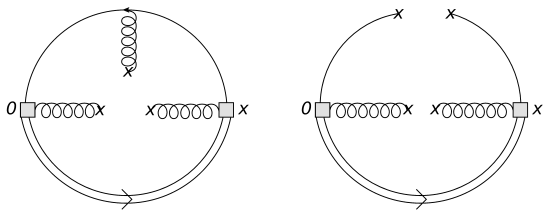

(a) (b)

Figure 11.4: Feynman diagrams for the dimension six and dimension seven condensate, which contribute to the leading order estimate of $\lambda^2_{E,H}$.

last two diagrams depicted in Fig. 11.4 are of mass dimension six and seven. Their contributions are expected to be smaller compared to the dimension five contributions, such that we observe that the OPE starts to converge. Other contributions to mass dimension six are vanishing or are of $\mathcal{O}(\alpha_s^2)$. Thus, the triple-gluon condensate is the only relevant condensate at this order and the Wilson coefficient reads:

$$C^{\mathrm{X}}_{G^3}(\omega) = \frac{\bar{\mu}^{2\epsilon}}{64\pi^2} \cdot B_{\mu\lambda\rho\nu\sigma\alpha} \cdot \Gamma(2\epsilon) \cdot \Gamma(1-\epsilon) \cdot \omega^{-2\epsilon} e^{2i\pi\epsilon}$$

$$\times \left[\mathrm{Tr}[-i \cdot \Gamma_1 P_+ \Gamma_2 \not{v} \sigma^{\lambda\alpha}] + \mathrm{Tr}[\Gamma_1 P_+ \Gamma_2 (v^\alpha \gamma^\lambda - v^\lambda \gamma^\alpha)] \right], \tag{11.40}$$

where the expression $B_{\mu\lambda\rho\nu\sigma\alpha}$ is defined in Appendix A. Finally, we state the expression for the dimension seven contribution:

$$C^{\mathrm{X}}_{\bar{q}qG^2}(\omega) = -\mathrm{Tr}[\Gamma_1 P_+ \Gamma_2] \cdot \frac{T^1_{\mu\rho\nu\sigma}}{\omega + i0^+} \cdot \frac{\pi^2}{2N_c(4-2\epsilon)(3-2\epsilon)}\,. \tag{11.41}$$

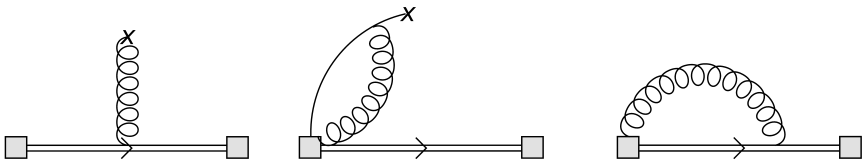

(a) (b) (c)

Figure 11.5: Vanishing subdiagrams in the Fock-Schwinger gauge.

According to Eq. (11.17) and (11.18), we still need to take the imaginary part of these diagrams. We choose to compute directly the loop diagrams and take the

imaginary part of the resulting expression. Following Cutkosky rules, another approach would be to perform the calculation by considering all possible cuts for the diagrams. Apart from the diagrams in Fig. 11.3, the diagrams are finite. (a) and (b) in Fig. 11.3 include both a three-particle and a two-particle cut, where the latter requires a non-trivial renormalization procedure [391]. The optical theorem states that both calculations yield the same result. Besides the diagram in Fig. 11.2 (b), all diagrams in Fig. 11.1-11.4 can generally be calculated by using perturbative methods. Fig. 11.2 (b) stems from higher order corrections in the expansion of the nonperturbative quark condensate in Eq. (11.61). Moreover, the diagrams contributing to the quark-gluon condensate in Fig. 11.3 (a) and (b) obey the same structure as the contributions in [356, 378] and hence a cross-check is possible after replacing the quark condensate by the quark-gluon condensate and keeping in mind that the Lorentz structures differ. By taking the imaginary part of all Wilson coefficients discussed above, plugging the results into Eq. (11.24), (11.25) and performing the integration over ω up to the threshold parameter ω_{th}, we obtain the final expression for the sum rules shown in Eq. (11.44) to Eq. (11.46).

For convenience, we introduced the function:

$$G_n(x) := 1 - \sum_{k=0}^{n} \frac{x^k}{k!} e^{-x}. \tag{11.42}$$

We see that the sum rules for $\lambda^4_{E,H}$ in Eq. (11.45) and (11.46) have got the same expression for the perturbative contribution. This contribution is in addition to that positive, since we are studying a positive-definite correlation function in Eq. (11.7). Furthermore, the quark, the gluon and the triple-gluon condensate in Eq. (11.45), (11.46) have different signs and the Wilson coefficients in Eq. (11.37), (11.38) and (11.39) vanish for λ^4_E. This will have implications on the stability of the sum rule for the parameter λ^4_E and will be investigated in Sec. 11.4. The dimension three, four and six condensates do not appear in Eq. (11.44), since the signs differ in Eq. (11.46) compared to (11.45).

All sum rules involve the decay constant $F(\mu)$, whose calculation in terms of the correlation function can be found, e.g. in Ref. [378]. For consistency, we will retain the result at leading order in α_s

$$\begin{aligned} F^2(\mu) \cdot e^{-\bar{\Lambda}/M} = \frac{2N_c M^3}{\pi^2} \cdot G_2\left(\frac{\omega_{th}}{M}\right) - \langle \bar{q} q \rangle \\ + \frac{1}{16 M^2} \langle \bar{q} g_s G \cdot \sigma q \rangle \,. \end{aligned} \tag{11.43}$$

$$F(\mu)^2\cdot(\lambda_H^2+\lambda_E^2)^2\,e^{-\bar{\Lambda}/M} = \frac{\alpha_s C_A C_F}{\pi^3}\cdot 24M^7\cdot G_6\Big(\frac{\omega_{th}}{M}\Big) - \frac{\alpha_s C_F C_A}{4\pi}\cdot\langle\bar{q}g_s\sigma\cdot Gq\rangle\cdot M^2\cdot$$
$$G_1\Big(\frac{\omega_{th}}{M}\Big) - \frac{3\alpha_s C_F}{2\pi}\cdot\langle\bar{q}g_s\sigma\cdot Gq\rangle\cdot M^2\cdot G_1\Big(\frac{\omega_{th}}{M}\Big) - \frac{\pi^2}{2N_c}\,\langle\bar{q}q\rangle\,\langle\frac{\alpha_s}{\pi}G^2\rangle\ , \tag{11.44}$$

$$F(\mu)^2\cdot\lambda_H^4\,e^{-\bar{\Lambda}/M} = \frac{\alpha_s C_A C_F}{\pi^3}\cdot 12M^7\cdot G_6\Big(\frac{\omega_{th}}{M}\Big) - \frac{\alpha_s C_F}{\pi}\,\langle\bar{q}q\rangle\cdot 6\cdot M^4\cdot G_3\Big(\frac{\omega_{th}}{M}\Big)$$
$$+\frac{1}{2}\,\langle\frac{\alpha_s}{\pi}G^2\rangle\cdot M^3\cdot G_2\Big(\frac{\omega_{th}}{M}\Big) - \frac{\alpha_s C_F C_A}{8\pi}\cdot\langle\bar{q}g_s\sigma\cdot Gq\rangle\cdot M^2\cdot G_1\Big(\frac{\omega_{th}}{M}\Big)$$
$$-\frac{3\alpha_s C_F}{4\pi}\cdot\langle\bar{q}g_s\sigma\cdot Gq\rangle\cdot M^2\cdot G_1\Big(\frac{\omega_{th}}{M}\Big) + \frac{\langle g_s^3 f^{abc}G^aG^bG^c\rangle}{64\pi^2}\cdot M\cdot$$
$$G_0\Big(\frac{\omega_{th}}{M}\Big) - \frac{\pi^2}{4N_c}\,\langle\bar{q}q\rangle\,\langle\frac{\alpha_s}{\pi}G^2\rangle\ , \tag{11.45}$$

$$F(\mu)^2\cdot\lambda_E^4\,e^{-\bar{\Lambda}/M} = \frac{\alpha_s C_A C_F}{\pi^3}\cdot 12M^7\cdot G_6\Big(\frac{\omega_{th}}{M}\Big) + \frac{\alpha_s C_F}{\pi}\,\langle\bar{q}q\rangle\cdot 6\cdot M^4\cdot G_3\Big(\frac{\omega_{th}}{M}\Big)$$
$$-\frac{1}{2}\,\langle\frac{\alpha_s}{\pi}G^2\rangle\cdot M^3\cdot G_2\Big(\frac{\omega_{th}}{M}\Big) - \frac{\alpha_s C_F}{2\pi}\cdot\langle\bar{q}g_s\sigma\cdot Gq\rangle\cdot M^2\cdot G_1\Big(\frac{\omega_{th}}{M}\Big)$$
$$-\frac{\langle g_s^3 f^{abc}G^aG^bG^c\rangle}{64\pi^2}\cdot M\cdot G_0\Big(\frac{\omega_{th}}{M}\Big) - \frac{\pi^2}{4N_c}\,\langle\bar{q}q\rangle\,\langle\frac{\alpha_s}{\pi}G^2\rangle\ . \tag{11.46}$$

11.4 Numerical Analysis

In this section we first compute the HQET parameters by using the sum rules in Eq. (11.43), (11.44), (11.45) and (11.46) following the procedure described in Sec. 11.3. In particular, we consider the ratios (11.44) to (11.46) divided by (11.43) in order to cancel the dependence on the low-energy parameter $\bar{\Lambda}$ and the decay constant $F(\mu)$. The numerical inputs for the necessary parameters are given in Table 11.1. But when we investigate the optimal window for the Borel parameter M, we observe that the sum rules are dominated by higher resonances and the continuum contribution. This questions the reliability of our estimates

Parameters	Value	Ref.
$\alpha_s(1\ \text{GeV})$	0.471	[195]
$\langle\bar{q}q\rangle$	$(-0.242 \pm 0.015)^3\ \text{GeV}^3$	[392]
$\langle\frac{\alpha_s}{\pi}G^2\rangle$	$(0.012 \pm 0.004)\ \ \text{GeV}^4$	[98]
$\langle\bar{q}gG\cdot\sigma q\rangle\,/\,\langle\bar{q}q\rangle$	$(0.8 \pm 0.2)\ \text{GeV}^2$	[393]
$\langle g_s^3 f^{abc} G^a G^b G^c\rangle$	$(0.045 \pm 0.045)\ \text{GeV}^6$	[89]
$\bar{\Lambda}$	$(0.55 \pm 0.06)\ \text{GeV}$	[206]

Table 11.1: List of the numerical inputs, which will be used in our analysis. The vacuum condensates are normalized at the point $\mu = 1$ GeV. For the strong coupling constant we use the two-loop expression with $\Lambda^{(4)}_{\text{QCD}} = 0.31$ GeV.

for $\lambda^2_{E,H}(1\ \text{GeV})$ and their ratio:

$$\mathcal{R}(\mu) = \frac{\lambda_E^2(\mu)}{\lambda_H^2(\mu)} \tag{11.47}$$

at $\mu = 1$ GeV. Hence, we study different combinations of Eq. (11.44), (11.45), (11.46) and (11.43).

We plot higher dimensional contributions for λ_H^4 in the lower part of Fig. 11.6 (a) and we observe that each power correction enhances the total value of λ_H^4. The dimension five contribution leads to the largest contribution in Fig. 11.6 (a). The fact that correlation functions with a large mass dimension experience large contributions from local condensates with a high mass dimension for small values of the Borel parameter M is a well known fact. Moreover, the contributions from dimensions greater than five become smaller indicating convergence of the OPE. The upper plot in Fig. 11.6 (a) shows the sum of all contributions up to mass dimension seven for different threshold parameters ω_{th}. This variation of the parameter ω_{th} indicates the stability of the sum rule, since the Borel parameter M and ω_{th} are correlated. Furthermore, it can be explicitly seen that in the highly nonperturbative regime with small M the condensate contributions become dominant and therefore the sum rule becomes unreliable. To find the optimal window for the threshold ω_{th}, we vary the function $F(\mu)$ in Eq. (11.43) for different values of ω_{th}, see Fig. 11.7 (a). As we can see, the decay constant $F(\mu)$ gives reliable values in the interval $0.8\,\text{GeV} \leq \omega_{th} \leq 1.0\,\text{GeV}$. In order to confirm that our threshold choice gives reasonable results, we compute the physical decay constant f_B by using Eq. (11.4), see Fig. 11.7 (b). We observe in Fig. 11.7 (b) that for $M \geq 0.8\,\text{GeV}$ the dependence on the threshold parameter ω_{th} between 0.8 GeV and 1.0 GeV becomes stable and reliable. Although the error of the decay constant f_B given in Eq. (11.5) is small, we assume a conservative uncertainty of 50%, because we neglect the $\mathcal{O}(\alpha_s)$ contributions for the HQET decay constant $F(\mu)$, which are known to be large and moreover our sum rules only account for the contributions up to mass dimension seven. The

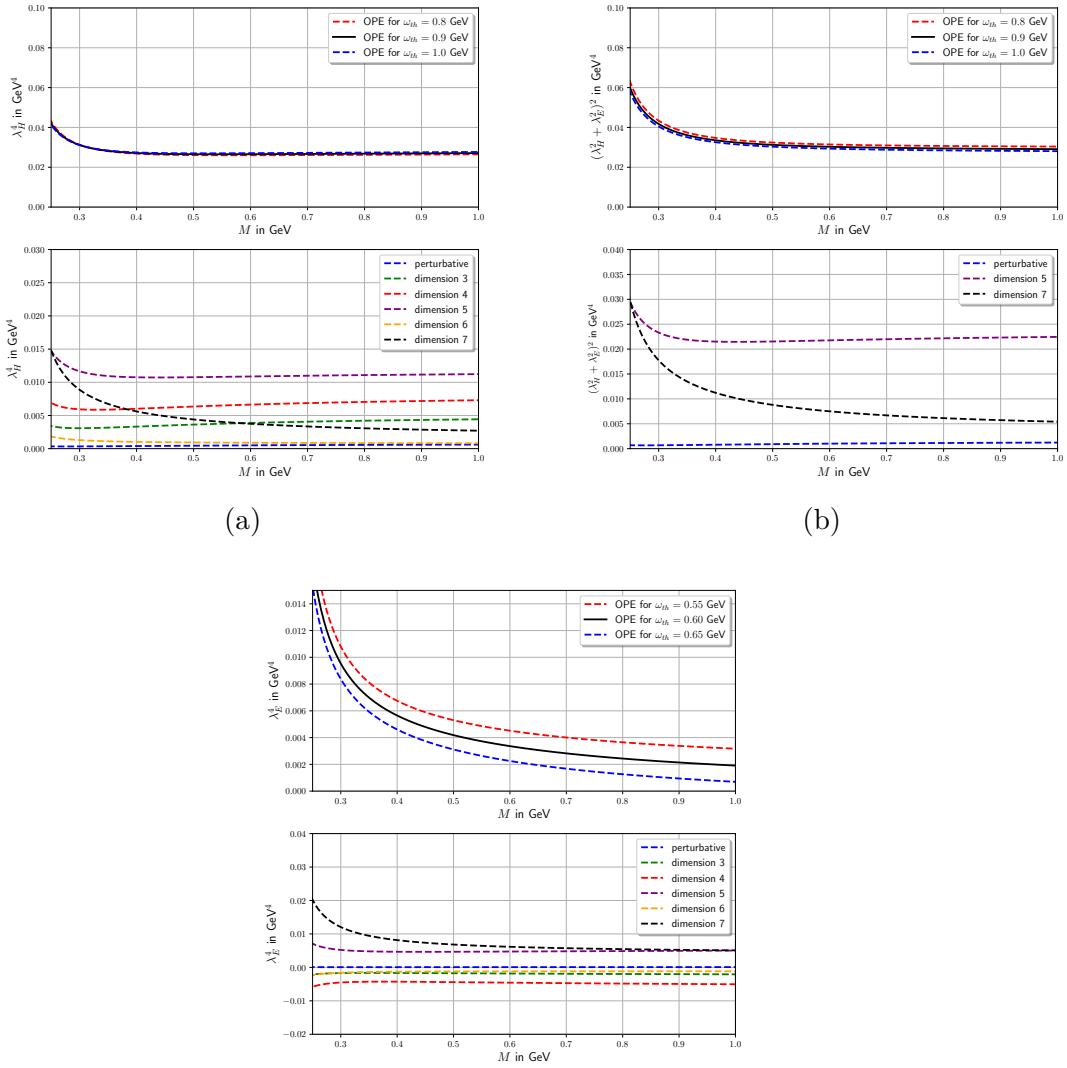

Figure 11.6: Fig. (a), (b) and (c) show the full OPE of Eq. (11.44), (11.45) and (11.46) within the threshold interval $0.8\,\text{GeV} \leq \omega_{th} \leq 1.0\,\text{GeV}$, respectively. The lower figures illustrate the individual contributions to the OPE for $\omega_{th} = 0.9$ GeV. The plots only show the central values.

corresponding analysis in [378] shows the impact of these corrections, which reduce the uncertainty of the analysis to $15\% - 20\%$. Another method to determine the interval for the threshold parameter ω_{th} is by taking the derivative with respect to the Borel parameter $\partial/\partial(-1/M)$ in Eq. (11.45). Dividing this expression by the original sum rule in Eq. (11.45) yields an estimate for the parameter $\bar{\Lambda}$ which needs to be compatible with the value stated in Table 11.1. Both methods give the same interval for ω_{th}, namely $0.8\,\text{GeV} \leq \omega_{th} \leq 1.0\,\text{GeV}$.

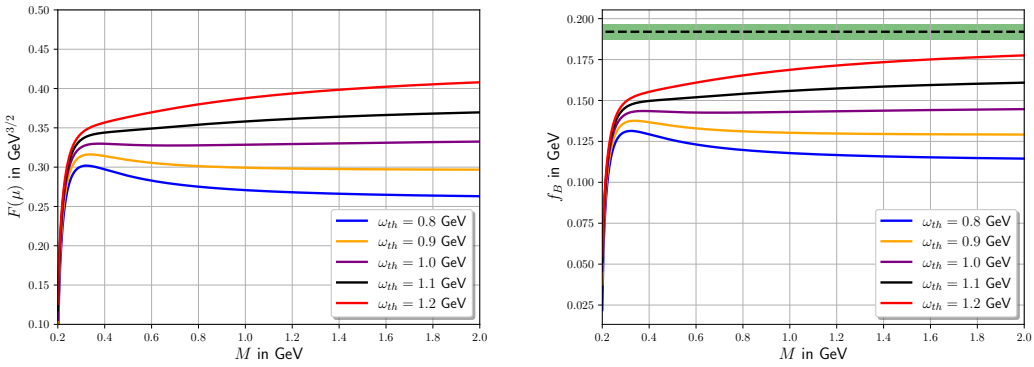

(a) (b)

Figure 11.7: Fig. (a) shows the comparison of the central values of the decay constant $F(\mu)$ for different values of ω_{th}. The value of the binding energy can be found in Table 11.1. Fig. (b) shows the comparison of the central values of the physical decay constant f_B with different values of ω_{th}. The dashed line indicates the lattice result and the shaded green area illustrates its corresponding uncertainty.

Similarly, we plot higher dimensional contributions for the sum rule in Eq. (11.44) in Fig. 11.6 (b). The lower plot illustrates each order of the power expansion individually. Here, we see that the dimension three, four and six condensates do not contribute to the sum rule. The terms corresponding to the dimension five condensate provide again the largest contribution and beyond this dimension the power expansion is expected to converge, which is indicated by the small contribution of mass dimension seven. Again, the upper plot in Fig. 11.6 (b) shows the value of $(\lambda_H^2 + \lambda_E^2)^2$ as a function of M for different threshold parameter ω_{th}. The determination of the threshold window for ω_{th} follows the same argumentation as for the sum rule in Eq. (11.45). In particular, both methods lead again to the same conclusion and we obtain the interval $0.8\,\text{GeV} \leq \omega_{th} \leq 1.0\,\text{GeV}$.

The sum rule for the parameter λ_E^4 in Eq. (11.46) requires further investigation. Fig. 11.6 (c) presents in the upper plot the sum of all contributions up to mass dimension seven, while in the lower plot each contribution is considered individually. In comparison to the sum rules in Eq. (11.44) and Eq. (11.45), the mass dimension three and four condensates contribute with the opposite sign to this sum rule. Since these contributions are large, this sum rule becomes unreliable and unstable compared to the previously studied sum rules. Additionally, the dominant dimension five contributions from Eq. (11.37), (11.38) and (11.39) do not appear in this sum rule, thus the extraction of an estimate for λ_E^2 from this sum rule gives an unreliable value. Moreover, we observe that the dimension seven contribution also gives a sizeable contribution, which questions the convergence of the OPE itself.

The fact that this sum rule becomes unstable can be seen from the threshold interval for ω_{th}. Only the argumentation via the decay constants $F(\mu)$ and f_B give

an appropriate interval, namely 0.55 GeV $\leq \omega_{th} \leq$ 0.65 GeV. Furthermore, the variation of the threshold seems to give larger deviations than for the sum rules in Eq. (11.44) and (11.45) indicating a less stable sum rule with larger uncertainties.

To obtain the lower bound for the Borel parameter M, we choose a value where the dimension seven condensate contribution is smaller than 40% of the total OPE. Notice that too small values of M spoil the convergence of the OPE since the condensate contributions become dominant. For the sum rules in Eq. (11.44) and (11.45), this condition is fulfilled for $0.5\,\text{GeV} \leq M$. Based on Fig. 11.6 (a) and 11.6 (b), we also see that for $0.5\,\text{GeV} \leq M$ the sum rule starts to become more reliable. As already mentioned, the sum rule for λ_E^4 in Eq. (11.46) is more unstable compared to λ_H^4 and $(\lambda_H^2 + \lambda_E^2)^2$. Hence, this method to obtain the lower bound of M does not work for λ_E^4. Instead, we choose the values based on Fig. 11.6 (c). We see that for $0.5\,\text{GeV} \leq M$ the OPE becomes more reliable and therefore a good choice for the lower bound. This estimate of the lower bound is taken into account in the uncertainty analysis.

For the determination of the upper bound of the Borel parameter we introduce:

$$R_{\text{cont.}} = 1 - \frac{\int_0^{\omega_{th}} \mathrm{d}\omega \frac{1}{\pi} \text{Im}\Pi_X^{\text{OPE}}(\omega) e^{-\omega/M}}{\int_0^{\infty} \mathrm{d}\omega \frac{1}{\pi} \text{Im}\Pi_X^{\text{OPE}}(\omega) e^{-\omega/M}} \tag{11.48}$$

for $X \in \{H, E, HE\}$. The value of $R_{\text{cont.}}$ guarantees that the ground state still gives a sizeable contribution compared to the higher resonances and continuum contribution. For reliable results of the sum rule we expect $R_{\text{cont.}} \leq 50\%$ for $M \leq M_{\text{max}}$. Thus, Eq. (11.48) fixes the upper bound for the Borel parameter. But in the case of Eq. (11.44), (11.45) and (11.46), the continuum contribution is dominant, which is to be expected from the large mass dimension of the considered correlation function in Eq. (11.7). Therefore, an upper bound for M is not feasible according to this method.

To resolve this problem, we consider two combinations of the sum rules in Sec. 11.3, which have the feature that $R_{\text{cont.}}$ becomes about 50% for a reasonable value of M. The combinations are the following:

$$\frac{(\lambda_H^2 + \lambda_E^2)^2}{\lambda_H^4} = (1 + \mathcal{R})^2 \quad \text{and} \quad \frac{F(\mu)^2 e^{-\bar{\Lambda}/M} + F(\mu)^2 e^{-\bar{\Lambda}/M} \lambda_H^4}{F(\mu)^2 e^{-\bar{\Lambda}/M} - F(\mu)^2 e^{-\bar{\Lambda}/M} \lambda_E^4} \tag{11.49}$$

with $\mathcal{R}$ defined in Eq. (11.47). The combination $(1 + \mathcal{R})^2$ is an appropriate choice, because the dominant mass dimension five contributions due to Eq. (11.45) lower the value of $R_{\text{cont.}}$ significantly. On the other hand, the second combination in Eq. (11.49) is dominated by the large $\mathcal{O}(\alpha_s^0)$ contributions from $F(\mu)$ such that $\lambda_{E,H}^4$ become only small corrections. For both combinations in Eq. (11.49) the parameter is $R_{\text{cont.}} \leq 50\%$ for $M_{\text{max}} = 0.8$ GeV.

In Table 11.2 we summarize the lower and upper bounds for the parameters M and ω_{th}.

Sum rule	Borel window	threshold window
Eq. (11.49)	$0.5\,\text{GeV} \leq M \leq 0.8\,\text{GeV}$	$0.8\,\text{GeV} \leq \omega_{th} \leq 1.0\,\text{GeV}$

Table 11.2: Summary of the threshold and Borel window for the combination in Eq. (11.49).

In Fig. 11.8 (a) and 11.8 (b) we plot both combinations as a function of M for different values of ω_{th} within its threshold window.

Finally, we are at the point to extract $\mathcal{R}$ and $\lambda^2_{E,H}$ based on Eq. (11.49). The uncertainties of $\lambda^2_{E,H}$ and for the ratio $\mathcal{R}$ are partially determined by varying each input parameter individually according to their uncertainty, see Table 11.1. For the strong coupling constant we use the two-loop expression with $\Lambda^{(4)}_{\text{QCD}} = 0.31$ GeV to obtain $\alpha_s(1\,\text{GeV}) = 0.471$. We vary $\Lambda^{(4)}_{\text{QCD}}$ in the interval $0.29\,\text{GeV} \leq \Lambda^{(4)}_{\text{QCD}} \leq 0.33\,\text{GeV}$, which corresponds to the running coupling $\alpha_s(1\,\text{GeV}) = 0.44 - 0.50$. In the last step, we square each uncertainty in quadrature:

$$\begin{aligned}
\mathcal{R}(1\,\text{GeV}) = 0.1 &+ \begin{pmatrix}+0.03\\-0.03\end{pmatrix}_{\omega_{th}} + \begin{pmatrix}+0.01\\-0.02\end{pmatrix}_{M} \\
&+ \begin{pmatrix}+0.01\\-0.01\end{pmatrix}_{\alpha_s} + \begin{pmatrix}+0.01\\-0.01\end{pmatrix}_{\langle\bar{q}q\rangle} + \begin{pmatrix}+0.02\\-0.03\end{pmatrix}_{\langle\frac{\alpha_s}{\pi}G^2\rangle} \\
&+ \begin{pmatrix}+0.05\\-0.04\end{pmatrix}_{\langle\bar{q}gG\cdot\sigma q\rangle} + \begin{pmatrix}+0.02\\-0.02\end{pmatrix}_{\langle g_s^3 f^{abc}G^aG^bG^c\rangle} \\
&= 0.1 \pm 0.07
\end{aligned} \tag{11.50}$$

$$\begin{aligned}
\lambda^2_H(1\,\text{GeV}) = \Big[0.150 &+ \begin{pmatrix}+0.002\\-0.003\end{pmatrix}_{\omega_{th}} + \begin{pmatrix}+0.002\\-0.004\end{pmatrix}_{M} \\
&+ \begin{pmatrix}+0.001\\-0.001\end{pmatrix}_{\langle\frac{\alpha_s}{\pi}G^2\rangle} + \begin{pmatrix}+0.001\\-0.001\end{pmatrix}_{\langle\bar{q}gG\cdot\sigma q\rangle} \\
&+ \begin{pmatrix}+0.001\\-0.001\end{pmatrix}_{\langle g_s^3 f^{abc}G^aG^bG^c\rangle}\Big]\,\text{GeV}^2 \\
&= (0.150 \pm 0.006)\,\text{GeV}^2
\end{aligned} \tag{11.51}$$

For λ_H^2, the variation of the strong coupling constant α_s, the dimension three and dimension six condensates do not change the central value significantly. Therefore, these uncertainties can be neglected.

$$\begin{aligned}\lambda_E^2(1\,\mathrm{GeV}) = \Bigg[0.010 &+ \begin{pmatrix}+0.004\\-0.005\end{pmatrix}_{\omega_{th}} + \begin{pmatrix}+0.002\\-0.003\end{pmatrix}_{M} \\ &+ \begin{pmatrix}+0.001\\-0.001\end{pmatrix}_{\alpha_s} + \begin{pmatrix}+0.003\\-0.003\end{pmatrix}_{\langle\bar{q}q\rangle} \\ &+ \begin{pmatrix}+0.003\\-0.004\end{pmatrix}_{\langle\frac{\alpha_s}{\pi}G^2\rangle} + \begin{pmatrix}+0.007\\-0.006\end{pmatrix}_{\langle\bar{q}gG\cdot\sigma q\rangle} \\ &+ \begin{pmatrix}+0.002\\-0.002\end{pmatrix}_{\langle g_s^3 f^{abc}G^aG^bG^c\rangle}\Bigg]\,\mathrm{GeV}^2 \\ &= (0.010 \pm 0.009)\,\mathrm{GeV}^2\,. \end{aligned} \tag{11.52}$$

Notice that the threshold parameter ω_{th} and the Borel parameter M are correlated, which can be deduced from the determination of the Borel window and the threshold interval. But since the variation of ω_{th} with respect to M is negligible, it is possible to choose one point in the parameter space of both parameters where the conditions from above are satisfied and obtain an estimate for the uncertainty by varying ω_{th}.

Besides these contributions, there are other uncertainties due to several approximations and systematic errors. Since we truncated the perturbative series at $\mathcal{O}(\alpha_s)$ and the power corrections at dimension seven, we introduce another error which is more complicated to determine. Moreover, there is also an intrinsic uncertainty caused by the sum rule approach, for instance generated by the use of the quark-hadron duality. The total uncertainties stated in Eq. (11.50), (11.51) and (11.52) only list those quantities, which give deviations from the central values.

Before we state our final results, we will first derive upper bounds on the parameters $\lambda_{E,H}^2$. Due to the diagonal structure of the correlation function, we know that the spectral density is positive definite. By performing the limit $\omega_{th} \to \infty$ in Eq. (11.45) and (11.46), we include all possible higher resonances and continuum contributions into our analysis. Thus, we obtain a consistent upper bound onto these parameters as it was already done in the case of f_D/f_{D_s} decay constants in [394]. The values for the upper bounds within the Borel window in Fig. 11.8 (a) and 11.8

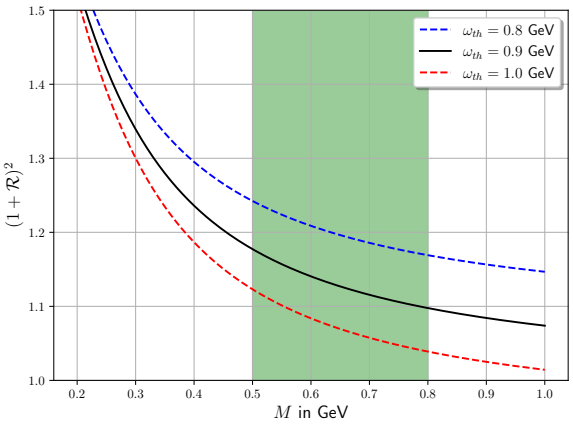

(a)

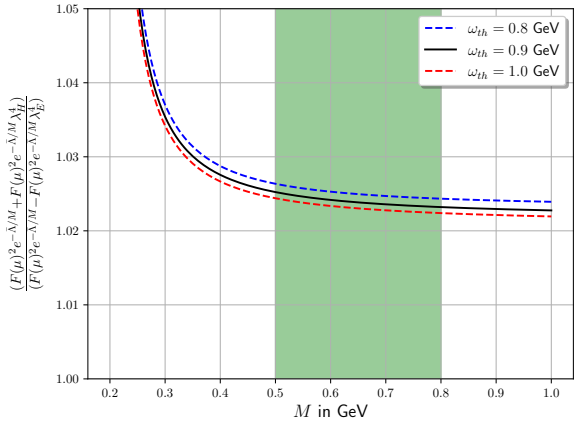

(b)

Figure 11.8: Fig. (a) shows the Borel sum rule for $(1+\mathcal{R})^2$ for the window $0.8\,\text{GeV} \leq \omega_{th} \leq 1.0\,\text{GeV}$. The shaded green area illustrates the Borel window. Similarly, Fig. (b) shows the Borel sum rule for $(F(\mu)^2 e^{-\bar{\Lambda}/M} + F(\mu)^2 e^{-\bar{\Lambda}/M} \lambda_H^4)/(F(\mu)^2 e^{-\bar{\Lambda}/M} - F(\mu)^2 e^{-\bar{\Lambda}/M} \lambda_E^4)$ for the window $0.8\,\text{GeV} \leq \omega_{th} \leq 1.0\,\text{GeV}$.

(b) are:

$$\lambda_H^2 < 0.48^{+0.17}_{-0.24}\ \text{GeV}^2\,, \tag{11.53}$$

$$\lambda_E^2 < 0.41^{+0.19}_{-0.24}\ \text{GeV}^2\,. \tag{11.54}$$

Now we extract our predictions for these parameters based on our sum rule analysis. We expect that these estimates should lie within the bounds of (11.53) and (11.54).

A conservative estimate of the uncertainties leads to the following final results:

$$\lambda_E^2(1\text{ GeV}) = (0.01 \pm 0.01)\text{ GeV}^2\,, \tag{11.55}$$

$$\lambda_H^2(1\text{ GeV}) = (0.15 \pm 0.05)\text{ GeV}^2\,, \tag{11.56}$$

$$\mathcal{R} = 0.1 \pm 0.1\,. \tag{11.57}$$

If we consider instead directly Eq. (11.44), (11.45) and take the Borel window and the threshold parameter ω_{th} as shown in Table 11.2, we obtain the values:

$$\lambda_E^2(1\text{ GeV}) = (0.05 \pm 0.03)\text{ GeV}^2\,, \tag{11.58}$$

$$\lambda_H^2(1\text{ GeV}) = (0.16 \pm 0.05)\text{ GeV}^2\,, \tag{11.59}$$

$$\mathcal{R} = 0.3 \pm 0.2\,. \tag{11.60}$$

Note that we can also use (11.46) to obtain the value for λ_E^2, however the threshold window must be chosen as $0.55\,\text{GeV} \leq \omega_{th} \leq 0.65\,\text{GeV}$ as shown in Fig. 11.6 (c).

Although the sum rules in Eq. (11.44) to (11.46) are dominated by continuum contributions and higher resonances for the Borel window given in Table 11.2, we see that the set of parameters and their ratio $\mathcal{R}$ in Eq. (11.58) to (11.60) reproduce the values for $\lambda_{E,H}^2$ and $\mathcal{R}$ in Eq. (11.55) to (11.57) within the errors. In particular the estimate for λ_H^2 does not change much, which indicates that the continuum contributions are well approximated by the sum rules in Eq. (11.45). All values lie within the bounds given in Eq. (11.53) and (11.54). Our result for λ_E^2 in Eq. (11.55) is close to the result in [378] and agrees within the error, see Table 11.3. Additionally, our result for λ_H^2 tends towards the result in [356].

11.5 Conclusion

In this work we suggested alternative diagonal QCD sum rules in order to estimate the HQET parameters $\lambda_{E,H}^2$ and their ratio $\mathcal{R} = \lambda_E^2/\lambda_H^2$. We included all leading contributions to the diagonal correlation function of three-particle quark-antiquark-gluon currents up to mass dimension seven. The advantage of these sum rules are that they are positive definite and we expect that the quark-hadron duality is more accurate compared to the previously studied correlation functions in [356, 378]. But we observe dominant contributions from the continuum and higher resonances due to the large mass dimension of the correlation function within these sum rules. This is why we consider combinations of these sum rules studied in Section 11.4, which satisfy the condition that the ground state contribution still gives a sizeable effect. Moreover, the OPE is expected to converge for the two sum rules in Eq. (11.44) and

(11.45) shown in Fig. 11.6 (a) and 11.6 (b), because the investigated contributions beyond mass dimension five become smaller. However, the OPE in Eq. (11.46) needs additional higher order corrections, since the contribution of dimension five and seven are both large, which makes the sum rule unstable, see Fig. 11.6 (c).

For a consistent treatment of the leading order contributions we also included only the $\mathcal{O}(\alpha_s^0)$ contributions for the HQET decay constant $F(\mu)$, although it is known that the $\mathcal{O}(\alpha_s)$ contributions are sizeable [379]. Our results compared to the values obtained in [356, 378] are listed in Table 11.3.

Parameters	Ref. [356]	Ref. [378]	**this work**
$\mathcal{R}(1\text{ GeV})$	(0.6 ± 0.4)	(0.5 ± 0.4)	(0.1 ± 0.1)
$\lambda_H^2(1\text{ GeV})$	(0.18 ± 0.07) GeV^2	(0.06 ± 0.03) GeV^2	(0.15 ± 0.05) GeV^2
$\lambda_E^2(1\text{ GeV})$	(0.11 ± 0.06) GeV^2	(0.03 ± 0.02) GeV^2	(0.01 ± 0.01) GeV^2

Table 11.3: Comparison of our results for the parameters $\lambda_{E,H}^2$ and $\mathcal{R}$ at $\mu = 1$ GeV.

With these new sum rules we obtain independent estimates for the parameters $\lambda_{E,H}^2$ and the $\mathcal{R}$-ratio, which are important ingredients for the second moments of the B-meson light-cone distribution amplitudes in B-meson factorization theorems. For future improvements of our sum rules we suggest to include $\mathcal{O}(\alpha_s^2)$ corrections to the OPE and consider even higher mass dimension in the power expansion of local vacuum condensates. In this case it would also be necessary to include the $\mathcal{O}(\alpha_s)$ contributions for $F(\mu)$. Especially the sum rule in (11.46) will benefit greatly since we expect the convergence of the OPE, which results in better determination of $\lambda_{E,H}^2$ and consequently $\mathcal{R}$.

Acknowledgements

We would like to thank Alexander Khodjamirian for proposing this project to us, for his constant feedback throughout the work and for reading the manuscript. We thank Thomas Mannel for useful discussion and reading the manuscript. Additionally, we are grateful to Thorsten Feldmann and Alexei Pivovarov for helpful discussions. This research was supported by the Deutsche Forschungsgemeinschaft (DFG, German Research Foundation) under grant 396021762 - TRR 257.

Appendix A Parametrization of the QCD condensates

Here we present the condensates that we have used in the work. All results are based on [395] if not stated otherwise. First, we Taylor expand the following matrix

element:

$$\begin{aligned}\langle 0|\,\bar{q}(0)\Gamma_1 P_+\Gamma_2\, q(x)\,|0\rangle &= \langle 0|\,\bar{q}(0)\Gamma_1 P_+\Gamma_2 q(0)\,|0\rangle \\ &+ x^\mu\,\langle 0|\,\bar{q}(0)\Gamma_1 P_+\Gamma_2 D_\mu q(0)\,|0\rangle \\ &+ \frac{x^\mu x^\nu}{2}\,\langle 0|\,\bar{q}(0)\Gamma_1 P_+\Gamma_2 D_\mu D_\nu q(0)\,|0\rangle \\ &+ \cdots \end{aligned} \tag{11.61}$$

The first term in Eq.(11.61) corresponds to the quark condensate.

$$\langle 0|\,\bar{q}^i_\alpha(0)\Gamma_{1,\alpha\beta}P_{+,\beta\gamma}\Gamma_{2,\gamma\delta}\,q^j_\delta(0)\,|0\rangle = \frac{1}{4N_c}\cdot \mathrm{Tr}[\Gamma_1 P_+\Gamma_2]\,\langle\bar{q}q\rangle\,\delta^{ij}, \tag{11.62}$$

where (i,j) are color indices and $(\alpha,\beta,\gamma,\delta)$ are spinor indices. The second term in Eq.(11.61) does not contribute. Making use of the Dirac equation, we can rewrite the covariant derivative as:

$$\not{D} q = -i m_q q\,. \tag{11.63}$$

We assume $m_q = 0$ for light quarks.

Before we consider the third term in more detail, we parametrize the dimension five matrix element:

$$\langle 0|\,\bar{q}^i_\alpha(0) g_s G_{\mu\nu}(0) q^j_\delta(0)\,|0\rangle = \langle 0|\,\bar{q} g_s \sigma\cdot G q\,|0\rangle\cdot\frac{1}{4N_c d(d-1)}\delta^{ij}\cdot(\sigma_{\mu\nu})_{\delta\alpha}\,. \tag{11.64}$$

The third term in Eq.(11.61) corresponds to the quark-gluon condensate.

$$\frac{x^\mu x^\nu}{2}\,\langle 0|\,\bar{q}^i_\alpha(0) D_\mu D_\nu q^j_\delta(0)\,|0\rangle = \frac{x^2}{16N_c d}\,\delta^{ij}\delta_{\alpha\delta}\,\langle 0|\,\bar{q} g_s\sigma\cdot G q\,|0\rangle\ . \tag{11.65}$$

The gluon condensate can be parametrized as:

$$\langle 0|\,G^a_{\mu\nu}G^b_{\rho\sigma}\,|0\rangle = \frac{\delta^{ab}}{d(d-1)(N_c^2-1)}\,\langle G^2\rangle\,(g_{\mu\rho}g_{\nu\sigma} - g_{\mu\sigma}g_{\nu\rho})\,. \tag{11.66}$$

Next is the parametrization of the triple-gluon condensate, which was denoted as $B_{\mu\lambda\rho\nu\sigma\alpha}$ in Eq. (11.40). The decomposition of the triple-gluon condensate has been investigated in [396]:

$$\begin{aligned}\langle g_s^3 f^{abc} G^a_{\mu\nu}G^b_{\rho\sigma}G^c_{\alpha\lambda}\rangle = \frac{\langle g_s^3 f^{abc}G^aG^bG^c\rangle}{d(d-1)(d-2)}\cdot\Big(&g_{\mu\lambda}g_{\rho\nu}g_{\sigma\alpha} + g_{\mu\sigma}g_{\rho\alpha}g_{\lambda\nu} + g_{\rho\lambda}g_{\mu\alpha}g_{\nu\sigma} + g_{\alpha\nu}g_{\mu\rho}g_{\sigma\lambda} - \\ &g_{\mu\sigma}g_{\rho\lambda}g_{\alpha\nu} - g_{\mu\lambda}g_{\rho\alpha}g_{\nu\sigma} - g_{\rho\nu}g_{\mu\alpha}g_{\sigma\lambda} - g_{\sigma\alpha}g_{\mu\rho}g_{\nu\lambda}\Big)\,.\end{aligned} \tag{11.67}$$

The expression in Eq. (11.67) corresponds to the tensor $B_{\mu\lambda\rho\nu\sigma\alpha}$ introduced in Eq. (11.40).

Chapter 12

Summary

In recent years, we have seen small deviations between Standard Model (SM) predictions and experimental measurements, especially in the quark and lepton flavour sectors, which may indicate the presence of New Physics (NP). B mesons in particular open up a wide range of possibilities for flavour studies. The large mass of the bottom-quark allows us to perform calculations within the framework of Heavy Quark Effective Theory (HQET). Given the increasing amount of data that Belle II and the LHCb will make available, we must aim to reduce theoretical uncertainty to the same level as experimental uncertainty in order to probe the Standard Model while also constraining potential NP effects.

This thesis has contributed to the systematic improvement of the precision of flavour physics prediction while also shedding light on the tension between theory prediction and experimental measurement by incorporating NP effects and their impact on observables.

First, we looked into how to improve the precision of the inclusive determination of $|V_{cb}|$, which employs the $B \to X_c \ell \bar{\nu}$ rate calculated from the measured $B \to X \ell$. In the current stage, the background signals $b \to u \ell \bar{\nu}$ and $b \to c(\tau \to \ell \bar{\nu} \nu) \bar{\nu}$ (among others) are simulated using Monte-Carlo data and subtracted from $B \to X \ell$, introducing uncertainties. We argue that the background signals can be computed precisely within the Heavy Quark Expansion (HQE) and thus could be included in the $B \to X \ell$ analysis without the need to subtract these contributions in order to obtain a more precise value of $|V_{cb}|$. We computed different moments for the $b \to u \ell \bar{\nu}$ process at next-to-leading order including power-corrections. We compared our findings to generator-level Monte-Carlo data and we observe significant differences between Monte-Carlo and HQE, particularly for the hadronic invariant mass moments, which might be avoided by employing the suggested approach. In addition, for the first time, we calculated $b \to c(\tau \to \ell \bar{\nu} \nu) \bar{\nu}$ contributions (which contribute at a rate of 4 %). Despite the lack of Monte-Carlo data to compare it, we report our findings so that future comparisons can be made. In order to prepare for the Belle II experimental study of inclusive $|V_{cb}|$, which will achieve an

unprecedented level of precision, we argue for using the full $B \to X\ell$ rate without subtracting the $b \to u\ell\bar{\nu}$ and $b \to c(\tau \to \ell\bar{\nu}\nu)\bar{\nu}$ contributions. With this strategy, the experimental uncertainties on $|V_{cb}|$ could be reduced even further.

The Lepton Flavour Universality (LFU) ratios of semileptonic inclusive B meson decays were also investigated. In the SM, the coupling of electroweak gauge bosons to leptons is independent of lepton flavour. The LFU symmetry of the SM can be investigated in the semileptonic $B \to X_c\ell\bar{\nu}$ decays. The observables used to probe the LFU hypothesis are ratios of branching fractions between decays with $\ell = \tau, \mu, e$. In the case of small deviations between SM predictions and experimental measurements, this could indicate the presence of NP effects. Additionally, since there are tensions between SM predictions and experimental measurements in the exclusive $B \to D^{(*)}\ell\bar{\nu}$ modes, the inclusive ratios serve as an important cross-check of those modes. Our calculation of the LFU ratios for the semileptonic inclusive B decay takes into account the mass effects in the total rate. Furthermore, we include next-to-leading order corrections in the strong coupling constant and HQE parameters up to $1/m_b^3$. We revised an earlier result concerning the ρ_D^3 contribution of the total rate. We provide updated results for the branching ratio of the $B \to X_c\tau\nu$ decay, which is in agreement with LEP measurements. Additionally, we can compare our inclusive calculation against the sum over exclusive B decays. Using the HFLAV-averaged SM predictions for $R(D)$ and $R(D^*)$ and the measured rates for the light-modes, combined with the prediction for the branching ratio $\mathcal{B}(B \to D^{**}\ell\bar{\nu})$, we observe that the sum over exclusive modes does not saturate our calculated inclusive rate.

The standard method for determining the CKM element $|V_{cb}|$ is the inclusive semileptonic $B \to X_c\ell\bar{\nu}$ decay. These determinations rely on the HQE and use moments of decay spectra to extract non-perturbative parameters directly from data under the SM assumption. We explored the possibility that NP may be present in the inclusive semileptonic $B \to X_c\ell\bar{\nu}$ decay but the extraction of HQE parameters is done assuming the SM. Hence, we investigate the NP effects in the semileptonic decay as well as their potential impact on the moments of the inclusive decay and thus on the extraction of non-perturbative parameters in HQE. We accomplish this by computing power-corrections up to $1/m_b^3$ and next-to-leading order corrections in the strong coupling constant to the full basis of dimension-six NP operators for the first time. In the next step, we compared SM predictions to the moments of lepton energy, hadronic invariant mass, dilepton momentum and the forward-backward asymmetry for various toy NP scenarios using HQE parameters obtained from experimental data and experimental measurements. Furthermore, we want to look into the potential impact of the HQE parameters under the assumption of NP. To begin, we generate pseudo data points for the moments of lepton energy, hadronic invariant mass and dilepton momentum in a realistic NP scenario. In principle,

these pseudo data points can then be used to fit the HQE parameters using the SM expressions. In this way our toy fit simulates a real-world situation: NP is present, but HQE parameters are extracted assuming the SM. We observe $1-2\sigma$ shifts between our toy fit result and the result obtained by assuming simply SM. We should note that the fit is fairly flexible in compensating for such variation, so it merely helps to illustrate how NP can be mimicked in the HQE extraction. The primary goal of this work is to lay the groundwork for a global fit analysis that includes the complete set of NP operators, allowing for the extraction of $|V_{cb}|$ with NP effects.

We also studied the Lepton Flavour Violating (LFV) $\Lambda_b \to \Lambda \ell_1^- \ell_2^+$ decay using for the first time a full basis of NP operators. We provide the analytical result for the angular distribution of $\Lambda_b \to \Lambda \ell_1^- \ell_2^+$ decay and investigate the interaction between baryonic and mesonic searches for LFV, where upper bounds for the latter are available already. In a model-independent approach, we convert these upper limits into constraints on the branching ratio and forward-backward asymmetry for $\Lambda_b \to \Lambda \ell_1^- \ell_2^+$ decays. We found that the $\Lambda_b \to \Lambda \ell_1^- \ell_2^+$ decay provides different constraints on the NP Wilson coefficients than the $\bar{B}_s \to \ell_1^- \ell_2^+$ and $B^+ \to K^+ \ell_1^- \ell_2^+$ decays and has the potential to reduce the allowed parameter space for NP models. We investigate the branching ratio and forward-backward symmetry of the $\Lambda_b \to \Lambda \ell_1^- \ell_2^+$ decay quantitatively in two model-dependent approaches with specific NP scenarios that could address the b-anomalies. Our findings suggest that the predicted branching ratio for $\Lambda_b \to \Lambda \ell_1^- \ell_2^+$ for these scenarios can constrain the NP couplings further.

We can also improve the constraint of the NP models by reducing the hadronic uncertainties caused by the ten independent $\Lambda_b \to \Lambda$ local form factors. We investigate a new parametrization for the local form factors in order to better control the hadronic uncertainties. Our parametrization has the advantage that it bounds the parameters due to the use of orthonormal polynomials that diagonalize the form factors contribution within their respective dispersive bounds. We show that our parametrization provides excellent control of systematic uncertainties when extrapolating from low to large hadronic recoil by performing a Bayesian analysis of the available lattice QCD results for the $\Lambda_b \to \Lambda$ form factors. We investigate our parametrization for various truncation's and find that the extrapolation uncertainty of $\Lambda_b \to \Lambda$ decays does not increase significantly within the kinematic phase space. We show how dispersive bounds can constrain form factor uncertainties to the point where massively underconstrained analyses still show stable uncertainty estimates. This is a clear advantage over other parametrizations. Unlike ad-hoc parametrizations of these form factors, our parametrization allows us to control the form-factor uncertainties at large hadronic recoil, which is phenomenologically interesting for theoretical predictions of processes such as $\Lambda_b \to \Lambda\gamma$ and $\Lambda_b \to \Lambda \ell^- \ell^+$ decay. We propose to incorporate the framework of dispersive bounds directly into the lattice-QCD analysis. In addition, these results can be improved even further by including the one-particle contributions and other two-particle contributions in a global anal-

ysis of the available $b \to s$ form factor data, as the upper bound would be even more saturated.

As part of this thesis's final project, we investigated the light-cone distribution amplitude (LCDA) of the B meson. LCDAs are important in exclusive B meson decays such as $B \to \pi\pi$ or $B \to \pi K$, because they allow us to study CP violation in weak interactions. We focus on three-particle LCDAs of the B meson, which are found in higher dimensional vacuum to meson matrix elements with non-local quark operators. These matrix elements can be parametrized in terms of the $\lambda^2_{E,H}$ parameters for local quark operators, which also contribute to the second moments of the three-particle B meson distribution amplitudes. In order to estimate the two HQET parameters $\lambda^2_{E,H}$ and their ratio $\mathcal{R} = \lambda^2_E/\lambda^2_H$, we proposed alternative diagonal QCD sum rules. We included all leading contributions to the diagonal correlation function of three-particle quark-antiquark gluon currents up to mass dimension seven. The advantage of these sum rules is that they are positive definite, and we anticipate that the quark-hadron duality will be more accurate than previously studied correlation functions in the literature. The dominant contributions from the continuum and higher resonances due to the large mass dimension of the correlation function within these sum rules are a disadvantage of our approach. We can overcome this limitation by considering sum rule combinations that satisfy the condition that the ground state contribution still has a significant effect. Our sum rule for the parameter λ^2_H yields a result within the $1 - 2\sigma$ interval of existing literature results. The sum rule seems to be stable because the operator-product expansion (OPE) is expected to converge as the investigated contributions beyond mass dimension five become smaller. While the sum rule of parameter λ^2_E produces unreliable results due to OPE convergence. The OPE requires additional higher order corrections because the contributions of dimensions five and seven are both large, making the sum rule unstable. In order to improve our sum rules in the future, we suggested to include next-to-leading order corrections to the OPE and considering even higher mass dimension in the power expansion of local vacuum condensates. The sum rule of λ^2_E, in particular, will benefit greatly because we anticipate convergence of the OPE, resulting in better determination of the parameter.

Flavour physics has advanced significantly thanks to a collaborative theoretical and experimental effort, yet there are still many intriguing problems and mysteries to be explored. We may finally know whether the tension between the Standard Model predictions and experimental measurements of the b-anomalies will either vanish or persist. Thanks to the enormous amount of data from the Belle II and LHCb experiments. We will be able to narrow the scope of NP effects in both cases and gain additional knowledge about the nature of bottom-quark decays.

Chapter 13

Acknowledgements

I'd like to start by thanking the most important people in my life. First i would like to express my gratitude towards my parents for their unwavering support while I was writing this thesis and generally during my entire academic career. I am thankful to my beloved wife for her immense love and support. You are the best thing that could have happened to me. You are the best thing that is still happening to me, and you will be the best thing that ever happens to me. Thank you very much!

I am grateful to my supervisor Prof. Dr. Thomas Mannel for always encouraging me on my path to completing my PhD thesis and for always responding to my open questions in such amazing detail, which I greatly appreciated. But also for the stimulating discussions we've had on topics unrelated to physics. I am grateful for the opportunity to be writing my thesis in his group, as well as his great support for my future path. Thanks to his excellent supervision, I learned a lot. He gave me the opportunity to present my findings and learn from other excellent groups at workshops and conferences. I am grateful to Prof. Dr. Alexander Khodjamirian for agreeing to be the second referee, for proposing the project to us in Chapter 11 and his constant feedback throughout the work.

I'd like to thank my collaborators Thomas Blake, Matteo Fael, Marzia Bordone, Stefan Meinel, Danny van Dyk, K. Keri Vos, and Marcel Wald for the opportunity to work with and learn from you all over the last three years. I also appreciate my supervisor's and K. Keri Vos's feedback on my thesis during the writing stage.

Thank you all for accompanying and guiding me on my journey.

Bibliography

[1] M. Rahimi and M. Wald, *QCD sum rules for parameters of the B-meson distribution amplitudes*, *Phys. Rev. D* **104** (2021) 016027 [2012.12165].

[2] T. Mannel, M. Rahimi and K. K. Vos, *Impact of background effects on the inclusive V_{cb} determination*, *JHEP* **09** (2021) 051 [2105.02163].

[3] M. Bordone, M. Rahimi and K. K. Vos, *Lepton flavour violation in rare Λ_b decays*, *Eur. Phys. J. C* **81** (2021) 756 [2106.05192].

[4] M. Rahimi and K. K. Vos, *Standard Model predictions for lepton flavour universality ratios of inclusive semileptonic B decays*, *JHEP* **11** (2022) 007 [2207.03432].

[5] T. Blake, S. Meinel, M. Rahimi and D. van Dyk, *Dispersive bounds for local form factors in $\Lambda_b \to \Lambda$ transitions*, 2205.06041.

[6] M. Fael, M. Rahimi and K. K. Vos, *New physics contributions to moments of inclusive $b \to c$ semileptonic decays*, 2208.04282.

[7] R. Allahverdi et al., *The First Three Seconds: a Review of Possible Expansion Histories of the Early Universe*, 2006.16182.

[8] J. J. S. Thomson, *Xl. cathode rays*, *Philosophical Magazine Series 1* **44** (1897) 293.

[9] E. Rutherford, *Bakerian lecture: nuclear constitution of atoms*, *Proc.Roy.Soc.Lond.* **A 97** (1920) 374.

[10] J. Chadwick, *The existence of a neutron*, *Proc.Roy.Soc.Lond.* **A 136** (1932) 692.

[11] S. L. Glashow, *Partial Symmetries of Weak Interactions*, *Nucl. Phys.* **22** (1961) 579.

[12] S. Weinberg, *A Model of Leptons*, *Phys. Rev. Lett.* **19** (1967) 1264.

[13] S. L. Glashow, J. Iliopoulos and L. Maiani, *Weak Interactions with Lepton-Hadron Symmetry*, *Phys. Rev. D* **2** (1970) 1285.

[14] M. Bordone, B. Capdevila and P. Gambino, *Three loop calculations and inclusive V_{cb}*, 2107.00604.

[15] F. Bernlochner, M. Fael, K. Olschewsky, E. Persson, R. van Tonder, K. K. Vos et al., *First extraction of inclusive V_{cb} from q^2 moments*, 2205.10274.

[16] A. Salam, *Weak and Electromagnetic Interactions*, *Conf. Proc. C* **680519** (1968) 367.

[17] G. 't Hooft and M. J. G. Veltman, *Regularization and Renormalization of Gauge Fields*, *Nucl. Phys. B* **44** (1972) 189.

[18] ATLAS collaboration, *Observation of a new particle in the search for the Standard Model Higgs boson with the ATLAS detector at the LHC*, *Phys. Lett. B* **716** (2012) 1 [1207.7214].

[19] CMS collaboration, *Observation of a New Boson at a Mass of 125 GeV with the CMS Experiment at the LHC*, *Phys. Lett. B* **716** (2012) 30 [1207.7235].

[20] P. W. Anderson, *Plasmons, Gauge Invariance, and Mass*, *Phys. Rev.* **130** (1963) 439.

[21] P. W. Higgs, *Broken Symmetries and the Masses of Gauge Bosons*, *Phys. Rev. Lett.* **13** (1964) 508.

[22] F. Englert and R. Brout, *Broken Symmetry and the Mass of Gauge Vector Mesons*, *Phys. Rev. Lett.* **13** (1964) 321.

[23] G. S. Guralnik, C. R. Hagen and T. W. B. Kibble, *Global Conservation Laws and Massless Particles*, *Phys. Rev. Lett.* **13** (1964) 585.

[24] M. Ogilvie, *Dynamics of the standard model, 2nd edition, john f. donoghue, eugene golowich and barry r. holstein*, *Contemporary Physics* **57** (2015) 1.

[25] M. E. Peskin and D. V. Schroeder, *An Introduction to quantum field theory*. Addison-Wesley, Reading, USA, 1995.

[26] M. D. Schwartz, *Quantum Field Theory and the Standard Model*. Cambridge University Press, 3, 2014.

[27] S. Weinberg, *The Quantum theory of fields. Vol. 1: Foundations*. Cambridge University Press, 6, 2005.

[28] S. Weinberg, *The quantum theory of fields. Vol. 2: Modern applications*. Cambridge University Press, 8, 2013.

[29] N. Cabibbo, *Unitary Symmetry and Leptonic Decays*, *Phys. Rev. Lett.* **10** (1963) 531.

[30] M. Kobayashi and T. Maskawa, *CP Violation in the Renormalizable Theory of Weak Interaction*, *Prog. Theor. Phys.* **49** (1973) 652.

[31] CKMfitter Group collaboration, *CP violation and the CKM matrix: Assessing the impact of the asymmetric B factories*, *Eur. Phys. J. C* **41** (2005) 1 [hep-ph/0406184].

[32] L. Wolfenstein, *Parametrization of the Kobayashi-Maskawa Matrix*, *Phys. Rev. Lett.* **51** (1983) 1945.

[33] A. J. Buras, M. E. Lautenbacher and G. Ostermaier, *Waiting for the top quark mass, K+ —> pi+ neutrino anti-neutrino, B(s)0 - anti-B(s)0 mixing and CP asymmetries in B decays*, *Phys. Rev. D* **50** (1994) 3433 [hep-ph/9403384].

[34] F. Halzen and A. D. Martin, *QUARKS AND LEPTONS: AN INTRODUCTORY COURSE IN MODERN PARTICLE PHYSICS*. 1984.

[35] D. J. Gross and F. Wilczek, *Ultraviolet Behavior of Nonabelian Gauge Theories*, *Phys. Rev. Lett.* **30** (1973) 1343.

[36] M. B. Green, J. H. Schwarz and E. Witten, *SUPERSTRING THEORY. VOL. 1: INTRODUCTION*, Cambridge Monographs on Mathematical Physics. 7, 1988.

[37] M. B. Green, J. H. Schwarz and E. Witten, *SUPERSTRING THEORY. VOL. 2: LOOP AMPLITUDES, ANOMALIES AND PHENOMENOLOGY*. 7, 1988.

[38] A. O. Sushkov, W. J. Kim, D. A. R. Dalvit and S. K. Lamoreaux, *New Experimental Limits on Non-Newtonian Forces in the Micrometer Range*, *Phys. Rev. Lett.* **107** (2011) 171101 [1108.2547].

[39] J. F. Donoghue, *The effective field theory treatment of quantum gravity*, *AIP Conf. Proc.* **1483** (2012) 73 [1209.3511].

[40] M. Persic, P. Salucci and F. Stel, *The Universal rotation curve of spiral galaxies: 1. The Dark matter connection*, *Mon. Not. Roy. Astron. Soc.* **281** (1996) 27 [astro-ph/9506004].

[41] L. Hernquist, N. Katz, D. H. Weinberg and J. Miralda-Escude, *The Lyman alpha forest in the cold dark matter model*, *Astrophys. J. Lett.* **457** (1996) L51 [astro-ph/9509105].

[42] G. Bertone, D. Hooper and J. Silk, *Particle dark matter: Evidence, candidates and constraints*, *Phys. Rept.* **405** (2005) 279 [hep-ph/0404175].

[43] P. J. E. Peebles and B. Ratra, *The Cosmological Constant and Dark Energy*, *Rev. Mod. Phys.* **75** (2003) 559 [astro-ph/0207347].

[44] E. J. Copeland, M. Sami and S. Tsujikawa, *Dynamics of dark energy*, *Int. J. Mod. Phys. D* **15** (2006) 1753 [hep-th/0603057].

[45] Planck collaboration, *Planck 2018 results. VIII. Gravitational lensing*, *Astron. Astrophys.* **641** (2020) A8 [1807.06210].

[46] A. D. Sakharov, *Violation of CP Invariance, C asymmetry, and baryon asymmetry of the universe*, *Pisma Zh. Eksp. Teor. Fiz.* **5** (1967) 32.

[47] J. H. Christenson, J. W. Cronin, V. L. Fitch and R. Turlay, *Evidence for the 2π Decay of the K_2^0 Meson*, *Phys. Rev. Lett.* **13** (1964) 138.

[48] Belle collaboration, *Observation of large CP violation in the neutral B meson system*, *Phys. Rev. Lett.* **87** (2001) 091802 [hep-ex/0107061].

[49] BaBar collaboration, *Observation of CP violation in the B^0 meson system*, *Phys. Rev. Lett.* **87** (2001) 091801 [hep-ex/0107013].

[50] BELLE collaboration, *Evidence for D^0 - $\bar{D}^0$ Mixing*, *Phys. Rev. Lett.* **98** (2007) 211803 [hep-ex/0703036].

[51] BaBar collaboration, *Evidence for $D^0 - \overline{D}^0$ Mixing*, *Phys. Rev. Lett.* **98** (2007) 211802 [hep-ex/0703020].

[52] Super-Kamiokande collaboration, *Evidence for oscillation of atmospheric neutrinos*, *Phys. Rev. Lett.* **81** (1998) 1562 [hep-ex/9807003].

[53] LSND collaboration, *Evidence for neutrino oscillations from the observation of $\bar{\nu}_e$ appearance in a $\bar{\nu}_\mu$ beam*, *Phys. Rev. D* **64** (2001) 112007 [hep-ex/0104049].

[54] SNO collaboration, *Measurement of day and night neutrino energy spectra at SNO and constraints on neutrino mixing parameters*, *Phys. Rev. Lett.* **89** (2002) 011302 [nucl-ex/0204009].

[55] KamLAND collaboration, *First results from KamLAND: Evidence for reactor anti-neutrino disappearance*, *Phys. Rev. Lett.* **90** (2003) 021802 [hep-ex/0212021].

[56] Super-Kamiokande collaboration, *A Measurement of atmospheric neutrino oscillation parameters by SUPER-KAMIOKANDE I*, *Phys. Rev. D* **71** (2005) 112005 [hep-ex/0501064].

[57] T2K collaboration, *Indication of Electron Neutrino Appearance from an Accelerator-produced Off-axis Muon Neutrino Beam*, *Phys. Rev. Lett.* **107** (2011) 041801 [1106.2822].

[58] Double Chooz collaboration, *Indication of Reactor $\bar{\nu}_e$ Disappearance in the Double Chooz Experiment*, *Phys. Rev. Lett.* **108** (2012) 131801 [1112.6353].

[59] RENO collaboration, *Observation of Reactor Electron Antineutrino Disappearance in the RENO Experiment*, *Phys. Rev. Lett.* **108** (2012) 191802 [1204.0626].

[60] Z. Maki, M. Nakagawa and S. Sakata, *Remarks on the unified model of elementary particles*, *Prog. Theor. Phys.* **28** (1962) 870.

[61] B. Pontecorvo, *Neutrino Experiments and the Problem of Conservation of Leptonic Charge*, *Zh. Eksp. Teor. Fiz.* **53** (1967) 1717.

[62] Muon g-2 collaboration, *Measurement of the Positive Muon Anomalous Magnetic Moment to 0.46 ppm*, *Phys. Rev. Lett.* **126** (2021) 141801 [2104.03281].

[63] J. Polchinski, *Effective field theory and the Fermi surface*, in *Theoretical Advanced Study Institute (TASI 92): From Black Holes and Strings to Particles*, pp. 0235–276, 6, 1992, hep-th/9210046.

[64] M. Neubert, *Effective field theory and heavy quark physics*, in *Theoretical Advanced Study Institute in Elementary Particle Physics: Physics in $D \geqq 4$*, pp. 149–194, 12, 2005, DOI [hep-ph/0512222].

[65] I. Brivio and M. Trott, *The Standard Model as an Effective Field Theory*, *Phys. Rept.* **793** (2019) 1 [1706.08945].

[66] G. Buchalla, A. J. Buras and M. E. Lautenbacher, *Weak decays beyond leading logarithms*, *Rev. Mod. Phys.* **68** (1996) 1125 [hep-ph/9512380].

[67] T. Mannel, W. Roberts and Z. Ryzak, *A Derivation of the heavy quark effective Lagrangian from QCD*, *Nucl. Phys. B* **368** (1992) 204.

[68] S. Balk, J. G. Korner and D. Pirjol, *Heavy quark effective theory at large orders in 1/m*, *Nucl. Phys. B* **428** (1994) 499 [hep-ph/9307230].

[69] H. Georgi, *An Effective Field Theory for Heavy Quarks at Low-energies*, *Phys. Lett. B* **240** (1990) 447.

[70] M. A. Shifman and M. B. Voloshin, *On Production of d and D* Mesons in B Meson Decays*, *Sov. J. Nucl. Phys.* **47** (1988) 511.

[71] N. Isgur and M. B. Wise, *Weak Decays of Heavy Mesons in the Static Quark Approximation*, *Phys. Lett. B* **232** (1989) 113.

[72] N. Isgur and M. B. Wise, *WEAK TRANSITION FORM-FACTORS BETWEEN HEAVY MESONS*, *Phys. Lett. B* **237** (1990) 527.

[73] M. J. Dugan, M. Golden and B. Grinstein, *On the Hilbert space of the heavy quark effective theory*, *Phys. Lett. B* **282** (1992) 142.

[74] M. E. Luke and A. V. Manohar, *Reparametrization invariance constraints on heavy particle effective field theories*, *Phys. Lett. B* **286** (1992) 348 [hep-ph/9205228].

[75] Y.-Q. Chen, *On the reparametrization invariance in heavy quark effective theory*, *Phys. Lett. B* **317** (1993) 421.

[76] J. Heinonen, R. J. Hill and M. P. Solon, *Lorentz invariance in heavy particle effective theories*, *Phys. Rev. D* **86** (2012) 094020 [1208.0601].

[77] A. V. Manohar, *Reparametrization Invariance Constraints on Inclusive Decay Spectra and Masses*, *Phys. Rev. D* **82** (2010) 014009 [1005.1952].

[78] T. Mannel and K. K. Vos, *Reparametrization Invariance and Partial Re-Summations of the Heavy Quark Expansion*, *JHEP* **06** (2018) 115 [1802.09409].

[79] B. M. Dassinger, T. Mannel and S. Turczyk, *Inclusive semi-leptonic B decays to order* $1/m_b^4$, *JHEP* **03** (2007) 087 [hep-ph/0611168].

[80] T. Mannel, S. Turczyk and N. Uraltsev, *Higher Order Power Corrections in Inclusive B Decays*, *JHEP* **11** (2010) 109 [1009.4622].

[81] A. Kobach and S. Pal, *Reparameterization Invariant Operator Basis for NRQED and HQET*, *JHEP* **11** (2019) 012 [1810.02356].

[82] S. Turczyk, *Additional Information on Heavy Quark Parameters from Charged Lepton Forward-Backward Asymmetry*, *JHEP* **04** (2016) 131 [1602.02678].

[83] HPQCD collaboration, *Rare decay* $B \to K\ell^+\ell^-$ *form factors from lattice QCD*, *Phys. Rev. D* **88** (2013) 054509 [1306.2384].

[84] HPQCD collaboration, $B \to Dl\nu$ *form factors at nonzero recoil and extraction of* $|V_{cb}|$, *Phys. Rev. D* **92** (2015) 054510 [1505.03925].

[85] R. R. Horgan, Z. Liu, S. Meinel and M. Wingate, *Lattice QCD calculation of form factors describing the rare decays* $B \to K^*\ell^+\ell^-$ *and* $B_s \to \phi\ell^+\ell^-$, *Phys. Rev. D* **89** (2014) 094501 [1310.3722].

[86] Fermilab Lattice, MILC collaboration, *Update of $|V_{cb}|$ from the $\bar{B} \to D^* \ell \bar{\nu}$ form factor at zero recoil with three-flavor lattice QCD*, *Phys. Rev. D* **89** (2014) 114504 [1403.0635].

[87] R. R. Horgan, Z. Liu, S. Meinel and M. Wingate, *Rare B decays using lattice QCD form factors*, *PoS* **LATTICE2014** (2015) 372 [1501.00367].

[88] HPQCD collaboration, *Lattice QCD calculation of the $B_{(s)} \to D^*_{(s)} \ell \nu$ form factors at zero recoil and implications for $|V_{cb}|$*, *Phys. Rev. D* **97** (2018) 054502 [1711.11013].

[89] M. A. Shifman, A. I. Vainshtein and V. I. Zakharov, *QCD and Resonance Physics. Theoretical Foundations*, *Nucl. Phys. B* **147** (1979) 385.

[90] B. L. Ioffe, *Calculation of Baryon Masses in Quantum Chromodynamics*, *Nucl. Phys. B* **188** (1981) 317.

[91] L. J. Reinders, H. Rubinstein and S. Yazaki, *Hadron Properties from QCD Sum Rules*, *Phys. Rept.* **127** (1985) 1.

[92] E. V. Shuryak, *Correlation functions in the QCD vacuum*, *Rev. Mod. Phys.* **65** (1993) 1.

[93] S. Narison, *QCD spectral sum rules for heavy flavors*, *Acta Phys. Polon. B* **26** (1995) 687 [hep-ph/9503234].

[94] E. de Rafael, *An Introduction to sum rules in QCD: Course*, in *Les Houches Summer School in Theoretical Physics, Session 68: Probing the Standard Model of Particle Interactions*, pp. 1171–1218, 7, 1997, hep-ph/9802448.

[95] P. Colangelo and A. Khodjamirian, *QCD sum rules, a modern perspective*, hep-ph/0010175.

[96] B. L. Ioffe, *Condensates in quantum chromodynamics*, *Phys. Atom. Nucl.* **66** (2003) 30 [hep-ph/0207191].

[97] HPQCD collaboration, *Determination of the quark condensate from heavy-light current-current correlators in full lattice QCD*, *Phys. Rev. D* **100** (2019) 034506 [1811.04305].

[98] P. Gubler and D. Satow, *Recent Progress in QCD Condensate Evaluations and Sum Rules*, *Prog. Part. Nucl. Phys.* **106** (2019) 1 [1812.00385].

[99] Flavour Lattice Averaging Group collaboration, *FLAG Review 2019: Flavour Lattice Averaging Group (FLAG)*, *Eur. Phys. J. C* **80** (2020) 113 [1902.08191].

[100] E. C. Poggio, H. R. Quinn and S. Weinberg, *Smearing the Quark Model*, *Phys. Rev. D* **13** (1976) 1958.

[101] M. A. Shifman, *Quark hadron duality*, in *8th International Symposium on Heavy Flavor Physics*, vol. 3, (Singapore), pp. 1447–1494, World Scientific, 7, 2000, DOI [hep-ph/0009131].

[102] D. Boito, I. Caprini, M. Golterman, K. Maltman and S. Peris, *Hyperasymptotics and quark-hadron duality violations in QCD*, *Phys. Rev. D* **97** (2018) 054007 [1711.10316].

[103] A. V. Manohar and M. B. Wise, *Heavy quark physics*, vol. 10. 2000.

[104] A. G. Grozin, *Heavy quark effective theory*, *Springer Tracts Mod. Phys.* **201** (2004) 1.

[105] T. Mannel and A. A. Pivovarov, *QCD corrections to inclusive heavy hadron weak decays at $\Lambda^3_{\rm QCD}/m^3_Q$*, *Phys. Rev. D* **100** (2019) 093001 [1907.09187].

[106] P. Gambino and C. Schwanda, *Inclusive semileptonic fits, heavy quark masses, and V_{cb}*, *Phys. Rev. D* **89** (2014) 014022 [1307.4551].

[107] A. Alberti, P. Gambino, K. J. Healey and S. Nandi, *Precision Determination of the Cabibbo-Kobayashi-Maskawa Element V_{cb}*, *Phys. Rev. Lett.* **114** (2015) 061802 [1411.6560].

[108] M. Jezabek and J. H. Kuhn, *QCD Corrections to Semileptonic Decays of Heavy Quarks*, *Nucl. Phys. B* **314** (1989) 1.

[109] A. Pak and A. Czarnecki, *Heavy-to-heavy quark decays at NNLO*, *Phys. Rev. D* **78** (2008) 114015 [0808.3509].

[110] K. Melnikov, *O(alpha(s)**2) corrections to semileptonic decay b —> cl anti-nu(l)*, *Phys. Lett. B* **666** (2008) 336 [0803.0951].

[111] S. Biswas and K. Melnikov, *Second order QCD corrections to inclusive semileptonic b —> X(c) l anti-nu(l) decays with massless and massive lepton*, *JHEP* **02** (2010) 089 [0911.4142].

[112] P. Gambino, *B semileptonic moments at NNLO*, *JHEP* **09** (2011) 055 [1107.3100].

[113] P. Gambino, K. J. Healey and S. Turczyk, *Taming the higher power corrections in semileptonic B decays*, *Phys. Lett. B* **763** (2016) 60 [1606.06174].

[114] F. Bernlochner, M. Fael, K. Olschewsky, R. van Tonder, K. K. Vos and M. Welsch, *Work in Progress*, .

[115] M. Fael, T. Mannel and K. Keri Vos, *V_{cb} determination from inclusive $b \to c$ decays: an alternative method*, *JHEP* **02** (2019) 177 [1812.07472].

[116] M. Fael, K. Schönwald and M. Steinhauser, *Third order corrections to the semi-leptonic $b \to c$ and the muon decays*, 2011.13654.

[117] M. Bordone, M. Jung and D. van Dyk, *Theory determination of $\bar{B} \to D^{(*)}\ell^-\bar{\nu}$ form factors at $\mathcal{O}(1/m_c^2)$*, *Eur. Phys. J. C* **80** (2020) 74 [1908.09398].

[118] M. Bordone, N. Gubernari, D. van Dyk and M. Jung, *Heavy-Quark expansion for $\bar{B}_s \to D_s^{(*)}$ form factors and unitarity bounds beyond the $SU(3)_F$ limit*, *Eur. Phys. J. C* **80** (2020) 347 [1912.09335].

[119] P. Gambino, M. Jung and S. Schacht, *The V_{cb} puzzle: An update*, *Phys. Lett. B* **795** (2019) 386 [1905.08209].

[120] D. Bigi, P. Gambino and S. Schacht, *$R(D^*)$, $|V_{cb}|$, and the Heavy Quark Symmetry relations between form factors*, *JHEP* **11** (2017) 061 [1707.09509].

[121] P. Gambino, G. Ossola and N. Uraltsev, *Hadronic mass and q^2 moments of charmless semileptonic B decay distributions*, *JHEP* **09** (2005) 010 [hep-ph/0505091].

[122] I. I. Y. Bigi and N. G. Uraltsev, *Weak annihilation and the endpoint spectrum in semileptonic B decays*, *Nucl. Phys. B* **423** (1994) 33 [hep-ph/9310285].

[123] M. B. Voloshin, *Nonfactorization effects in heavy mesons and determination of /V(ub)/ from inclusive semileptonic B decays*, *Phys. Lett. B* **515** (2001) 74 [hep-ph/0106040].

[124] M. Prim, *b2-hive/effort v0.1.0*, July, 2020. 10.5281/zenodo.3965699.

[125] B. O. Lange, M. Neubert and G. Paz, *Theory of charmless inclusive B decays and the extraction of V(ub)*, *Phys. Rev. D* **72** (2005) 073006 [hep-ph/0504071].

[126] F. De Fazio and M. Neubert, *$B \to X_u$ lepton anti-neutrino lepton decay distributions to order α_s*, *JHEP* **06** (1999) 017 [hep-ph/9905351].

[127] A. L. Kagan and M. Neubert, *QCD anatomy of $B \to X_s\gamma$ decays*, *Eur. Phys. J. C* **7** (1999) 5 [hep-ph/9805303].

[128] O. Buchmuller and H. Flacher, *Fit to moment from $B \to X_c\ell\bar{\nu}$and $B \to X_s\gamma$ decays using heavy quark expansions in the kinetic scheme*, *Phys. Rev. D* **73** (2006) 073008 [hep-ph/0507253].

[129] Belle collaboration, *Measurements of Partial Branching Fractions of Inclusive $B \to X_u \ell^+ \nu_\ell$ Decays with Hadronic Tagging*, 2102.00020.

[130] Belle collaboration, *Search for $B^+ \to \mu^+ \nu_\mu$ and $B^+ \to \mu^+ N$ with inclusive tagging*, *Phys. Rev. D* **101** (2020) 032007 [1911.03186].

[131] C. Ramirez, J. F. Donoghue and G. Burdman, *Semileptonic $b \to u$ decay*, *Phys. Rev. D* **41** (1990) 1496.

[132] M. Bordone, G. Isidori and D. van Dyk, *Impact of leptonic τ decays on the distribution of $B \to P\mu\bar{\nu}$ decays*, *Eur. Phys. J. C* **76** (2016) 360 [1602.06143].

[133] R. Alonso, A. Kobach and J. Martin Camalich, *New physics in the kinematic distributions of $\bar{B} \to D^{(*)}\tau^-(\to \ell^-\bar{\nu}_\ell\nu_\tau)\bar{\nu}_\tau$*, *Phys. Rev.* **D94** (2016) 094021 [1602.07671].

[134] T. Mannel, A. V. Rusov and F. Shahriaran, *Inclusive semitauonic B decays to order $\mathcal{O}(\Lambda^3_{QCD}/m^3_b)$*, *Nucl. Phys. B* **921** (2017) 211 [1702.01089].

[135] T. Mannel, M. Rahimi and K. K. Vos, *Work in Progress*, .

[136] P. Gambino, P. Giordano, G. Ossola and N. Uraltsev, *Inclusive semileptonic B decays and the determination of $|V_{ub}|$*, *JHEP* **10** (2007) 058 [0707.2493].

[137] P. Gambino and N. Uraltsev, *Moments of semileptonic B decay distributions in the $1/m_b$ expansion*, *Eur. Phys. J. C* **34** (2004) 181 [hep-ph/0401063].

[138] Belle collaboration, *Measurements of q^2 Moments of Inclusive $B \to X_c\ell^+\nu_\ell$ Decays with Hadronic Tagging*, *Phys. Rev. D* **104** (2021) 112011 [2109.01685].

[139] C. Bobeth, M. Bordone, N. Gubernari, M. Jung and D. van Dyk, *Lepton-flavour non-universality of $\bar{B} \to D^*\ell\bar{\nu}$ angular distributions in and beyond the Standard Model*, *Eur. Phys. J. C* **81** (2021) 984 [2104.02094].

[140] F. Herren, *The forward-backward asymmetry and differences of partial moments in inclusive semileptonic B decays*, 2205.03427.

[141] M. Beneke, P. Böer, J.-N. Toelstede and K. K. Vos, *QED factorization of non-leptonic B decays*, *JHEP* **11** (2020) 081 [2008.10615].

[142] M. Beneke, P. Böer, G. Finauri and K. K. Vos, *QED factorization of two-body non-leptonic and semi-leptonic B to charm decays*, *JHEP* **10** (2021) 223 [2107.03819].

[143] M. Papucci, T. Trickle and M. B. Wise, *Radiative semileptonic $\overline{B}$ decays*, *JHEP* **02** (2022) 043 [2110.13154].

[144] S. Calí, S. Klaver, M. Rotondo and B. Sciascia, *Impacts of radiative corrections on measurements of lepton flavour universality in $B \to D\ell\nu_\ell$ decays*, *Eur. Phys. J. C* **79** (2019) 744 [1905.02702].

[145] Particle Data Group collaboration*Prog. Theor. Exp. Phys.* **2020 083C01** (2020) .

[146] J. Hasenbusch, *Analysis of inclusive semileptonic B meson decays with τ lepton final states at the Belle experiment*, Ph.D. thesis, U. Bonn (main), 2018.

[147] F. U. Bernlochner, Z. Ligeti, M. Papucci, M. T. Prim, D. J. Robinson and C. Xiong, *Constrained second-order power corrections in HQET: $R(D^{(*)})$, $|V_{cb}|$, and new physics*, 2206.11281.

[148] Z. Ligeti and F. J. Tackmann, *Precise predictions for $B \to X_c\tau\bar{\nu}$ decay distributions*, *Phys. Rev. D* **90** (2014) 034021 [1406.7013].

[149] A. Sirlin, *Radiative corrections to g(v)/g(mu) in simple extensions of the su(2) x u(1) gauge model*, *Nucl. Phys. B* **71** (1974) 29.

[150] M. Gremm and A. Kapustin, *Order 1/m(b)**3 corrections to $B \to X(c)$ lepton anti-neutrino decay and their implication for the measurement of Lambda-bar and lambda(1)*, *Phys. Rev. D* **55** (1997) 6924 [hep-ph/9603448].

[151] A. F. Falk, Z. Ligeti, M. Neubert and Y. Nir, *Heavy quark expansion for the inclusive decay anti-B —> tau anti-neutrino X*, *Phys. Lett. B* **326** (1994) 145 [hep-ph/9401226].

[152] S. Balk, J. G. Korner, D. Pirjol and K. Schilcher, *Inclusive semileptonic B decays in QCD including lepton mass effects*, *Z. Phys. C* **64** (1994) 37 [hep-ph/9312220].

[153] D. King, A. Lenz, M. L. Piscopo, T. Rauh, A. V. Rusov and C. Vlahos, *Revisiting Inclusive Decay Widths of Charmed Mesons*, 2109.13219.

[154] P. Colangelo, F. De Fazio and F. Loparco, *Inclusive semileptonic Λ_b decays in the Standard Model and beyond*, *JHEP* **11** (2020) 032 [2006.13759].

[155] D. Moreno, *NLO QCD corrections to inclusive semitauonic weak decays of heavy hadrons up to $1/m_b^3$*, 2207.14245.

[156] A. Czarnecki, M. Jezabek and J. H. Kuhn, *Radiative corrections to $b \to c$ tau anti-tau-neutrino*, *Phys. Lett. B* **346** (1995) 335 [hep-ph/9411282].

[157] M. Jezabek and L. Motyka, *Tau lepton distributions in semileptonic B decays*, *Nucl. Phys. B* **501** (1997) 207 [hep-ph/9701358].

[158] M. Fael, K. Schönwald and M. Steinhauser, *A first glance to the kinematic moments of $B \to X_c \ell \nu$ at third order*, 2205.03410.

[159] M. Fael, K. Schönwald and M. Steinhauser, *Kinetic Heavy Quark Mass to Three Loops*, *Phys. Rev. Lett.* **125** (2020) 052003 [2005.06487].

[160] M. Freytsis, Z. Ligeti and J. T. Ruderman, *Flavor models for $\bar{B} \to D^{(*)} \tau \bar{\nu}$*, *Phys. Rev. D* **92** (2015) 054018 [1506.08896].

[161] A. Alberti, P. Gambino and S. Nandi, *Perturbative corrections to power suppressed effects in semileptonic B decays*, *JHEP* **01** (2014) 147 [1311.7381].

[162] M. Fael, T. Mannel and K. K. Vos, *The Heavy Quark Expansion for Inclusive Semileptonic Charm Decays Revisited*, *JHEP* **12** (2019) 067 [1910.05234].

[163] P. Gambino and J. F. Kamenik, *Lepton energy moments in semileptonic charm decays*, *Nucl. Phys. B* **840** (2010) 424 [1004.0114].

[164] CLEO collaboration, *Measurement of absolute branching fractions of inclusive semileptonic decays of charm and charmed-strange mesons*, *Phys. Rev. D* **81** (2010) 052007 [0912.4232].

[165] M. Fael and K. K. Vos, *Work in Progress*, .

[166] D. Leljak, B. Melić and D. van Dyk, *The $\overline{B} \to \pi$ form factors from QCD and their impact on $|V_{ub}|$*, *JHEP* **07** (2021) 036 [2102.07233].

[167] Belle collaboration, *Measurements of Partial Branching Fractions of Inclusive $B \to X_u \, \ell^+ \, \nu_\ell$ Decays with Hadronic Tagging*, *Phys. Rev. D* **104** (2021) 012008 [2102.00020].

[168] F. U. Bernlochner, M. F. Sevilla, D. J. Robinson and G. Wormser, *Semitauonic b-hadron decays: A lepton flavor universality laboratory*, *Rev. Mod. Phys.* **94** (2022) 015003 [2101.08326].

[169] F. U. Bernlochner, Z. Ligeti, M. Papucci and D. J. Robinson, *Combined analysis of semileptonic B decays to D and D^*: $R(D^{(*)})$, $|V_{cb}|$, and new physics*, *Phys. Rev. D* **95** (2017) 115008 [1703.05330].

[170] T. Mannel, M. Rahimi and K. K. Vos, *Work in Progress*, .

[171] B. Grinstein and A. Kobach, *Model-Independent Extraction of $|V_{cb}|$ from $\bar{B} \to D^* \ell \overline{\nu}$*, *Phys. Lett. B* **771** (2017) 359 [1703.08170].

[172] F. U. Bernlochner, Z. Ligeti and D. J. Robinson, *$N = 5$, 6, 7, 8: Nested hypothesis tests and truncation dependence of $|V_{cb}|$*, *Phys. Rev. D* **100** (2019) 013005 [1902.09553].

[173] P. Gambino et al., *Challenges in semileptonic B decays*, *Eur. Phys. J. C* **80** (2020) 966 [2006.07287].

[174] Fermilab Lattice, MILC collaboration, *Semileptonic form factors for $B \to D^* \ell \nu$ at nonzero recoil from 2 + 1-flavor lattice QCD*, 2105.14019.

[175] G. Martinelli, S. Simula and L. Vittorio, *Exclusive determinations of $|V_{cb}|$ and $R(D^*)$ through unitarity*, 2109.15248.

[176] P. Colangelo and F. De Fazio, *Tension in the inclusive versus exclusive determinations of $|V_{cb}|$: a possible role of new physics*, *Phys. Rev. D* **95** (2017) 011701 [1611.07387].

[177] M. Jung and D. M. Straub, *Constraining new physics in $b \to c\ell\nu$ transitions*, *JHEP* **01** (2019) 009 [1801.01112].

[178] A. Crivellin and S. Pokorski, *Can the differences in the determinations of V_{ub} and V_{cb} be explained by New Physics?*, *Phys. Rev. Lett.* **114** (2015) 011802 [1407.1320].

[179] B. Dassinger, R. Feger and T. Mannel, *Complete Michel Parameter Analysis of inclusive semileptonic $b \to c$ transition*, *Phys. Rev. D* **79** (2009) 075015 [0803.3561].

[180] EOS Authors collaboration, *EOS: a software for flavor physics phenomenology*, *Eur. Phys. J. C* **82** (2022) 569 [2111.15428].

[181] R. Mandal, C. Murgui, A. Peñuelas and A. Pich, *The role of right-handed neutrinos in $b \to c\tau\bar{\nu}$ anomalies*, *JHEP* **08** (2020) 022 [2004.06726].

[182] B. Grzadkowski, M. Iskrzynski, M. Misiak and J. Rosiek, *Dimension-Six Terms in the Standard Model Lagrangian*, *JHEP* **10** (2010) 085 [1008.4884].

[183] J. Aebischer, A. Crivellin, M. Fael and C. Greub, *Matching of gauge invariant dimension-six operators for $b \to s$ and $b \to c$ transitions*, *JHEP* **05** (2016) 037 [1512.02830].

[184] A. Celis, M. Jung, X.-Q. Li and A. Pich, *Scalar contributions to $b \to c(u)\tau\nu$ transitions*, *Phys. Lett. B* **771** (2017) 168 [1612.07757].

[185] A. Czarnecki, K. Melnikov and N. Uraltsev, *NonAbelian dipole radiation and the heavy quark expansion*, *Phys. Rev. Lett.* **80** (1998) 3189 [hep-ph/9708372].

[186] M. Trott, *Improving extractions of $|V_{cb}|$ and m_b from the hadronic invariant mass moments of semileptonic inclusive B decay*, *Phys. Rev. D* **70** (2004) 073003 [hep-ph/0402120].

[187] V. Aquila, P. Gambino, G. Ridolfi and N. Uraltsev, *Perturbative corrections to semileptonic b decay distributions*, *Nucl. Phys. B* **719** (2005) 77 [hep-ph/0503083].

[188] A. Alberti, P. Gambino, K. J. Healey and S. Nandi, *The Inclusive Determination of $|V_{cb}|$*, *Nucl. Part. Phys. Proc.* **273-275** (2016) 1325.

[189] V. Shtabovenko, R. Mertig and F. Orellana, *FeynCalc 9.3: New features and improvements*, *Comput. Phys. Commun.* **256** (2020) 107478 [2001.04407].

[190] J. Aebischer, M. Fael, C. Greub and J. Virto, *B physics Beyond the Standard Model at One Loop: Complete Renormalization Group Evolution below the Electroweak Scale*, *JHEP* **09** (2017) 158 [1704.06639].

[191] C. Anastasiou and K. Melnikov, *Higgs boson production at hadron colliders in NNLO QCD*, *Nucl. Phys. B* **646** (2002) 220 [hep-ph/0207004].

[192] S. A. Larin, *The Renormalization of the axial anomaly in dimensional regularization*, *Phys. Lett. B* **303** (1993) 113 [hep-ph/9302240].

[193] I. I. Y. Bigi, M. A. Shifman, N. Uraltsev and A. I. Vainshtein, *High power n of m_b in beauty widths and $n = 5 \to \infty$ limit*, *Phys. Rev. D* **56** (1997) 4017 [hep-ph/9704245].

[194] M. Fael, K. Schönwald and M. Steinhauser, *Relation between the $\overline{\text{MS}}$ and the kinetic mass of heavy quarks*, *Phys. Rev. D* **103** (2021) 014005 [2011.11655].

[195] F. Herren and M. Steinhauser, *Version 3 of RunDec and CRunDec*, *Comput. Phys. Commun.* **224** (2018) 333 [1703.03751].

[196] M. González-Alonso, J. Martin Camalich and K. Mimouni, *Renormalization-group evolution of new physics contributions to (semi)leptonic meson decays*, *Phys. Lett. B* **772** (2017) 777 [1706.00410].

[197] Q.-Y. Hu, X.-Q. Li and Y.-D. Yang, *$b \to c\tau\nu$ transitions in the standard model effective field theory*, *Eur. Phys. J. C* **79** (2019) 264 [1810.04939].

[198] Belle collaboration, *Moments of the electron energy spectrum and partial branching fraction of B —> X(c) e nu decays at Belle*, *Phys. Rev. D* **75** (2007) 032001 [hep-ex/0610012].

[199] BaBar collaboration, *Measurement of the electron energy spectrum and its moments in inclusive $B \to Xe\nu$ decays*, *Phys. Rev. D* **69** (2004) 111104 [hep-ex/0403030].

[200] CLEO collaboration, *Moments of the B meson inclusive semileptonic decay rate using neutrino reconstruction*, *Phys. Rev. D* **70** (2004) 032002 [hep-ex/0403052].

[201] Belle collaboration, *Moments of the Hadronic Invariant Mass Spectrum in $B \to X_c \ell \nu$ Decays at BELLE*, *Phys. Rev. D* **75** (2007) 032005 [hep-ex/0611044].

[202] BaBar collaboration, *Measurement and interpretation of moments in inclusive semileptonic decays $\overline{B} \to X_c l \bar{\nu} u$*, *Phys. Rev. D* **81** (2010) 032003 [0908.0415].

[203] Belle-II collaboration, *Measurement of Hadronic Mass Moments $\langle M_X^n \rangle$ in $B \to X_c \ell \nu$ Decays at Belle II*, 2009.04493.

[204] Belle-II collaboration, *Measurement of Lepton Mass Squared Moments in $B \to X_c \ell \bar{\nu}_\ell$ Decays with the Belle II Experiment*, 2205.06372.

[205] P. D. Group, P. A. Zyla, R. M. Barnett, J. Beringer, O. Dahl, D. A. Dwyer et al., *Review of Particle Physics*, *Progress of Theoretical and Experimental Physics* **2020** (2020) .

[206] P. Gambino, A. Melis and S. Simula, *Extraction of heavy-quark-expansion parameters from unquenched lattice data on pseudoscalar and vector heavy-light meson masses*, *Phys. Rev. D* **96** (2017) 014511 [1704.06105].

[207] P. Gambino and S. Hashimoto, *Inclusive Semileptonic Decays from Lattice QCD*, *Phys. Rev. Lett.* **125** (2020) 032001 [2005.13730].

[208] P. Gambino, S. Hashimoto, S. Mächler, M. Panero, F. Sanfilippo, S. Simula et al., *Lattice QCD study of inclusive semileptonic decays of heavy mesons*, *JHEP* **07** (2022) 083 [2203.11762].

[209] LHCb collaboration, *Test of lepton universality in beauty-quark decays*, 2103.11769.

[210] LHCb collaboration, *Angular Analysis of the $B^+ \to K^{*+} \mu^+ \mu^-$ Decay*, *Phys. Rev. Lett.* **126** (2021) 161802 [2012.13241].

[211] LHCb collaboration, *Measurement of CP-Averaged Observables in the $B^0 \to K^{*0} \mu^+ \mu^-$ Decay*, *Phys. Rev. Lett.* **125** (2020) 011802 [2003.04831].

[212] LHCb collaboration, *Test of lepton universality using $B^+ \to K^+ \ell^+ \ell^-$ decays*, *Phys. Rev. Lett.* **113** (2014) 151601 [1406.6482].

[213] LHCb collaboration, *Test of lepton universality with $B^0 \to K^{*0} \ell^+ \ell^-$ decays*, *JHEP* **08** (2017) 055 [1705.05802].

[214] LHCb collaboration, *Search for lepton-universality violation in $B^+ \to K^+ \ell^+ \ell^-$ decays*, *Phys. Rev. Lett.* **122** (2019) 191801 [1903.09252].

[215] LHCb collaboration, *Angular analysis of the $B^0 \to K^{*0}\mu^+\mu^-$ decay using 3 fb^{-1} of integrated luminosity*, *JHEP* **02** (2016) 104 [1512.04442].

[216] BaBar collaboration, *Evidence for an excess of $\bar{B} \to D^{(*)}\tau^-\bar{\nu}_\tau$ decays*, *Phys. Rev. Lett.* **109** (2012) 101802 [1205.5442].

[217] BaBar collaboration, *Measurement of an Excess of $\bar{B} \to D^{(*)}\tau^-\bar{\nu}_\tau$ Decays and Implications for Charged Higgs Bosons*, *Phys. Rev. D* **88** (2013) 072012 [1303.0571].

[218] LHCb collaboration, *Measurement of the ratio of branching fractions $\mathcal{B}(\bar{B}^0 \to D^{*+}\tau^-\bar{\nu}_\tau)/\mathcal{B}(\bar{B}^0 \to D^{*+}\mu^-\bar{\nu}_\mu)$*, *Phys. Rev. Lett.* **115** (2015) 111803 [1506.08614].

[219] Belle collaboration, *Measurement of the τ lepton polarization and $R(D^*)$ in the decay $\bar{B} \to D^*\tau^-\bar{\nu}_\tau$*, *Phys. Rev. Lett.* **118** (2017) 211801 [1612.00529].

[220] Belle collaboration, *Measurement of the τ lepton polarization and $R(D^*)$ in the decay $\bar{B} \to D^*\tau^-\bar{\nu}_\tau$ with one-prong hadronic τ decays at Belle*, *Phys. Rev. D* **97** (2018) 012004 [1709.00129].

[221] LHCb collaboration, *Measurement of the ratio of the $B^0 \to D^{*-}\tau^+\nu_\tau$ and $B^0 \to D^{*-}\mu^+\nu_\mu$ branching fractions using three-prong τ-lepton decays*, *Phys. Rev. Lett.* **120** (2018) 171802 [1708.08856].

[222] LHCb collaboration, *Test of Lepton Flavor Universality by the measurement of the $B^0 \to D^{*-}\tau^+\nu_\tau$ branching fraction using three-prong τ decays*, *Phys. Rev. D* **97** (2018) 072013 [1711.02505].

[223] Belle collaboration, *Measurement of $\mathcal{R}(D)$ and $\mathcal{R}(D^*)$ with a semileptonic tagging method*, 1904.08794.

[224] R. Alonso, B. Grinstein and J. Martin Camalich, *Lepton universality violation and lepton flavor conservation in B-meson decays*, *JHEP* **10** (2015) 184 [1505.05164].

[225] L. Calibbi, A. Crivellin and T. Ota, *Effective Field Theory Approach to $b \to s\ell\ell^{(\prime)}$, $B \to K^{(*)}\nu\overline{\nu}$ and $B \to D^{(*)}\tau\nu$ with Third Generation Couplings*, *Phys. Rev. Lett.* **115** (2015) 181801 [1506.02661].

[226] L. Di Luzio, A. Greljo and M. Nardecchia, *Gauge leptoquark as the origin of B-physics anomalies*, *Phys. Rev. D* **96** (2017) 115011 [1708.08450].

[227] L. Calibbi, A. Crivellin and T. Li, *Model of vector leptoquarks in view of the B-physics anomalies*, *Phys. Rev. D* **98** (2018) 115002 [1709.00692].

[228] R. Barbieri and A. Tesi, *B-decay anomalies in Pati-Salam SU(4)*, *Eur. Phys. J. C* **78** (2018) 193 [1712.06844].

[229] M. Blanke and A. Crivellin, *B Meson Anomalies in a Pati-Salam Model within the Randall-Sundrum Background*, *Phys. Rev. Lett.* **121** (2018) 011801 [1801.07256].

[230] L. Di Luzio, J. Fuentes-Martin, A. Greljo, M. Nardecchia and S. Renner, *Maximal Flavour Violation: a Cabibbo mechanism for leptoquarks*, *JHEP* **11** (2018) 081 [1808.00942].

[231] T. Faber, M. Hudec, M. Malinský, P. Meinzinger, W. Porod and F. Staub, *A unified leptoquark model confronted with lepton non-universality in B-meson decays*, *Phys. Lett. B* **787** (2018) 159 [1808.05511].

[232] J. Heeck and D. Teresi, *Pati-Salam explanations of the B-meson anomalies*, *JHEP* **12** (2018) 103 [1808.07492].

[233] A. Angelescu, D. Bečirević, D. A. Faroughy and O. Sumensari, *Closing the window on single leptoquark solutions to the B-physics anomalies*, *JHEP* **10** (2018) 183 [1808.08179].

[234] M. Schmaltz and Y.-M. Zhong, *The leptoquark Hunter's guide: large coupling*, *JHEP* **01** (2019) 132 [1810.10017].

[235] A. Greljo, J. Martin Camalich and J. D. Ruiz-Álvarez, *Mono-τ Signatures at the LHC Constrain Explanations of B-decay Anomalies*, *Phys. Rev. Lett.* **122** (2019) 131803 [1811.07920].

[236] B. Fornal, S. A. Gadam and B. Grinstein, *Left-Right SU(4) Vector Leptoquark Model for Flavor Anomalies*, *Phys. Rev. D* **99** (2019) 055025 [1812.01603].

[237] M. J. Baker, J. Fuentes-Martín, G. Isidori and M. König, *High- p_T signatures in vector–leptoquark models*, *Eur. Phys. J. C* **79** (2019) 334 [1901.10480].

[238] C. Cornella, J. Fuentes-Martin and G. Isidori, *Revisiting the vector leptoquark explanation of the B-physics anomalies*, *JHEP* **07** (2019) 168 [1903.11517].

[239] L. Da Rold and F. Lamagna, *A vector leptoquark for the B-physics anomalies from a composite GUT*, *JHEP* **12** (2019) 112 [1906.11666].

[240] M. Bordone, C. Cornella, J. Fuentes-Martin and G. Isidori, *A three-site gauge model for flavor hierarchies and flavor anomalies*, *Phys. Lett. B* **779** (2018) 317 [1712.01368].

[241] M. Bordone, C. Cornella, J. Fuentes-Martín and G. Isidori, *Low-energy signatures of the* PS^3 *model: from B-physics anomalies to LFV*, *JHEP* **10** (2018) 148 [1805.09328].

[242] M. Bordone, O. Catà and T. Feldmann, *Effective Theory Approach to New Physics with Flavour: General Framework and a Leptoquark Example*, *JHEP* **01** (2020) 067 [1910.02641].

[243] D. Marzocca, *Addressing the B-physics anomalies in a fundamental Composite Higgs Model*, *JHEP* **07** (2018) 121 [1803.10972].

[244] D. Bečirević, I. Doršner, S. Fajfer, N. Košnik, D. A. Faroughy and O. Sumensari, *Scalar leptoquarks from grand unified theories to accommodate the B-physics anomalies*, *Phys. Rev. D* **98** (2018) 055003 [1806.05689].

[245] I. Bigaran, J. Gargalionis and R. R. Volkas, *A near-minimal leptoquark model for reconciling flavour anomalies and generating radiative neutrino masses*, *JHEP* **10** (2019) 106 [1906.01870].

[246] A. Crivellin, D. Müller and F. Saturnino, *Flavor Phenomenology of the Leptoquark Singlet-Triplet Model*, *JHEP* **06** (2020) 020 [1912.04224].

[247] S. Saad, *Combined explanations of $(g-2)_\mu$, $R_{D^{(*)}}$, $R_{K^{(*)}}$ anomalies in a two-loop radiative neutrino mass model*, *Phys. Rev. D* **102** (2020) 015019 [2005.04352].

[248] V. Gherardi, D. Marzocca and E. Venturini, *Low-energy phenomenology of scalar leptoquarks at one-loop accuracy*, *JHEP* **01** (2021) 138 [2008.09548].

[249] K. S. Babu, P. S. B. Dev, S. Jana and A. Thapa, *Unified framework for B-anomalies, muon $g-2$ and neutrino masses*, *JHEP* **03** (2021) 179 [2009.01771].

[250] A. Crivellin, D. Müller and T. Ota, *Simultaneous explanation of $R(D^{(*)})$ and $b \to s\mu^+\mu^-$: the last scalar leptoquarks standing*, *JHEP* **09** (2017) 040 [1703.09226].

[251] D. Buttazzo, A. Greljo, G. Isidori and D. Marzocca, *B-physics anomalies: a guide to combined explanations*, *JHEP* **11** (2017) 044 [1706.07808].

[252] M. Bordone, O. Catà, T. Feldmann and R. Mandal, *Constraining flavour patterns of scalar leptoquarks in the effective field theory*, *JHEP* **03** (2021) 122 [2010.03297].

[253] C. Cornella, D. A. Faroughy, J. Fuentes-Martín, G. Isidori and M. Neubert, *Reading the footprints of the B-meson flavor anomalies*, 2103.16558.

[254] D. Marzocca and S. Trifinopoulos, *A Minimal Explanation of Flavour Anomalies: B-Meson Decays, Muon Magnetic Moment, and the Cabbibo Angle*, 2104.05730.

[255] A. Greljo, P. Stangl and A. E. Thomsen, *A Model of Muon Anomalies*, 2103.13991.

[256] J. Davighi, *Anomalous Z' bosons for anomalous B decays*, 2105.06918.

[257] J. S. Alvarado, S. F. Mantilla, R. Martinez and F. Ochoa, *A non-universal $U(1)_X$ extension to the Standard Model to study the B meson anomaly and muon $g-2$*, 2105.04715.

[258] P. Fileviez Pérez, C. Murgui and A. D. Plascencia, *Leptoquarks and Matter Unification: Flavor Anomalies and the Muon $g-2$*, 2104.11229.

[259] J.-Y. Cen, Y. Cheng, X.-G. He and J. Sun, *Flavor Specific $U(1)_{B_q-L_\mu}$ Gauge Model for Muon $g-2$ and $b \to s\bar{\mu}\mu$ Anomalies*, 2104.05006.

[260] J. Chen, Q. Wen, F. Xu and M. Zhang, *Flavor Anomalies Accommodated in A Flavor Gauged Two Higgs Doublet Model*, 2104.03699.

[261] T. Nomura and H. Okada, *Explanations for anomalies of muon anomalous magnetic dipole moment, $b \to s\mu\bar{\mu}$ and radiative neutrino masses in a leptoquark model*, 2104.03248.

[262] H. M. Lee, *Leptoquark Option for B-meson Anomalies and Leptonic Signatures*, 2104.02982.

[263] G. Arcadi, L. Calibbi, M. Fedele and F. Mescia, *Muon $g-2$ and B-anomalies from Dark Matter*, 2104.03228.

[264] R. Barbieri, *A view of flavour physics in 2021*, 2103.15635.

[265] G. Hiller, D. Loose and I. Nišandžić, *Flavorful leptoquarks at the LHC and beyond: Spin 1*, 2103.12724.

[266] A. Angelescu, D. Bečirević, D. A. Faroughy, F. Jaffredo and O. Sumensari, *On the single leptoquark solutions to the B-physics anomalies*, 2103.12504.

[267] J. Alda, J. Guasch and S. Peñaranda, *Anomalies in B mesons decays: A phenomenological approach*, 2012.14799.

[268] G. Arcadi, L. Calibbi, M. Fedele and F. Mescia, *Systematic approach to B-physics anomalies and t-channel dark matter*, 2103.09835.

[269] T. Blake, S. Meinel and D. van Dyk, *Bayesian Analysis of $b \to s\mu^+\mu^-$ Wilson Coefficients using the Full Angular Distribution of $\Lambda_b \to \Lambda(\to p\,\pi^-)\mu^+\mu^-$ Decays*, *Phys. Rev. D* **101** (2020) 035023 [1912.05811].

[270] M. Algueró, B. Capdevila, S. Descotes-Genon, J. Matias and M. Novoa-Brunet, ***b → sℓℓ*** *global fits after Moriond 2021 results*, in *55th Rencontres de Moriond on Electroweak Interactions and Unified Theories*, 4, 2021, 2104.08921.

[271] W. Altmannshofer and P. Stangl, *New Physics in Rare B Decays after Moriond 2021*, 2103.13370.

[272] T. Hurth, F. Mahmoudi, D. M. Santos and S. Neshatpour, *More Indications for Lepton Nonuniversality in $b \to s\ell^+\ell^-$*, 2104.10058.

[273] M. Ciuchini, A. M. Coutinho, M. Fedele, E. Franco, A. Paul, L. Silvestrini et al., *New Physics in $b \to s\ell^+\ell^-$ confronts new data on Lepton Universality*, *Eur. Phys. J. C* **79** (2019) 719 [1903.09632].

[274] LHCb collaboration, *Physics case for an LHCb Upgrade II - Opportunities in flavour physics, and beyond, in the HL-LHC era*, 1808.08865.

[275] S. Sahoo and R. Mohanta, *Effects of scalar leptoquark on semileptonic Λ_b decays*, *New J. Phys.* **18** (2016) 093051 [1607.04449].

[276] D. Das, *Lepton flavor violating $\Lambda_b \to \Lambda\ell_1\ell_2$ decay*, *Eur. Phys. J. C* **79** (2019) 1005 [1909.08676].

[277] T. Feldmann and M. W. Y. Yip, *Form factors for $\Lambda_b \to \Lambda$ transitions in the soft-collinear effective theory*, *Phys. Rev. D* **85** (2012) 014035 [1111.1844].

[278] W. Detmold and S. Meinel, *$\Lambda_b \to \Lambda\ell^+\ell^-$ form factors, differential branching fraction, and angular observables from lattice QCD with relativistic b quarks*, *Phys. Rev. D* **93** (2016) 074501 [1602.01399].

[279] A. Datta, S. Kamali, S. Meinel and A. Rashed, *Phenomenology of $\Lambda_b \to \Lambda_c\tau\overline{\nu}_\tau$ using lattice QCD calculations*, *JHEP* **08** (2017) 131 [1702.02243].

[280] P. Böer, T. Feldmann and D. van Dyk, *Angular Analysis of the Decay $\Lambda_b \to \Lambda(\to N\pi)\ell^+\ell^-$*, *JHEP* **01** (2015) 155 [1410.2115].

[281] Particle Data Group collaboration, *Review of Particle Physics*, *PTEP* **2020** (2020) 083C01.

[282] K. G. Chetyrkin, J. H. Kuhn and M. Steinhauser, *RunDec: A Mathematica package for running and decoupling of the strong coupling and quark masses*, *Comput. Phys. Commun.* **133** (2000) 43 [hep-ph/0004189].

[283] T. Blake and M. Kreps, *Angular distribution of polarised Λ_b baryons decaying to $\Lambda\ell^+\ell^-$*, *JHEP* **11** (2017) 138 [1710.00746].

[284] S. Descotes-Genon and M. Novoa-Brunet, *Angular analysis of the rare decay $\Lambda_b \to \Lambda(1520)(\to NK)\ell^+\ell^-$*, *JHEP* **06** (2019) 136 [1903.00448].

[285] M. Bordone, *Heavy Quark Expansion of $\Lambda_b \to \Lambda^*$ (1520) Form Factors beyond Leading Order*, *Symmetry* **13** (2021) 531 [2101.12028].

[286] D. Das and J. Das, *The $\Lambda_b \to \Lambda^*(1520)(\to N\bar{K})\ell^+\ell^-$ decay at low-recoil in HQET*, *JHEP* **07** (2020) 002 [2003.08366].

[287] HFLAV collaboration, *Averages of b-hadron, c-hadron, and τ-lepton properties as of 2018*, *Eur. Phys. J.* **C81** (2021) 226 [1909.12524].

[288] UTfit collaboration. http://www.utfit.org/UTfit/WebHome.

[289] C. Bobeth, G. Hiller and G. Piranishvili, *Angular distributions of $\bar{B} \to \bar{K}\ell^+\ell^-$ decays*, *JHEP* **12** (2007) 040 [0709.4174].

[290] G. Hiller and M. Schmaltz, *R_K and future $b \to s\ell\ell$ physics beyond the standard model opportunities*, *Phys. Rev. D* **90** (2014) 054014 [1408.1627].

[291] LHCb collaboration, *Search for the lepton-flavour-violating decays $B_s^0 \to \tau^\pm\mu^\mp$ and $B^0 \to \tau^\pm\mu^\mp$*, *Phys. Rev. Lett.* **123** (2019) 211801 [1905.06614].

[292] LHCb collaboration, *Search for the lepton-flavour violating decays $B_{(s)}^0 \to e^\pm\mu^\mp$*, *JHEP* **03** (2018) 078 [1710.04111].

[293] BaBar collaboration, *A search for the decay modes $B^{+-} \to h^{+-}\tau^{+-}l$*, *Phys. Rev. D* **86** (2012) 012004 [1204.2852].

[294] LHCb collaboration, *Search for the lepton flavour violating decay $B^+ \to K^+\mu^-\tau^+$ using B_{s2}^{*0} decays*, *JHEP* **06** (2020) 129 [2003.04352].

[295] LHCb collaboration, *Search for Lepton-Flavor Violating Decays $B^+ \to K^+\mu^\pm e^\mp$*, *Phys. Rev. Lett.* **123** (2019) 241802 [1909.01010].

[296] N. Gubernari, A. Kokulu and D. van Dyk, *$B \to P$ and $B \to V$ Form Factors from B-Meson Light-Cone Sum Rules beyond Leading Twist*, *JHEP* **01** (2019) 150 [1811.00983].

[297] D. Bečirević, N. Košnik, O. Sumensari and R. Zukanovich Funchal, *Palatable Leptoquark Scenarios for Lepton Flavor Violation in Exclusive $b \to s\ell_1\ell_2$ modes*, *JHEP* **11** (2016) 035 [1608.07583].

[298] J. Gratrex, M. Hopfer and R. Zwicky, *Generalised helicity formalism, higher moments and the $B \to K_{J_K}(\to K\pi)\bar{\ell}_1\ell_2$ angular distributions*, *Phys. Rev. D* **93** (2016) 054008 [1506.03970].

[299] R. Balasubramamian and B. Blossier, *Decay constant of B_s and B_s^* mesons from $\mathrm{N_f} = 2$ lattice QCD*, *Eur. Phys. J. C* **80** (2020) 412 [1912.09937].

[300] D. Lancierini, G. Isidori, P. Owen and N. Serra, *On the significance of new physics in $b \to s\ell^+\ell^-$ decays*, 2104.05631.

[301] C. D. Froggatt and H. B. Nielsen, *Hierarchy of Quark Masses, Cabibbo Angles and CP Violation*, *Nucl. Phys. B* **147** (1979) 277.

[302] R. Barbieri, G. Isidori, J. Jones-Perez, P. Lodone and D. M. Straub, *$U(2)$ and Minimal Flavour Violation in Supersymmetry*, *Eur. Phys. J. C* **71** (2011) 1725 [1105.2296].

[303] LHCb collaboration, *Measurement of b hadron fractions in 13 TeV pp collisions*, *Phys. Rev. D* **100** (2019) 031102 [1902.06794].

[304] LHCb collaboration, *Angular moments of the decay $\Lambda_b^0 \to \Lambda\mu^+\mu^-$ at low hadronic recoil*, *JHEP* **09** (2018) 146 [1808.00264].

[305] LHCb collaboration, *Test of lepton universality with $B^0 \to K^{*0}\ell^+\ell^-$ decays*, *JHEP* **08** (2017) 055 [1705.05802].

[306] LHCb collaboration, *Measurement of CP-averaged observables in the $B^0 \to K^{*0}\mu^+\mu^-$ decay*, *Phys. Rev. Lett.* **125** (2020) 011802 [2003.04831].

[307] LHCb collaboration, *Analysis of Neutral B-Meson Decays into Two Muons*, *Phys. Rev. Lett.* **128** (2022) 041801 [2108.09284].

[308] LHCb collaboration, *Branching Fraction Measurements of the Rare $B_s^0 \to \phi\mu^+\mu^-$ and $B_s^0 \to f_2'(1525)\mu^+\mu^-$ Decays*, *Phys. Rev. Lett.* **127** (2021) 151801 [2105.14007].

[309] LHCb collaboration, *Angular analysis of the rare decay $B_s^0 \to \phi\mu^+\mu^-$*, *JHEP* **11** (2021) 043 [2107.13428].

[310] LHCb collaboration, *Test of lepton universality in beauty-quark decays*, 2103.11769.

[311] ATLAS collaboration, *Study of the rare decays of B_s^0 and B^0 mesons into muon pairs using data collected during 2015 and 2016 with the ATLAS detector*, *JHEP* **04** (2019) 098 [1812.03017].

[312] ATLAS collaboration, *Angular analysis of $B_d^0 \to K^*\mu^+\mu^-$ decays in pp collisions at $\sqrt{s} = 8$ TeV with the ATLAS detector*, *JHEP* **10** (2018) 047 [1805.04000].

[313] CMS collaboration, *Measurement of properties of $B_s^0 \to \mu^+\mu^-$ decays and search for $B^0 \to \mu^+\mu^-$ with the CMS experiment*, *JHEP* **04** (2020) 188 [1910.12127].

[314] CMS collaboration, *Measurement of angular parameters from the decay $B^0 \to K^{*0}\mu^+\mu^-$ in proton-proton collisions at $\sqrt{s} = 8$ TeV*, *Phys. Lett. B* **781** (2018) 517 [1710.02846].

[315] CMS collaboration, *Angular analysis of the decay $B^+ \to K^*(892)^+\mu^+\mu^-$ in proton-proton collisions at $\sqrt{s} = 8$ TeV*, *JHEP* **04** (2021) 124 [2010.13968].

[316] Belle collaboration, *Lepton-Flavor-Dependent Angular Analysis of $B \to K^*\ell^+\ell^-$*, *Phys. Rev. Lett.* **118** (2017) 111801 [1612.05014].

[317] LHCb collaboration, *Differential branching fraction and angular analysis of $\Lambda_b^0 \to \Lambda\mu^+\mu^-$ decays*, *JHEP* **06** (2015) 115 [1503.07138].

[318] LHCb collaboration, *First Observation of the Radiative Decay $\Lambda_b^0 \to \Lambda\gamma$*, *Phys. Rev. Lett.* **123** (2019) 031801 [1904.06697].

[319] T. Hurth, F. Mahmoudi and S. Neshatpour, *Implications of the new LHCb angular analysis of $B \to K^*\mu^+\mu^-$: Hadronic effects or new physics?*, *Phys. Rev. D* **102** (2020) 055001 [2006.04213].

[320] J. Bhom, M. Chrzaszcz, F. Mahmoudi, M. T. Prim, P. Scott and M. White, *A model-independent analysis of $b \to s\mu^+\mu^-$ transitions with GAMBIT 's FlavBit*, *Eur. Phys. J. C* **81** (2021) 1076 [2006.03489].

[321] S. Meinel and D. van Dyk, *Using $\Lambda_b \to \Lambda\mu^+\mu^-$ data within a Bayesian analysis of $|\Delta B| = |\Delta S| = 1$ decays*, *Phys. Rev. D* **94** (2016) 013007 [1603.02974].

[322] C. G. Boyd and R. F. Lebed, *Improved QCD form-factor constraints and $\Lambda_b \to \Lambda_c\ell\bar{\nu}$*, *Nucl. Phys. B* **485** (1997) 275 [hep-ph/9512363].

[323] R. J. Hill and G. Paz, *Model independent extraction of the proton charge radius from electron scattering*, *Phys. Rev. D* **82** (2010) 113005 [1008.4619].

[324] B. Bhattacharya, R. J. Hill and G. Paz, *Model independent determination of the axial mass parameter in quasielastic neutrino-nucleon scattering*, *Phys. Rev. D* **84** (2011) 073006 [1108.0423].

[325] T. D. Cohen, H. Lamm and R. F. Lebed, *Precision Model-Independent Bounds from Global Analysis of $b \to c\ell\nu$ Form Factors*, *Phys. Rev. D* **100** (2019) 094503 [1909.10691].

[326] G. Hiller and R. Zwicky, *Endpoint relations for baryons*, *JHEP* **11** (2021) 073 [2107.12993].

[327] S. Okubo, *Exact bounds for K_{l3} decay parameters*, *Phys. Rev. D* **3** (1971) 2807.

[328] S. Okubo, *New improved bounds for K_{l3} parameters*, *Phys. Rev. D* **4** (1971) 725.

[329] S. Okubo and I.-F. Shih, *Exact inequality and test of chiral SW(3) theory in K_{l3} decay problem*, *Phys. Rev. D* **4** (1971) 2020.

[330] T. Becher and R. J. Hill, *Comment on form-factor shape and extraction of $|V_{ub}|$ from $B \to \pi l \nu$*, *Phys. Lett. B* **633** (2006) 61 [hep-ph/0509090].

[331] C. Bourrely, I. Caprini and L. Lellouch, *Model-independent description of $B \to \pi l \nu$ decays and a determination of $|V_{ub}|$*, *Phys. Rev. D* **79** (2009) 013008 [0807.2722].

[332] C. G. Boyd, B. Grinstein and R. F. Lebed, *Constraints on form-factors for exclusive semileptonic heavy to light meson decays*, *Phys. Rev. Lett.* **74** (1995) 4603 [hep-ph/9412324].

[333] C. G. Boyd and M. J. Savage, *Analyticity, shapes of semileptonic form-factors, and $\bar{B} \to \pi l \bar{\nu}$*, *Phys. Rev. D* **56** (1997) 303 [hep-ph/9702300].

[334] L. Lellouch, *Lattice constrained unitarity bounds for $\bar{B}^0 \to \pi^+ \ell^- \bar{\nu}$ decays*, *Nucl. Phys. B* **479** (1996) 353 [hep-ph/9509358].

[335] M. Di Carlo, G. Martinelli, M. Naviglio, F. Sanfilippo, S. Simula and L. Vittorio, *Unitarity bounds for semileptonic decays in lattice QCD*, *Phys. Rev. D* **104** (2021) 054502 [2105.02497].

[336] G. Martinelli, S. Simula and L. Vittorio, *Constraints for the semileptonic $B \to D^{(*)}$ form factors from lattice QCD simulations of two-point correlation functions*, *Phys. Rev. D* **104** (2021) 094512 [2105.07851].

[337] G. Martinelli, S. Simula and L. Vittorio, *$|V_{cb}|$ and $R(D)^{(*)}$) using lattice QCD and unitarity*, *Phys. Rev. D* **105** (2022) 034503 [2105.08674].

[338] G. Martinelli, M. Naviglio, S. Simula and L. Vittorio, *$|V_{cb}|$, Lepton Flavour Universality and $SU(3)_F$ symmetry breaking in $B_s \to D_s^{(*)} \ell \nu_\ell$ decays through unitarity and lattice QCD*, 2204.05925.

[339] I. Caprini, *Functional Analysis and Optimization Methods in Hadron Physics*, SpringerBriefs in Physics. Springer, 2019, 10.1007/978-3-030-18948-8.

[340] I. Caprini, L. Lellouch and M. Neubert, *Dispersive bounds on the shape of $\bar{B} \to D^{(*)} \ell \bar{\nu}$*, *Nucl. Phys. B* **530** (1998) 153 [hep-ph/9712417].

[341] A. Bharucha, T. Feldmann and M. Wick, *Theoretical and Phenomenological Constraints on Form Factors for Radiative and Semi-Leptonic B-Meson Decays*, *JHEP* **09** (2010) 090 [1004.3249].

[342] A. Bazavov et al., *B- and D-meson leptonic decay constants from four-flavor lattice QCD*, *Phys. Rev. D* **98** (2018) 074512 [1712.09262].

[343] C. B. Lang, D. Mohler, S. Prelovsek and R. M. Woloshyn, *Predicting positive parity B_s mesons from lattice QCD*, *Phys. Lett. B* **750** (2015) 17 [1501.01646].

[344] P. Gelhausen, A. Khodjamirian, A. A. Pivovarov and D. Rosenthal, *Decay constants of heavy-light vector mesons from QCD sum rules*, *Phys. Rev. D* **88** (2013) 014015 [1305.5432].

[345] B. Pullin and R. Zwicky, *Radiative decays of heavy-light mesons and the $f^{(T)}_{H,H^*,H_1}$ decay constants*, *JHEP* **09** (2021) 023 [2106.13617].

[346] M. C. Arnesen, B. Grinstein, I. Z. Rothstein and I. W. Stewart, *A Precision model independent determination of $|V_{ub}|$ from $B \to \pi l \nu$*, *Phys. Rev. Lett.* **95** (2005) 071802 [hep-ph/0504209].

[347] B. Simon, *Orthogonal polynomials on the unit circle: New results*, *International Mathematics Research Notices* **2004** (2004) 2837.

[348] Particle Data Group collaboration, *Review of particle physics*, *Prog. Theor. Exp. Phys.* **2020** (2020) 083C01.

[349] D. van Dyk et al., *EOS - A Software for Flavor Physics Phenomenology*, 2111.15428.

[350] D. van Dyk, F. Beaujean, T. Blake, C. Bobeth, M. Bordone, E. Eberhard et al., EOS v1.0.2 — A software for flavor physics phenomenology, May, 2022. 10.5281/zenodo.6532243.

[351] N. Metropolis, A. W. Rosenbluth, M. N. Rosenbluth, A. H. Teller and E. Teller, *Equation of state calculations by fast computing machines*, *J. Chem. Phys.* **21** (1953) 1087.

[352] W. K. Hastings, *Monte Carlo Sampling Methods Using Markov Chains and Their Applications*, *Biometrika* **57** (1970) 97.

[353] C. Bobeth, M. Chrzaszcz, D. van Dyk and J. Virto, *Long-distance effects in $B \to K^* \ell\ell$ from analyticity*, *Eur. Phys. J. C* **78** (2018) 451 [1707.07305].

[354] N. Gubernari, D. van Dyk and J. Virto, *Non-local matrix elements in $B_{(s)} \to \{K^{(*)}, \phi\} \ell^+ \ell^-$*, 2011.09813.

[355] M. Beneke and T. Feldmann, *Factorization of heavy to light form-factors in soft collinear effective theory*, *Nucl. Phys. B* **685** (2004) 249 [hep-ph/0311335].

[356] A. G. Grozin and M. Neubert, *Asymptotics of heavy meson form-factors*, *Phys. Rev. D* **55** (1997) 272 [hep-ph/9607366].

[357] M. Beneke, G. Buchalla, M. Neubert and C. T. Sachrajda, *QCD factorization for exclusive, nonleptonic B meson decays: General arguments and the case of heavy light final states*, *Nucl. Phys. B* **591** (2000) 313 [hep-ph/0006124].

[358] M. Beneke, G. Buchalla, M. Neubert and C. T. Sachrajda, *QCD factorization for B —> pi pi decays: Strong phases and CP violation in the heavy quark limit*, *Phys. Rev. Lett.* **83** (1999) 1914 [hep-ph/9905312].

[359] B. O. Lange and M. Neubert, *Renormalization group evolution of the B meson light cone distribution amplitude*, *Phys. Rev. Lett.* **91** (2003) 102001 [hep-ph/0303082].

[360] G. Bell, T. Feldmann, Y.-M. Wang and M. W. Y. Yip, *Light-Cone Distribution Amplitudes for Heavy-Quark Hadrons*, *JHEP* **11** (2013) 191 [1308.6114].

[361] V. M. Braun, Y. Ji and A. N. Manashov, *Scale-dependence of the B-meson LCDA beyond leading order from conformal symmetry*, in *14th International Symposium on Radiative Corrections: Application of Quantum Field Theory to Phenomenology*, 12, 2019, DOI [1912.03210].

[362] V. M. Braun, Y. Ji and A. N. Manashov, *Two-loop evolution equation for the B-meson distribution amplitude*, *Phys. Rev. D* **100** (2019) 014023 [1905.04498].

[363] A. M. Galda and M. Neubert, *Evolution of the B-Meson Light-Cone Distribution Amplitude in Laplace Space*, *Phys. Rev. D* **102** (2020) 071501 [2006.05428].

[364] V. M. Braun, Y. Ji and A. N. Manashov, *Higher-twist B-meson Distribution Amplitudes in HQET*, *JHEP* **05** (2017) 022 [1703.02446].

[365] M. Beneke and J. Rohrwild, *B meson distribution amplitude from B –> \gamma l \nu*, *Eur. Phys. J. C* **71** (2011) 1818 [1110.3228].

[366] M. Beneke, V. M. Braun, Y. Ji and Y.-B. Wei, *Radiative leptonic decay $B \to \gamma \ell \nu_\ell$ with subleading power corrections*, *JHEP* **07** (2018) 154 [1804.04962].

[367] Y.-L. Shen, Z.-T. Zou and Y.-B. Wei, *Subleading power corrections to $B \to \gamma l \nu$ decay in PQCD approach*, *Phys. Rev. D* **99** (2019) 016004 [1811.08250].

[368] V. M. Braun and A. Khodjamirian, *Soft contribution to $B \to \gamma \ell \nu_\ell$ and the B-meson distribution amplitude*, *Phys. Lett. B* **718** (2013) 1014 [1210.4453].

[369] A. Khodjamirian, R. Mandal and T. Mannel, *Inverse moment of the B_s-meson distribution amplitude from QCD sum rule*, *JHEP* **10** (2020) 043 [2008.03935].

[370] Y.-M. Wang, *Factorization and dispersion relations for radiative leptonic B decay*, *JHEP* **09** (2016) 159 [1606.03080].

[371] Y.-M. Wang and Y.-L. Shen, *Subleading-power corrections to the radiative leptonic $B \to \gamma \ell \nu$ decay in QCD*, *JHEP* **05** (2018) 184 [1803.06667].

[372] H. Kawamura, J. Kodaira, C.-F. Qiao and K. Tanaka, *B-meson light cone distribution amplitudes in the heavy quark limit*, *Phys. Lett. B* **523** (2001) 111 [hep-ph/0109181].

[373] V. A. Novikov, M. A. Shifman, A. I. Vainshtein and V. I. Zakharov, *Calculations in External Fields in Quantum Chromodynamics. Technical Review*, *Fortsch. Phys.* **32** (1984) 585.

[374] M. A. Shifman, A. I. Vainshtein and V. I. Zakharov, *QCD and Resonance Physics: Applications*, *Nucl. Phys. B* **147** (1979) 448.

[375] K. G. Wilson, *Nonlagrangian models of current algebra*, *Phys. Rev.* **179** (1969) 1499.

[376] V. M. Braun and I. E. Filyanov, *Conformal Invariance and Pion Wave Functions of Nonleading Twist*, *Z. Phys. C* **48** (1990) 239.

[377] P. Ball, V. M. Braun, Y. Koike and K. Tanaka, *Higher twist distribution amplitudes of vector mesons in QCD: Formalism and twist - three distributions*, *Nucl. Phys. B* **529** (1998) 323 [hep-ph/9802299].

[378] T. Nishikawa and K. Tanaka, *QCD Sum Rules for Quark-Gluon Three-Body Components in the B Meson*, *Nucl. Phys. B* **879** (2014) 110 [1109.6786].

[379] D. J. Broadhurst and A. G. Grozin, *Operator product expansion in static quark effective field theory: Large perturbative correction*, *Phys. Lett. B* **274** (1992) 421 [hep-ph/9908363].

[380] A. A. Penin and M. Steinhauser, *Heavy light meson decay constant from QCD sum rules in three loop approximation*, *Phys. Rev. D* **65** (2002) 054006 [hep-ph/0108110].

[381] M. Neubert, *Heavy meson form-factors from QCD sum rules*, *Phys. Rev. D* **45** (1992) 2451.

[382] S. Aoki et al., *Review of lattice results concerning low-energy particle physics*, *Eur. Phys. J. C* **77** (2017) 112 [1607.00299].

[383] A. F. Falk, M. Neubert and M. E. Luke, *The Residual mass term in the heavy quark effective theory*, *Nucl. Phys. B* **388** (1992) 363 [hep-ph/9204229].

[384] M. Neubert, *Heavy quark symmetry*, *Phys. Rept.* **245** (1994) 259 [hep-ph/9306320].

[385] R. Hofmann, *Operator product expansion and local quark hadron duality: Facts and riddles*, *Prog. Part. Nucl. Phys.* **52** (2004) 299 [hep-ph/0312130].

[386] R. Thomas, T. Hilger and B. Kampfer, *Four-quark condensates in nucleon QCD sum rules*, *Nucl. Phys. A* **795** (2007) 19 [0704.3004].

[387] V. Fock, *Proper time in classical and quantum mechanics*, *Phys. Z. Sowjetunion* **12** (1937) 404.

[388] J. S. Schwinger, *On gauge invariance and vacuum polarization*, *Phys. Rev.* **82** (1951) 664.

[389] D. Binosi, J. Collins, C. Kaufhold and L. Theussl, *JaxoDraw: A Graphical user interface for drawing Feynman diagrams. Version 2.0 release notes*, *Comput. Phys. Commun.* **180** (2009) 1709 [0811.4113].

[390] R. N. Lee, *LiteRed 1.4: a powerful tool for reduction of multiloop integrals*, *J. Phys. Conf. Ser.* **523** (2014) 012059 [1310.1145].

[391] A. G. Grozin and M. Neubert, *Hybrid renormalization of penguins and five-dimension heavy light operators*, *Nucl. Phys. B* **495** (1997) 81 [hep-ph/9701262].

[392] M. Jamin, *Flavor symmetry breaking of the quark condensate and chiral corrections to the Gell-Mann-Oakes-Renner relation*, *Phys. Lett. B* **538** (2002) 71 [hep-ph/0201174].

[393] V. M. Belyaev and B. L. Ioffe, *Determination of Baryon and Baryonic Resonance Masses from QCD Sum Rules. 1. Nonstrange Baryons*, *Sov. Phys. JETP* **56** (1982) 493.

[394] A. Khodjamirian, *Upper bounds on f(D) and f(D(s)) from two-point correlation function in QCD*, *Phys. Rev. D* **79** (2009) 031503 [0812.3747].

[395] P. Pascual and R. Tarrach, *QCD: RENORMALIZATION FOR THE PRACTITIONER*, vol. 194. 1984.

[396] S. N. Nikolaev and A. V. Radyushkin, *Vacuum Corrections to QCD Charmonium Sum Rules: Basic Formalism and O (G^3) Results*, *Nucl. Phys. B* **213** (1983) 285.